

UNIVERSITY OF LONDON

Imperial College of Science and Technology

The Blackett Laboratory

Optics Section

STUDIES OF MODE-LOCKING THE C.W. DYE LASER

Ivan Speer Ruddock B.Sc.(Q.U.B.)

Thesis submitted for the Degree of Doctor of Philosophy

of The University of London, 1976.

ABSTRACT

The characteristics of a continuous wave (C.W.) Rhodamine 6G dye laser are described and configurations in which the active medium flows in either a dye cell or an open "jet-stream" are compared and the thermal limitations considered. Continuous laser action of Rhodamine B and Sodium Fluorescein and the associated problems are discussed.

Passive mode-locking, involving the inclusion of a saturable absorber dye in the cavity, was investigated (for Rhodamine 6G) with the dye in contact with one of the cavity mirrors or situated at a distance from it. Pulse durations were determined by the second harmonic autocorrelation method and the electron-optical streak camera. The contacted system generated the shortest and most reproducible mode-locking and produced second harmonic traces to which the best fit was by the autocorrelation function of pulses of sech^2 intensity profile. Mode-locking of the non-contacted system was only possible close to threshold and the corresponding traces suggested asymmetric exponential pulses.

Pulse durations for the contacted dye cell were reduced from ~ 1 ps to a minimum of 0.3 ps by narrowing the cell from 0.6 mm to 0.2 mm. The tuning range for mode-locking of Rhodamine 6G by DODCI (3,3'-diethyloxadicyanin iodide), 595-620 nm, was extended to 580 nm by the use of DQOCI (1,3'-diethyl 4,2'-quinolyoxacarbocyanin iodide) as absorber. Further extension was achieved by mode-locking Rhodamine B (610-630 nm) and Sodium Fluorescein (545 nm). In common with flashlamp pumped mode-locked dye lasers, pulse durations were largely independent of the saturable absorber recovery time.

A review is also given of the theoretical models of the passive mode-locking mechanism and compared with the experimental system.

CONTENTS

	<u>PAGE</u>
GENERAL INTRODUCTION	6
CHAPTER 1: PHOTOPHYSICS OF DYE LASERS	
1.1 Introduction	8
1.2 Dyes	8
1.3 Triplet State Effects	16
1.4 Pumping of C.W. Dye Lasers	19
1.5 Rate Equation Description of Dye Lasers	21
CHAPTER 2: THE C.W. DYE LASER	
2.1 Introduction	26
2.2 Review of C.W. Dye Laser Development	26
2.3 The Astigmatically Compensated Cavity	28
2.4 The Dye Cell Laser	32
2.5 The Rhodamine 6G Dye Cell Laser	36
2.6 The Jet-stream Laser	41
2.7 Thermal Effects	46
2.8 C.W. Dye Laser Stability	51
2.9 Tuning of the C.W. Dye Laser	55
2.10 Loss Analysis of the Rhodamine 6G C.W. Dye Laser	60
2.11 The C.W. Rhodamine B Laser	66
2.12 The C.W. Sodium Fluorescein Laser	67
2.13 Conclusion	70
CHAPTER 3: MEASUREMENT OF ULTRASHORT PULSES	
3.1 Introduction	71
3.2 Fourier Spectroscopy	72

3.3	Second Harmonic Autocorrelation	74
3.4	The Electron-Optical Streak Camera	83
3.5	Conclusion	89
CHAPTER 4: MODE-LOCKING OF THE C.W. RHODAMINE 6G DYE LASER		
4.1	Introduction	90
4.2	Review of Mode-Locked Dye Lasers	91
4.3	The Mode-Locking Dyes	95
4.4	The Passively Mode-Locked C.W. Dye Laser Cavity	95
4.5	The Contacted Dye Cell	102
4.6	The Mode-Locked C.W. Rhodamine 6G Laser:-Contacted Absorber	
a	Phenomenological characteristics	103
b	Pulse durations	108
c	Pulse shapes	120
d	Generation of subpicosecond pulses	123
e	Spectral characteristics	127
f	Tuning characteristics	143
g	The effect of saturable absorber lifetime	145
4.7	Conclusion	152
CHAPTER 5: TUNING OF THE MODE-LOCKED C.W. DYE LASER AND THE MODE-LOCKED CHARACTERISTICS OF THE NON-CONTACTED ABSORBER SYSTEM		
5.1	Introduction	153
5.2	The Mode-Locked C.W. Rhodamine B laser	153
5.3	The Mode-Locked Sodium Fluorescein Laser	155
5.4	The Mode-Locked C.W. Rhodamine 6G Laser:-Non-Contacted Absorber	
a	Mode-locking characteristics	159
b	Spectral characteristics	169
5.5	The Mechanism of Passive Mode-Locking	172

5.6 Conclusion	178
GENERAL CONCLUSION	179
REFERENCES	182
ACKNOWLEDGMENTS	190
PUBLICATIONS	191

GENERAL INTRODUCTION

With the early solid-state and gas laser materials most of the basic output parameters were variable with one important exception. The inability to frequency tune the laser emission restricted the potential of the laser especially in the study of resonant interactions. The use of organic dye solutions as the active media with their broad emission bands of tens of nanometers satisfied this basic requirement and was first demonstrated by Sorokin and Lankard¹ in 1966 by optically pumping with a pulsed ruby laser a solution of chloro-aluminium phthalocyanine.

In addition to tunability, organic dye solutions in flashlamp pumped operation², were able to provide similar output energies to those currently available from solid state systems (up to 400 J)³. The dye laser by virtue of its liquid structure does not suffer from the ever present risks of damage at high power densities caused by self-focussing and other non-linear phenomena in the media. Also they are considerably cheaper than other laser materials and high optical quality is obtainable with the correct choice of solvent. Due to the homogeneous nature of the dye emission there is in addition to gross tuning of the laser wavelength, the possibility of spectral narrowing down to \sim MHz⁴.

A major advance in dye laser and laser technology in general occurred with the development of continuous wave (C.W.) operation⁵. The possibility of stable tunable narrow linewidth radiation has made it of prime importance in high resolution spectroscopy⁶. The subsequent discovery and synthesis of new laser dyes enables C.W. laser operation to be continuously tunable over the entire visible and

near infra-red spectrum ⁷. With their broad bandwidth, dye lasers also promised the possibility of generating very short pulses of sub-picosecond durations. The application of passive mode-locking to pulsed ⁸ and C.W. dye lasers ⁹ led towards this end and generated tunable pulses of ~ 1 ps ¹⁰.

The mode-locked C.W. dye laser, capable of producing continuous trains of short pulses, is in conjunction with signal averaging and low noise detection methods, an ideal instrument for the measurement of molecular relaxation times ^{10,12}. Tunable transform limited pulses also find application in investigations of coherent photon phenomena such as self-induced transparency ¹³. They are also important in communications and the study of propagation in optical fibres.

The mode-locked C.W. dye laser has, however, become the centre of mode-locking research as it allows a large amount of control over the cavity parameters and an unlimited number of resonator transits are available for pulse compression. It is this feature that is studied in this work with a view to extending the tuning range for mode-locked operation to increase its versatility and to investigate the steady-state pulse durations to improve the available temporal resolution and to gain an insight into the mode-locking process itself.

CHAPTER I

PHOTOPHYSICS OF DYE LASERS

1.1 Introduction

The use of organic dye solutions as the active media in pulsed and continuous lasers creates significant differences from solid state or gas systems. In particular, the performance of continuous wave (C.W.) dye lasers depends strongly on the competing loss mechanisms in the dye solutions and they are also more exacting with respect to the physical tolerances of the cavity. In this chapter, the basic photophysics of dye solutions is reviewed with special reference to the factors important in continuous operation, and the rate equation theory for the dynamics of laser action is discussed. For a more comprehensive description, the reader is referred to accounts by other authors e.g. "Dye Lasers" ¹⁴ edited by F.P. Schäfer and the work of Snavely ¹⁵.

The important thermal effects encountered in C.W. dye lasers are described in Chapter 2 along with the resonator design and the operating characteristics of the "unmode-locked" C.W. dye laser.

1.2 Dyes

In general, a dye may be considered as a substance which can impart a characteristic colour to other materials due to its high absorption in the visible part of the spectrum. This property is associated with the dye containing several conjugated double bonds which are double bonds separated by a single bond, causing absorption at wavelength longer than 200 nm ¹⁶. The light absorption mechanism by such compounds is the same in all parts of the spectrum including

the ultraviolet and near infrared and so the term 'dye' may be extended to include all substances containing conjugated double bands.

The electronic ground states of dye molecules are singlet (S_0) and the excited electronic states can be considered either singlet or triplet but because some state mixing occurs in large polyatomic molecules, pure singlet and triplet states do not exist. The manifold of singlet ($S_0, S_1, S_2 \dots$) and triplet states (T_1, T_2, \dots) are shown in Figure 1. The electronic levels separated by $10,000 - 30,000 \text{ cm}^{-1}$, extend over a range of frequencies due to the quantized vibrational and electronic excitation of the large number of atoms in the organic dye molecule. The spacing of the vibrational levels (shown schematically in Figure 1) is 1000 cm^{-1} , but due to the rotational levels separated by a 10 cm^{-1} each electronic state extends over a near continuum. In addition, the vibrational and rotational levels are broadened by collisional and electrostatic perturbations caused by the surrounding solvent molecules. The populations of the levels in each electronic state are determined by a Boltzmann distribution and after an electronic transition, the relaxation to thermal equilibrium occurs on a time-scale of $\sim 1\text{ps}$, due to collisions with the solvent molecules and the radiationless decay is shown in Figure I. The vibrational relaxation times for the S_1 level of Rhodamine 6G and Rhodamine B have been measured by Ricard et al ¹⁷ to be $\sim 2\text{ps}$ and $\sim 1.4\text{ps}$ respectively and for the S_0 level of the former to be $\sim 4\text{ps}$.

Transitions between the singlet levels are spin-allowed and the $S_0 - S_1$ transition gives rise to the strong, broad absorption bands characteristic of dyes. Radiative decay from the first excited singlet state S_1 to the higher vibrational levels of S_0 gives rise to fluorescence and it is by stimulation of this transition that laser action in dyes occurs. The fluorescence lifetime, which for the dyes

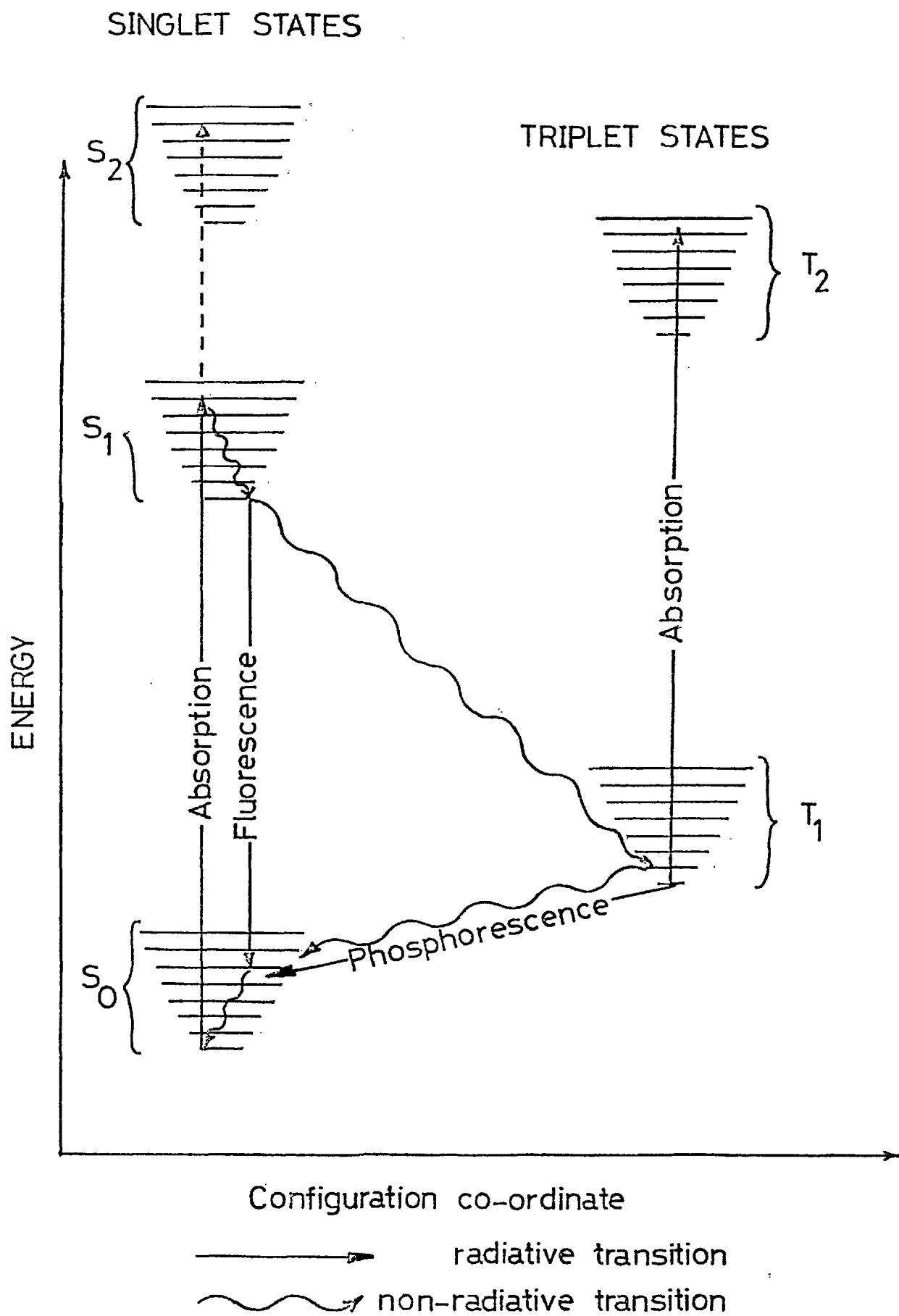


FIG:1 Schematic Energy Level Diagram for a Dye Molecule

used in this work was $\sim 3 - 5\text{ns}$ ^{18, 19, 20}, depends on the dye molecules' environment and is influenced by the solvent, and the temperature, concentration and pH of the solution. The absorption and fluorescence spectra for Rhodamine 6G dissolved in ethylene glycol are shown in Figure 2, along with the stimulated emission cross-section $\sigma_e(\lambda)$ given by ¹⁴

$$\sigma_e(\lambda) = \frac{\lambda^4 E(\lambda)}{8\pi n^2 c \tau} \quad \text{per unit wavelength} \quad (1.1)$$

where $E(\lambda)$ is the fluorescence intensity at wavelength λ , n is the refractive index of the solution, c is the velocity of light in vacuo, and τ is the fluorescence radiative lifetime. The fluorescence profile is normalized to the quantum efficiency ϕ , defined as the ratio of the number of fluorescence photons to the number of absorbed photons, by $\int_0^\infty E(\lambda) d\lambda = \phi$. The quantum efficiency (0.68) was determined for this solution by comparison to one of Rhodamine 6G in ethanol for which $\phi = 0.93$ was assumed ¹⁴. The absorption measurements were made on a working strength solution (6.7×10^{-4} M), such that losses could be estimated in the lasing region centred on 600 nm, using a Perkin - Elmer Model 124 spectrophotometer. The mirror symmetry of the absorption and the Stokes shifted fluorescence spectra is a consequence of the Franck-Condon principle showing that the nuclear configurations of the S_0 and S_1 states are similar.

Absorption from the ground state and the first excited state to higher excited states is also possible, followed by radiationless decay back to the S_1 level and subsequent fluorescence, resulting in a fluorescence spectrum which does not normally depend

RHODAMINE 6G

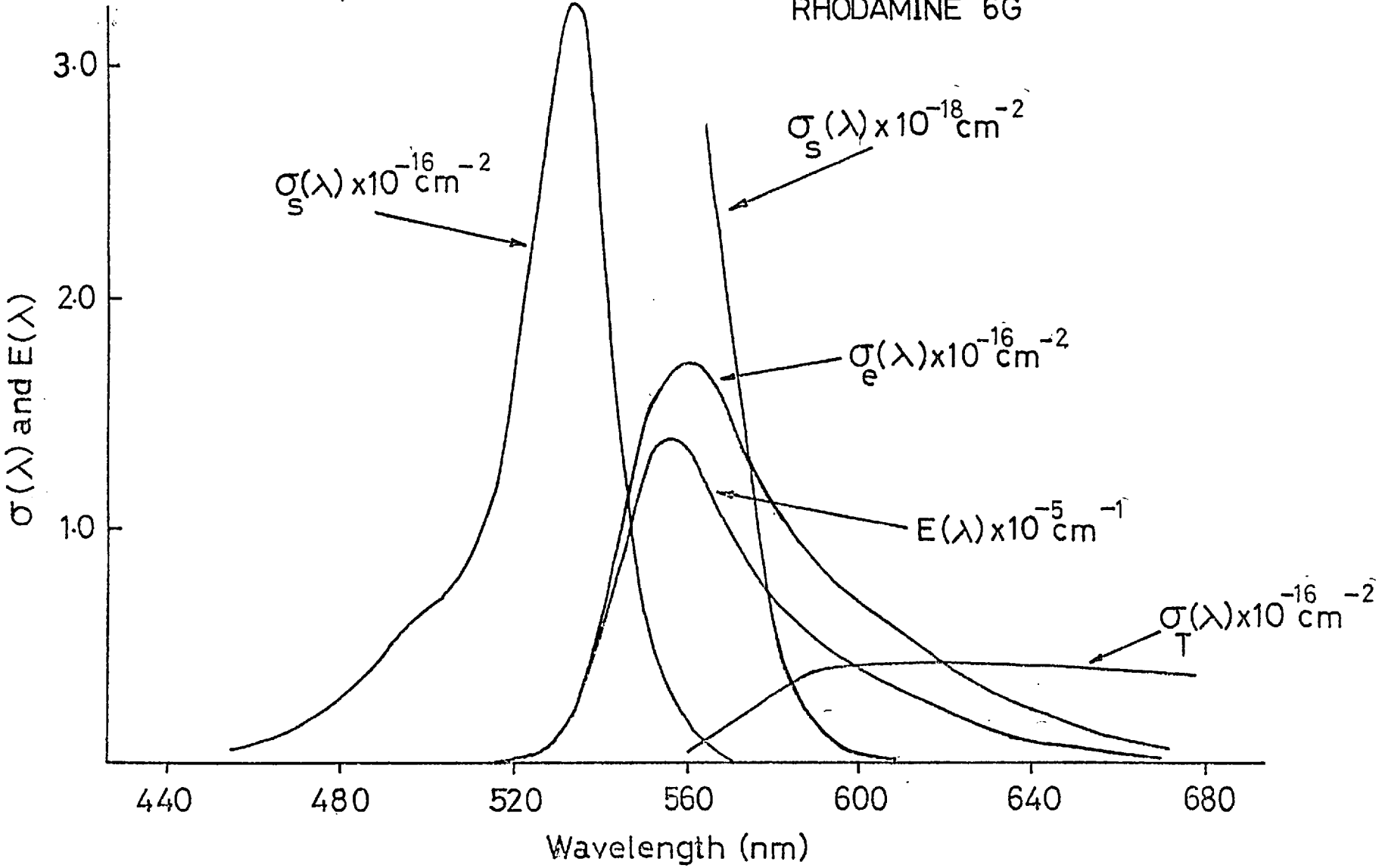


FIG: 2
12

on the wavelength of excitation. The $S_2 - S_1$ relaxation time in cresyl violet has been measured to be $\sim 3 \times 10^{-11}$ seconds by Lin and Dienes²¹. However, the aromatic molecule azulene is an exception and exhibits fluorescence from S_2 to the ground state while internal conversion from S_1 to the ground state is sufficiently fast to prevent the detection of fluorescence except with very high power laser pulses^{22,23}.

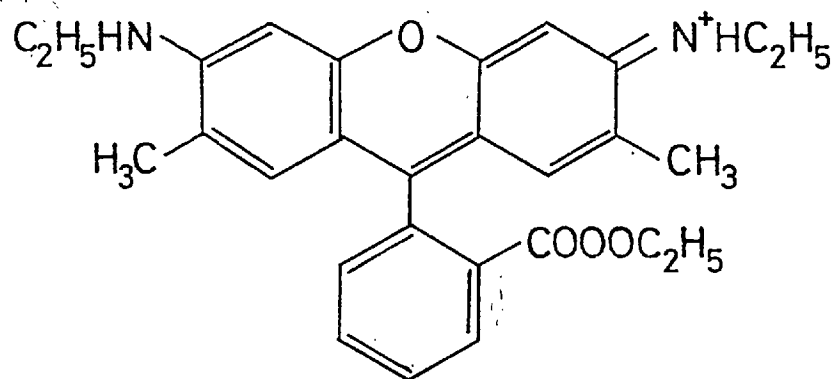
Intersystem crossing by radiationless transitions from the excited singlet state S_1 to the lower lying triplet state T_1 can be induced by internal or external perturbations such as spin-orbit coupling and the influence of dye solvent molecules with high atomic number nuclei. Intersystem crossing, shown in Figure 1 by a wavy line, and denoted by the intersystem crossing rate constant k_{ST} , competes with fluorescence and is detrimental to the efficiency of laser operation in several ways.

As the $T_1 - S_0$ transition is spin-forbidden, the lifetime for decay of the triplet state τ_T , is considerably longer than τ and can be in the $\mu s - ms$ range depending on the solvent conditions and if the transition is radiative the ensuing radiation is termed phosphorescence. The triplet decay time in a C.W. dye laser in which the active medium was a Rhodamine 6G in ethylene glycol solution has been measured directly to be ~ 120 ns by Teschke et al²⁴. Owing to its relatively long lifetime, the triplet state acts as a trap for the excited molecules and depletes the number available for amplification in the laser process. In addition, T_1 is the lowest lying triplet level among which transitions are spin-allowed and the associated absorption band generally overlaps

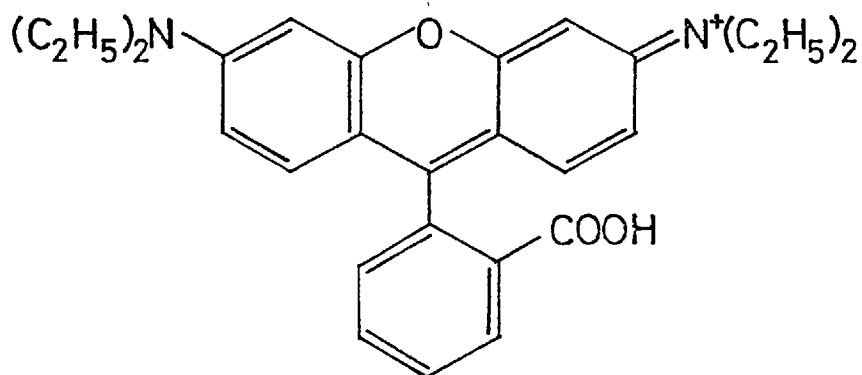
the singlet-state fluorescence spectrum. In Figure 2, the triplet-triplet absorption cross-section σ_T is reproduced for a Rhodamine 6G in ethanol solution²⁵. The triplet-triplet absorption can be strong enough to quench or prevent laser action, and so to minimize the deleterious effects, either sufficient quenching of the triplet state must be achieved or a rapid risetime pumping source is necessary such that threshold is reached before a significant number of molecules have accumulated there²⁶.

The laser dyes in addition to Rhodamine 6G, employed in this work, were Rhodamine B and Sodium Fluorescein (Eastman Kodak) and were used without further purification. The structure of the dyes, members of the Xanthene dye family, is shown in Figure 3 along with the basic Xanthene structure. The saturable absorber dyes used in the passive mode-locking process are members of the polymethine branch of the cyanine group and are discussed in Chapter 4.

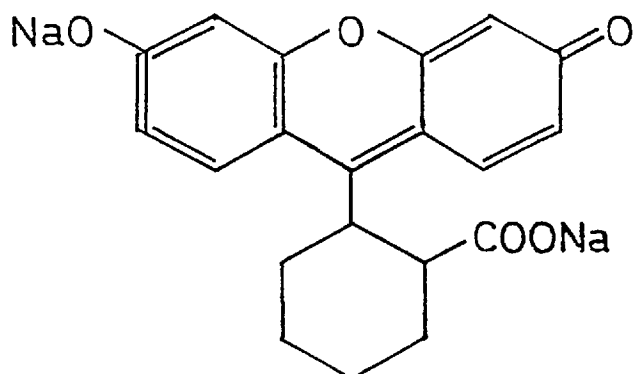
As already pointed out, the dye parameters are greatly influenced by the conditions prevailing in the solution. However, the prospective use of the dye may determine the solvent required e.g. in continuous operation, one with a high thermal conductivity and a low thermal refractive index gradient is desirable, and for this reason, water was widely used in the earlier lasers²⁷. In highly polar solvents like water, dimerization of the dye molecules occurs at normal working concentrations leading to an absorptive loss of pump power as the dimers' fluorescence is normally quenched. The addition of a deaggregating agent to the solution which forms micelles containing one dye molecule each, prevents dimerization and for this purpose the surfactant "Ammonyx L0" has been widely used²⁸.



RHODAMINE 6G



RHODAMINE B



SODIUM FLUORESCIEIN

FIG: 3

1.3 Triplet State Effects

The accumulation of dye molecules in the metastable triplet state was initially considered to be a barrier to the operation of pulsed and later C.W. dye lasers. To surmount this problem, Sorokin and Lankard²⁹ used a Q-switched laser as a pump source such that the high pumping rate was rapid enough to create sufficient inversion before the build-up of the triplet population. Even with a rapid risetime flashlamp, laser emission was still limited to approximately $1\mu\text{s}$ ³², but by using an air saturated Rhodamine 6G in methanol solution, Snavely and Schäfer³⁰ produced pulses of $\sim 140\mu\text{s}$, and after removal of the oxygen, threshold was unobtainable up to seven times the original pumping level. This was attributed to a quenching of the triplet state lifetime reducing it to $\sim 10^{-7}\text{s}$ at the oxygen concentration of $\sim 0.2 \times 10^{-2}\text{M}$. The termination of the laser pulse which still occurred before the end of the pump was later shown to be due to thermal inhomogenities in the active medium. Oxygen by its paramagnetic nature increases spin-orbit coupling and produces quenching, but simultaneously there is a fluorescence quenching action by enhancing intersystem crossing from the excited singlet to the triplet states. The predominance of either of these phenomena determines whether oxygen helps or hinders lasing and this point is discussed further in Chapter 2 with respect to Sodium Fluorescein. However for Rhodamine 6G, the most commonly used dye, and for many others³¹, oxygen is a very efficient triplet quencher and was sufficient for most of this work.

From the dynamics of the dye laser, the limiting effect of an uncontrolled triplet population can be seen¹⁴, for the typical

case in which the triplet lifetime τ_T is long compared to the spontaneous lifetime τ for the $S_1 - S_0$ process.

If the intersystem crossing rate for S_1-T_1 is k_{ST} (s^{-1}), the rate at which molecules enter T_1 , the triplet ground state is given by $N_{1C}k_{ST}$ when N_{1C} is the critical inversion, the population of S_1 required for the gain of the pumped active medium to overcome the intrinsic cavity losses. The population of T_1 , N_T will be given by

$$\frac{dN_T}{dt} = N_{1C}k_{ST} - N_T/\tau_T$$

Assuming the critical inversion is produced at time $t = 0$ and that τ_T is large, then

$$N_T = N_{1C}k_{ST}\tau_T$$

From Figure 2, at the peak of the stimulated emission cross-section, $\sigma_T(\lambda) \sim \sigma_e(\lambda)/10$.

When

$$N_1\sigma_e = N_T\sigma_T$$

the intrinsic gain just balances the loss due to the triplet state and so at the peak of σ_e , the gain vanishes when

$$N_T = 10N_{1C}$$

and a maximum value of $k_{ST}\tau_T/10$ exists for C.W. operation.

Experimental values for $k_{ST}\tau_T$ in the Rhodamine 6G C.W. laser have been measured by Teschke and Dienes³² to be $\sim 0.8 - 1.6$ depending

on the solvent. Similar values of ~ 0.9 have been estimated by Webb et al³⁴ for a Rhodamine 6G - ethanol flashlamp pumped laser.

From (1.2), (for an unquenched system) the maximum laser pulse length t_{\max} is given by

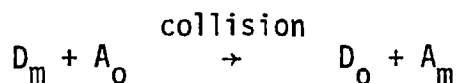
$$t_{\max} \sim 10/k_{ST}$$

The intersystem crossing rate is related to the fluorescence quantum efficiency ϕ , and the fluorescence lifetime τ by

$$k_{ST} = \tau^{-1}(1-\phi)$$

Substitution of Rhodamine 6G parameters, $\phi = 0.93$ and $\tau \sim 5 \times 10^{-9}$ s gives $k_{ST} \sim 1.4 \times 10^{-7} \text{ s}^{-1}$, resulting in $t_{\max} \sim 7 \times 10^{-7}$ s, consistent with the laser pulses in a system without a triplet state quenching agent (TSQA)³⁰.

As an alternative to oxygen, various chemical additives may be used to reduce the triplet population. The most common one has been cyclooctatetraene (COT) with which Pappalardo et al²⁴ produced laser pulses of up to 500 μ s from a flashlamp pumped Rhodamine 6G laser with a pumping pulse of ~ 600 μ s FWHM. The depopulation of a dye metastable state by a chemical additive results from collisional transfer of energy from the triplet state to the additive molecule by the transition



provided the energy condition $E(D_m) \geq E(A_m)$ is satisfied. A and

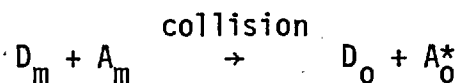
D represent acceptor and donor molecules respectively, and m and o denote metastable and ground state.

To be effective in improving dye laser performance, a triplet state quenching agent must also fulfil the following conditions for the energy levels ³¹.

$$\begin{aligned} E(A_m) &\leq E(D_m) \\ E(A_o^*) &> E(D_o^*) \\ E(A_m^* - A_m) &\neq E(D_o^* - D_o) \end{aligned}$$

The asterisk represents an electronic excited state.

The latter two conditions ensure that the TSQA does not absorb laser emission by allowed transitions from either its ground state or from its metastable state. If the first condition is not satisfied, an additive may still be effective by collisionally induced spin-energy transfer.



This form of indirect triplet quenching can occur with flashlamp pumped systems as the TSQA usually have absorption bands in the UV by which they can be excited to be in their metastable level.

1.4 Pumping of C.W. Dye Lasers

The continuous operation of a laser places restrictions on the pump source and consequently introduces imaging and thermal problems. The latter topic will be discussed in Chapter 2, but in this section consideration will be given to the method of optical excitation.

The minimum pumping power density necessary to reach laser threshold, W_{pT} / S where W_{pT} is the threshold pump power, S the area of the excited region, is given by¹⁵

$$\frac{W_{pT}}{S} \approx \frac{N_{1c} h \nu_p d}{\tau} \quad \text{watts. cm}^{-2}.$$

where d is the active length of the dye solution and ν_p is the frequency of the pumping radiation in a longitudinally excited cavity.

The critical inversion N_{1c} has been shown to be related to the solution and cavity parameters by¹⁴

$$\frac{N_{1c}}{N} = \frac{1}{\gamma(\lambda)} \left\{ \sigma_s(\lambda) + \frac{r(\lambda)}{N} \right\}$$

where $\gamma(\lambda) = \{ \sigma_e(\lambda) + \sigma_s(\lambda) + k_{ST} \tau_T (\sigma_s(\lambda) - \sigma_T(\lambda)) \}$, N is the total dye molecule number density, and $r(\lambda) = -(1/2d) \times \ln\{R_1(\lambda)R_2(\lambda)\}$, with $R_1(\lambda)$ and $R_2(\lambda)$ being the reflectances of the cavity mirrors.

For a typical Rhodamine 6G C.W. dye laser with $d = 0.1$ cm, $R_1, R_2 \sim 1$, the calculated power density is approximately ~ 4 KW. cm^{-2} at 530 nm. The lowest thresholds required in practical systems are ~ 20 KW. cm^{-2} and for useful applications a continuous pumping power density of $\sim 100 - 200$ KW. cm^{-2} is necessary. Although these power densities may be possible with conventional arc lamps, the losses involved in the transfer optics have so far precluded their use as practical sources of excitation.

Reported C.W. dye lasers have been optically pumped by argon-ion²⁷ and He - Ne³⁵ beams, which are focussed to spot sizes of $\sim 20\mu\text{m}$ diameter. The use of such small beam waists in

the laser cavity imposes severe restrictions on the cavity design and requires intra-cavity imaging components.

In this work, the excitation sources were Spectra-Physics argon-ion lasers, (Models 164 and 170) which gave maximum powers of $\sim 3\text{W}$ and 12W all-lines respectively. The spectral distribution of the output power among the laser lines is given below for the Model 170.

Wavelength (nm)	Output Power (W)
514.5	4.0
501.7	0.5
496.5	1.2
488.0	3.2
476.5	1.0
472.7	0.2
465.8	0.1
457.9	0.3
454.5	0.1

1.5 Rate Equation Description of Dye Lasers

A rate equation analysis of the populations of the dye states can give an expression relating the output power to the cavity output coupling in the case of a C.W. or a long pulse dye laser in which the pumping pulse is long compared to the singlet and triplet decay times.

Rate equation descriptions of a dye laser have been given by many authors^{15,16} and the following discussion is based upon

that of Polloni ³⁶.

The rate equations for a dye laser may be written as:-

$$\frac{dN_1}{dt} = W_p N_0 - B_e N_1 q - N_1/\tau + B_s N_0 q \quad (1.3a)$$

$$\frac{dN_T}{dt} = k_{ST} N_1 - N_T/\tau_T \quad (1.3b)$$

$$\frac{dq}{dt} = V B_e N_1 q - K_i q - K_o q - V B_s N_0 q - V B_T N_T q \quad (1.3c)$$

where N_1 is the number density of the first excited singlet level S_1 , W_p is proportional to the pump power, N_0 is the number density of active molecules, the B's are the stimulated emission (or absorption) coefficients per photon such that $B_k = \sigma_k c/V$, where c is the velocity of light in the medium and V is the laser mode volume, and σ_k the transition cross-section, q is the number of photons at the laser frequency ν_L in the cavity, and K_i accounts for the internal losses in the cavity excluding those due to re-absorption in the dye. $K_i = \gamma_i c/d$, γ_i being the fraction of power lost per transit and d is the length of the active medium. The power coupled out of the cavity is represented by $K_o = \gamma_o c/d$ where γ_o is the output mirror transmission. It is assumed in equations (1.3) that the decay time of the S_0 vibrational levels is very rapid such that the number density of active molecules in the lower level is not significantly altered by the pumping and can be considered constant and equal to N_0 . Also the triplet levels T_1 and T_2 are considered to be in equilibrium.

Under steady state conditions, the situation is represented by setting the derivatives in (1.3) to zero to give,

$$W_p N_0 - B_e N_1 q - N_1/\tau + B_s N_0 q = 0 \quad (1.4a)$$

$$k_{ST} N_1 - N_1/\tau_T = 0 \quad (1.4b)$$

$$V B_e N_1 q - K_i q - K_o q - V B_s N_0 q - V B_T N_1 q = 0 \quad (1.4c)$$

Elimination of N_1 from equations (1.4) gives for the number of photons in the cavity q ,

$$q = \frac{V}{\tau} \left[\frac{1}{K_i + K_o + B_T k_{ST} \tau_T \cdot \frac{K_i + K_o + V B_s N_0}{B_e - B_T k_{ST} \tau_T}} \right] \quad (1.5)$$

$$\times \left[W_p N_0 \tau - \frac{K_i + K_o + V B_s N_0}{V B_e - V B_T k_{ST} \tau_T} \right]$$

The number of photons leaving the cavity via the output mirror per unit time is given by

$$Q_o = K_o q \quad (1.6)$$

The threshold pumping level W_{p_T} required for when the output mirror is 100% reflecting i.e. $K_o = 0$ is derived from (1.4) again by elimination of N_1

$$W_{p_T} = \frac{K_i + V B_s N_0}{N_0 V \tau (B_e - k_{ST} \tau_T B_T)}$$

Normalizing the pumping level W_p by defining $\theta = W_p/W_{pT}$, substitution into (1.6) gives

$$Q_0 = \frac{K_0}{\tau B_e} \frac{1}{\{K_i + K_0 + \frac{a}{1+a} \cdot V B_s N_0\}} \cdot \left\{ \theta - \frac{K_0}{K_i + V B_s N_0} - 1 \right\} \quad (1.7)$$

where $a = \frac{B_T k_{ST} \tau_T}{B_e - B_T k_{ST} \tau_T}$ and includes the triplet effects which if negligible, can be set to zero.

Using the definition of the loss term, (1.7) becomes

$$Q_0 = \frac{V \gamma_0}{d \tau \sigma_e} \frac{\gamma_i + \gamma_0}{\{\gamma_i + \gamma_0 + \frac{a}{1+a} \cdot \gamma_s\}} \cdot \left\{ \theta - \frac{\gamma_0}{\gamma_i + \gamma_s} - 1 \right\} \quad (1.8)$$

The power coupled out of the cavity $P_0 = h\nu Q_0$ is given by

$$P_0 = \frac{h\nu S \gamma_0}{\sigma_e \tau \{\gamma_i + \gamma_0 + \frac{a}{1+a} \cdot \gamma_s\}} \cdot \left\{ \theta - \frac{\gamma_0}{\gamma_i + \gamma_s} - 1 \right\} \quad (1.9)$$

where S is the average mode area in the active medium.

As most of the terms in (1.9) can be easily derived experimentally, this provides a means of determining the microscopic parameters of the dye solution by macroscopic methods and also of verifying the rate equation model of the C.W. dye laser. A loss analysis of a C.W. dye laser was first performed by Jacobs et al³⁷ by using a set of output mirrors of varying reflectivities and later

by Marowsky et al³⁸ using a continuously adjustable prism output coupler. In the latter report, the authors obtained good agreement between experiment and theoretical predictions from equation (1.9) for output power variation with loss and between the calculated value of σ_e and that from Spectrophotofluorimeter measurements of a Rhodamine 6G - ethylene glycol solution.

Equation (1.9) does not take into account the decrease in ground state population with increased pumping rate. The term $W_p N_0$ should be written as $W_p(N_0 - N_1 - N_T)$ implying an increase in pump power more rapid with increasing γ_0 than predicted by (1.9). However, ground state depletion is of minor importance at low pumping power, and at higher power levels thermal distortion changes the imaging conditions, and the condition of constant pumped area no longer holds.

In Chapter 2, using measurements of $\gamma_i + \gamma_s$ for the Rhodamine 6G - ethylene glycol system, equation (1.9) is fitted to output power measurements from which the stimulated emission cross-section at 590 nm is estimated.

CHAPTER 2

THE C.W. DYE LASER

2.1 Introduction

Following an historical survey of C.W. dye lasers, the design and operational requirements of an experimental C.W. dye laser are discussed. The topics covered are the resonator optics, the dye flow system using both a cell and an open flowing "jet-stream" of dye, thermal problems associated with the choice of solvent, stability and tuning. The operation of Rhodamine 6G, Rhodamine B and Sodium Fluorescein lasers is described and using a Rhodamine 6G in a jet-stream configuration, the intrinsic cavity losses are measured giving an estimation of the stimulated emission cross-section.

2.2 Review of C.W. Dye Laser Development

C.W. operation of a dye laser was first demonstrated by Peterson et al⁵ using a short hemispherical cavity excited longitudinally by a focussed argon-ion laser beam. The dye cuvette which formed the cavity consisted of a plane mirror and a spherical mirror of 4.55 mm radius separated by a 4.5 mm channel through which the Rhodamine 6G-water solution flowed. The plane mirror coating was such that $\sim 76\%$ of the argon-ion power at 514.5 nm was transmitted to couple the pumping radiation into the cavity, and reflected $\sim 99\%$ of the dye laser power at ~ 595 nm. As the pumping beam was focussed to $\sim 11\mu\text{m}$ diameter spot inside the cuvette, the plane mirror substrate was chosen to be of sapphire such that with its high thermal conductivity, the formation of a hot spot on the dielectric coating was prevented.

In the absence of a dispersive element in the resonator, the output spectrum was ~ 3.0 nm halfwidth and exhibited channeling due to beating between the modes of the various subresonances, and was comparable in width to an untuned pulsed Rhodamine 6G laser operated near threshold. The measured threshold power was 200 mW, and with a pumping power of 960 mW, an output power of ~ 30 mW was achieved when the transmission of the curved mirror was increased to 2.5%.

Tuning of the C.W. dye laser was demonstrated by Hercher and Pike³⁹ by including a Brewster's angle prism in the cavity. Again the active medium was flowed transversely in a dye cell but the mirrors were isolated from it to avoid damage to the coatings and to lengthen the laser to include the tuning element. A second lens was introduced to recollimate the internal dye laser beam and to minimize aberrations due to the prism. With a Rhodamine 6G solution, tuning in this configuration was possible over the range 564 - 615 nm with a bandwidth of 0.01 nm.

The basic longitudinally pumped C.W. dye laser has since been developed to produce a single longitudinal mode by Hercher and Pike⁴⁰ with a short term bandwidth of 35MHz and more recently by Hartig and Walther⁴¹ who locked the output to the Sodium D_1 - line resulting in a long term stability of 1.5 MHz and a bandwidth of 20 MHz. In addition, mode-locking by O'Neill⁴² has generated pulses of ~ 4 ps.

This design, however, has been largely superseded by the astigmatically compensated cavity involving the use of concave mirrors for focussing and this configuration, which has been used throughout this work, is described in the following section.

2.3 The Astigmatically Compensated Cavity

In Chapter 1, it was shown that pumping requirements demand a tight focussing of the input beam to spot sizes, typically of $\sim 10\mu\text{m}$ diameter. This was provided for in the earlier lasers by the use of lenses and dichoric mirrors, but apart from the stringent requirements on the input mirror which can restrict the available tuning range, there was always the risk of damage at high power levels as the focus was generally adjacent to one of the dye cell reflectors. Variations on this technique, in which the dye cell is separated from the resonator mirrors e.g. by using a short focal length mirror such that the beam waist falls away from the dielectric coating, result in additional reflections. There is no simple way of eliminating these reflections by mounting the cell at Brewster's angle due to astigmatism, for which compensation cannot be easily achieved.

To overcome these disadvantages, and also to provide a cavity long enough to permit the inclusion of tuning and mode-locking elements, Kogelnik et al⁴³ examined the stability of a three-element reflecting resonator, the basic form of which is shown in Figure 4. This type of folded cavity requires an oblique angle of incidence at the central mirror which will introduce astigmatism into the system. For use as a C.W. dye laser cavity, a dye cell must be inserted at the focus, preferably oriented at the Brewster angle to minimize losses. A dye cell at this angle has itself astigmatic properties, and both distortions become more severe with a reduced spot size.

Compensation can be obtained by offsetting the astigmatism of the central mirror by that of the dye cell. In a resonator of the type shown in Figure 4 with two internal astigmatic components, it is necessary to consider the ray and mode characteristics of the sagittal (xz) and the tangential (yz) planes separately.

Two adjustment measures δ_x and δ_y can be defined by

$$d_{\text{air}} + d_x = R_1 + f_x + \delta_x$$

$$d_{\text{air}} + d_y = R_1 + f_y + \delta_y$$

where f_x and f_y are the effective focal lengths of the centre mirror, and d_x and d_y are the effective distances through the Brewster cell; the optical path distance in air, d_{air} being the same for the x and y cases.

From the geometry of Figure 4, the distances d_x and d_y which the rays have to traverse in each plane are given by

$$d_x = t \sqrt{(n^2 + 1)/n^2}$$

$$d_y = t \sqrt{(n^2 + 1)/n^4}$$

where t is the thickness of the cell and n is the refractive index.

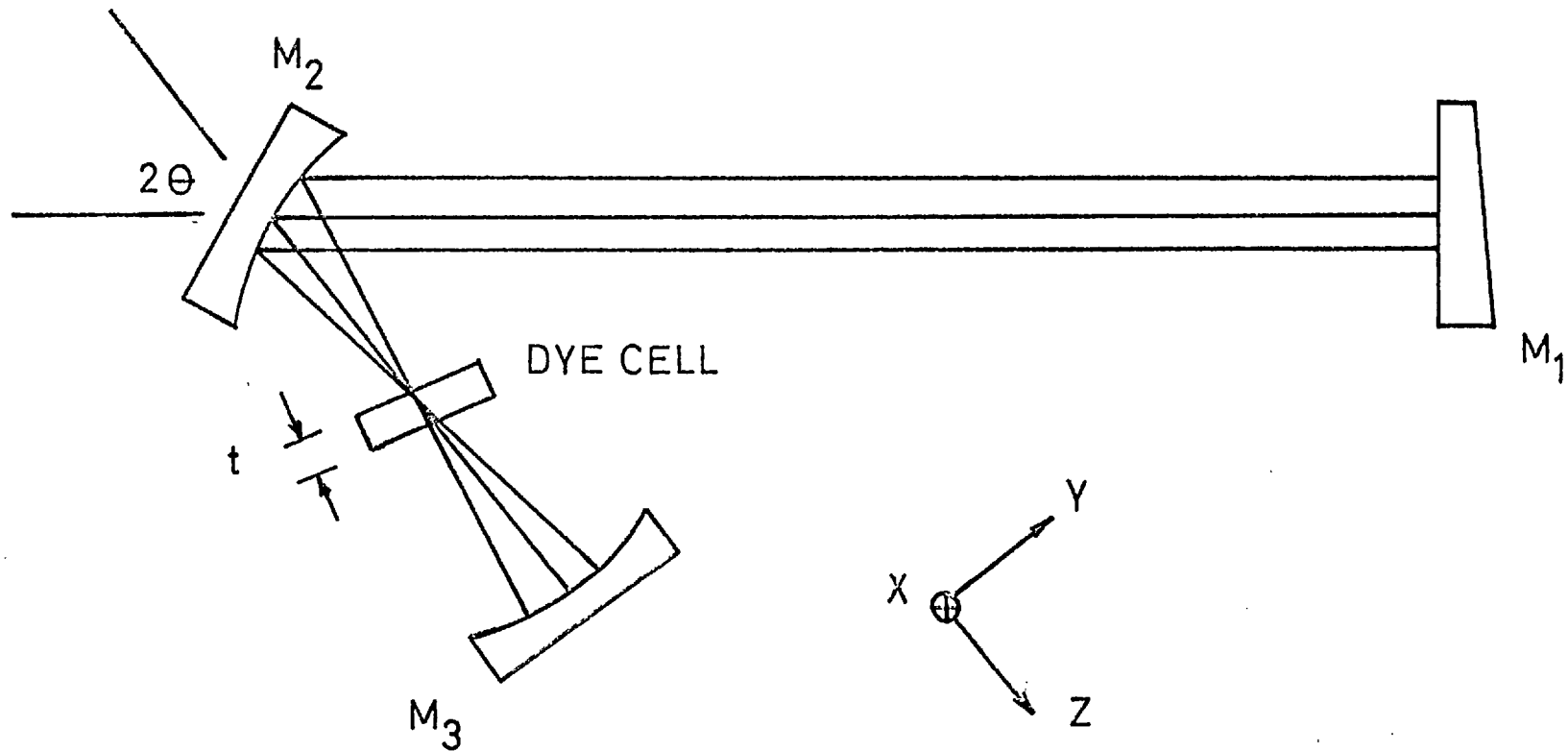
With a given d_{air} , the resonator will generally operate in a different portion of the x stability range than that of the y stability range and may only be stable in one plane at a time. For compensation there is a maximum overlap of the x and y stability ranges which leads to adjustment measures, more or less equal in x and y.

The difference in the adjustment measures are given by

$$\begin{aligned} \delta_x - \delta_y &= (d_x - d_y) - (f_x - f_y) \\ &= t(n^2 - 1) \sqrt{(n^2 + 1)/n^4} - f \sin\theta \tan\theta \end{aligned} \quad (2.1)$$

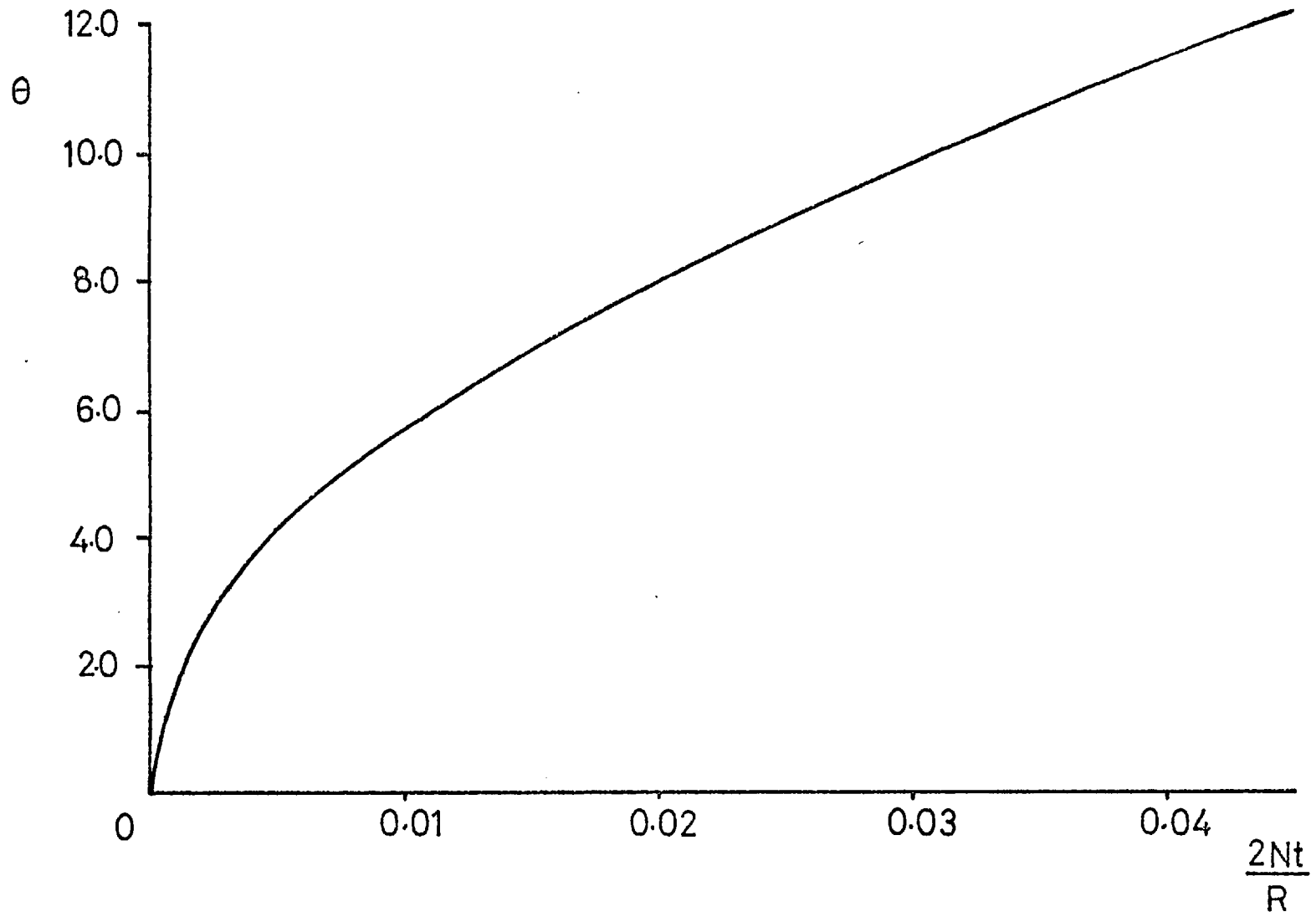
where $f_x = f/\cos \theta$, $f_y = f \cos \theta$.

FIG:4
30



Astigmatically Compensated Cavity

FIG:5



At compensation $\delta_x = \delta_y$ leading to

$$2Nt = 2f \sin\theta \tan\theta \cong R \sin\theta \tan\theta \quad (2.1)$$

where $N = \{(n^2 - 1)/n^4\} \sqrt{(n^2 + 1)}$

Equation (2.1) shows that compensation can be maintained by adjusting the cell thickness with the angle of incidence θ on the central mirror. The variation of the compensation angle with the normalized cavity parameter $2Nt/R$ is shown in Figure (5). In a typical C.W. dye laser system as used in this work, with a dye flow of 0.5 mm thickness and of refractive index 1.43, the corresponding angle of incidence θ for compensation is $3^{\circ}30'$.

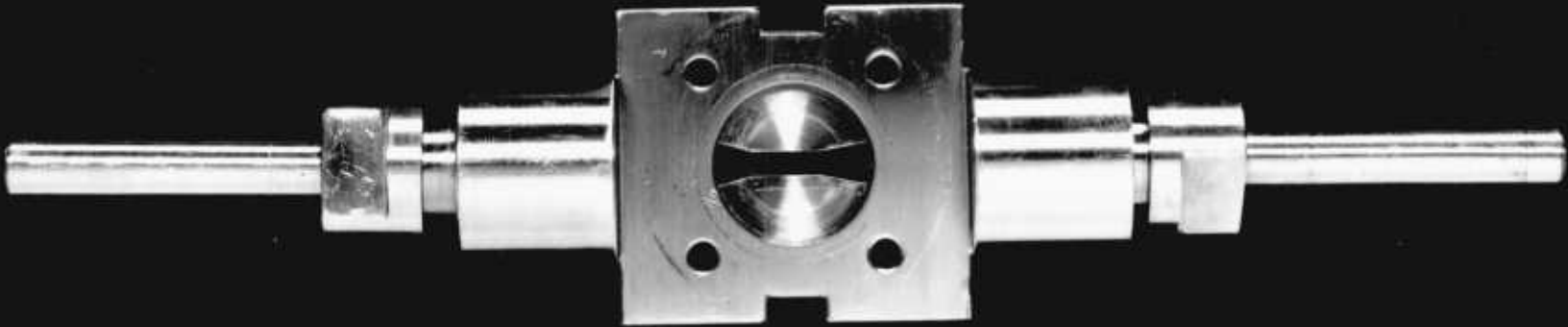
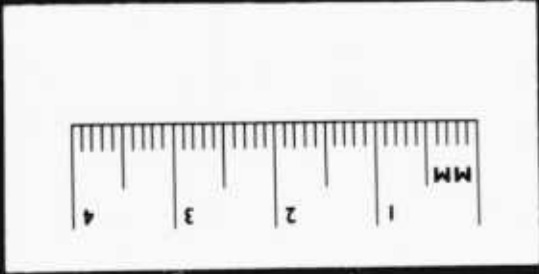
Operation of the laser at values of θ away from the optimum resulted in increased thresholds, reduced stability and degraded the mode characteristics. Apart from use as a dye laser resonator, astigmatically compensated focussing arrangements are widely used in acousto-optic dumpers and mode-lockers for continuous gas and dye lasers using a crystal located at the focus and excited by an R.F. pulse. In this work, the active medium was flowed either through a narrow dye cell or as an open flowing stream of dye placed at the beam waist of the cavity and they are described in the following sections.

2.4 Dye Cell Laser

The dye cell developed for use with the folded focussing arrangement was as shown in Plate 1. It was constructed throughout of stainless steel and sealed by silicon rubber O-rings. The fused quartz windows were of 0.4 mm thickness, polished to $\lambda/10$ and when positioned on each side of the central section, the dye flow

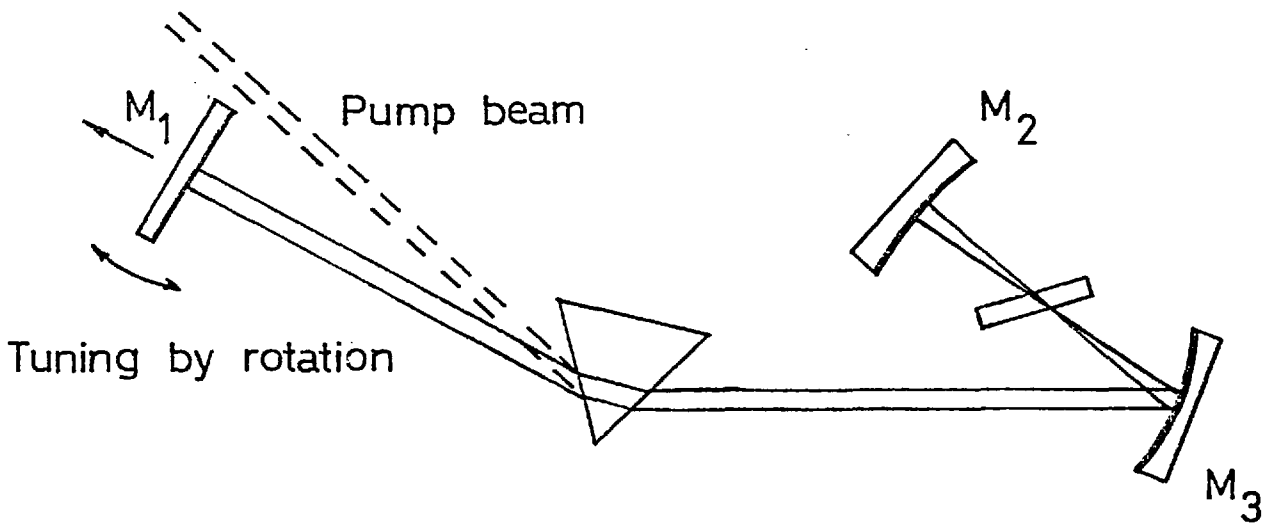
PLATE 1

DYE CELL AND WINDOW HOLDER

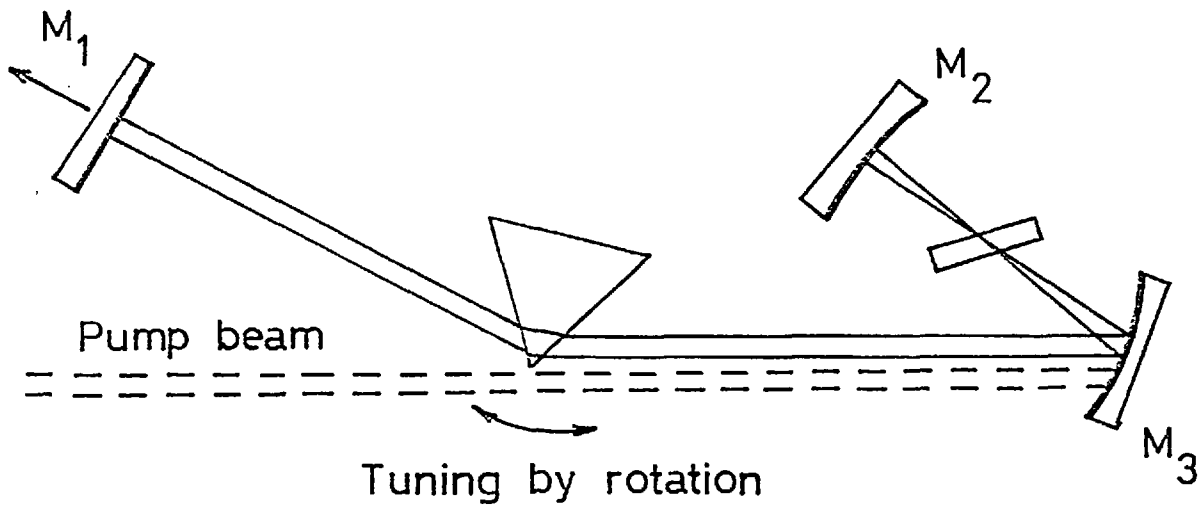


rate was determined by the gap between them and the shape of the channel. This shape was chosen to increase the dye speed as it passed the focus point of the argon-ion laser. With P.T.F.E. gear pumps (Micropump Corporation) an overall flow rate of 3 l.min^{-1} was possible giving the dye a speed of 18 m.s^{-1} at the focal spot. The cell thickness was 0.5 mm and one of the windows was recessed into its holder to give an effective wedge of 1° to combat etalon effects from spurious reflections. The dye solutions were filtered continuously by a 142 mm diameter, $1 \mu\text{m}$ pore size P.T.F.E. membrane (Millipore Ltd.) which in addition to removing scattering particles also minimized bubbles and thus improved laser stability.

The two configurations used for the basic C.W. laser are shown in Figure 6. In Figure 6a, the argon-ion pump beam was coupled into the cavity by the tuning prism such that the dye laser internal beam was collinear with it between the prism and the dye cell. This pumping method was first reported by Dienes et al⁴⁴ and has been used extensively in astigmatically compensated cavities. An advantage is that the pump and dye laser beams have maximum overlap at the focus of the mirrors, but the pumping is limited to one line at any time and tuning by rotation of the prism is not possible due to the resulting misalignment. This method was used successfully in the earlier part of this work but the need for all-line pumping for dyes other than Rhodamine 6G necessitated the modification shown in Figure 6b. The excitation beam now passes the apex of the prism and so allows tuning by rotation as well as all-line pumping. Similar thresholds were obtained with both methods as the two beams were still close together, within $\sim 2 \text{ mm}$ on the mirror surface. Without changing alignment, laser threshold was



(a)



(b)

increased by a factor of 1.6 when pumping all-lines due to the decreased absorption of the 488 nm line and the negligible absorption of the other blue lines in the argon-ion output. The spherical mirrors of 10 and 5 cm radii were broadband reflectors ($R \sim 99.9\%$, 500 - 700 nm) and the plane mirror had reflectivities in the range, 90 - 99% at 600 nm.

Alignment of the cavity to produce overlap of the small beam waists was only possible when it was derived from the dye fluorescence. Using the pump beam as a guide, the system was initially aligned such that the components were all in the same horizontal plane. Then by tilting mirror M_1 (Figure 6a) the spectra of the fluorescence collected by mirrors M_2 and M_3 could be displayed on a screen placed 3 - 4 m away. Adjustment of M_2 sharply focussed one of the spectra and hence focussed the argon-ion beam into the dye solution. Then M_3 was manipulated until the other spectrum was also in focus and overlapped that due to M_2 . The alignment was completed by the reorientation of M_1 to return the spectra to the plane of the laser cavity and the threshold then was improved upon by further fine adjustments to the prism and mirrors.

2.5. The Rhodamine 6G Dye Cell Laser

For each dye studied the concentration of both the dye and Ammonyx LO (water solutions) were optimized. The variation of threshold power required and output power with dye concentration is shown in Figure 7. At low concentrations the amount of pump light absorbed was reduced whereas at higher levels the increase in ground state absorption at the dye laser wavelength and heating

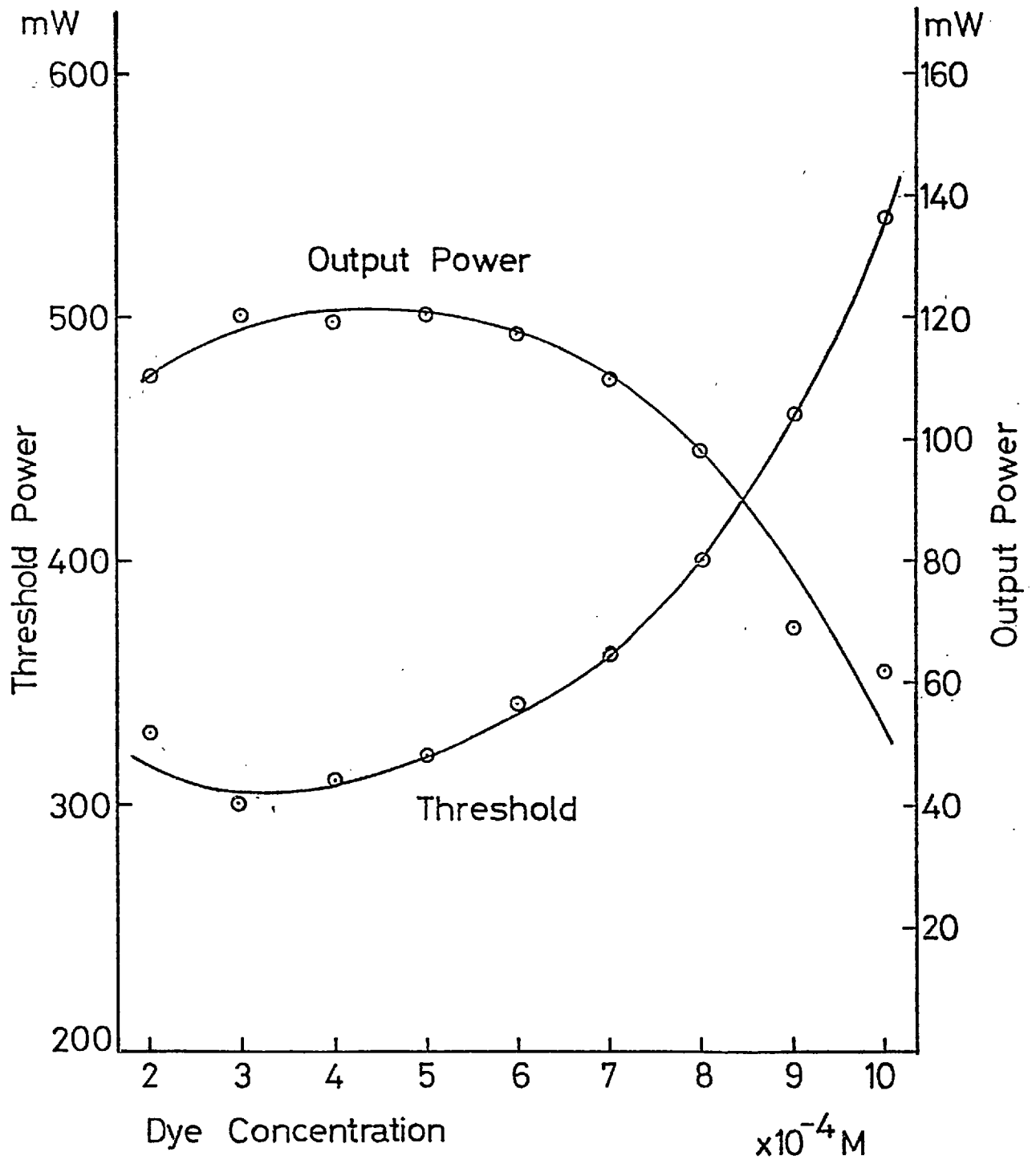


FIG:7

in the dye solution raised the threshold. At the optimum concentration of 4×10^{-4} M, 90% of the 514.5 nm pump light power was absorbed in the cell of 0.6 mm path-length. The Ammonyx LO concentration caused a similar variation in threshold as at low amounts complete deaggregation of the dye molecules did not occur while beyond optimum the additive itself formed conglomerates which acted as scattering centres. The effect of the variation of dye concentration on the tuning of the laser is illustrated in Figure 8 for three different dye concentrations. The shift of the peak of the tuning curve to longer wavelengths with the concentration is anticipated from the increase in self-absorption at shorter wavelengths.

Typical output powers for the dye cell cavity were ~ 150 mW for a pump power of 2.4 W and an output coupling of $\sim 5\%$ at a wavelength of 590 nm. Under these conditions, thresholds were $\sim 300 - 400$ mW depending on the adjustment of the focussing mirrors. The alignment which produced the most favourable thresholds was not that at which the maximum output power levels could be obtained due to refractive index gradients in the solution and is discussed in section 2.6.

For single line pumping (514.5 nm) of Rhodamine 6G, a linear increase in pumping up to 3W input was observed at which level the beam quality deteriorated. With the water solution - dye cell combination, slope efficiencies of $\sim 10\%$ were measured and typical data are given in Figure 9 for the laser operating at 590 nm with an output coupling of $\sim 5\%$, which although not optimum, was convenient in the mode-locking investigations. The use of a mirror of $\sim 11.5\%$ transmission produced a decrease in

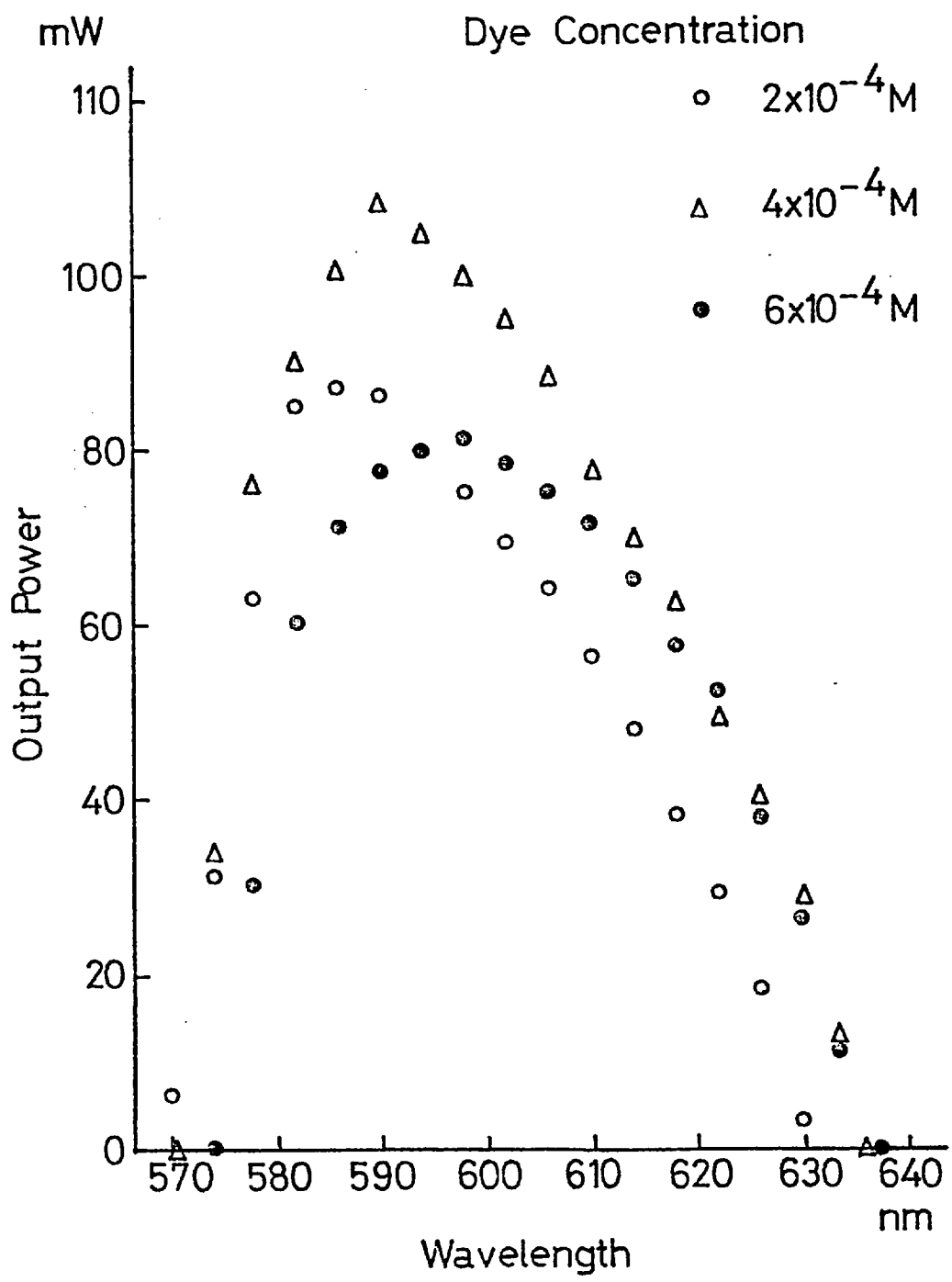


FIG:8

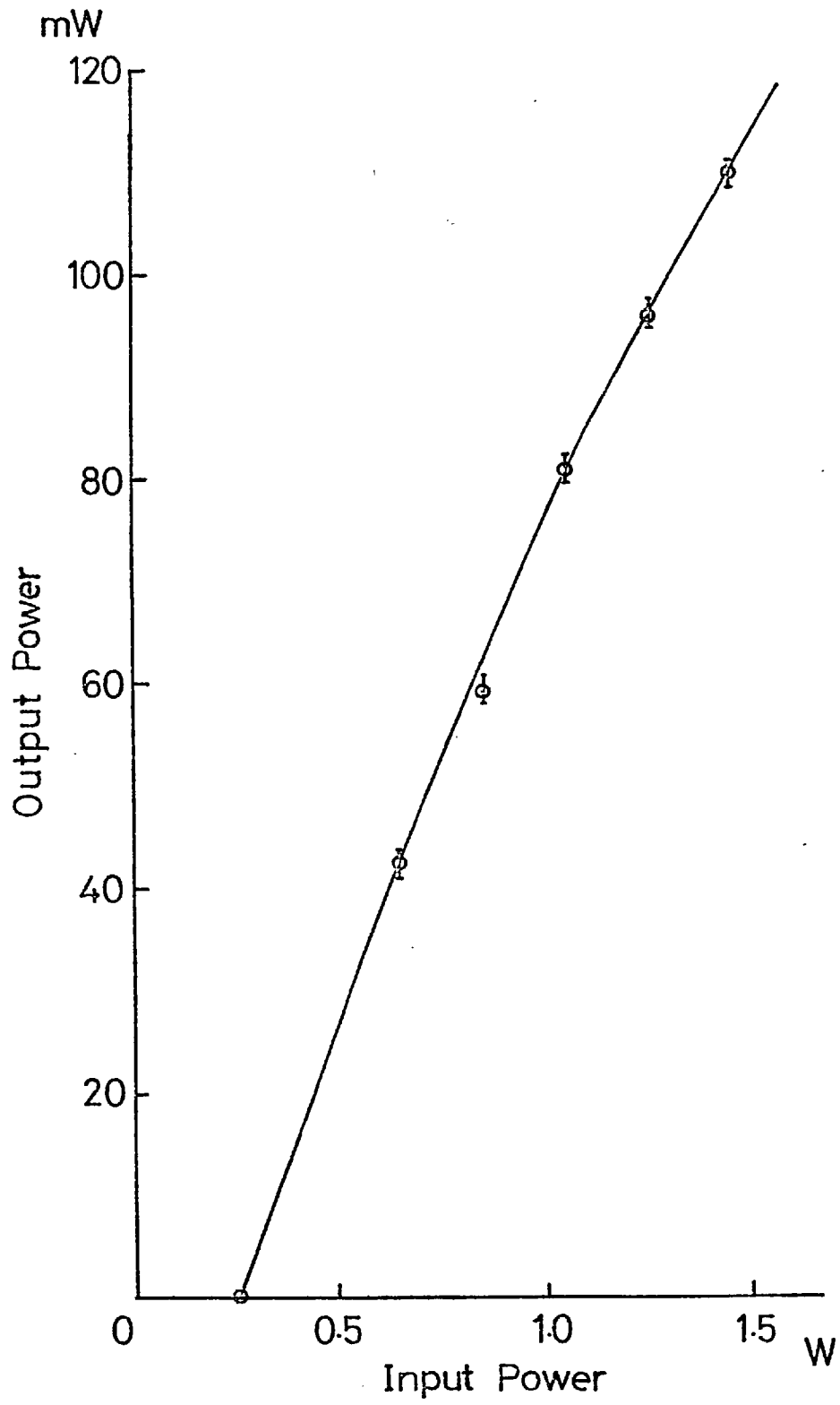


FIG:9

output power of $\sim 50\%$, implying that higher transmissions were tolerable and increased power levels were possible. More detailed studies of the losses in the laser cavity were made for the jet-stream system and are described in Section 2.9.

2.5 The Dye Cell Laser

Although the dye cell laser described above operated satisfactorily with a Rhodamine 6G - water solution, there were a number of inherent disadvantages associated with placing it at the focus of a high power laser which eventually reduced the efficiency. After long term use, the windows became contaminated by particles burning onto the inner surface due to the high power density of the focussed beam and in addition localized heating of the windows degraded the optical quality, with both effects giving rise to poor long term stability. Also in an astigmatically compensated cavity, the windows have to be thin to reduce aberration losses and the stresses due to cementing them to the holders introduce a birefringence that is equivalent to an added loss in a linearly polarized laser.

To overcome these problems, Runge and Rosenberg⁴⁵ investigated the use of free-flowing films of dye and obtained laser action in intra-cavity pumped C.W. lasers and passive mode-locking of the He - Ne laser. Also with the more viscous solvent, ethylene glycol, they found that some dyes e.g. Cresyl Violet, were more stable than when dissolved in methanol.

The requirement on a jet for it to be of sufficient quality for use as the optical medium is that the flow must be a stable laminar sheet. For flow in a pipe or past an obstacle,

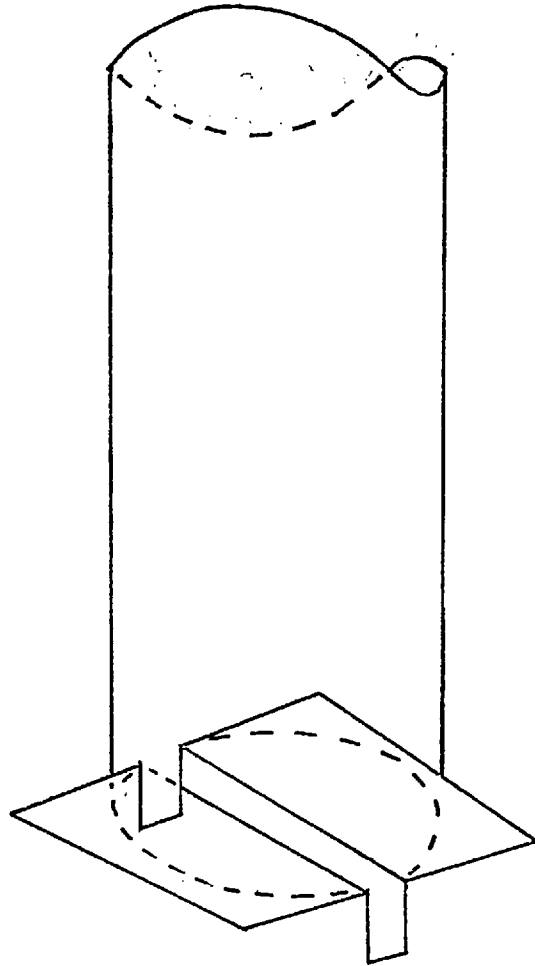
a critical velocity exists at which the flow becomes turbulent. In dealing with this transition, the most commonly used empirical criterion is the Reynolds number, R , defined as

$$R = \frac{v \ell \rho}{\eta}$$

where v is the fluid velocity, η is the fluid viscosity, ρ is the fluid density and ℓ is the pipe width. The Reynolds number relates the basic flow factors and so there will be a critical value R_{CR} beyond which the flow is unstable with respect to infinitesimal disturbances. For Reynolds numbers below R_{CR} , disturbances are damped and the flow remains laminar.

Two types of nozzle were tried in the flow system. The first and least successful was similar to that of Runge and Rosenberg⁴⁵ and consisted of a copper tube of 6 mm internal diameter, flattened and polished at one end to form a slot. A sheet of dye was produced by this method but the flow rate was limited as it became wide at increased pump speeds. It also had the disadvantage that the optical quality of the film of dye was determined by the smoothness of the end of the tube and imperfections at the slot produced surface waves.

Figure 10 shows the second type of nozzle similar to that of Ezeliek et al⁴⁶, and that used throughout this work. The slit was formed by two razor blades cemented (with a spacing of 0.5 mm), to the end of a stainless steel tube of 6 mm internal diameter. The tube was filed such that two pillars were left to act as guides for the dye film after attaching the blades. These were necessary



Jet Nozzle

FIG:10

at high flow-rates to counteract the spreading of the sheet encountered with the first jet. The resulting jet-stream was narrower than the opening as the approach to the slit was from every part of the interior and the change in direction of the streamlines was not completed inside but continued downstream.

In a free flowing system the correct choice of solvent is essential for stable laser operation. Surface waves produced by imperfections will have a higher damping constant for a high viscosity solvent. With ethylene glycol, the dye flowed under normal conditions at a rate of $\sim 1.3 \text{ l. min}^{-1}$ which corresponded to a nozzle speed of $\sim 7 \text{ m.s}^{-1}$ and a pipe speed of $\sim 0.8 \text{ m.s}^{-1}$. For a viscosity of 20 cp at 20°C , this leads to Reynolds numbers of 266 and 170 for the pipe and nozzle flows respectively. As both are below the critical value of ~ 2000 , turbulence is thus avoided enabling the use of the film as a laser medium.

Theoretical treatments of simple jets show that small thickness fluctuations caused by pressure changes in the flow are obtained near the exit of the nozzle for high flow velocities, high viscosity solvents and a thin jet. As the damping of surface waves is a function of time, the flow velocity should be low enough for them to be attenuated close to the slot. Hence, due to both these factors, there exists an optimum velocity for the jet. A quantitative investigation of viscosity and flow velocity has been made by Wellegehausen et al ⁴⁸ using interferometric methods, and by flowing mixtures of ethylene glycol and water to vary the viscosity in the range 20cp - 1cp they observed the thickness fluctuations to increase from $\sim 4\text{nm}$ to $\sim 15\text{nm}$. A pressure change of 1 Torr in the flow was also found to introduce a thickness

variation of $\sim 5\text{nm}$ for a viscosity of 1.3cp . To maintain a steady flow with water, the jet thickness had to be kept below 0.2 mm and velocity about 2m.s^{-1} . Operation with a water jet of thickness greater than 0.5 mm led to only intermittent laser action whereas with a very thin jet, the high dye concentrations required caused increased self-absorption and the low flow rate led to thermal problems.

At first sight, high stability jet-stream dye lasers would not seem feasible due to the optical surfaces of the active medium being defined by the liquid flow. However, the single mode C.W. dye laser of Ezekiel et al ⁴⁶ has a free running jitter of 6 MHz in one second after single frequency operation is achieved by two intracavity prisms, two etalons and a Fox-Smith mode selector.

In the jet-stream used in this work, the tube leading to the slit was chosen to be $\sim 45\text{ cm}$ long so that it could be rigidly clamped to the optical bench and hence any movement of the flexible dye flow pipes would not cause eddies in the dye just before the exit from the jet. After passage through the mirror foci, the dye was collected in a tube at grazing incidence to prevent shock-waves from travelling back up the film creating jitter and also to prevent the formation of bubbles. The diameter of the collection tube was greater than that on the high pressure side to avoid trapping of air pockets which would be carried back into the reservoir.

Following the conversion to an open dye flow, the operating characteristics of the system remained similar to those with the dye cell except for threshold and conversion efficiencies. With the optimum Rhodamine 6G - ethylene glycol concentration of 10^{-3}M , the minimum threshold for the cavity of Figure 6b was 120 mW of 514.5 nm

pumping radiation. The output mirror reflectivity was $> 99\%$ at the wavelength concerned (590 nm), and this compared favourably to that of 200 mW for the dye cell under similar conditions. Similarly, output powers and efficiencies were improved. In Section 2.3, output powers of 150 mW and a slope efficiency of $\sim 8\%$ were obtained at 590 nm for an input of 2.4 W with the dye cell. In the jet-stream laser, power levels increased to 400 mW at a pump power of 2.4 W with a slope efficiency of $\sim 18\%$. The maximum outputs obtained for an output coupling of $\sim 6\%$ at 590 nm have been ~ 800 mW at 6W (514.5 nm) input and ~ 1 W at an all-line pump power of 10 W. At low power levels, slope efficiencies of $\sim 17\%$ were measured for multi-line excitation, comparable to those with the single line, but as a consequence of the increased thermal effects, the efficiency decreased to $\sim 10\%$ when the laser was adjusted for high power pumping. This point is discussed further in the next section.

2.7 Thermal Effects

In their work on triplet quenching in pulsed dye lasers, Snively and Schäfer³¹ observed that even with an oxygen saturated solution, lasing still terminated while the flashlamp intensity was above threshold. This was attributed to the formation of a thermal refractive index gradient in the dye solution misaligning the resonator and for which they were able to compensate by mirror adjustment such that the onset of laser action was delayed relative to the pump pulse. The C.W. dye laser presents considerable thermal problems as the pumping light is focussed to a power density of $\sim 10^7$ W.cm⁻². Due to the radiationless transitions in the dye, the focussed beam produces a local heating and results in an inhomogeneous

temperature rise ΔT which neglecting thermal conductivity is given by ⁴⁹

$$\Delta T \propto \frac{\epsilon W_p \gamma}{\omega_a \rho \xi v} \cdot \left\{ \phi\left(\frac{2x}{\omega_a}\right) + 1 \right\} \cdot e^{-\gamma z} \cdot e^{-2y^2/\omega_a^2}$$

γ is the absorption coefficient of the pump radiation in the dye, while ϵ expresses the percentage of the pump power converted into heat. ρ , ξ and v are the dye density, specific heat and flow velocity respectively. The function ϕ is the Gaussian profile of the temperature increase in the direction of the flow and $e^{-\gamma z}$ represents the exponential decrease in the pump intensity. The Gaussian distribution of the focussed pump beam is given by e^{-2y^2/ω_a^2} where ω_a is the argon-ion beam waist.

In the yz plane in the dye, normal to the flow direction, the temperature change is symmetric while in the xz plane, it is highly asymmetric. The non-uniform thermal distribution and hence refractive index, causes a number of effects with both dye cells and jet-streams. In the boundary regions where the flow is low the temperature rise for pump powers above ~ 5 W might be sufficiently high to cause permanent damage in a dye cell. This limitation is further enhanced by the presence of any small impurities which can be burnt onto the windows at the hot spot. This occurred with a water solution of Sodium Fluorescein containing cyclooctatetraene as triplet quencher, (Section 2.11). Pump power levels had to be less than 2W as otherwise the cell windows were rapidly degraded.

The thermal lens resulting from the non-uniform refractive index can alter the stability of the cavity and hence lower the efficiency and output power, and deform the beam profile. The

change in refractive index, $|\Delta n|$ for a particular pump power W_p is given by⁴⁸

$$|\Delta n|_{\max} \propto \frac{\epsilon \gamma W_p}{\omega_a \rho \xi v_{\max}} \cdot \left| \frac{dn}{dT} \right|$$

where $\frac{dn}{dT}$ is the thermal coefficient of the refractive index. For various solvents under the same pumping conditions, $\left| \frac{dn}{dT} \right| \{\rho \xi v_{\max}\}^{-1}$ can be taken as a figure of merit. Among the common solvents, water is best due to its low $\left| \frac{dn}{dT} \right|$ and larger values for ρ and ξ , which made it the choice for use in the enclosed dye cell. The other common solvents like methanol and ethanol were found to cause blooming of the cell windows which was at times permanent. Water was also convenient for use in the cell in that high flow rates of $\sim 30 \text{ m.s}^{-1}$ could be attained.

Although the threat of damage was now absent, thermal effects in the jet were responsible for the fall-off in output power and changes in the transverse mode structure with increasing pump power. Compared to water with a refractive index coefficient of $\sim 0.00014 \text{ T}^{-1}$ at 20°C , ethylene glycol has a value of $\sim 0.001 \text{ T}^{-1}$ such that the parameter $\frac{dn}{dT} \cdot \{\rho \xi v_{\max}\}^{-1}$ for water flowing at 30 m.s^{-1} and ethylene glycol at 10 m.s^{-1} is $\sim 4 \times 10^{-8}$ and $\sim 4 \times 10^{-7}$ respectively. Consequently, thermal problems are more severe in the higher viscosity solvent due to the lower flow rates required for stable laser action.

The effect of all-line pumping on output power is shown in Figure 11 in which the thermal distortions are maximized due to the large Stokes losses produced by those below 514.5 nm . For curve(a)

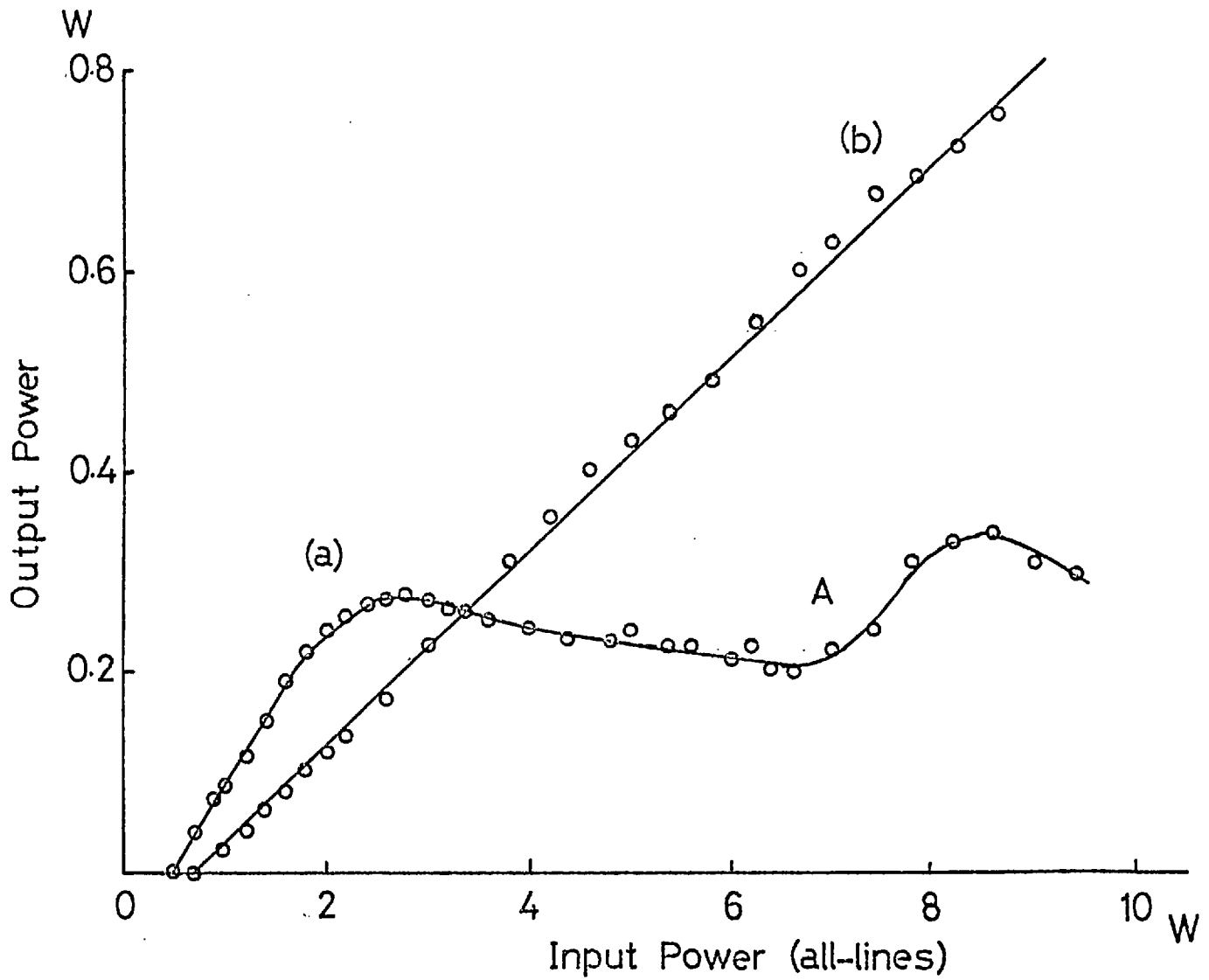


FIG:11

the laser was aligned to give lowest threshold (tightest focus) resulting at 2.5W in the cavity becoming unstable. Just below this critical power level, higher order modes started to appear as the inner parts of the dye laser beam were affected first. At the point A where the power increased again, the cavity was stable for a different transverse mode structure which also became unstable. By slightly adjusting the focussing mirror to reduce the power density, a linear dependence of output on pump power was obtained (curve (b)) although with increased threshold. In addition, a decrease in the slope efficiency from 17% to 10% when compared to the lower portion of curve (a) can be observed. Thus by careful operation and cavity design, ethylene glycol should be suitable for pump powers of up to ~ 20 W but should higher power pump sources (~ 100 W) become available, it might be necessary to reconsider water as the solvent.

An interesting variation of this thermal effect occurred when Cresyl Violet Perchlorate was being investigated. Due to its low absorption at the argon-ion wavelength of 514.5 nm, C.W. laser action requires it to be mixed with Rhodamine 6G⁵⁰ whose fluorescence peak overlaps the Cresyl Violet absorption such that Cresyl Violet is pumped by excitation transfer between the dye molecules. With high reflectivity cavity mirrors, thresholds of ~ 700 mW were obtained, and the laser was tunable over the range 644-692 nm. However, above ~ 3 W input, thermal effects became severe due to the combined Stokes shifts of both dyes. Beisser and Eilenberger⁵¹ have compared the Cresyl Violet-Rhodamine 6G C.W. dye laser with a system in which the output of a Rhodamine 6G laser directly pumps a

Cresyl Violet solution. In the tandem configuration they found a linear increase in gain up to an argon-ion input power of 10W, which they attributed to the distribution of the heating between the two dye streams.

2.8 C.W. Dye Laser Stability

The successful operation of a continuous dye laser as implied by the name, depends on the isolation of any external influences which would otherwise affect the laser characteristics. Its use as a scientific tool requires that there are no uncontrollable amplitude and frequency fluctuations. In this section, the mechanical factors involved in the stability of the dye laser cavity are considered, whereas those involving the dye flow and solvent have been discussed in Sections 2.6 and 2.7 respectively.

The combined system of argon-ion and C.W. dye lasers was attached to a steel surface table ensuring that the relative positions of the components did not change. Earlier work on wooden tables suffered from bending of the table top depending on the location of ancillary equipment resulting in misalignment of the laser cavity. Isolation of the entire experiment from building vibrations was possible by supporting the system on air. Due to the water cooling requirements of the argon-ion laser, pumping was necessary to provide the pressure and high flow rate needed, so to prevent coolant vibrations from affecting the dye laser, the two cavities were mounted on separate optical benches on the surface table.

The individual components of the dye laser were attached to standard kinematic mounts which, in the case of the concave mirrors, also had y - z micrometer controlled translation stages.

The macroscopic stability was such that the laser normally remained in alignment from day to day.

Instabilities due to velocity and pressure fluctuations in the jet could be traced back to pulsations caused by the gear pump. This becomes more extreme when the pump wears or if the gears are not perfectly balanced. The resulting vibrations in the jet could be seen as an amplitude modulation in the dye laser output as shown in Plate 2a. The ripple at 66 Hz could be alleviated (Plate 2b) by the inclusion of a surge reservoir before the jet reducing the noise to $\sim \pm 3\%$ and which also acted as a trap for bubbles.

In the dye cell cavity, the outer surfaces of the active medium were already defined by the windows so provided large scale vibrations in the flow did not occur, the effect of turbulence would only have been important in single frequency operation. Non-stationary heating of the solution arising from highly turbulent flow has been observed⁵² to cause a thermal detuning which fluctuates with time. The measured frequency jitter (ref.52) of 80 MHz was reduced to less than 0.8 MHz by using a cell designed to give laminar flow and short term temperature changes of $\sim 0.01^\circ\text{C}$. In the mode-locked laser however with bandwidths of $\sim 10^{12}$ Hz spectral perturbations of this magnitude are negligible.

At high power levels, the argon-ion output contained amplitude spikes at a frequency of 100 Hz as illustrated in Plate 3 along with the corresponding dye laser output. Reducing the laser current to below 40 amps (4W) removed this source of noise (Plate 3c) with the Spectra-Physics Model 170 laser, but with the smaller Model 164, threshold requirements demanded maximum power operation.

PLATE 2

AMPLITUDE STABILITY OF THE JET-STREAM

C.W. DYE LASER

(a) Without surge reservoir

TIMESCALE: 10ms/div

(b) With surge reservoir

TIMESCALE: 10ms/div

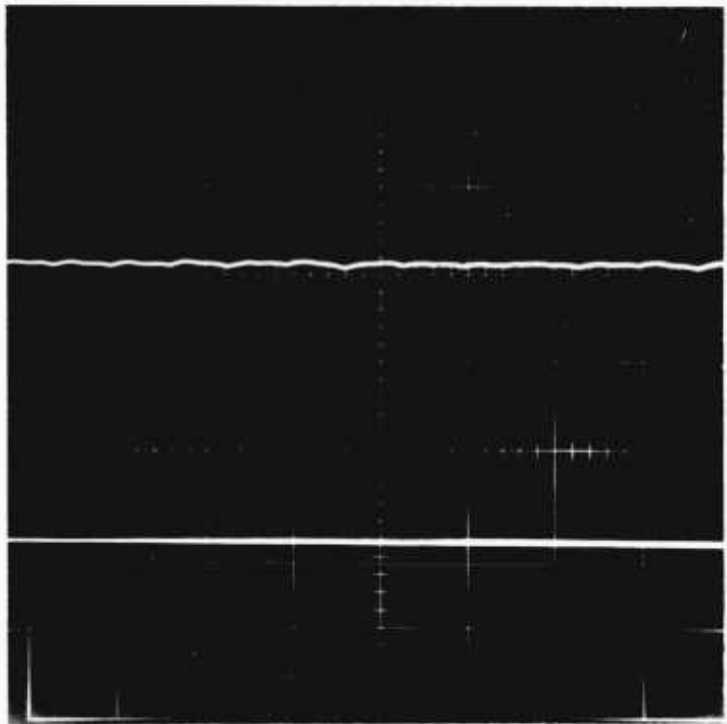
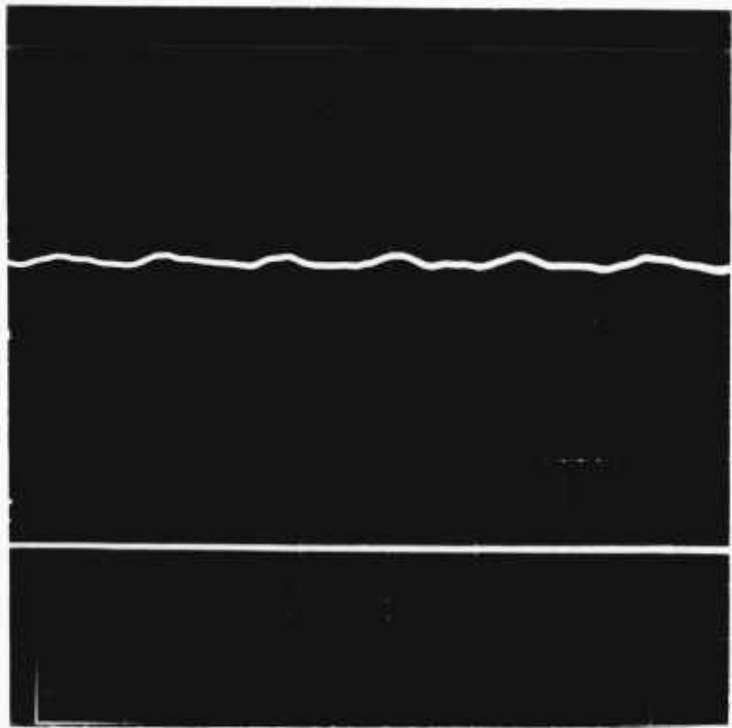


PLATE 3

AMPLITUDE FLUCTUATIONS ARISING IN THE
PUMPING SOURCE

(a) Output of argon-ion laser - current 45 Amps.

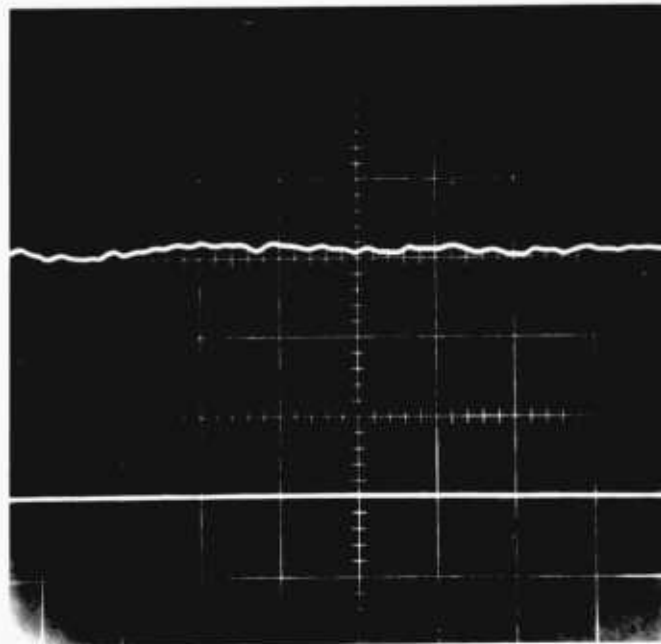
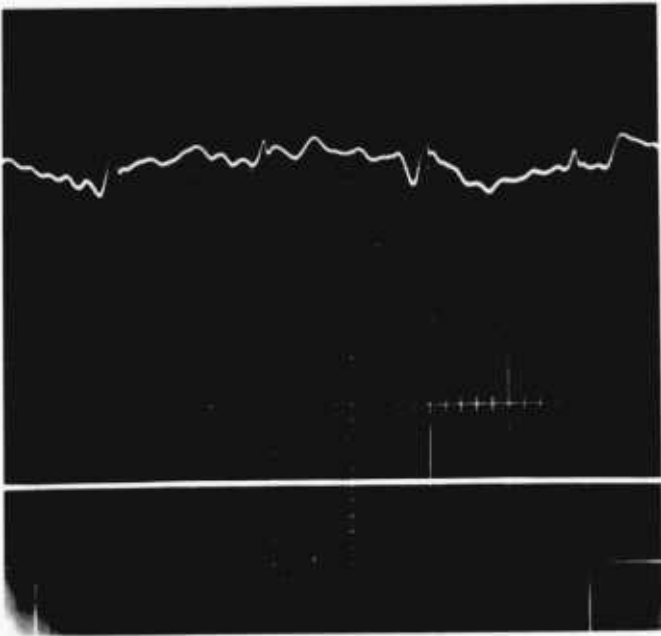
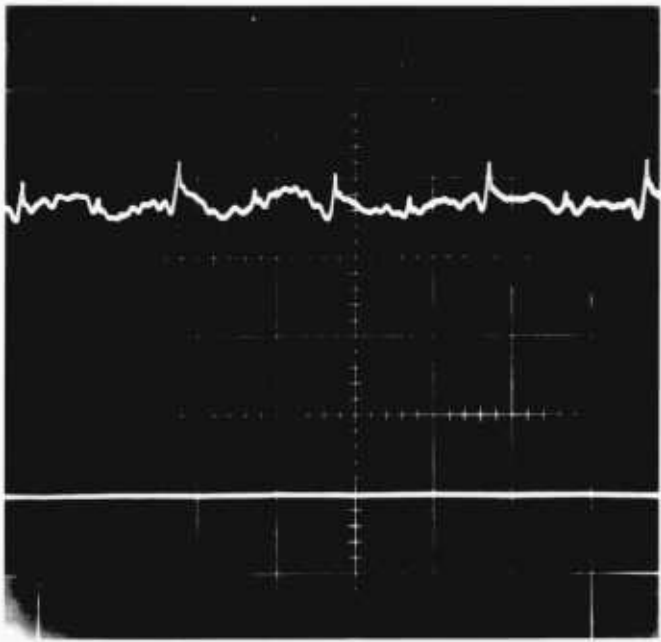
TIMESCALE: 5ms/div.

(b) Output of C.W. dye laser (argon-ion current 45 Amps)

TIMESCALE: 2ms/div.

(c) Output of C.W. dye laser (argon-ion current < 40 Amps)

TIMESCALE: 2ms/div.



The cavity alignment itself also influenced the stability as the transverse mode structure depended on it. Normally the system lased in the TEM_{00} mode without the inclusion of apertures and the resulting stability was at its highest. For higher orders, mode competition led to oscillation between different patterns and introduced rapid amplitude and spectral variations.

2.9 Tuning of the C.W. Dye Laser

To exploit the available bandwidth of the lasing dyes several tuning methods are used both for varying the laser wavelength over broad spectral ranges and also for reducing the linewidth to that of a single longitudinal mode. The four most common techniques for C.W. and pulsed dye lasers are the prism⁵³, the diffraction grating^{54,55}, the Fabry-Perot etalon⁵⁶ and the birefringent filter⁵⁷. For single frequency applications of the C.W. dye laser, it is usual to employ a combination of a prism or birefringent filter and Fabry-Perot etalons⁴⁶. Although the internal power in a C.W. dye laser cavity is relatively low, the attractiveness of using uncoated tuning elements has increased the use of the birefringent filter and it will doubtless be chosen more often especially for high power pulsed systems where the preferred state of polarization can be achieved quite rapidly by the inclusion of extra non-dispersive plates at Brewster's angle.

In this work, a Brewster's angle prism was used for tuning as it facilitated the coupling into the cavity of the pump beam. The prism in most of the mode-locking investigations was of fused quartz, and 2 cms aperture with faces polished to $\lambda/4$ and cut for

Brewster's angle at 600 nm when in minimum deviation. Alignment of the prism in the optical plane of the cavity resulted in negligible losses from the surfaces and along with the jet, maintained the polarization at >99%. Rotation of the prism about an axis passing through its apex swept the dispersed dye fluorescence across the end resonator mirror hence selecting the desired portion of the spectrum in which the laser operated. With the extension to mode-locking in mind, the material was chosen to have a low dispersion, $\frac{dn}{d\lambda}$, which for fused quartz is $\sim 3.5 \times 10^{-5} \text{ nm}^{-1}$ at 600 nm.

To determine the maximum bandwidth which could oscillate in a laser tuned by this prism from geometrical considerations only, an estimate was made of the misalignment tolerance $\Delta\theta$ which was the angle through which the end mirror could be tilted before the output power dropped by a factor of 2. For the untuned laser of Figure 12 in which the argon-ion beam was coupled via a dichloric mirror M_1 , a value of $\Delta\theta \sim 4 \times 10^{-4}$ radians for mirror M_2 was obtained. The jet-output mirror distance was equal to the jet-prism-output mirror distance in the normal tuned cavity. The spectral interval $\Delta\lambda$ for which feed-back is possible is given by¹⁴

$$\Delta\lambda = \frac{d\lambda}{d\theta} \cdot \Delta\theta \quad (2.4)$$

where $\frac{d\lambda}{d\theta}$ is the angular dispersion of the prism. Knowledge of the dispersion of the glass enables (2.4) to be written as

$$\begin{aligned} \Delta\lambda &= \frac{dn}{d\lambda}^{-1} \cdot \frac{dn}{d\theta} \cdot \Delta\theta \\ &= \frac{dn}{d\lambda}^{-1} \cdot \frac{a}{t} \cdot \Delta\theta \end{aligned} \quad (2.5)$$

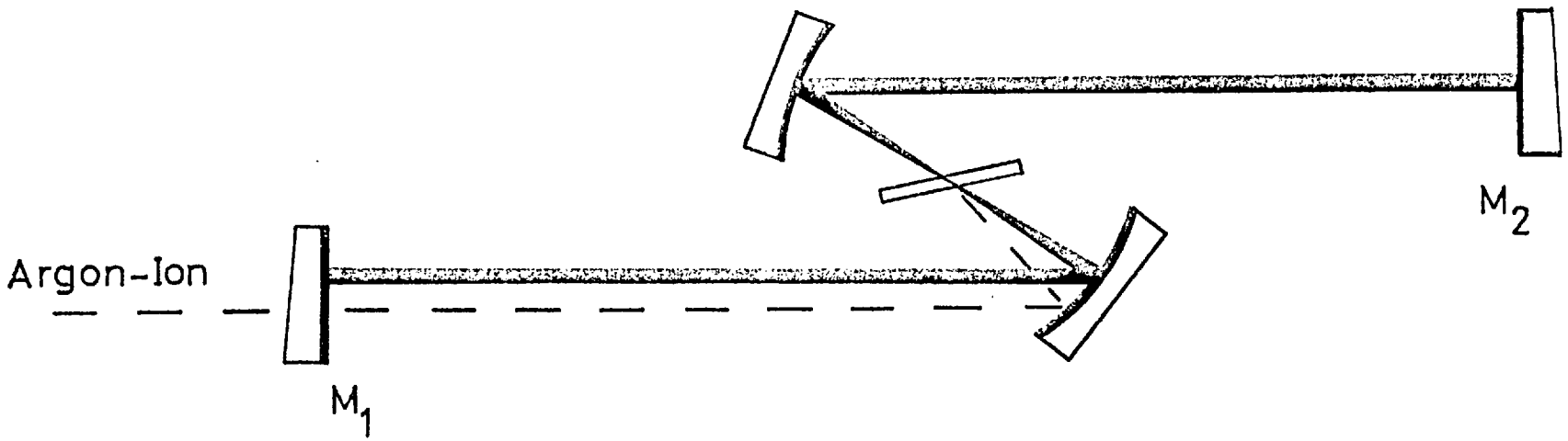


FIG:12

where a is the beam width and t is the path difference through the prism. Substitution of the relevant parameters into (2.5) gives $\Delta\lambda \sim 11$ nm representing the passive band-pass of the prism. Mode-locked operation with a more highly dispersive prism (Pilkington-Chance Double Extra Dense Flint), for which $\Delta\lambda \sim 4.5$ nm was estimated, resulted in longer pulse durations and is discussed in Chapter 4.

An interesting phenomenon observable with the untuned laser cavity was an etalon effect arising in the jet-stream. The channeled spectrum of the untuned laser is shown in Plate 4 recorded on a Monospek 1000, 1m spectrograph with a grating of 1200 lines. mm^{-1} blazed at 300 nm and operated in second order to give a dispersion of $0.4 \text{ nm} \cdot \text{mm}^{-1}$ on the plate. From the theory of a Fabry-Perot etalon, the free-spectral range is given by⁵⁸

$$\Delta\lambda_{\text{FSR}} = \frac{\lambda^2}{2nd} \quad (2.6)$$


where d is the separation of the reflecting surfaces and n is the refractive index of the enclosed medium. From the periodicity of the spectrum, $\Delta\lambda_{\text{FSR}}$ was ~ 0.2 nm and from (2.6) for ethylene glycol of refractive index 1.43 at a wavelength of 590 nm the corresponding thickness was ~ 0.7 mm, equal to that estimated for the jet-stream at Brewster's angle. The channeling could be avoided in the dye cell by wedging but even with a non-parallel jet slit, the effect remained due to the negligible wedge over the focal region in the dye. The etalon effect was useful as it enabled accurate values for the dye film thickness to be calculated without resorting to absorption measurements.

PLATE 4

SPECTRUM OF THE UN-TUNED JET-STREAM

C.W. DYE LASER

10mm

A horizontal dimension line with arrows at both ends, indicating a width of 10mm.

λ

A horizontal arrow pointing to the right, labeled with the Greek letter lambda (λ), representing the wavelength of the light.

The inclusion of the prism in the cavity narrowed the laser spectrum to ~ 0.1 nm from ~ 3.0 nm and hence only one of the components was selected. Due to gain effects, the actual laser bandwidth is usually 50-100 times smaller than the passive band-pass of the tuning element estimated earlier. The spectral profile of the laser with the fused quartz prism at 50% above threshold is shown in Plate 5a recorded using a scanning Fabry-Perot (Spectra-Physics Model 410) driven from the 90 V sawtooth of the time-base of an oscilloscope. The free spectral range was 1.5nm and the instrument profile was 0.05nm indicating a laser linewidth of 0.13nm. The narrower spectrum ($\Delta\lambda = 0.06$ nm) with the high dispersive prism is shown in Plate 5b. Spectral stability was normally $\sim \pm 0.05$ nm on a millisecond timescale.

2.10 Loss Analysis of the Rhodamine 6G C.W. Dye Laser

An estimate of the cavity internal losses consisting of those due to reabsorption in the dye solution (γ_s) and the intrinsic losses of the resonator (γ_i) is necessary for comparison of the mode-locking rate equation theory with the experimental behaviour of the system. Also the cavity loss, γ_i , is a useful figure of merit for comparing different configurations e.g. dye cell and jet-stream.

The method used for determining $\gamma_s + \gamma_i$ was to measure the variation of threshold power W_{pT} with output mirror coupling γ_o . This was performed for the cavity of Figure 6b by using a range of mirrors of transmission at 590 nm in the range 0.1 - 12.5%. A similar technique for a C.W. dye laser was first used by Jacobs et al ³⁷ and more recently by Marowsky and Polloni ³⁸. The latter authors employed frustrated total internal reflection to provide a continuously adjustable output coupler.

PLATE 5a

SPECTRUM OF C.W. DYE LASER (FUSED SILICA PRISM)

CALIBRATION: 0.3 nm per major division

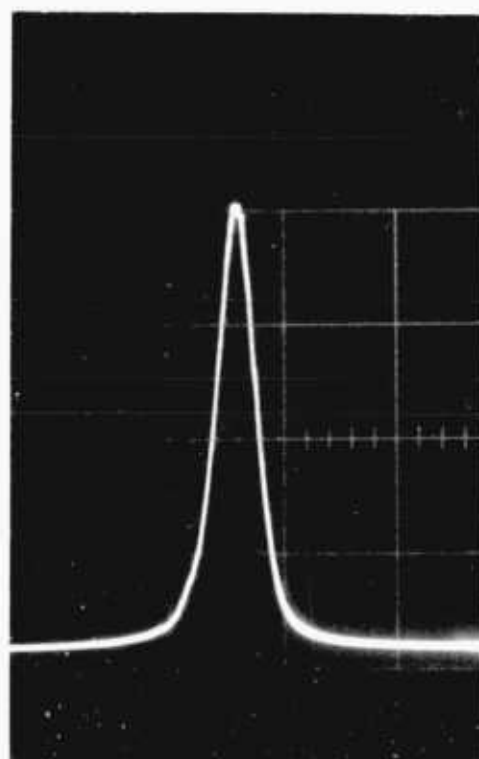


PLATE 5b

SPECTRUM OF C.W. DYE LASER (DEDF PRISM)

CALIBRATION: 0.3 nm per major division

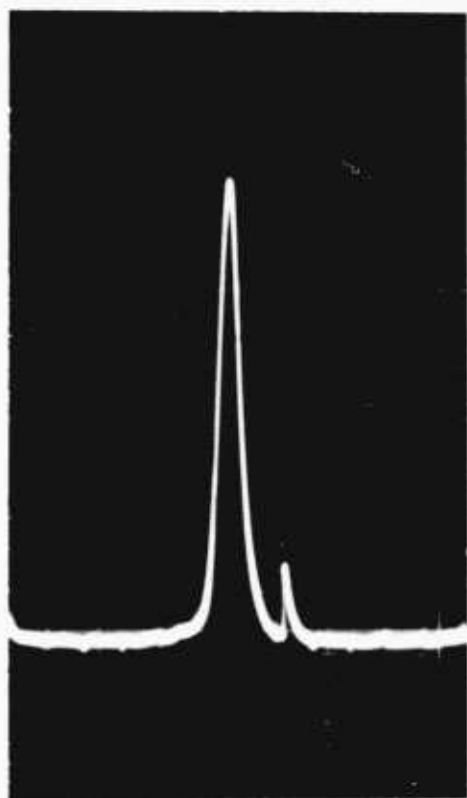
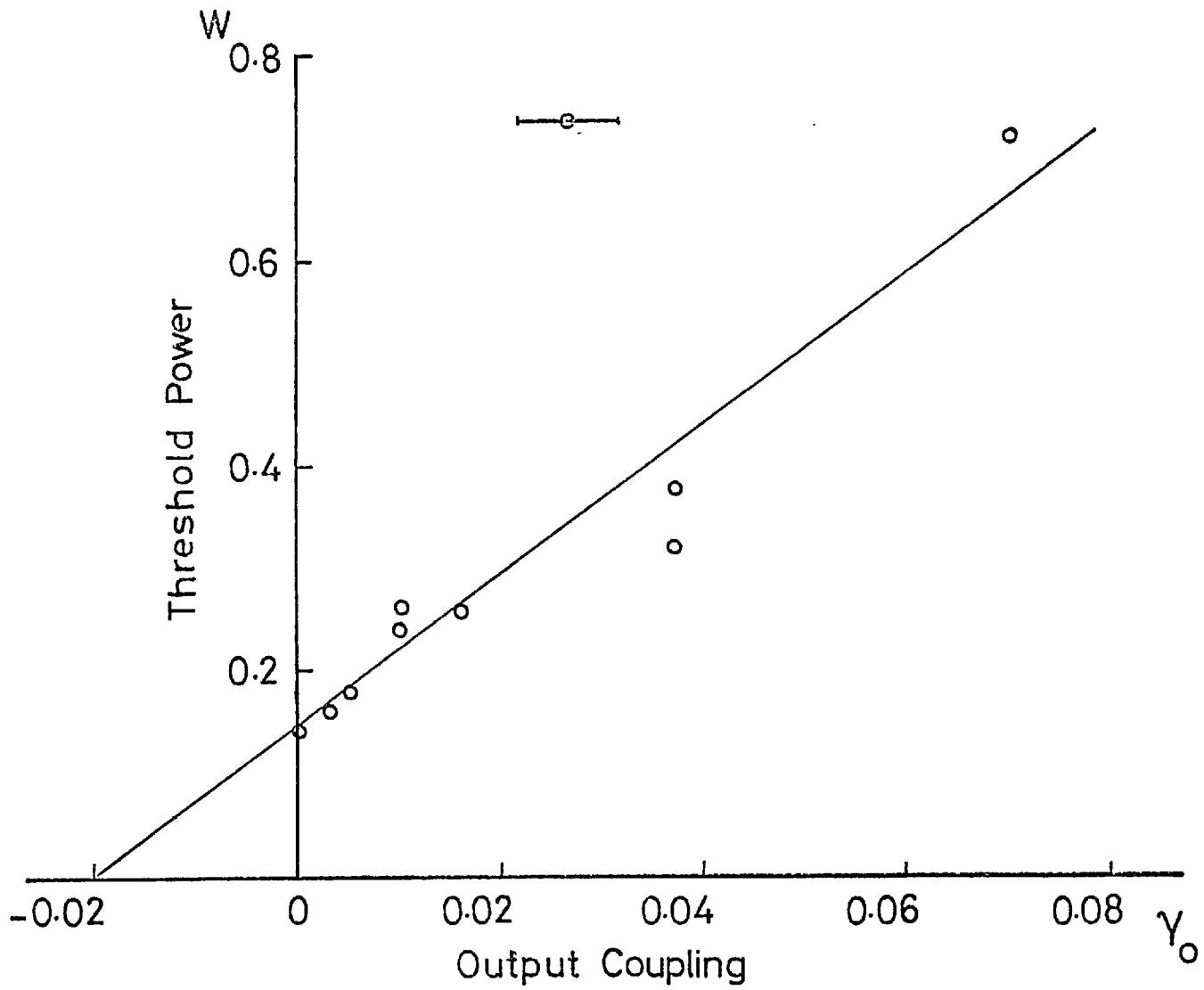


Figure 13 shows a typical set of results of threshold power W_{P_T} versus γ_0 . Between successive experimental points care was taken to ensure that the cavity alignment and tuning remained constant each time the mirror was changed. The total loss, $\gamma_i + \gamma_s$ was obtained by extrapolation onto the γ_0 axis and in this example a value of $\sim 2\%$ was deduced. For the dye at a concentration of 6.7×10^{-4} M, in a jet of path-length 0.4 mm, the reabsorption γ_s was, at 590 nm, $\sim 0.5\%$. Hence the basic tuned cavity loss was $\sim 1.5\%$ and the additional losses associated with the introduction of the mode-locking elements could be determined from the increase in the threshold.

By a similar method, the cavity small signal gain may be obtained which can serve as a means of comparing dye solutions and solvents under identical experimental conditions. This would require the dependence of the output power P_0 on γ_0 to be recorded, but as a complete range of mirrors was not available, only the initial portion of the curve was plotted (Figure 14) for input powers of 500 mW and 2 W. The pumping rate from the ground state to the first excited state is proportional to the input pumping power provided the pumped area remains constant. To satisfy this condition, the largest γ_0 used (0.13) resulted in a threshold power of 1 W at 514.5 nm at which level thermal effects were negligible. For the entire series of observations, the laser alignment was such that a linear increase in output power with input was obtained up to 3 W, which was above the level normally required for mode-locking.

FIG:13



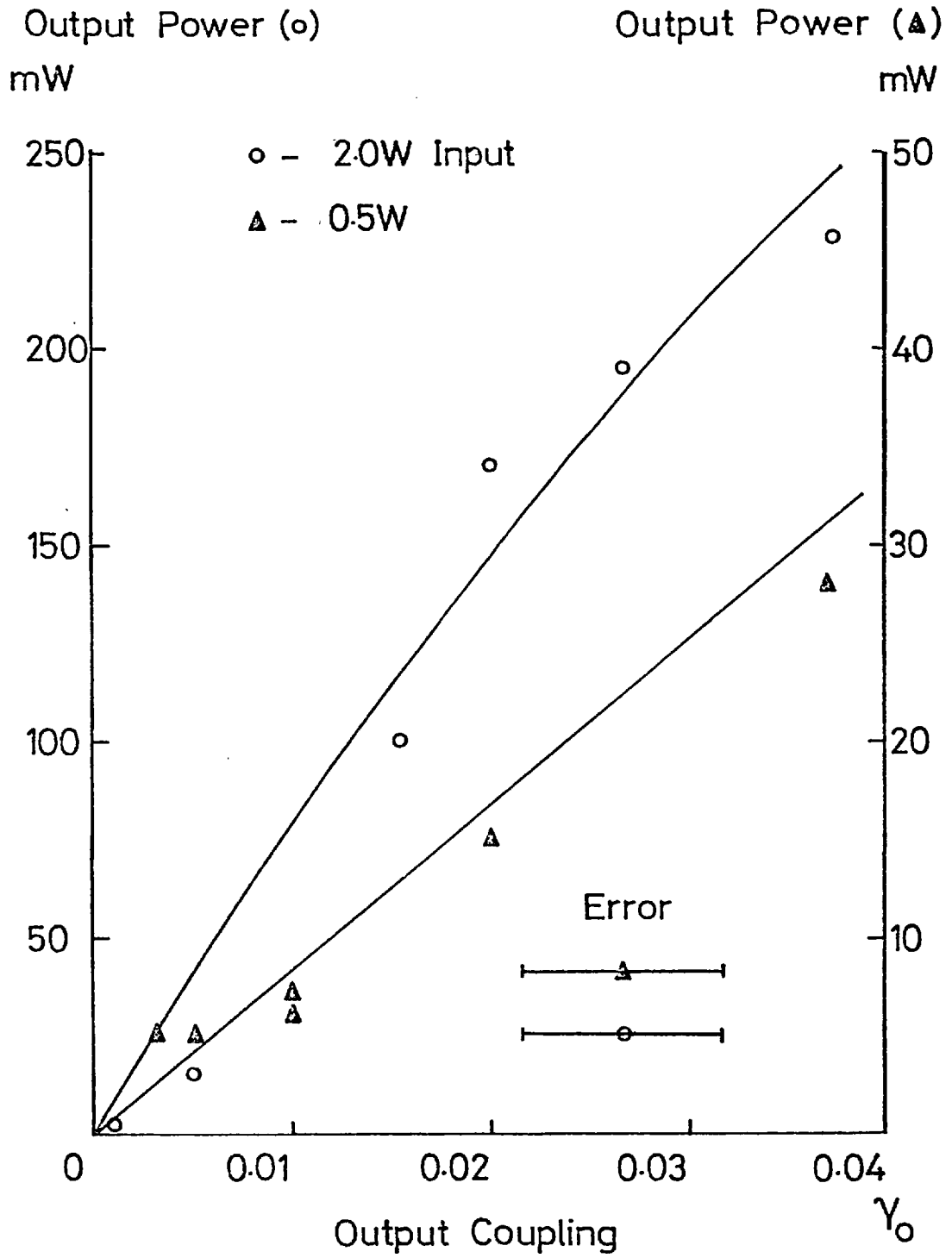


FIG:14

In Chapter 1, the relationship between output power and output coupling was derived, given by

$$P_o = hvS \cdot \frac{\gamma_i + \gamma_s}{\tau \sigma_e} \cdot \frac{\gamma_o}{\gamma_i + \gamma_o + \frac{a}{1+a} \cdot \gamma_s} \cdot \left\{ \theta - \frac{\gamma_o}{\gamma_i + \gamma_s} - 1 \right\} \quad (1.9)$$

where S is the average mode area in the active region, θ is the ratio of the pumping level to the threshold level when $\gamma_o = 0$ and $\frac{a}{1+a}$ is a triplet loss factor. Fitting equation (1.9) to the experimental points of Figure 14 enables a value for σ_e to be estimated by making only macroscopic measurements on the laser as terms in $\sigma_e \gamma_i$ and $\sigma_e \cdot a \gamma_s / (1+a)$

may be eliminated using simultaneous equations. For a laser spot size of $\sim 20 \mu\text{m}$ diameter in the jet, estimated from the laser beam divergence, the calculated value for σ_e at 590 nm was $\sim 1.3 \times 10^{-16} \text{ cm}^{-2}$ in good agreement with that of $0.8 \times 10^{-16} \text{ cm}^{-2}$ obtained by spectrophotofluorimeter methods as uniform pumping was assumed in the analysis.

2.11 The C.W. Rhodamine B Laser.

To eventually extend the mode-locking range to longer wavelengths, Rhodamine B was investigated as an active medium. Using the dye cell in the cavity of Figure 6b, all-line pumping with the Spectra-Physics Model 164 laser gave a maximum input power of 3w. This was necessary due to the lower efficiency of Rhodamine B and the simultaneous decrease in the power available at 514.5 nm from the pump laser in use at that time.

The characteristics of the Rhodamine B laser were similar to those of Rhodamine 6G described previously. For the optimum concentration ($8 \times 10^{-4} \text{ M}$, water + 10% Ammonyx LO), typical tuning

behaviour was as shown in Figure 15 at a pumping level of 3W all-lines. The mirror transmission was 3% at 620 nm with a resulting threshold of ~ 1 W.

In one respect the operation of Rhodamine B differed significantly from Rhodamine 6G in that the threshold depended strongly on the solution's temperature. Without cooling, the temperature of the circulating dye solutions normally rose to $\sim 35^{\circ}\text{C}$, but for Rhodamine B, the necessary threshold powers increased by $\sim 30\%$ from those required when the dye was placed in a bath maintaining its temperature at $\sim 5^{\circ}\text{C}$. This phenomenon can be shown to be due to variation of the populations of the molecular vibrational levels. A decrease in the solution temperature leads to a lower population of the upper vibrational levels of the singlet ground state manifold S_0 as it is in thermal equilibrium with the solvent. The subsequent enhancement in the transition probability from the bottom of the S_1 state to the higher vibrational levels of S_0 is manifest either as a thermal tuning of the laser⁵⁹ or in the prism tuned cavity used in this work, an improvement in laser efficiency.⁶⁰ Although a reduction in temperature has been shown to lead to increased dimerization in aqueous solutions of Xanthene dyes, this is unlikely to have occurred due to the amount of deaggregating agent present.

2.12 The C.W. Sodium Fluorescein Laser

The fluorescence spectrum of Sodium Fluorescein is shown in Figure 36 (Page 157) and from this the lasing region is expected to be at shorter wavelengths than the Rhodamine 6G tuning

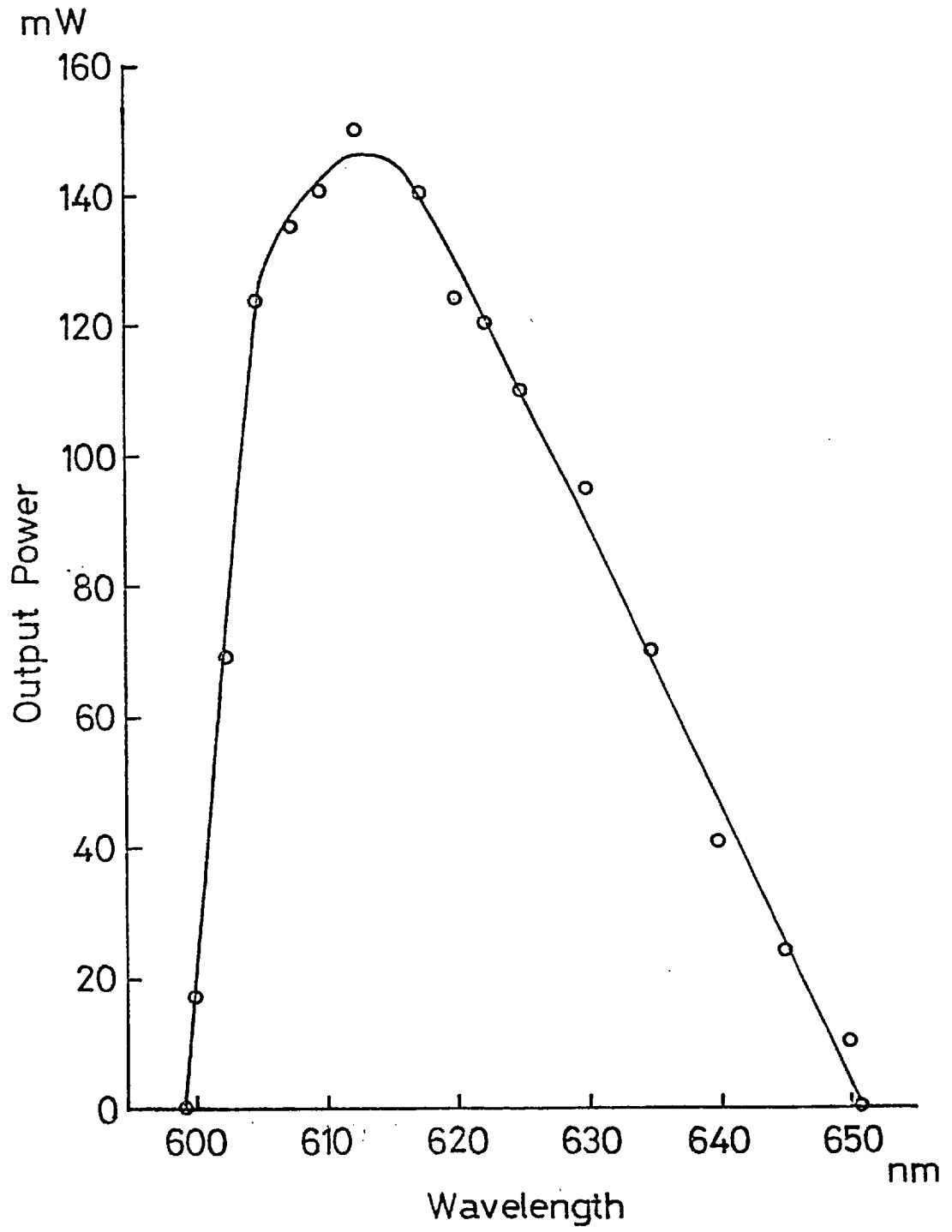


FIG:15

limit giving a new C.W. mode-locking region. Also the dye is conveniently placed for pumping by the 488 nm and 514.5 nm lines of the argon-ion laser.

In a study of the selectivity of various triplet state quenching agents (TSQA), Marling et al^{31,61} showed for a Sodium Fluorescein flashlamp pumped laser, that the output power dropped by $\sim 20\%$ in the presence of one atmosphere of oxygen. In addition to acting as a successful triplet quencher in some dyes, (Rhodamine 6G), oxygen can also quench the excited singlet state by enhancing transitions between it and the triplet state thus decreasing the quantum efficiency and increasing the triplet absorption loss. As both processes are probably operative in dyes, the predominating one determines whether oxygen helps or hinders laser action, and for some dyes an optimum concentration is observable³¹.

With the dye cell system of Figure 6b, lasing was possible for a 6×10^{-4} M/water + 10% Ammonyx LO solution at a threshold of ~ 1.5 W all-lines. However, within minutes the threshold rose to the pumping limit (3W) and the dye eventually lost its bright fluorescing colour. The addition of $\sim 0.2\%$ cyclooctatetraene (COT) reduced the threshold to $\sim 50\%$ of that for a fresh solution but limited the input power to ~ 2 W due to the burning of COT particles onto the cell windows⁴⁴. For an output mirror of transmission $\sim 5\%$ at 550 nm, a maximum tuning range of 530 - 580 nm was obtained and output powers of ~ 220 mW for a pump level of 2.0 W were measured giving an overall conversion efficiency of $\sim 10\%$ comparable to the Rhodamine 6G dye cell cavity.

With Sodium Fluorescein there was an extra source of instability due to lasing taking place past the apex of the prism onto the front mirror of the argon-ion laser. This caused the dye laser beam to oscillate between the two cavities as well as producing a background signal. By introducing a glass plate at the output of the argon-ion laser sufficient loss was provided to prevent feedback along the pumping axis.

2.13 Conclusion

The dye cell and jet-stream C.W. Rhodamine 6G dye lasers have been compared and it was shown that with the latter system high stability operation was possible with increased efficiency (8% → 18%). The thermal problems involved in the choice of dye solvent were discussed and although ethylene glycol has a greater thermal refractive index gradient than water, careful focussing of the pump beam enabled high power levels to be used (10 W). In addition to Rhodamine 6G, the basic parameters of Rhodamine B and Sodium Fluorescein C.W. dye lasers were measured as a prerequisite for the extension of mode-locking to longer and shorter wavelengths respectively than the Rhodamine 6G tuning range.

CHAPTER 3

MEASUREMENT OF ULTRASHORT PULSE DURATIONS

3.1 Introduction

The generation of ultrashort pulses from mode-locked lasers initiated the development of new methods for studying such short durations. The mode-locked pulse train may be displayed directly using a photo-diode and oscilloscope combination. The repetitive signal from the mode-locked C.W. dye laser, in this work, was detected by a Spectra-Physics Model 403 avalanche silicon photo-diode and a sampling oscilloscope (Tektronix 561B and S4 Sampling Head) with a risetime of 25ps giving an overall resolution of ~ 100 ps. This was sufficient for qualitative diagnosis of the mode-locking, however for the picosecond and subpicosecond regions, additional techniques were required.

Those most commonly used may be classified either as linear, the electron-optical streak camera⁶² or non-linear comprising the second order correlation measurements of two-photon fluorescence⁶³ second harmonic generation⁶⁴ and the optical Kerr effect⁶⁵. A linear method gives information concerning the pulse shape whereas the second order correlation functions only provide unique information regarding the pulse duration. Three photon fluorescence⁶⁶ and third harmonic⁶⁷ measurements have also been made, and although they are not in widespread use, they can along with the second order correlation methods define the pulse intensity profile. Of the above techniques, the streak camera and the second harmonic autocorrelation methods

have been used^{42,68} to measure pulse durations from mode-locked C.W. dye lasers as they are the most convenient and sensitive in practice.

3.2 Fourier Spectroscopy

If the mode-locked laser modes, within the oscillating bandwidth, are known to be locked in phase the pulse duration could be determined by measuring the power spectrum of the laser output. This could be obtained using a conventional spectrometer or with Fourier spectroscopy in a Michelson interferometer.

In the latter method, the quantity measured is $\gamma^{(r)}(\tau)$, which is the real part of the amplitude autocorrelation quantity given by⁶⁹

$$\gamma^{(r)}(\tau) = \frac{2\langle V^{(r)}(t + \tau)V^{(r)}(t) \rangle}{\langle V(t)V^*(t) \rangle} \quad (3.1)$$

where τ is the time delay introduced in one arm of the interferometer between the two beams produced at the beamsplitter. The signal electric field is represented by $V^{(r)}(t)$ and is related to the amplitude frequency spectrum $\tilde{V}(\nu)$ by

$$V^{(r)}(t) = \int_{-\infty}^{\infty} \tilde{V}(\nu) e^{2\pi i \nu t} d\nu$$

As $V^{(r)}(t)$ is the real field, $\tilde{V}(-\nu) = \tilde{V}^*(\nu)$ where the asterisk denotes the complex conjugate.

The amplitude energy spectrum is given by $|\tilde{V}(\nu)|$ and hence the power spectrum may be defined as

$$W(\nu) = \lim_{T \rightarrow \infty} \frac{1}{2T} \left| \int_{-T}^T V^{(r)}(t) e^{-2\pi i \nu t} dt \right|^2 \equiv \langle |\tilde{V}(\nu)|^2 \rangle$$

where the angular brackets represent a time average.

A normalized form of $W(\nu) = \phi^2(\nu)$ can be defined by

$$\int_{-\infty}^{\infty} \phi(\nu) d\nu = 1$$

From the normalized complex amplitude autocorrelation function

$$\gamma(\tau) = \frac{\langle V(t + \tau) V^*(t) \rangle}{\langle V(t) V^*(t) \rangle} = \frac{1}{I} \int_{-\infty}^{\infty} V(t + \tau) V^*(t) dt \quad (3.2)$$

it can be shown that⁶⁹

$$\gamma(\tau) = \int_{-\infty}^{\infty} \phi(\nu) e^{2\pi i \nu \tau} d\nu$$

such that $\gamma(\tau)$ and $\phi(\nu)$ are a Fourier pair and hence each contain the same information.

The function measured in a Michelson interferometer, $|\gamma^{(r)}(\tau)|^2$, is given by the real part of (3.2) and the resulting fringe visibility by

$$|\gamma(\tau)|^2 = \frac{I_{\max} - I_{\min}}{I_{\max} + I_{\min}}$$

If the coherence time of the signal, $\Delta\tau_c$, is defined by⁶⁹

$$\Delta\tau_c = \int_{-\infty}^{\infty} |\gamma(\tau)|^2 d\tau$$

and the spectral width $\Delta\nu$ by

$$\Delta\nu = \left\{ \int_0^{\infty} \phi^2(\nu) d\nu \right\}^{-1}$$

then by Parseval's theorem

$$\Delta\tau_c \Delta\nu = 1$$

Hence a measurement of the spectral bandwidth with e.g. a Michelson interferometer yields only the coherence time and no information about the pulse duration. However, the use of the Michelson as an instrument to determine pulse lengths has been suggested⁷⁰ but as fringes are only observable for delay times less than $\Delta\tau_c$ this only represents a lower limit for the pulse durations except in the case of ideal mode-locking.

As an alternative to observing the amplitude autocorrelation of the laser pulses as described above, a method in which the coherence requirements are eliminated would give the pulse duration. This is provided by the second order intensity autocorrelation involving second harmonic generation of the output of the Michelson interferometer and is the method used for most of this work.

3.3 Second Harmonic Autocorrelation

Measurement of the second harmonic autocorrelation function was first proposed by Weber⁶⁴ to study the pulses from a mode-locked Nd: glass laser. The method used was to polarize orthogonally the beams in each arm of the interferometer which were then propagated as the ordinary and extraordinary rays in a Potassium Dihydrogen Sulphide crystal. The crystal's orientation was chosen such that the second harmonic was generated only by the superposition of the pulses. The pulse duration was then determined from the dependence of the second harmonic intensity on the relative delay between them.

Previously, the enhancement of second harmonic generation (SHG) during mode-locking was used by Di Domenico et al⁷¹ to estimate the duration of pulses from a mode-locked Nd: Yag laser, however the

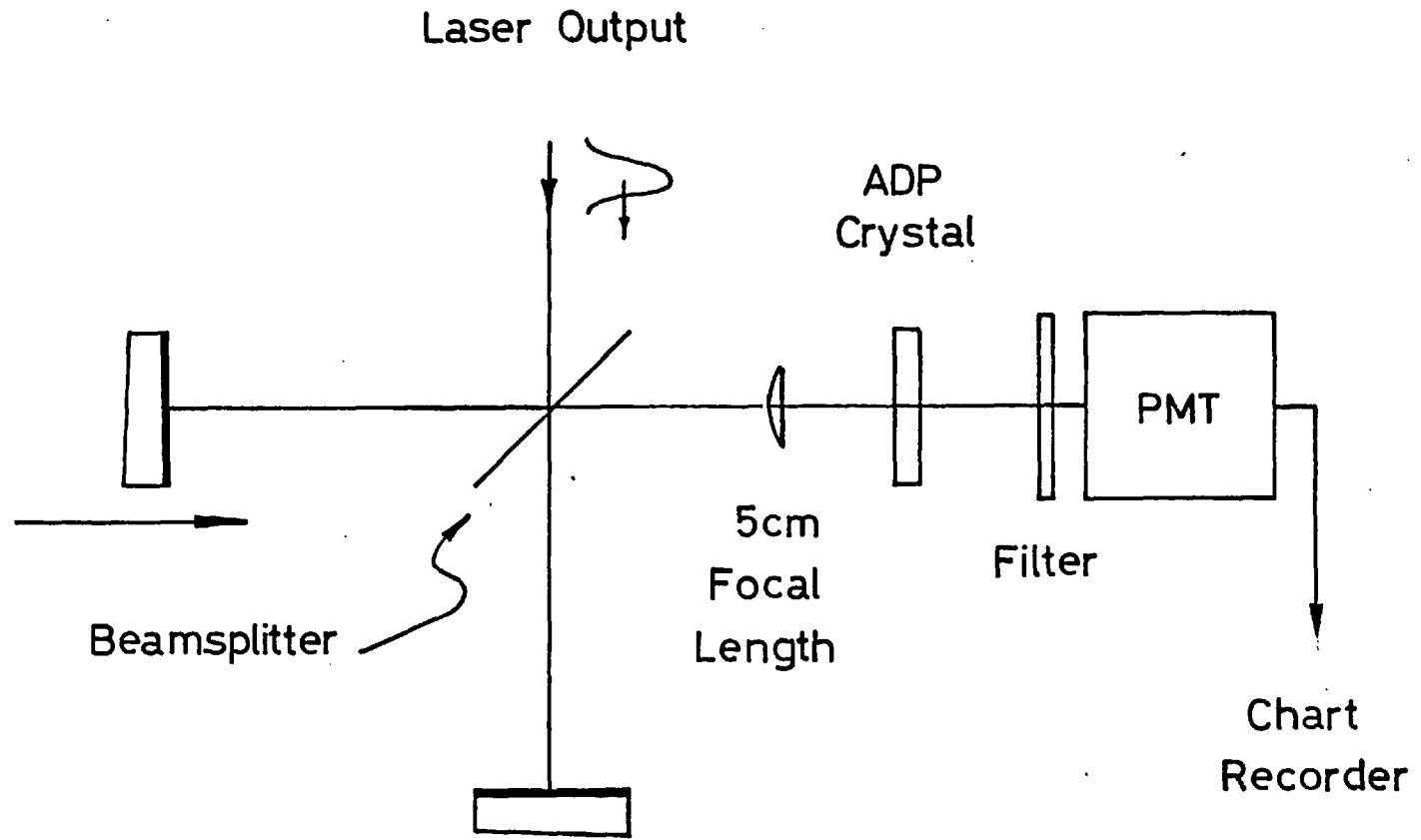
additional measurements of the laser's spectral profile made it an indirect method in which misinterpretation was likely.

Weber's arrangement⁶⁴ using beams of orthogonal polarizations is only applicable to the infra-red as the commonly available crystals KDP and Ammonium Dihydrogen Phosphate (ADP) do not have phase matching conditions in the visible. The alternative method in which the two beams have parallel polarization and a background signal is present has been used extensively with mode-locked C.W. dye lasers^{68, 72} and the experimental system used in this work is shown in Figure 16.

The laser output, after filtering by passage through a prism entered the interferometer consisting of a 50% beamsplitter B and two high reflectivity mirrors M_1 and M_2 . The beam was then focussed into the ADP crystal by a 5 cms focal length lens and the second harmonic signal was detected by a photomultiplier (Mullard 56TUVP) with Kodak 18B filters at the input to remove the fundamental. The relative delay between the pulses produced by the interferometer path difference ($2\Delta\ell$) was continuously variable by a small motor-micrometer arrangement which pushed one of the mirror mounts along an optical bench. The second harmonic signal was simultaneously displayed on an x-t chart-recorder. A slight misalignment of the mirrors M_1 and M_2 was sufficient to prevent feedback into the laser cavity.

The crystal used for Rhodamine 6G and Rhodamine B was cut such that the fundamental radiaticn. of wavelength $\lambda = 605$ nm, normal to the input face was incident at the phase-matching angle of 61° for a crystal temperature of 25°C . The intensity of the second harmonic signal is a maximum for $\Delta\ell = 0$ and varies rapidly with changes in $2\Delta\ell$ comparable to the pulse duration. As SHG of the first kind is

FIG:16



being used in which the fundamental beams propagate as ordinary rays, there is always a background signal in the absence of overlap due to the independent frequency conversion of each beam.

As the SHG with respect to time delay corresponds to the second order autocorrelation function, the profiles recorded are identical to those in the two photon fluorescence method. The theoretical basis for correlation measurements has been treated extensively⁷³, so only the main features will be discussed in this chapter.

The relative second harmonic signal detected and displayed on the chart-recorder $S_2(\tau)$ is given by^{64, 73}

$$S_2(\tau) = 1 + 2G_2(\tau) \quad (3.2)$$

where $G_2(\tau)$ is the normalized second order autocorrelation function

$$G_2(\tau) = \frac{\int_{-\infty}^{\infty} I(t) I(t + \tau) dt}{\int_{-\infty}^{\infty} I^2(t) dt}$$

and τ is the time delay in the interferometer. By definition the autocorrelation of any function is symmetric and so from measurements of either two photon fluorescence or SHG conclusions regarding the symmetry of the fundamental pulses cannot be made. The autocorrelation function is the Fourier transform of $|I(\nu)|^2$ where $I(\nu)$ denotes the Fourier spectrum of the original pulse shape $I(t)$ ⁶⁹. In $|I(\nu)|^2$ and hence also in $G_2(\tau)$ all phase information of the Fourier spectrum of the pulse is lost. In addition, although the autocorrelation function is unique for a given pulse shape, the back transform is not,

TABLE 3.1

Pulse profile: $I(t) = I_0 F(t)$

	<u>F(t)</u>	<u>M value</u>
Gaussian	$\exp-(t/T)^2$	$\sqrt{2}$
Lorentzian	$(1 + (t/T)^2)^{-1}$	2.00
Sech ²	$1/\cosh^2(t/T)$	1.55
Exponential	$\exp-(t /T)$	2.442
Exponential (single-sided)	$\exp-(t/T)$	2

but to calculate the pulse durations, assumptions about the pulse profile must be made.

The pulse width, t_p , is given by

$$t_p = \frac{2\ell}{Mc}$$

where ℓ is the distance travelled by the interferometer mirror corresponding to the half maximum intensity of the second harmonic peak, c is the velocity of light in air and the factor of 2 in the numerator is due to the delay changing twice as fast as the distance travelled by the mirror. The constant M depends on the pulse envelope and reflects the variation in width of the autocorrelation function for different fundamental profiles of the same halfwidth. Table (3.1) gives the autocorrelation functions and the values of M for a number of simple pulse shapes.

The pulse profiles assumed were found by fitting the expressions in Table (3.1) to the experimental second harmonic traces. To distinguish between them, accurate measurement of the intensity in the wings was necessary down to ~ 0.01 of the peak height as the autocorrelation functions for Gaussian, Lorentzian, Sech^2 and Exponential of the the same duration agree closely down to ~ 0.3 of the maximum. In Chapters 4 and 5 the traces obtained are shown to be characteristic of the laser configurations used for mode-locking and a comparison with the theoretical curves is made.

In common with the two photon fluorescence method, the contrast ratio of the peak to the background signal must be measured to obtain an indication of the mode-locking quality⁷³. From equation (3.2)

it can be seen that the expected contrast ratio (C.R.) for isolated pulses is 3:1 and this is illustrated in the second harmonic trace in Figure 17. The importance of the C.R. as an aid to the evaluation of the mode-locking was pointed out by Klauder et al⁷⁴ and Picard and Schweitzer⁷⁵. A peak in the second harmonic output is not indicative of mode-locking as a laser operating with completely randomly phased modes and with noise spikes of duration corresponding to the inverse bandwidth also produces a peak (C.R. - 1.5:1)

Frequently the second harmonic trace consists of a broad base of contrast ratio 2:1 with a narrow spike superimposed on it to give an overall contrast ratio of 3:2:1. In this case the laser output contains amplitude modulated noise with the pulse envelope duration being related to the base and the noise components to the spike. The presence of the spike may be dependent on the interferometer alignment due to spatial incoherence of the two beams when they are not oscillating in the fundamental mode⁷³. Hence contrast ratios of 2:1 may indicate isolated pulses for which imperfect alignment of the beams exists as well as structured pulses.

The degree of mode-locking is difficult to deduce from the autocorrelation traces as a sizeable decrease in the C.R. is not observed until the fraction of the laser energy in the pulses is small. Von der Linde⁷⁶ has shown that the C.R. will drop to 2.92:1 for a Gaussian pulse t_p containing only 10% of the energy where the background duration T is the time between successive pulses and given by $t_p/T = 10^{-4}$, e.g. 1ps pulse every 10 ns.

The background signal due to SHG of the first kind is convenient as it enables accurate measurement of the C.R. and verifies the alignment

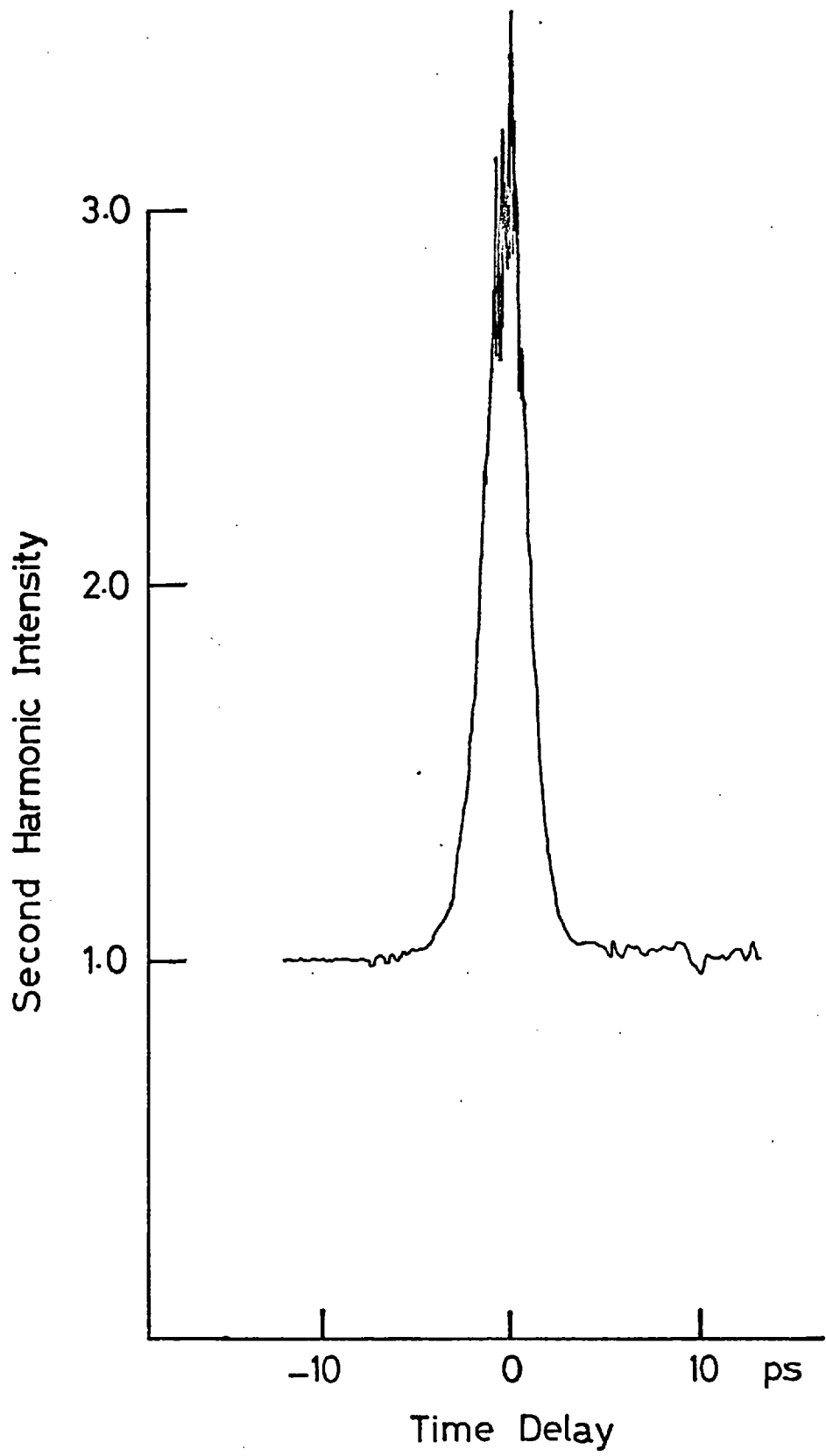


FIG:17

of the interferometer. A zero background method for use in the visible has been reported by Shank and Ippen⁷⁷ in which the two fundamental beams are not quite collinear as they impinge on the crystal such that the sum frequency generated at the overlap is detected along the bisector of the angle between them. Away from coincidence, the second harmonic signals generated by each beam independently are not recorded and this allows accurate determination of the intensity in the wings.

The resolution of the second harmonic method is related to the degree of phase-matching of the fundamental pulses and depends on the crystal thickness due to dispersion between the ordinary fundamental and extraordinary harmonic photons. Miller⁷⁸ has shown that the second harmonic intensity drops to half its peak value at λ_1 for a bandwidth $\delta\lambda_1$ given by

$$\delta\lambda_1 = 1.39\lambda_1 / \pi d \left\{ \frac{1}{2} \frac{\partial n^e}{\partial \lambda_2} - \frac{\partial n^o}{\partial \lambda_1} \right\} \quad (3.3)$$

where $\partial n^e / \partial \lambda_2$ and $\partial n^o / \partial \lambda_1$ are the dispersions of the extraordinary harmonic and ordinary frequencies respectively. In this work, with an ADP crystal of $d \sim 0.3\text{mm}$, substitution of the crystal parameters gives a maximum phase-matchable bandwidth at 600 nm of $\delta\lambda_1 \sim 2.6\text{ nm}$. In a thick crystal, SHG still occurs with a broad bandwidth laser but as the pulses propagate phase-matching will only take place over a decreasing spectral region centred on λ_1 . Hence the second harmonic intensity is no longer proportional to the square of the fundamental intensity and the autocorrelation function measured will not bear a simple relationship to the second order

autocorrelation of the input pulses. From $\delta\lambda_1 \sim 2.6$ nm, the corresponding minimum pulse duration detected with any accuracy is given by

$$t_p = K/\delta\nu_1 = 0.1\text{ps} \quad (3.4)$$

where $\delta\nu_1 = c\lambda_1/\lambda_1^2$ and $K = 0.32$ for pulses of a Sech^2 intensity profile.

The chart-recorder which displayed the second harmonic signal had a response time of 0.5 s for a full scale deflection and so for a typical micrometer drive rate of ~ 1.55 mm.min⁻¹ equivalent to a delay of ~ 7.0 ps.min⁻¹ the minimum displayable trace was not greater than ~ 0.05 ps in duration. Normally the complete scan lasted ~ 2 minutes, slow enough to resolve some of the interferometer fringes at the peak of the curve.

It has been stressed above that although easy to operate, care must be exercised in interpreting the results as a C.R. close to 3:1 does not necessarily mean that $> 10 - 30\%$ of the energy is located in the pulses. Also the study of low intensity components or interpulse background is precluded due to the non-linear nature of the technique. For these applications and to quantify the distribution of pulse structure it is necessary to use an electron-optical streak camera.

3.4 The Electron-Optical Streak Camera

High speed streak cameras up to 1970 were of such a design that the instrumental response function was ~ 40 ps arising from the initial spread of photoelectron transit times in the first stage of the image tube ⁷⁹. Zavoiskii and Fanchenko ⁷⁹ showed that the distribution of

photoelectron transit times in the image tube has a halfwidth

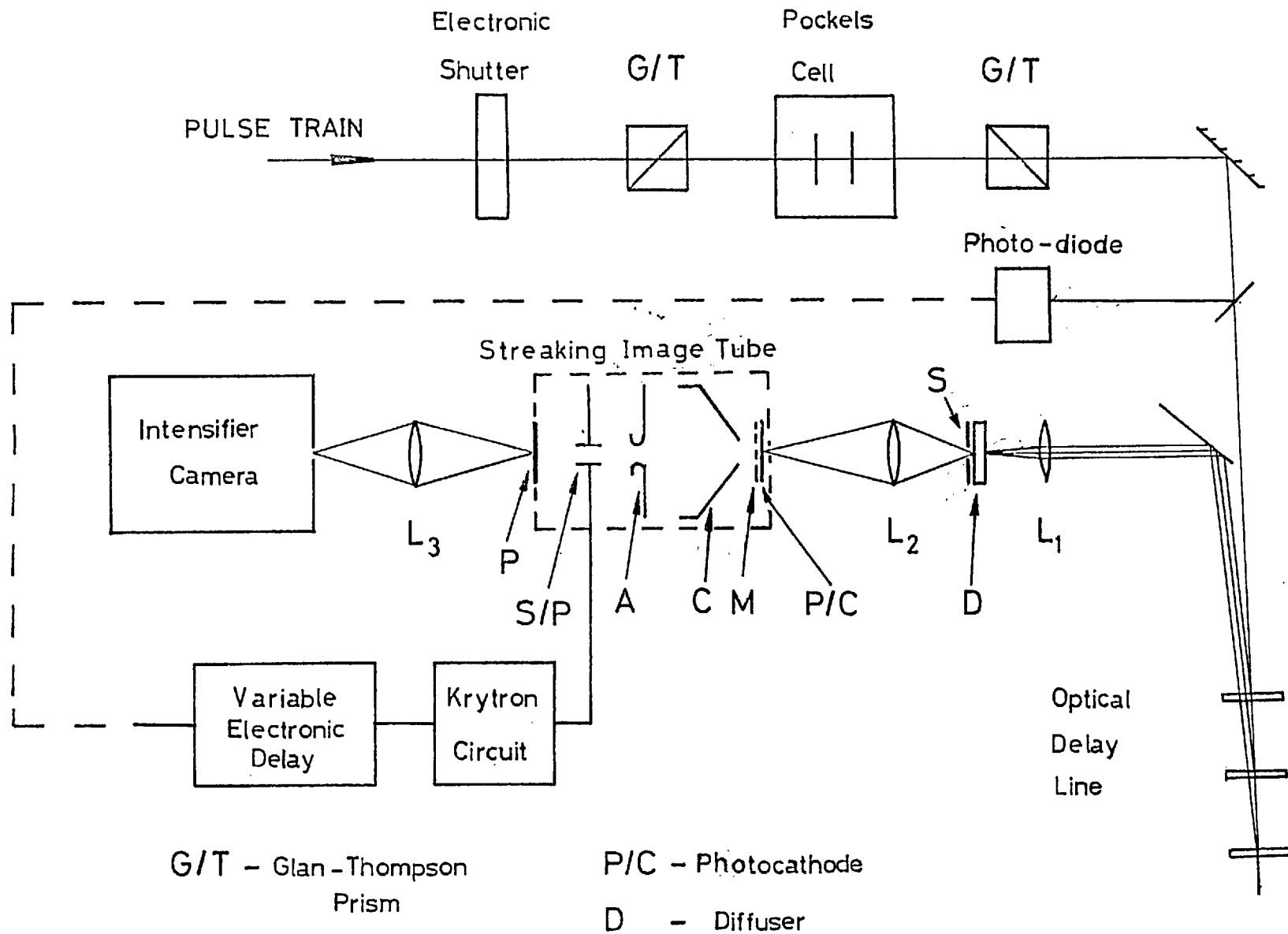
$$\Delta\tau_D = \frac{m \Delta u}{eE}$$

where Δu is the halfwidth of the initial velocity distribution and e and m are the electron charge and mass respectively. By employing large extraction fields E and choosing the photocathode such that it is operated near the long wavelength cut-off for the incident light (thus reducing Δu), $\Delta\tau_D$ may be minimized⁶².

The operation of the streak camera can be outlined with reference to Figure 18. The laser pulses to be studied were subdivided by reflection from an optical delay line consisting of 3 uncoated parallel plates to provide a means of calibrating the streak and also to provide better synchronization. The resulting pulses were then focussed onto the 50 μ m input slit (s) by the cylindrical lens (L_1) which was imaged at a demagnification of $\times 3$ by L_2 (Biotar 75 mm f 1.5) onto the S20 photocathode. The streak limited or technical resolution $\Delta\tau_S$ of the camera is given by $\Delta\tau_S = \frac{1}{v\delta}$ where v is the streak speed and δ is the spatial resolution in the streak mode. Typically, for the Photochron II camera used in this work, $v \sim 10^{10}$ cm.s⁻¹ and $\delta \sim 120$ lp. cm⁻¹ giving $\Delta\tau_S \sim 0.8$ ps⁸⁰.

The high extraction field of 20KV. cm⁻¹, produced by positioning a fine mesh electrode (M) 0.5 mm away from the photocathode, was sufficient to reduce the time dispersion of the photoelectrons to ~ 0.5 ps for incident light at 750 nm on an S20 photocathode. These photoelectrons, retaining an image of the original pulse were focussed at the phosphor (P) by suitable potentials on the cone (C) and anode (A).

FIG:18



A photodiode signal (150 mV) derived from a portion of the original pulse train was fed into a Tektronix 7904 oscilloscope from which the Gate Out signal ($\sim 2V$) triggered the time base of a Tektronix 519 oscilloscope. The '519' Gate Out triggered an avalanche transistor-Krytron circuit generating the streak deflection voltage ramp of 5KV. The risetime of the ramp was ~ 1 ns and the central 1.5 KV region was utilized as the ramp on the streak plates (S/P) sweeping the electron beam across the phosphor changing the temporal to a spatial image with a jitter of ± 50 ps.

To avoid saturation of the photocathode and loss of spatial and temporal resolution resulting from high photoelectron current densities, the illuminating light level is kept low. Intensification of the image at the phosphor was provided by an image intensifier system (EMI T2001 with type 9912 cascade tube) with a gain of $\sim 10^6$ for an overall accelerating potential of ~ 35 KV, optically coupled to the streak tube by lens L_3 (f1.5, 80mm Dallmeyer Optac Ltd.). The final image was photographed either on Polaroid for setting-up purposes or on Ilford Type HP4 film for quantitative use in microdensitometry.

The streaked pulse duration t_p must be deconvolved from the recorded pulse width $\Delta\tau_R$ and for a Gaussian pulse and instrumental function, is given by

$$(\Delta\tau_R)^2 = (\Delta\tau_S)^2 + (\Delta\tau_D)^2 + (t_p)^2 \quad (3.5)$$

where for the Photochron II camera at 600 nm, $\Delta\tau_S \sim 0.8$ ps and $\Delta\tau_D \sim 0.9$ ps. Calibration of the film by a neutral density step

wedge enabled the halfwidth (FWHM) to be determined.

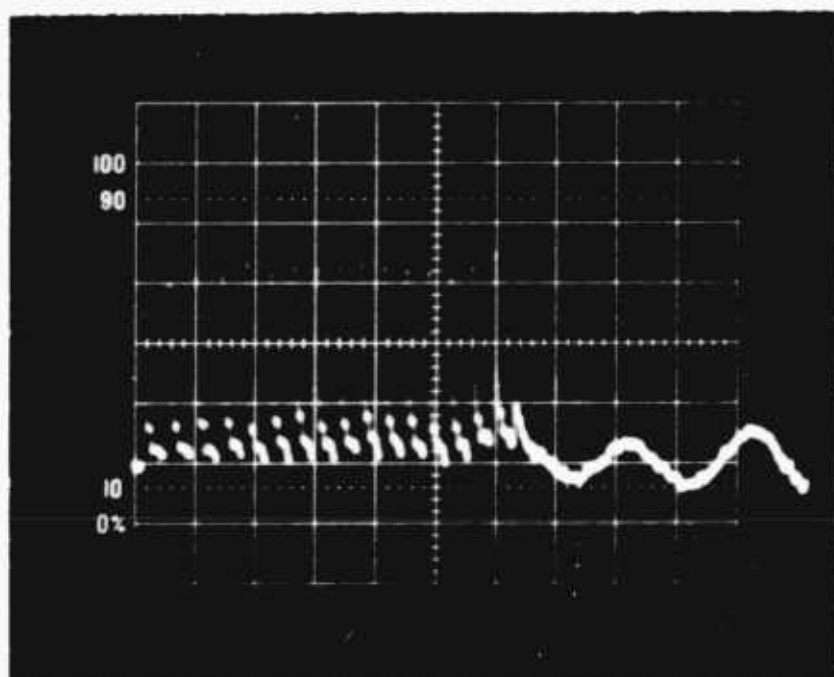
As the laser signal under investigation was continuous, experimental problems arose which are not normally encountered with pulsed mode-locked lasers. For all types of mode-locked lasers, it is customary to employ an electro-optic switch to either isolate a single pulse or select a group to minimize signal induced background arising from scattering inside the image tube. Alternatively the tube could be gated but this does not prevent damage to the photocathode by prolonged continuous exposure. The switch also allows one to examine pulses from any portion of the pulse train synchronizing the camera to one of the switched out packet. Figure 18 also shows the switching system used for the C.W. dye laser. It consisted of an electronic shutter and Pockels cell (E.O.D. Ltd., Type 12KD) placed between crossed Glan-Thompson prisms aligned to give zero transmission. The electronic shutter was opened remotely in coincidence with the shutter on the streak camera recording lens to provide an origin for the sequence of events in streaking a pulse. A reflection from the second polarizer triggered a photodiode-oscilloscope combination to give an output signal of $\sim 2V$ which was further amplified to $\sim 30V$ to operate a Krytron switch. This generated a 5KV half-wave voltage of 150ns which was applied to the Pockels cell. Approximately 13 pulses were selected from the laser output (Plate 6) and they were then incident on the optical delay line and streak camera.

Due to strain birefringence and the laser beam divergence there was always a small amount of leakage ($\sim 10^{-3}$) through the Pockels cell and crossed polarizers which was integrated on the streak exposure

PLATE 6

SWITCHED-OUT PORTION OF MODE-LOCKED PULSE TRAIN

TIMESCALE: 20 ns/DIV



during the slow reset of the ramp generator. To overcome this, the extraction mesh was biased negative⁸¹ relative to the photocathode immediately after the streak and held negative for the period during which the streak bias voltage was being restored. A small pick-up voltage pulse was derived from the output of the ramp generator and this was used to trigger the mesh gating circuit after a delay of $\sim 50\text{ns}$. The circuit consisted of an avalanche transistor network and a krytron with an applied anode voltage of $\sim 1400\text{V}$. Thus after the streak, the mesh potential was reduced to $\sim -400\text{V}$ and the camera remained effectively switched-off until the ramp generator had reset. Without this modification, the streak photographs were masked by the continuous trace produced by integration of the leakage.

3.5 Conclusion

For most investigations on the mode-locking of the C.W. dye laser, the second harmonic method sufficed and supplied reliable information on the pulse durations provided care was taken with alignment and the interpretation of the contrast ratio. Although the result obtained was averaged over a large number of pulses, this is the value which is important in most C.W. applications e.g. the measurement of organic dye recovery times.⁷²

Apart from the high resolution of the autocorrelation method, there is a need for a linear technique capable of observing low intensity components and intra-pulse background⁸² and determining the shape and distribution of structure in pulses. In this work, along with verification of the autocorrelation measurements, the streak camera was used to compare quickly the effect on mode-locking of variations in the laser parameters and show the form and stability of the pulses from different cavity configurations.

CHAPTER 4

MODE-LOCKING OF THE C.W. RHODAMINE 6G DYE LASER

4.1 Introduction

In the early applications of lasers, it was apparent that high power pulses were necessary especially in the study of non-linear phenomena and this was partly achieved by the method of Q-switching for solid-state lasers⁸³ increasing the available power from $\sim 10^3$ W to $\sim 10^8$ W. The method of Q-switching is not applicable to pulsed dye lasers due to their short storage time of ~ 5 ns compared to ~ 0.5 ms for a Neodymium:glass laser. The alternative approach to increasing laser power and simultaneously providing high temporal resolution is by decreasing the duration of the emission and is termed "mode-locking". This terminology refers to the case in which a laser output consists of a train of pulses each separated by the laser round trip time (T_{RT}) corresponding to a single pulse oscillating in the cavity and part of which is coupled out at each reflection from the output mirror. The term mode-locking has been used as the laser operation arises from the coupling of the longitudinal modes of the cavity such that a constant phase relationship exists between them, whereas normally the laser radiation is well distributed among the many oscillating modes. By Fourier analysis, this can be shown to be equivalent to the localization of the laser field to a small region inside the cavity.

The production of the fixed phase relationship can be brought about by non-linear effects in the gain medium⁸⁴ but is generally introduced by either the inclusion in the cavity of an "active" mode-locking element⁸⁵ or a "passive" saturable absorber which is capable of

generating the shortest pulses and has been used extensively with solid state ^{86,87} and both pulsed ⁸⁸ and C.W. dye lasers ¹¹.

Active mode-locking requires an intra-cavity loss modulator to be driven at a frequency equal to a multiple of the longitudinal mode spacing ($\delta\nu$) where

$$\delta\nu = c/2L$$

c is the speed of light and L is the cavity length.

Sidebands are created at a frequency spacing equal to the mode spacing which couple by interference and this continues until the modes under the gain curve are all locked together with a constant phase relationship.

Passive mode-locking involves the introduction of a saturable absorber dye where non-linear absorption causes selection and subsequent compression of a pulse from the initial build-up fluctuations which is equivalent to introducing phase-locking of the longitudinal modes.

In this chapter a review is given of the mode-locking methods used and in particular their application to the C.W. dye laser. The passive mode-locking of the C.W. Rhodamine 6G laser is studied in detail for various cavity parameters resulting in the direct generation of subpicosecond pulses.

4.2 Review of Mode-Locked Dye Lasers

From the time-bandwidth product for pulses, it is clear that the shortest pulses should be obtainable from the laser systems with the greatest bandwidth. Although in the Nd:glass laser ($\Delta\lambda \sim 10\text{nm}$) the theoretical minimum of $t_p \sim 0.3\text{ps}$ has not yet been observed, substructure of this duration has been measured in two photon

fluorescence patterns^{89,67}. It was apparent that the dye laser could be a source of very short pulses with the added advantage of tunability as the typical dye emission band is $\sim 50\text{nm}$ wide.

Dye lasers, both pulsed and C.W., have been mode-locked by active and passive methods. Using a mode-locked laser as a dye laser pump, thus modulating the gain, Glenn et al⁹⁰ and Bradley et al⁹¹ observed a mode-locked dye laser output. The dye laser resonator was adjusted in length to cause synchronism between the pumping pulses and the oscillating dye laser pulse. Although the high gains in the active medium are generated in a few picoseconds by the pumping pulses, the fluorescence lifetimes of the dyes used can be up to a few nanoseconds in duration. This is due to the intense internal powers experienced which act to deplete the gain by stimulated emission and so produce a net gain over a period approximately that of the pumping pulse. A mode-locked superradiant travelling wave dye laser was demonstrated by Mack⁹² which had the advantage of not requiring the matching of the pump and dye laser cavity transit times and produced pulses estimated to be $\sim 15\text{ ps}$ when excited by a mode-locked ruby laser.

Gain modulation due to pumping by an acousto-optically mode-locked argon-ion laser has generated pulses in the C.W. dye laser. Chan et al have obtained pulses of $\sim 2.8\text{ ps}$ from Rhodamine 6G lasers pumped by $\sim 160\text{ ps}$ pulses⁷² and $\sim 50\text{ ps}$ when pumped by 1-2 ns pulses⁹³. Mahr⁹⁴ has measured pulses of $\sim 12\text{ ps}$ using 250 ps argon-ion laser pulses as the pump source and with a similar arrangement, Harris et al⁹⁵ produced mode-locking over the range 570-640 nm and acousto-optically dumped pulses from the cavity.

Runge³⁵ used a variation of the gain modulation technique in which the dye was placed internal to a He - Ne laser cavity and acted both as the active medium and as a saturable absorber to mode-lock the pump beam. As the dye lased synchronously with the He - Ne laser in the same resonator, laser action was initially restricted to near strongly dispersive Ne transitions which compensated for the different effective cavity lengths seen by the pumping and dye laser pulses. Independent tuning of the dye laser emission gave pulses of ~ 270 ps over the range 673 - 701 nm with the dyes Cresyl Violet, Nile Blue, Nile Blue A, Resazurin, 3,3' - diethyloxadicarbocyanine iodide (DODCI) and 3,3' - diethylthiadicarbocyanine iodide (DTDCI)⁹⁶.

Active modulation of the cavity loss has been used for both pulsed and C.W. dye lasers as well as in the pumping laser. A flashlamp pumped 7-diethylamino - 4 - methyl coumarin laser operating at 460 nm was mode-locked to produce subnanosecond pulses⁸⁵ using an acoustically driven fused quartz block but the shortest pulses were not observed until near the end of the 600 ns pulse train.

By using a similar technique, Dienes et al⁶⁸ generated stable pulses of ~ 55 ps in a C.W. Rhodamine 6G laser. The pulses (measured by SHG) exhibited substructure corresponding to the inverse bandwidth of the laser and peak powers were estimated to be of a few watts. Less stable mode-locking was obtained by Kuizenga⁹⁷ with a phase modulator driven at the cavity longitudinal mode spacing frequency. Multiple structured pulses of 200-500 ps were obtained attributed to the effect of dispersion resulting in a different mode-locking frequency for each part of the laser spectrum. The presence of a sharp spike on the broad (6.0 nm) bandwidth led the author to conclude that only

part of the spectrum was well mode-locked.

Mode-locking of dye lasers by active modulation methods has not reliably produced pulses of picosecond duration. Due to the large number of round trips needed to compress the circulating pulse ($\sim 10^8$), for an actively mode-locked system, it is unlikely that the modulation frequency can be set to the required accuracy for this period of time⁹⁸. However, active methods enable the generation of pulses at wavelengths for which saturable absorbers may not be available⁸⁵ and in conjunction with passive mode-locking may produce higher power pulses in C.W. dye lasers.

Passive mode-locking of a dye laser was first reported by Schmidt and Schäfer⁸ who obtained > 80% modulation in the output of a Rhodamine 6G flashlamp pumped system with 3,3' - diethyloxadicarbocyanine iodide (DODCI) as saturable absorber. Increasing the cavity length from 15cms to 180 cms also produced a modulation in the absence of an absorber. This had been observed earlier by Sorokin and attributed to self-absorption in the active medium⁹⁹. (The combination of Rhodamine 6G and DODCI is still the most popular for generating tunable picosecond pulses and has been used for producing the shortest pulses). The use of an absorber dye cell in which the dye was in contact with one of the cavity reflectors enabled Bradley and O'Neill¹⁰⁰ to obtain 100% modulation for the same dyes with the correct concentrations and pump level. Later development of the flashlamp pumped dye laser led to the production of transform limited pulses of ~ 3 ps duration by Arthurs et al,¹⁰¹ tunable by an intra-cavity Fabry-Perot over the range 602 - 625 nm when operated close to threshold to reduce the effects of self-phase-modulation¹⁰². By sampling between the mode-locked

pulses with a streak camera, it has been shown that <3% of the total energy is contained outside the pulses and that the ratio of signal to background power was $> 10^4$ ¹⁰³.

Similarly to the pulsed dye lasers, the application of passive mode-locking to the C.W. dye laser resulted in the production of picosecond pulses. By flowing DODCI in a cell at the focus of a second astigmatically compensated focussing arrangement, Ippen et al⁹ mode-locked Rhodamine 6G over the tuning range 590 - 610 nm. Pulses of ~ 1.5 ps were measured with the second harmonic method and with spectral information showed that the pulses were close to the bandwidth limit assuming Lorentzian profiles. O'Neill⁴² using a different configuration involving a contacted absorber cell obtained pulses of ~ 4 ps, measured with the electron-optical streak camera.

By mixing both the active and passive media in one jet-stream, Scavennac¹⁰⁴ simplified the mode-locked laser cavity. Using a similar system, Shank et al¹⁰⁵ generated pulses of ~ 0.7 ps which after acousto-optic dumping yielded peak powers of kilowatts. The same authors⁷⁷ have also compressed, using a grating pair¹⁰⁶, frequency chirped pulses from a double jet-stream cavity to give pulses of ~ 0.3 ps. In addition, by mixing the original chirped pulses and the compressed pulses to obtain a dynamic spectrogram¹⁰⁷, they showed that the laser output consisted of asymmetric pulses with exponential tails.

4.3 The Mode-Locking Dyes

The two dyes used in this work for both Rhodamine 6G and Rhodamine B were DODCI and DQOCI (1,3' - Diethyl - 4,2' - quinoly-oxocarbocyanine Iodide). The latter dye has been used with flashlamp pumped Rhodamine 6G lasers to generate pulses in the range 575-600nm¹⁰⁸.

Figure 19 shows the absorption spectra of DODCI¹⁰⁹ and DQOCI (as measured on a Perkin-Elmer spectrophotometer) from which both are seen to have peak absorption cross-sections of $\sigma_s \sim 8 \times 10^{-16} \text{ cm}^{-2}$. As the DODCI absorption peak is at $\sim 585 \text{ nm}$, its ability to mode-lock over the spectral range 600-630 nm has been attributed to the existence of a photoisomer^{10, 109}. The absorption spectrum of the photoisomer as measured by Dempster et al¹⁰⁹ is reproduced in Figure 19 and exhibits a peak absorption cross-section of $\sim 7 \times 10^{-16} \text{ cm}^{-2}$ at $\sim 620 \text{ nm}$.

Under low power excitation, a fluorescence lifetime and absorption recovery time of $\sim 1.2 \text{ ns}$ has been measured^{11, 109, 110} for DODCI. However with high power pulses similar to those experienced in a laser cavity, fluorescence and absorption recovery times of $\sim 300 \text{ ps}$ ^{111, 112} have been obtained for both forms of DODCI. The difference has been accounted for by stimulated depopulation¹¹³ of the upper state at the high photon flux used. The same authors also obtained a quantum efficiency of ~ 0.01 for photoisomer generation.

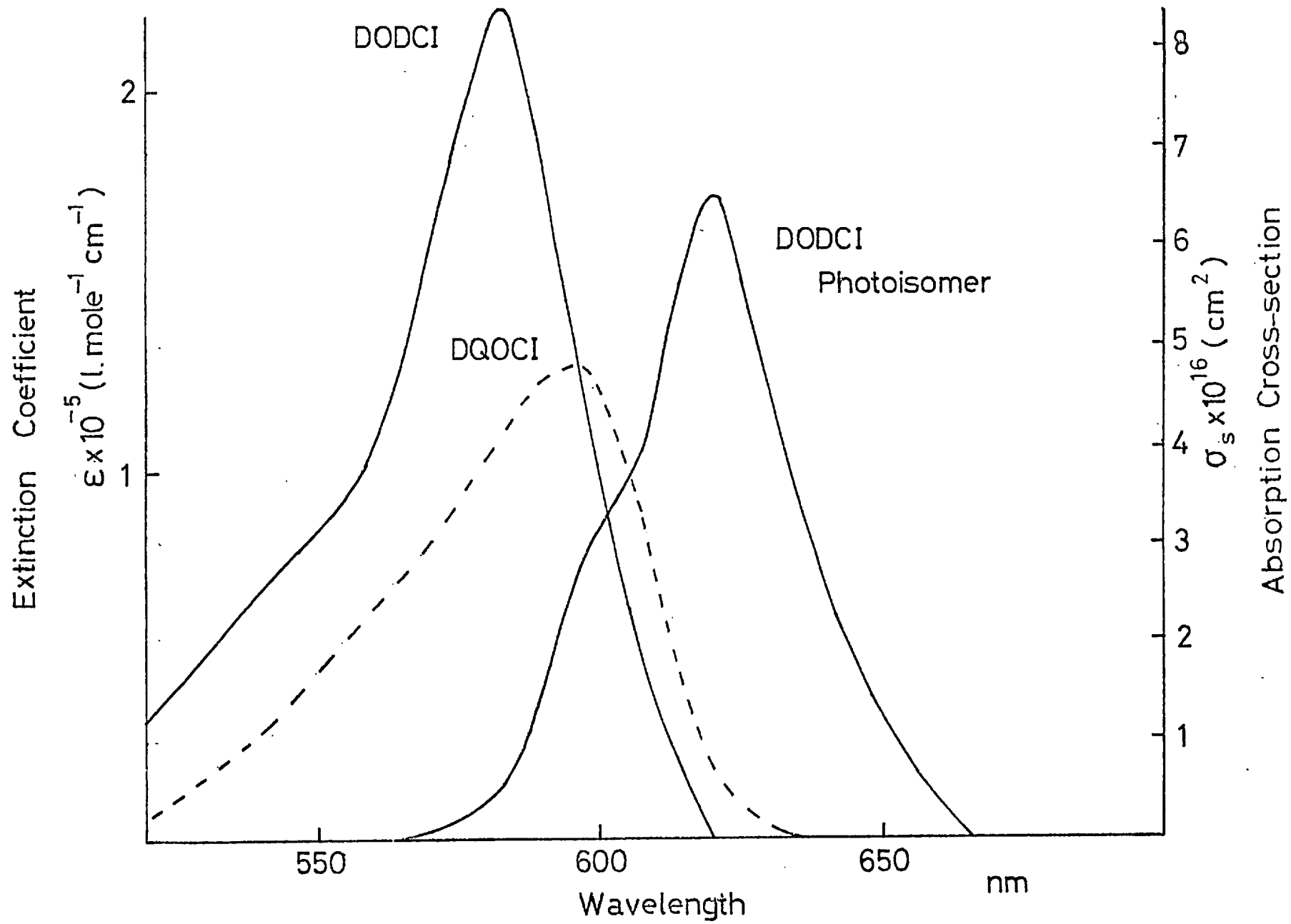
DQOCI has not been shown to have a photoisomer but from measurements of the rate of build-up of mode-locking it is thought to have a short recovery time \sim tens of picoseconds¹⁰⁸.

The structures of the two dyes, both of the polymethine family, are shown in Figure 20.

4.4 The Passively Mode-Locked C.W. Dye Laser Cavity

The two cavity configurations used for passive mode-locking differed in the location of the saturable absorber. In one, it was placed in contact with one of the mirrors and in the other, it was situated a short distance from it. Figure 21 shows the contacted

FIG. 19



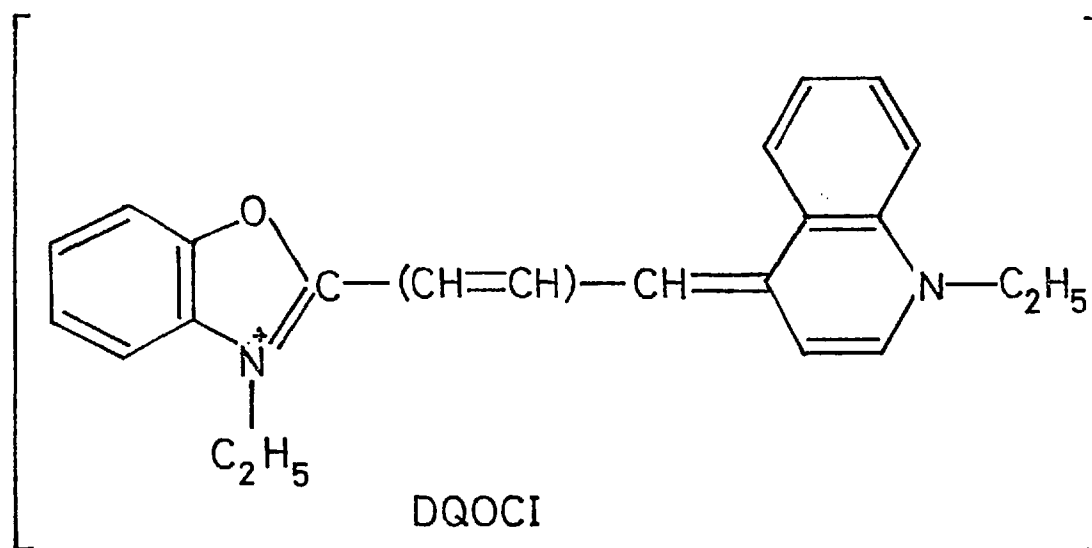
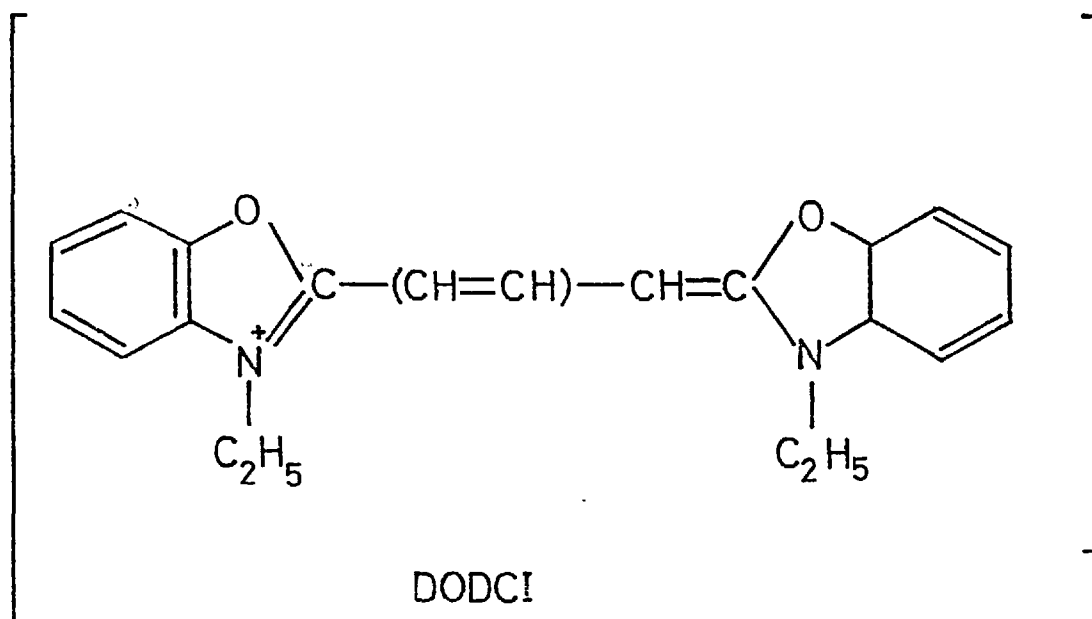
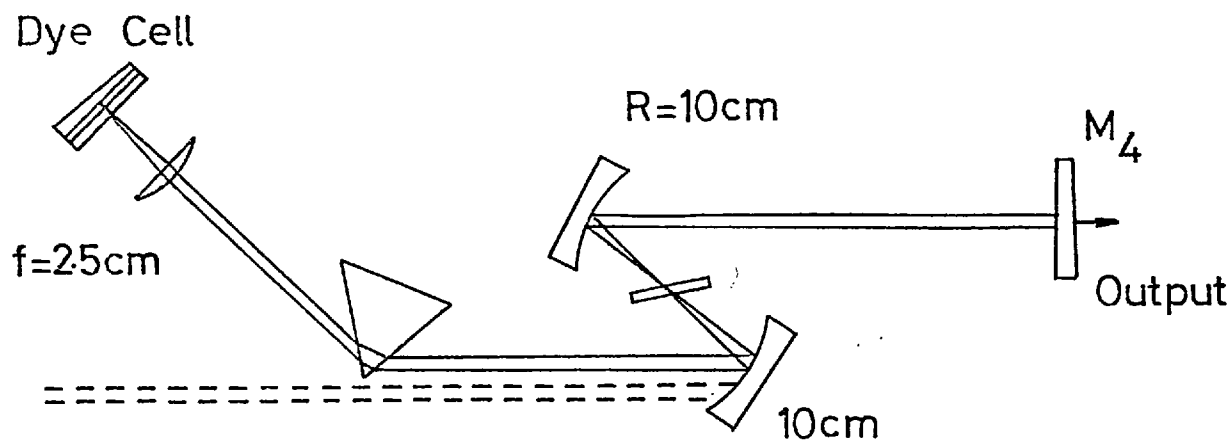
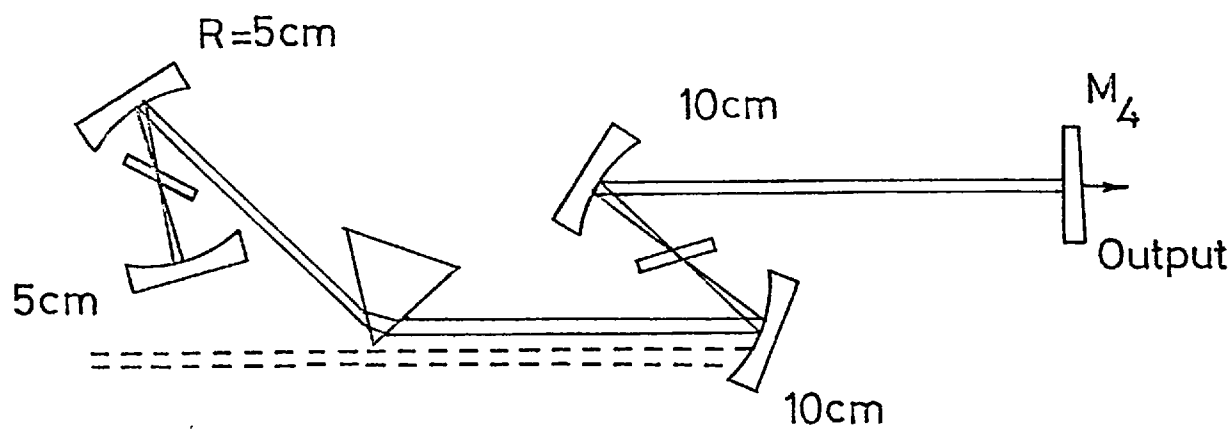


FIG: 20



(a)



(b)

FIG :21

and non-contacted variations. The basic cavity, common to each, differed from that of Figure 6b by two modifications. Replacing the 5 cms radius mirror by one of 10 cms radius, extended the cavity on the right-hand side to give a convenient output through the partially transmitting mirror (M_4). This also allowed the position of the active medium to be altered without changing the overall cavity length. The plane mirror (M_1 - Figure 6b) was replaced by the saturable absorber which flowed in a thin contacted cell or as a jet-stream in a folded focussing arrangement. In both cases, the dye laser was focussed to a smaller spot size in the mode-locking dye than in the active medium. For the contacted cell, an anti-reflection coated lens of a 2.5 cms focal length was used, whereas with the jet-stream, a 5 cms radius mirror performed the same function. The spot sizes produced were of approximately $10\mu\text{m}$ diameter compared to the mode size in the active medium of $\sim 20\mu\text{m}$ diameter ensuring a power density ratio of ~ 4 and facilitating saturation of the absorption of the dye.

In the mode-locking process, after the period of linear build-up of power in the cavity from the threshold level of spontaneous noise to that at which the non-linear effects of the absorption become noticeable, selection of noise bursts occur due to saturation. This leads to the selection of a pulse of duration comparable to the absorber relaxation time provided saturation of the absorption occurs before saturation of the amplification in the active medium. New ¹¹⁴ has shown that the condition $\sigma_b > 2\sigma_e$ where σ_b is the absorption cross-section of the saturable absorber, satisfies this requirement and as seen from the absorption spectra of DODCI and DQOCI (Figure 19), and the stimulated emission cross-section of Rhodamine 6G (Figure 2)

this is experimentally valid.

Assuming the saturable absorber to be a two-level system, the flux required for significant saturation F_{SAT} , is given by

$$F_{SAT} = 1/\tau_b \sigma_b$$

However, for DODCI at 600 nm with $\tau_b \sim 330$ ps and $\sigma_b \sim 3 \times 10^{-16} \text{ cm}^{-2}$, substitution gives $F_{SAT} \sim 10^{25} \text{ photons.cm}^{-2}$ ($\sim 3.3 \text{ MW.cm}^{-2}$). In the C.W. dye laser, prior to the addition of the mode-locking dye at a pump power of ~ 3 W, a power density of $\sim 5 \text{ MW.cm}^{-2}$ can be produced by focussing to a spot size of $\sim 10\mu\text{m}$ diameter in the absorber cell or jet.

The mode-locking continues from the selected noise burst and the pulse peak will be further enhanced relative to the background if there is a net loss at the leading and trailing edges. By arranging the cavity length such that T_{RT}/τ is not too large where T_{RT} is the laser cavity double transit time and τ is the lifetime of the active medium ensures that the amplifier does not completely recover to its fully pumped state between pulse transits. If this is satisfied, saturation of the gain at the peak of the pulse creates a net loss on the trailing edge¹¹⁵ and combined with the linear absorption at the leading edge the peak is favoured in both dyes¹¹⁴.

In the cavities of Figure 21, the transit time from the active medium to the saturable absorber was ~ 4 ns and the corresponding time to the plane mirror was ~ 1.5 ns. Hence for at least one transit of the amplifying dye, the pulse experienced gain saturation. Locating the active medium nearer the centre of the cavity also increases the energy extraction efficiency in a mode-locked dye laser. For a dye with

an upper state lifetime of ~ 5 ns situated at the end of a cavity of $T_{RT} \sim 12$ ns, a large fraction of the molecules pumped into the upper laser level in the interval between the pulse transits is lost by spontaneous emission.

4.5 The Contacted Dye Cell

The advantage of immersing the end cavity mirror in the mode-locking dye was first recognized in the generation of ultrashort pulses in Nd: glass lasers^{116, 117}. With the dye cell at an arbitrary position, the shot to shot reproducibility of the mode-locking was poor and the occurrence of laser outputs with one pulse per transit was ~ 1 in 10 ¹¹⁸. This was increased to 80% of pulse trains ideally mode-locked by contacting¹¹⁹. The improvement was attributed to the overlap of the laser flux near the mirror surface producing an intensity of four times that experienced for a single transit of a non-contacted cell. Hence in this region, saturation occurs more easily leading to the formation of a burst of noise or the selection of a noise fluctuation depending on the dye recovery time. In addition, multiple pulsing is more likely with a non-contacted absorber due to pulses crossing in the dye, giving groups extending over a distance related to the cell-mirror separation¹²⁰. With the advent of dye lasers, the contacted dye cell was again shown to be superior for generating reproducible pulse trains¹⁰¹ and was applied to the C.W. dye laser by O'Neill⁴².

The dye cell used in much of this work was similar to O'Neill's and was machined from stainless steel such that the dye flowed in a channel of ~ 0.6 mm width when the window mount was fitted into the cell body. The latter held the broadband high reflectivity mirror (Laser Energy Inc: $R > 99\%$ 500-700 nm). The 16mm diameter window (fused silica, polished to $\lambda/2$ over its entire diameter) was wedged at 1° as

was the dye channel. Plate 7 shows the cell dismantled with the dye flow connections visible. As with the active medium, the solution was pumped by a gear pump and filtered continuously. In the cell, the flow rate was $\sim 20\text{m.s}^{-1}$ which although not critical had to be maintained bubble free. The air-glass interface of the cell window and also both the surfaces of the plano-convex lens were anti-reflection coated (OCLI Ltd: H.E.A. coating) to reduce losses at normal incidence to $\sim 0.2\%$.

Preliminary alignment of the cavity was carried out with the solvent (ethanol) only flowing in the cell by the addition of it and then the lens to the unmode-locked configuration ensuring at each stage that the threshold was still low. The additional optical components increased the necessary pump level by $\sim 100\text{ mW}$ to $\sim 400\text{ mW}$ at minimum for 514.5 nm pump radiation.

4.6 The Mode-Locked C.W. Rhodamine 6G Laser - Contacted Absorber

a Phenomenological Characteristics

Mode-locking in the system described in the previous sections was achieved by the addition of DODCI from a high concentration stock solution to the ethanol used for alignment purposes. The concentration was increased until a stable pulse train was observed on the sampling oscilloscope. By turning the prism slightly away from Brewster's angle, a small reflection for monitoring with the photodiode was obtained. Plate 8 shows some stages in this sequence of events as the DODCI concentration was increased to 10^{-4} M with lasing at $\sim 600\text{ nm}$. The modulation, which was first observable close to threshold for a concentration of $\sim 0.2 \times 10^{-5}\text{ M}$, sharpened with

PLATE 7

CONTACTED ABSORBER DYE CELL AND WINDOW

HOLDER

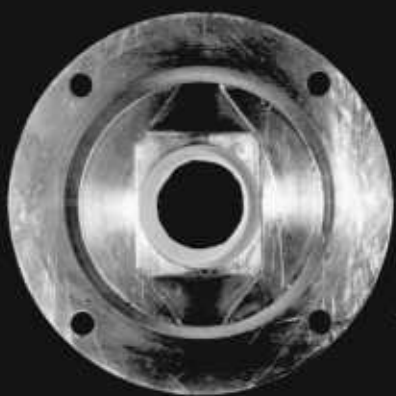
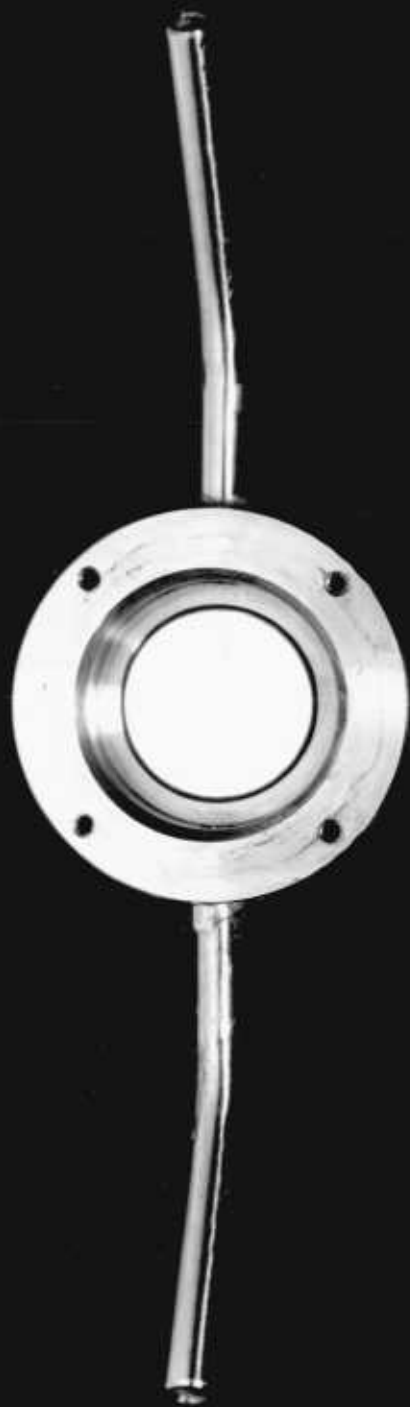


PLATE 8

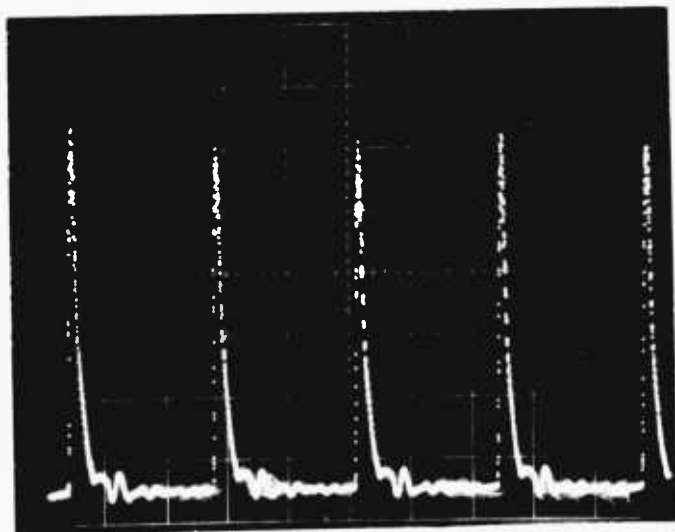
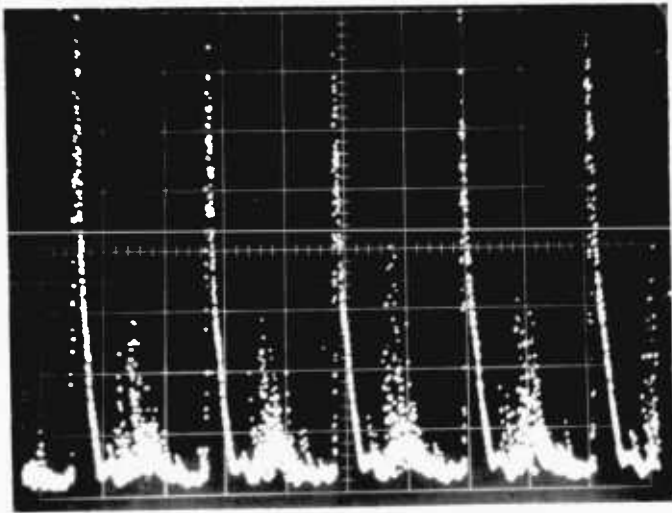
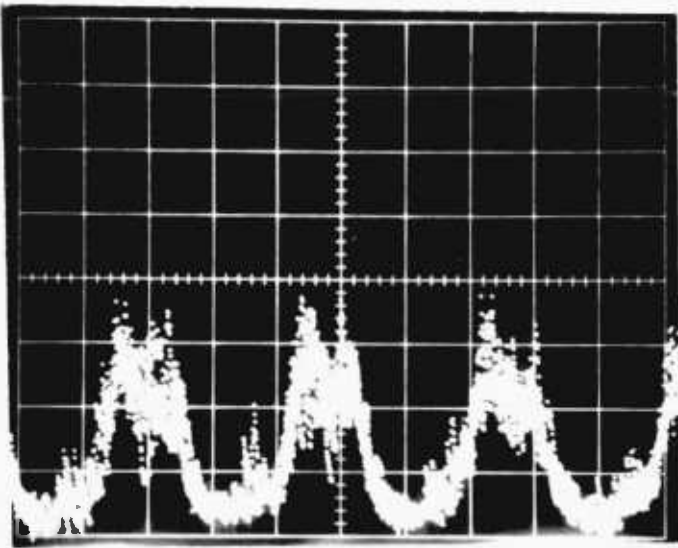
BUILD-UP OF MODE-LOCKED PULSE TRAIN

DODCI Concentration:

(a) $0.2 \times 10^{-5} \text{M}$

(b) $0.6 \times 10^{-5} \text{M}$

(c) $0.8 \times 10^{-5} \text{M}$



additional dye until at $\sim 0.8 \times 10^{-5} \text{M}$ instrument limited pulses separated by the cavity round trip time (T_{RT}) of 12 ns were detected. At this concentration, the low light transmission of the 0.6 mm cell was $\sim 80\%$.

At low dye strengths ($< 10^{-5} \text{M}$) the laser was prone to multiple pulsing in which either groups or equally spaced components were generated. Examples of each situation are illustrated in Plate 9. The conditions under which they existed depended largely on the cavity length and the pumping power. For cavities with T_{RT} less than ~ 13.5 ns equally spaced multiple pulsing was possible (Plate 9a). For example, in a cavity of $T_{\text{RT}} \sim 13$ ns, four pulses were generated which upon reduction of the cavity double transit time to 10.5 ns (by moving M_4 - Figure 21) decreased in number until a single pulse was oscillating. The pulses were detector limited up to ~ 700 mW above threshold after which they became longer and eventually $< 100\%$ modulated. Under these conditions, the round trip time from the jet to Mirror M_4 was < 4.5 ns. Maintaining the cavity at the same overall length but moving the jet away from M_4 until this double transit time was ~ 6.7 ns resulted in the generation of groups of discrete pulses (Plate 9b).

This pattern of discrete pulses was normal when the jet- M_4 round trip time was long and was observed up to ~ 9 ns for a cavity with $T_{\text{RT}} \sim 18$ ns. The spacing of the subpulses was ~ 1.5 ns, but at higher powers (~ 300 mW above threshold) they merged to form one pulse of 5 - 8 ns in duration. The relation between the pulse and the cavity was such that it occupied about one half and the laser (Plate 9c) was operating in a "flip-flop" mode. For long cavities at low concentrations

PLATE 9

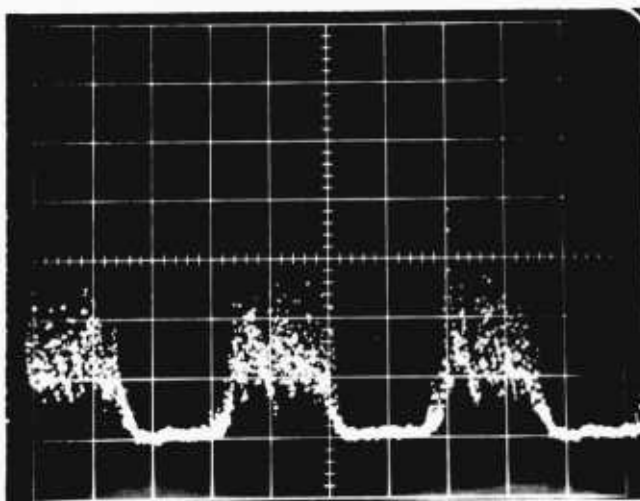
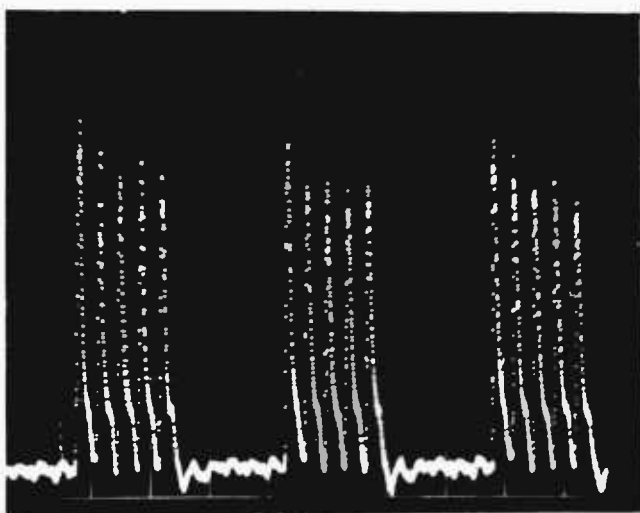
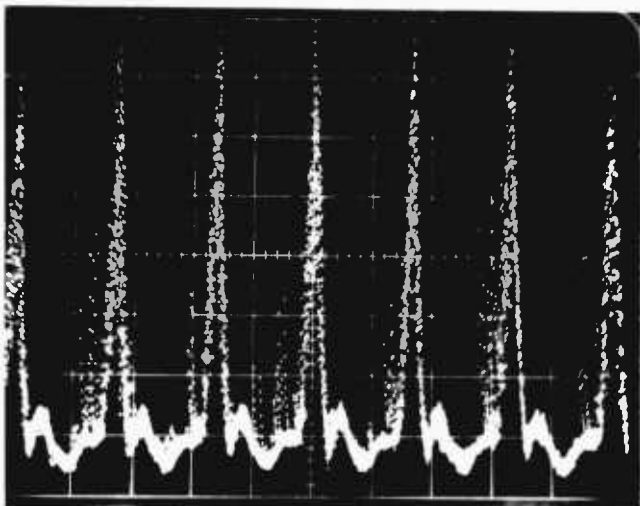
MODE-LOCKING PHENOMENA WITH CONTACTED ABSORBER CONFIGURATION

TIMESCALE:

(a) 2ns/DIV

(b) 5ns/DIV

(c) 5ns/DIV



only this form of laser action was attainable. However, at sufficiently high levels, e.g. $\sim 2 \times 10^{-5} \text{M}$, it was possible to progress from threshold through one to five pulses in a group with each stage separated by $\sim 150 \text{ mW}$. With increasing absorber strength, the tolerance for each section increased until at working solutions ($\sim 10^{-4} \text{M}$) the single pulse region was $\sim 700 - 800 \text{ mW}$ in extent.

Similarly for the shorter cavity the single and double pulse situations were present under normal conditions depending on pump power. Tuning of the laser away from the strong mode-locking regime for DODCI (590 - 620 nm) produced similar phenomena as a reduction in dye concentration.

The existence of two distinct modes of operation depending on the distance of the active medium from the cavity end mirror may be attributed to the degree of gain saturation. When the Rhodamine 6G was far away from M_4 , the combination of the rapid recovery of the DODCI solution ($\sim 300 \text{ ps}$) and the absence of gain saturation made long pulses possible in which components were selected by the absorber. However, it is not clear as to why this form of mode-locking was favoured as opposed to just a greater number of equally spaced pulses experienced with shorter cavities.

4.6b Pulse Durations

Pulses from a passively mode-locked Rhodamine 6G laser employing contacted absorber and amplifier dye cells were measured by O'Neill⁴² to be $\sim 4 \text{ ps}$ using the electron-optical streak camera. For a dye cell of similar thickness (0.5 - 0.6 mm) the pulse durations in this work were reduced to a minimum of $\sim 1 \text{ ps}$.

As anticipated from the results of 4.6 a, two equally spaced

pulses were generated at a DODCI concentration of $0.4 \times 10^{-4} \text{M}$ when the jet-mirror (M_4) double transit time was $\sim 2.6 \text{ ns}$. The corresponding second harmonic traces (with the high dispersion Double Extra Dense Flint prism) indicated pulses of $\sim 10 \text{ ps}$ and were of contrast ratio 2:1 implying structured pulses. Examples of these are shown in Figure 22 but the associated spikes were not fully recorded due to imperfect overlap of the interferometer⁷³. The spike was difficult to observe if the laser was not in the fundamental (0,0) mode. Adjustment of the dye cell generally improved the laser stability and beam quality.

In the single pulse region ($0.6 \times 10^{-4} \text{M}$, $\sim 600 \text{ nm}$) durations of 3.5 - 5 ps were measured for different cavity alignments. A second harmonic trace for a dye concentration of $0.8 \times 10^{-4} \text{M}$ with the laser being pumped 100 mW above threshold (1.4W) and tuned to 609 nm is shown in Figure 23. The pulse halfwidth of 3.6 ps was calculated assuming a sech^2 intensity profile. The smoothness of the trace is an indication of the overall stability of the mode-locked laser and in particular the stability of the pulse duration on a timescale of $\sim 10^{-2} \text{ s}$ as determined by the chart recorder response time. Plate 10 shows the amplitude stability of the mode-locked laser on a $\sim \text{ms}$ timescale. Isolated pulses were deduced from the contrast ratio of 3:1 in Figure 23 and the absence of wings and background on the trace. The average second harmonic signal was a useful diagnostic tool for both the optimum pumping power and cavity alignment. With the crystal perfectly phase-matched, a decrease in the pulse duration was clearly seen as an increase in the UV detected.

Further strengthening of the absorber concentration to $\sim 2 \times 10^{-5} \text{M}$ reduced the pulses to the 1.4 - 2.5 ps range at which level the threshold

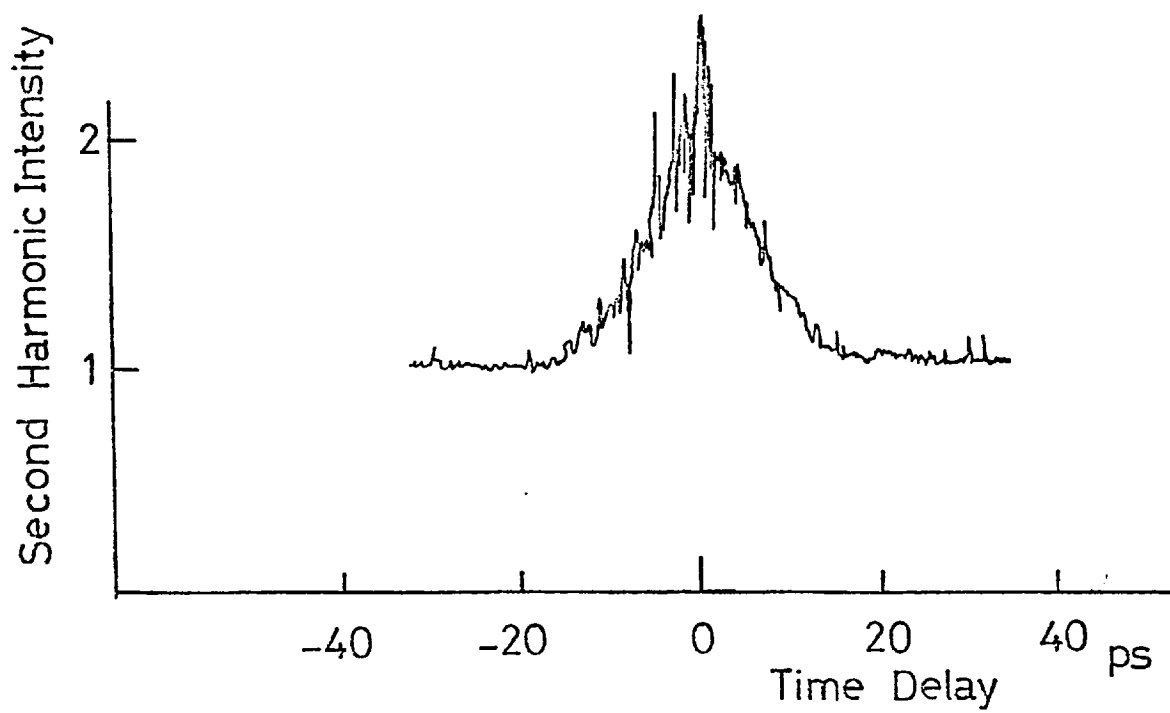
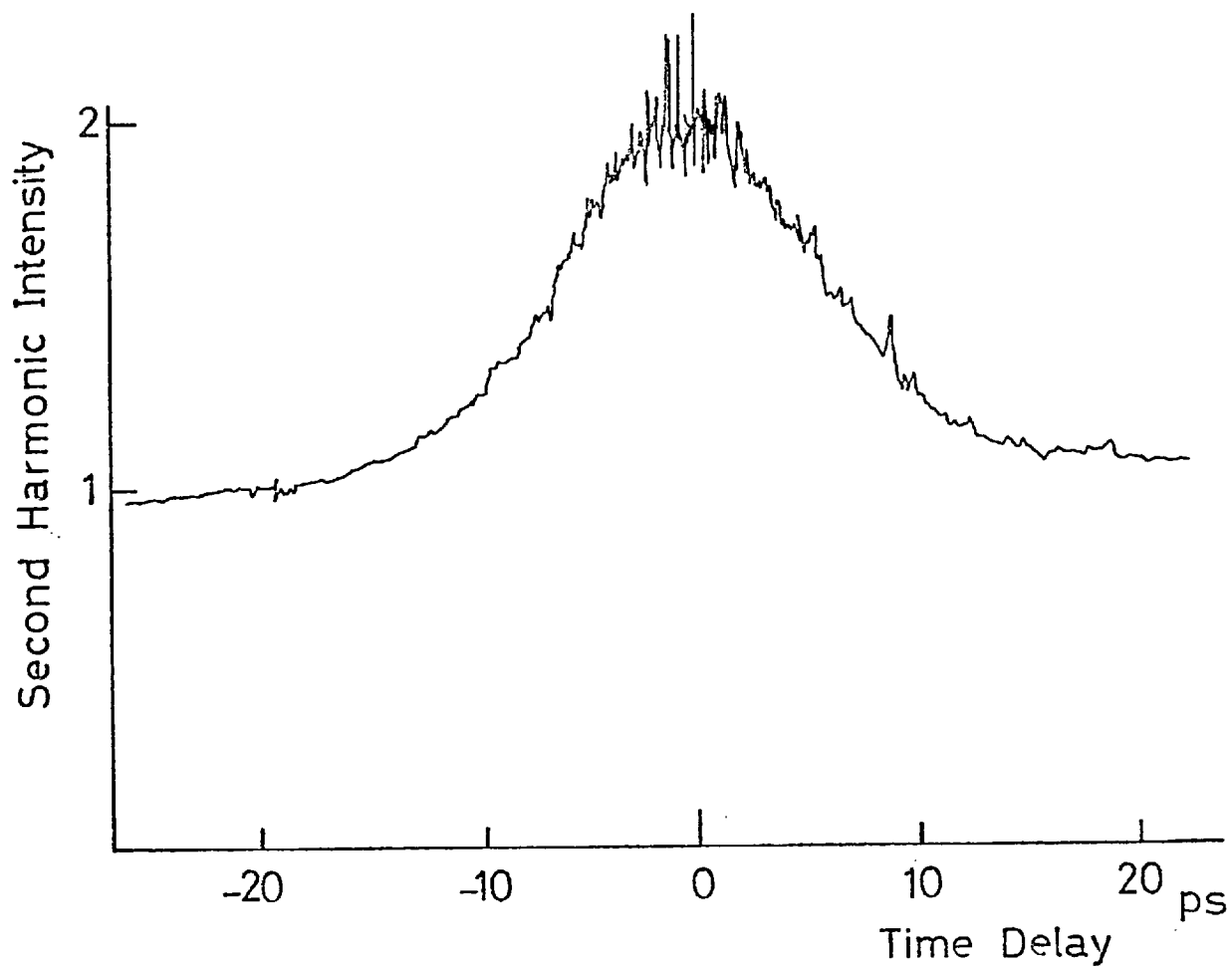


FIG: 22

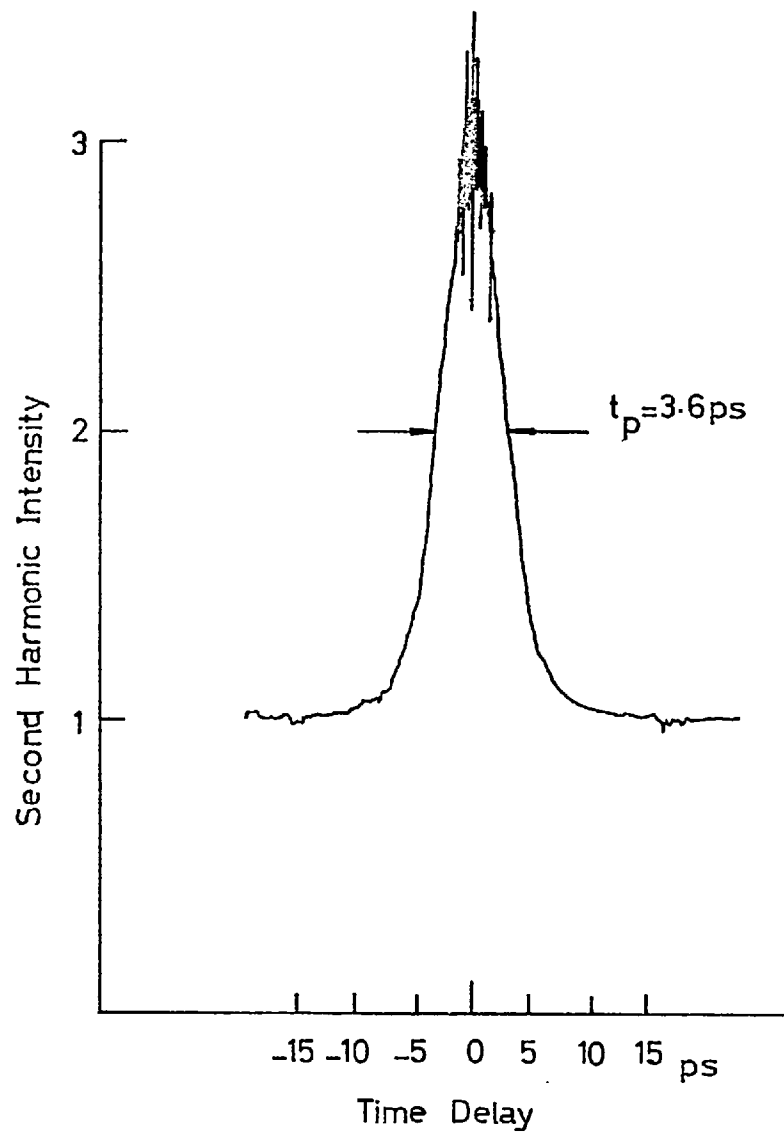
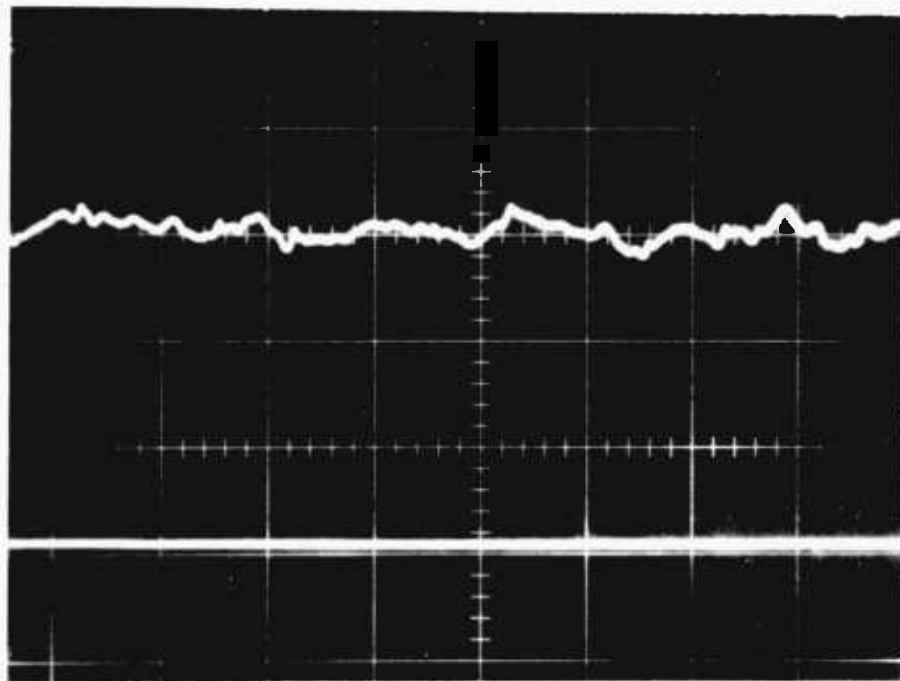


FIG: 23

PLATE 10

AMPLITUDE STABILITY OF MODE-LOCKED C.W. DYE LASER

TIMESCALE: 10ms/DIV



was ~ 3.8 W. However, the pump level could be increased to ~ 0.6 W above threshold maintaining the pulses in the 2 - 3 ps region. At the lower concentrations, short pulses were only obtained within ~ 0.2 W above threshold.

The dependence of the pulse duration on DODCI strength is shown in Figure 24 for the series of results described above. At the highest dye concentration (2×10^{-5} M) the pumping power required, ~ 4.5 W, was the maximum available on the 514.5 nm line of the Model 170 ion laser. The actual dependence of pulse duration on concentration is significant only for a particular cavity alignment but these results serve to illustrate for a fixed set of parameters the gross dependence on, and the effect of the dye. At this optimum level, corresponding to a small signal transmission of the cell of $\sim 60\%$ at 600 nm, operation at sufficiently high powers to generate double pulsing normally gave smooth autocorrelation traces of contrast ratio 3:1 similar to those associated with single pulsing.

To observe the dependence of the pulse durations on the cavity dispersion, the DEDF prism was replaced by that of lower dispersion fused silica. Its estimated passive bandpass was ~ 11 nm compared to ~ 4.5 nm for the DEDF prism when used in the basic tuned configuration. Following the change in dispersion, the pulse durations at ~ 603 nm decreased from 1.5 - 2.0 ps to 1.0 - 1.5 ps for the jet-stream system under the same conditions. The influence of the cavity dispersion in determining the equilibrium mode-locking behaviour has been treated recently by Haus¹²¹. The bandwidth narrowing effect of the tuning element was shown to eventually offset the pulse compression to give

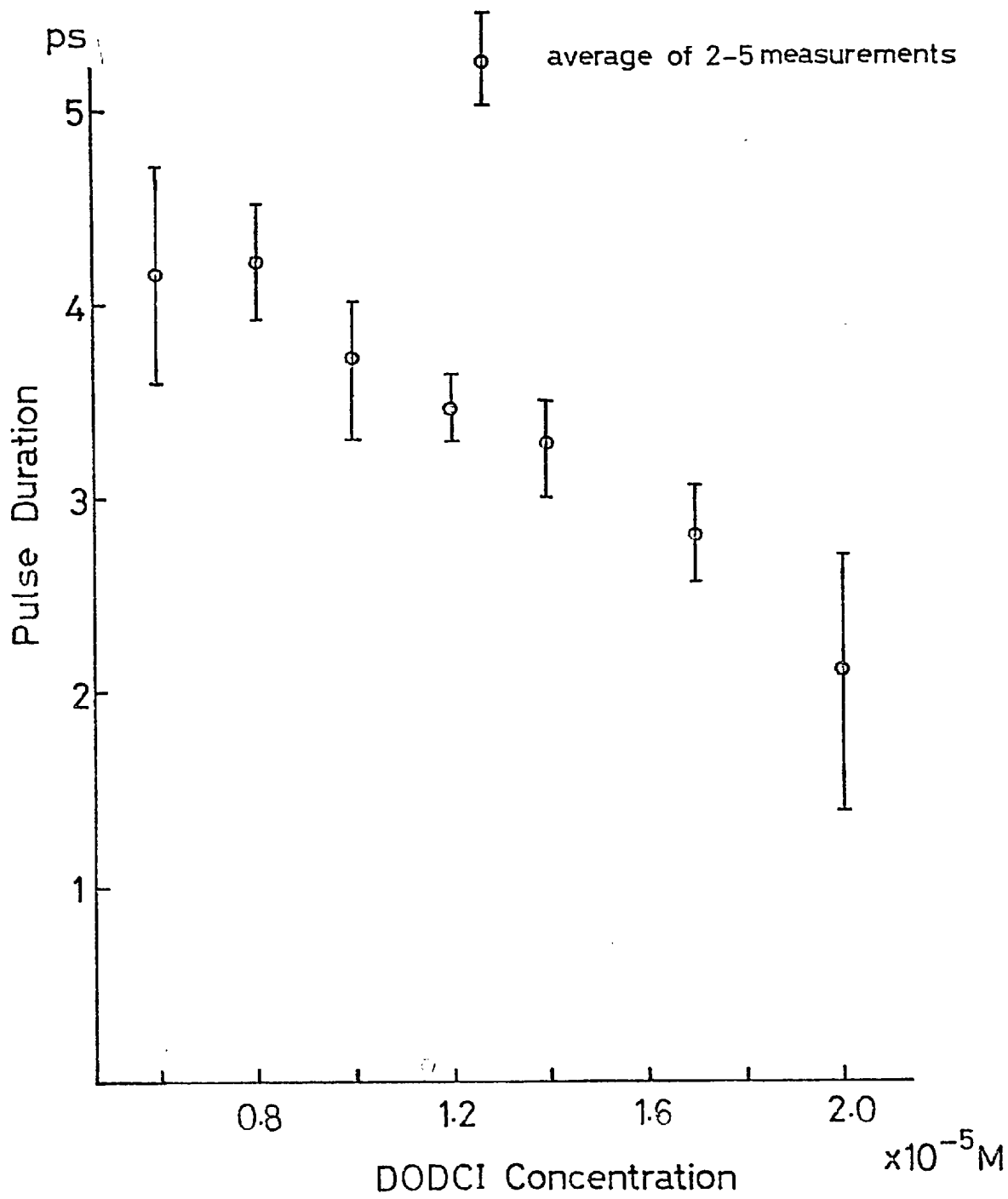


FIG: 24

a steady state pulse in the cavity. A decrease in the cavity dispersion would be expected to lead to a further reduction in the pulse width until equilibrium was once again restored. Previous modelling of the C.W. dye laser mode-locking demonstrated the mechanism of pulse shortening and predicted the parameter ranges within which pulses were generated ^{114, 122}.

Following this improvement, the fused silica prism was retained for production of sub-picosecond pulses (Section 4.6d) although the extension of the tuning range with Rhodamine B and Sodium Fluorescein had employed the DEDF prism.

The streak camera and pulse selection network outlined in Chapter 3 was used to examine the pulses in greater detail and to verify the autocorrelation measurements. Under the conditions which produced the low contrast traces e.g. poor beam quality, streak photographs similar to those in Plate 11a were recorded. The streaking speeds were 10^{10} cm.s⁻¹ and from the microdensitometer trace of Figure 25 the pulses extended over 45 ps with structure typically of 1 - 2 ps. Readjustment of the laser, usually at the absorber cell focus resulted in streaks as in Plates 11b and 11c for which high contrast second harmonic traces were associated, Figures 26a and 26b show the corresponding microdensitometer traces indicating pulse durations of 1.9ps and 0.9ps respectively, calculated using the sub-pulse spacing of 60 ps and the streak camera instrumental time resolution of ~ 1.2 ps at 610 nm for a writing speed of 10^{10} cm.s⁻¹. The latter result being the shortest pulse measured for the 0.6 mm contacted cell.

In general, pulses from the dye cell system were longer than those described above for the jet-stream. The lower efficiency of

PLATE 11

STREAKS OF THE CONTACTED ABSORBER

MODE-LOCKED C.W. RHODAMINE 6G LASER

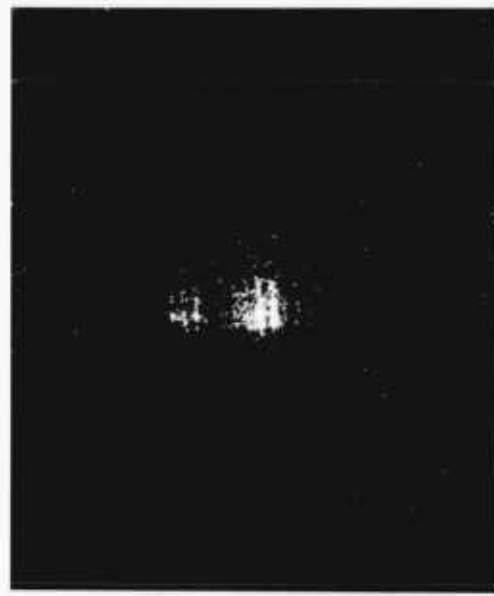
(a)

(b)

(c)

CALIBRATION: Separation of sub-pulses

- 60 ps



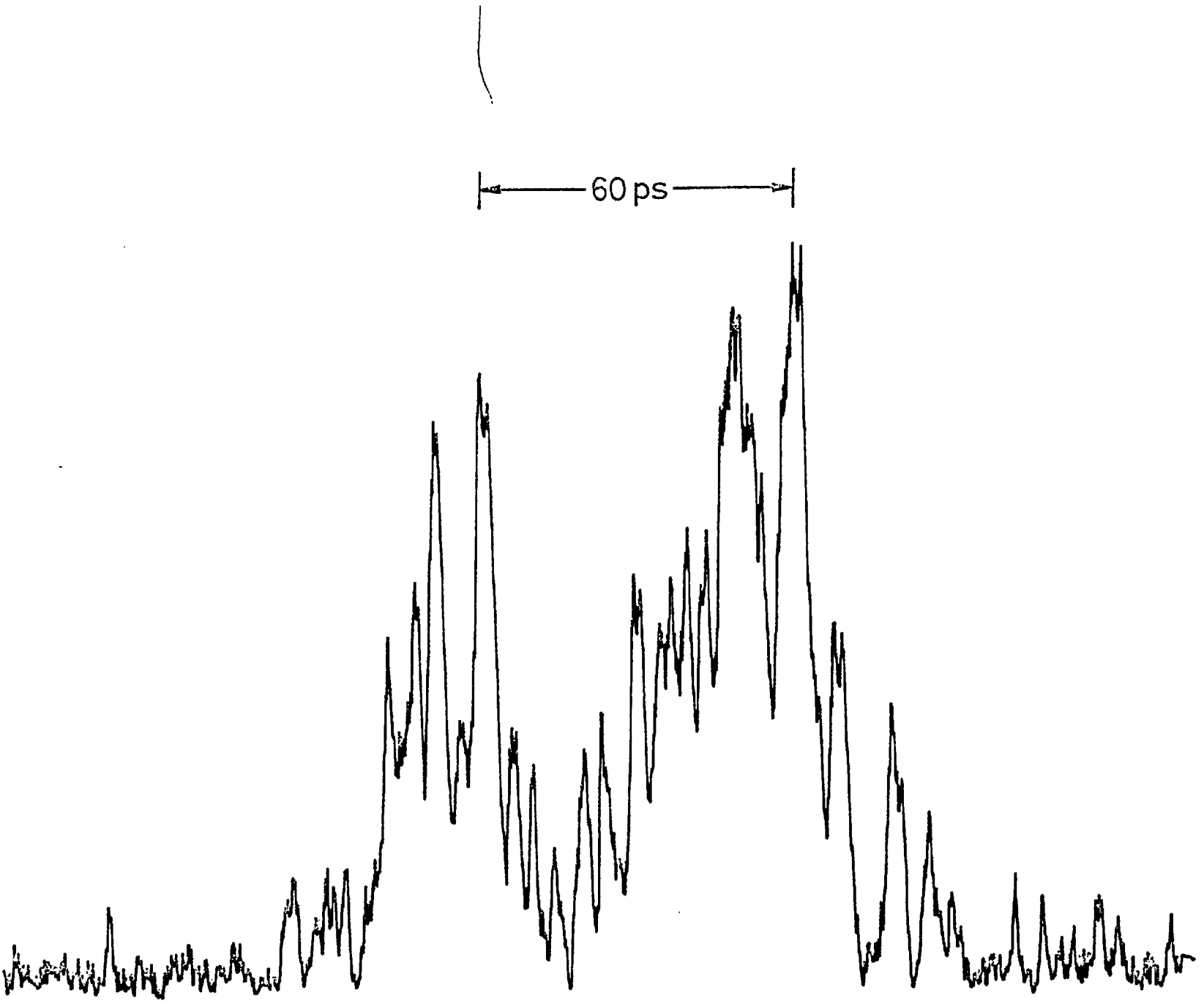
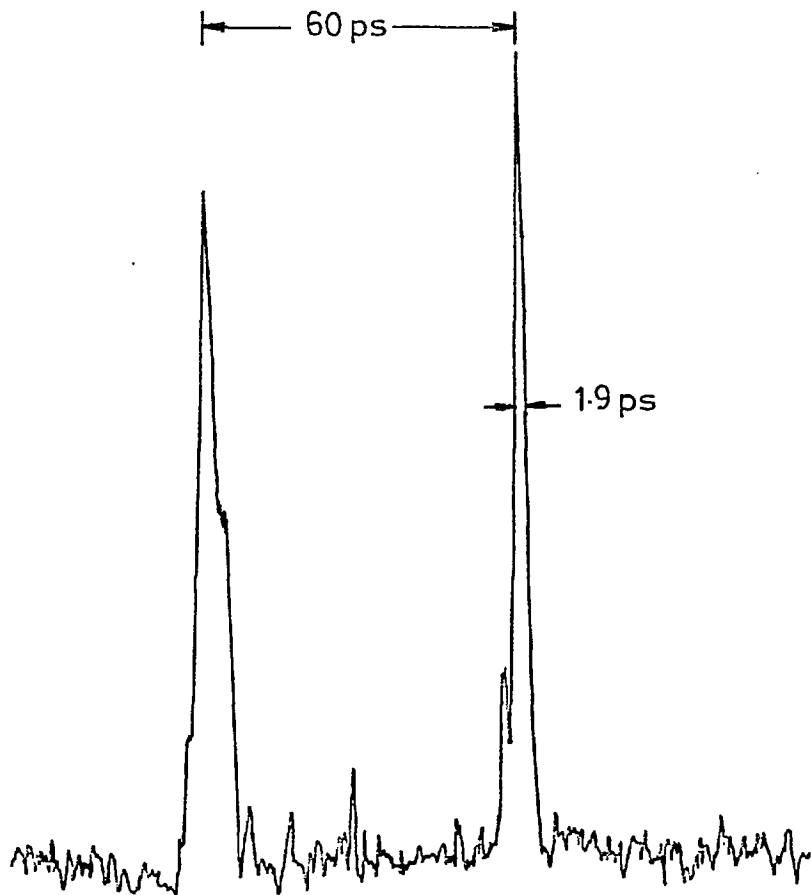
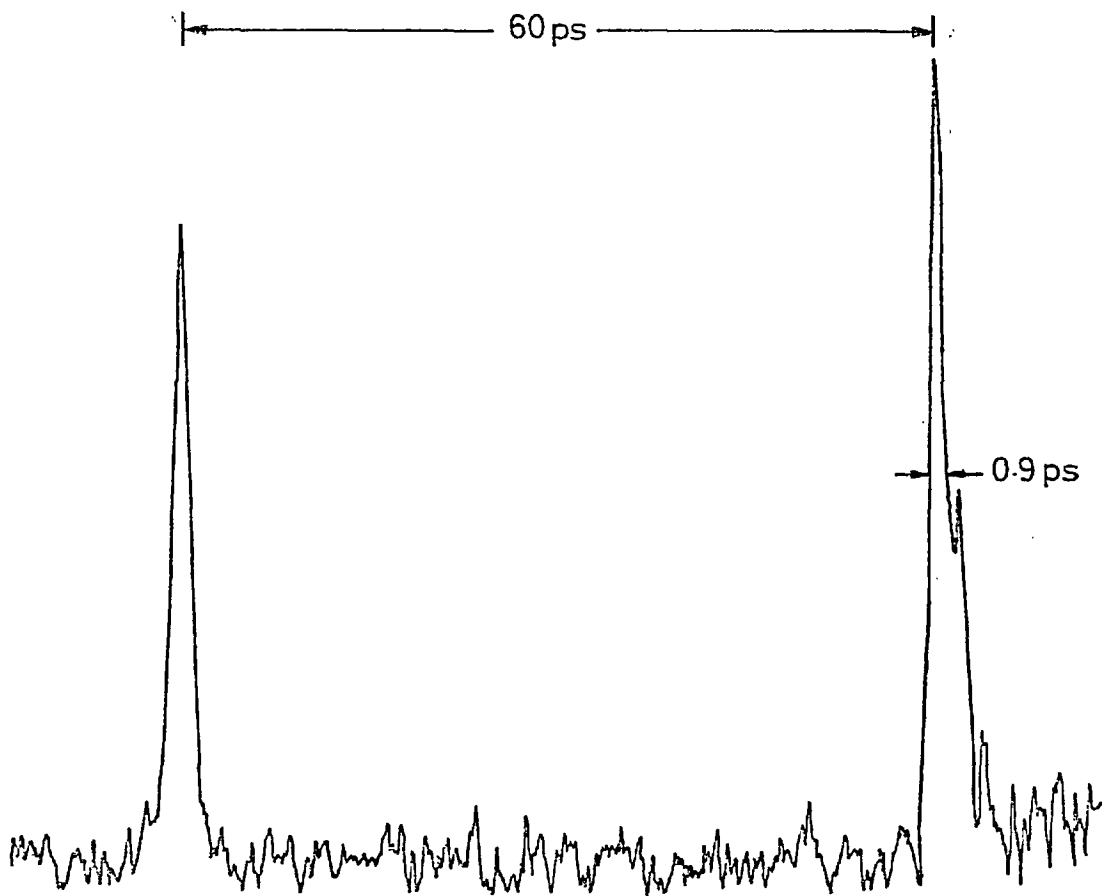


FIG: 25



(a)



(b)

FIG: 26

the cell and the lower available pumping power from the Model 164 argon-ion laser in use at that time restricted the absorber concentrations to $\sim 10^{-5}M$ producing pulses of minimum duration, 2.0 - 2.5 ps at ~ 603 nm at power levels of ~ 1.5 W. Conversion to an open flowing system reduced the pulses by ~ 0.5 ps to the range 1.5 - 2.0 ps under the same conditions (with the DEDF prism).

In the discussion of the autocorrelation method in Chapter 3 it was stressed that because of the inherent non-linearity, contrast ratios close to 3:1 would still be recorded even if a large fraction of the total energy lay outside of the main pulses. The interpulse background in a flashlamp pumped dye laser has been examined by Roddie⁸² using a streak camera. It was shown that the peak to background power was greater than 10^4 at distances removed from the pulse. Within 200 ps from the pulse on the trailing edge and 150 ps on the leading edge there was a limit to the resolution due to broadening of the streak at the high illumination intensity required. However within 15 ps of the pulse it was shown that the background was down by a factor of more than 150 and that the total interpulse energy content was less than 5% of that of the pulse. Due to the similarity in the mode-locking processes in pulsed and C.W. dye lasers it is likely that under the conditions for which high contrast traces were recorded, similar peak to background ratios existed. As the dynamic range of the camera at slower writing speeds (5×10^9 cm.s⁻¹) was ~ 10 , interpulse backgrounds of $> 10\%$ of the peak intensity would have been observable and on over-exposed streaks there was also no evidence of interpulse energy.

4.6c Pulse Shapes

In Chapter 3, it was also pointed out that by definition of the autocorrelation function deductions concerning the symmetry and the shape of pulses are open to error.

However a pulse shape must be assumed in order to calculate the pulse halfwidth and to do this the autocorrelation functions of Gaussian, Lorentzian and sech^2 intensity profiles were fitted to the experimental traces at the half maximum intensity points. An advantage with the second harmonic method is that the signal is displayed linearly whereas with the TPF technique it is normally recorded photographically.

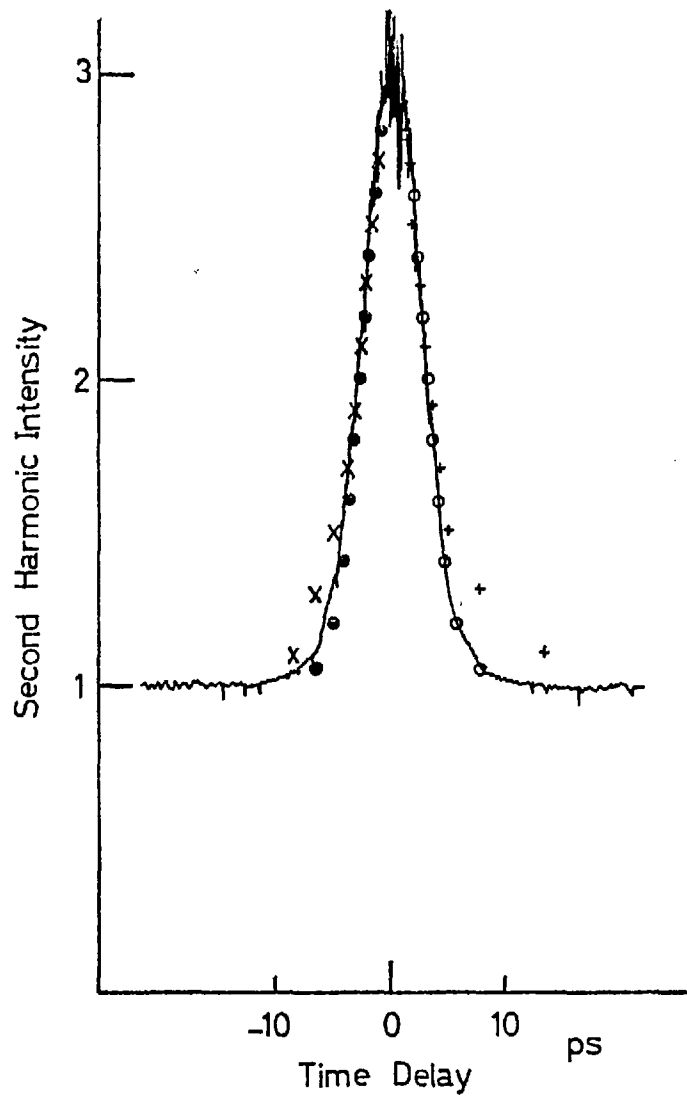
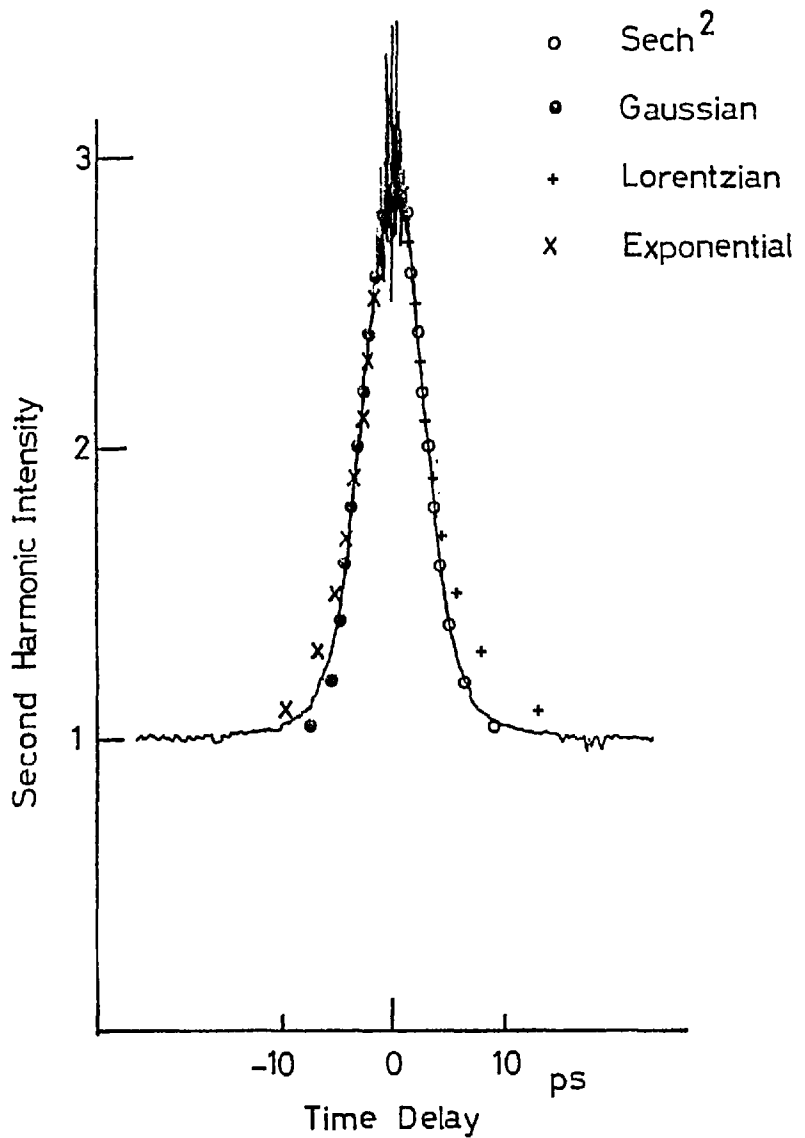
Gaussian and Lorentzian envelopes have been assumed in many cases for the deconvolution of pulses from TPF¹⁰² and streak photographs and second harmonic measurements^{9, 123}. Pulses of sech^2 intensity profile are encountered in self-induced transparency¹²⁴ and C.W. dye laser mode-locking theory¹²¹. Table 4.1 gives the autocorrelation functions $G^2(\tau)$ for four analytical pulse shapes and in Figure 27 they are fitted to second harmonic traces of halfwidth 4.3 ps and 3.9 ps. As the Gaussian, Lorentzian, Sech^2 and Exponential agree closely for $\sim 70\%$ of the trace, it is imperative that extremely accurate measurement of the second harmonic intensity is made for the longer delays in the wings. It is in this application that the background free method is useful, but as seen from the low noise traces in Figure 27, the intensity can be easily measured down to $\sim 2\%$ of the peak.

From the examples in Figure 27, the closest fit for the contacted dye cell is by the autocorrelation function for sech^2 pulses of

TABLE 4.1

Pulse profile:	$I(t)$	Halfwidth:	t_p
Autocorrelation function:	$G_2(\tau)$	Halfwidth:	$\Delta\tau_G$
<u>$I(t)$</u>	<u>$G_2(\tau)$</u>	<u>$\Delta\tau_G$</u>	<u>$\Delta\tau_G/t_p$</u>
Gaussian			
$\frac{I_0 \exp-(t/T)^2}{\sqrt{\pi T}}$	$\exp-(\tau/\sqrt{2}T)^2$	$2(2.1 \ln 2)^{\frac{1}{2}} T$	$\sqrt{2}$
Lorentzian			
$\frac{I_0}{\pi T} \{1 + (t/T)^2\}^{-1}$	$\{1 + (\tau/2T)^2\}^{-1}$	$4T$	2
Sech ²			
$I_0 \{2T \cosh^2(t/T)\}^{-1}$	$4T \frac{\cosh \tau/T - \tau/T \sinh \tau/T}{\sinh^3 \tau/T}$	$1.762T$	1.55
Exponential			
$\frac{I_0 \exp-(t /T)}{\sqrt{T}}$	$(T + \tau) \exp-(\tau /T)$	$3.35T$	2.44
Exponential (single-sided)			
$\sqrt{(2/T)} \exp-(t/T)$	$\exp-(\tau/T)$	$2T \ln 2$	2

FIG: 27



intensity $I(t)$ given by

$$I(t) = I_0 \operatorname{sech}^2 t/T$$

with pulse duration at half intensity $t_p = 1.762T$. With the contacted dye cell, the autocorrelation traces were always of this form even when of 2:1 contrast. In Chapter 5 it is shown that the second harmonic traces for the non-contacted absorber are characterized by exponential tails as in reference 77.

4.6d Generation of Subpicosecond Pulses

The shortest pulses generated directly in a passively mode-locked laser have been ~ 0.8 ps for a C.W. dye laser employing a composite dye medium. Flashlamp pumped solid state and dye lasers have produced pulses of minimum duration ~ 1.5 ps^{109, 119}. The generation of subpicosecond pulses has also been achieved indirectly by compression in a dispersive optical system, pulses possessing a linear frequency chirp. The output from mode-locked Nd: glass lasers are often far from transform-limited i.e. $\Delta\nu t_p > 1$ which has been attributed to the presence of phase modulation in the form of a frequency sweep¹²⁵. Treacy confirmed this hypothesis by crossing a TPF detector with a spectrograph showing from the tilted fluorescence tracks that the lower frequency components arrived first.¹²⁶ He also demonstrated direct temporal compression using a grating pair placed with rulings parallel such that the light leaves the system in a direction parallel to the entrance direction having been diffracted twice. Different wavelengths are diffracted by varying angles and so the transit time

increases approximately linearly with wavelength. In this arrangement, pulses from a Nd: glass laser were reduced to 0.4 ps, close to the limit set by the laser bandwidth. More recently, pulses of minimum duration 0.3 ps have been obtained by compressing chirped pulses of ~ 1 ps from a passively mode-locked C.W. dye laser⁷⁷. Alternatively the laser pulses may be chirped externally to the cavity by use of self-phase-modulation (SPM) in a medium with a large intensity dependent refractive index¹²⁷. Under these conditions a linear chirp occurs in the central region of the pulse which again can be exploited for compression. Lauberau and Von der Linde¹²⁸ succeeded in narrowing to 4 ps a 20 ps pulse from a Nd: glass laser which had a 5 cm^{-1} frequency modulation as a result of SPM in a CS_2 cell. However, indirect production of subpicosecond pulses is not always desirable or possible. For example, frequently in the Nd: glass laser the pulses are not only chirped due to SPM in the host material but also contain subpicosecond structure which prevents compression to the limit indicated by the bandwidth¹¹⁸. There may be deterioration of the laser beam quality and loss in power after telescoping and passage through the grating pair even if blazed at the correct wavelength. For the C.W. dye laser, the production of a chirp by SPM presents difficulties due to the low intensity of the pulses as focussing only produces a high intensity over a short path length. The possibility of compression by a factor of 2 or 3 has been demonstrated¹²⁹ by coupling the laser output to a 1m optical fibre filled with CS_2 . At the small beam waist created, the resulting power density of $\sim 2.6 \times 10^7 \text{ W.cm}^{-2}$ was sufficient to produce several interference peaks in the laser spectrum.

To avoid the use of such indirect methods, the possibility of the direct generation of subpicosecond pulses was investigated using an adjustable gap contacted dye cell. In Section 4.6a it was pointed out that in the dye laser mode-locking theory of Haus¹²¹, the steady state pulse duration was determined by the cavity dispersion. Hence to reduce the pulse widths below this value either the pulse compression or the tuning element parameters must be adjusted. Changing the prism was shown to shorten the pulses from 1.5 - 2.0 ps to 1.0 - 1.5 ps. Similarly by changing the path length in the dye cell, the pulse durations decreased to the subpicosecond range in agreement with earlier work on the Nd: glass laser¹¹⁷. The theoretical analysis of Bradley et al¹¹⁷ for the passage of a pulse through a thin contacted dye cell was based on the maximum emission principle as first introduced by Statz et al¹³⁰ and applied to mode-locking by Garmire and Yariv¹²⁰. Alternatively a simpler view of the role of the saturable absorber in the shaping of the leading edge of the pulse may be taken.

In the initial stages of the mode-locking build-up there is an advantage with a contacted cell when its length is short compared to the pulse in addition to that gained in the intensity at the mirror surface. As has been observed experimentally¹³¹ a long recovery time saturable absorber, such as DODCI, selects a portion of the noisy cavity radiation (50 - 100 ps). On transit through a thin contacted cell (0.5 - 1.0 mm) the leading edge experiences the small signal absorption of the dye for both the inward and outward passages before meeting the peak of the pulse. When the pulse has become short, the situation will arise that on the outward transit

the leading edge meets the peak in the cell and for the remainder of its journey it travels through a saturated medium. Hence with a very thin cell, there is more efficient shaping of the leading edge and depletion of the low intensity components on it. With a cell and pulse of comparable dimensions ¹¹⁷ the advantage is lost and it is then equivalent to a cell situated some distance from a cavity mirror as the dye will not have fully recovered when the pulse traverses for the second time after reflection. Due to the presence of saturable amplification in the C.W. dye laser, the steady state pulse would be less than the equivalent cell thickness and is determined by the overall balance between dispersion and pulse compression. In the Nd: glass laser, pulses of ~ 2.5 ps have been generated for a cell of $30 \mu\text{m}$ thickness ¹¹⁹ as the absorber in this case is responsible both for the selection and pulse compression.

In this work, a variable gap dye cell was employed, similar in most respects to that of 0.6 mm thickness described in Section 4.5 except the window and mirror were attached to sleeves sliding within one another. Rotation of an outer threaded sleeve adjusted the width of the channel in the dye cell. Calibration was achieved by closing the cell until the window and mirror made contact with a strip of Melinex (thickness $\sim 2\mu\text{m}$) from which any desired cell length could be set to within $10\mu\text{m}$.

With the cell initially at ~ 0.5 mm, pulses of 1.5 ps were measured at 609 nm for a DODCI concentration of $2.4 \times 10^{-5}\text{M}$. Narrowing the cell and simultaneously increasing the absorber concentration to maintain the same low-level transmission reduced the pulse durations until at a gap of 0.2 mm they were 0.7 ps. Further cavity adjustments

resulted in minimum durations of 0.3 ps being measured. The pulses increased to ~ 1 ps when the cell was further narrowed due to poor dye flow through such a thin channel.

The stability of the pulses at 0.3 ps was such that the variation over periods in excess of an hour was ~ 0.1 ps. Also the pulse durations did not depend strongly on input power. Pulses of 0.3 - 0.4 ps were generated at up to 25% (0.6W) above threshold (2.4W). At higher pumping powers they broadened to ~ 1.5 ps and became less stable. Average output powers coupled out of the cavity by the plane mirror of transmission $\sim 5\%$ at 600 nm were e.g. 15 mW for pulses of 0.5 ps, giving peak pulse powers of ~ 300 W. In this case the laser was operating at 605 nm with a DODCI concentration of 5×10^{-5} M and was pumped at 2.9W with a threshold of 2.5W. The tuning behaviour of the subpicosecond pulses and the mode-locking of Rhodamine 6G with other saturable absorbers are given in Section 4.6f.

Second harmonic traces of subpicosecond pulses are shown in Figure 28 with halfwidths 0.3ps and 0.5ps.

4.6e Spectral Characteristics

In addition to the temporal measurements, it was also essential to establish the laser bandwidth to determine the degree of mode-locking and coherence of the pulses. Coherent pulses for which the pulse duration and spectral bandwidth bear a fixed relationship to one another, by virtue of the Fourier transform, find application in the studies of the interaction of light with matter such as coherent photon response¹³², self-induced transparency¹²⁴ and photon echoes¹³³. Before discussing the experimental results pertaining to the C.W. dye laser, the

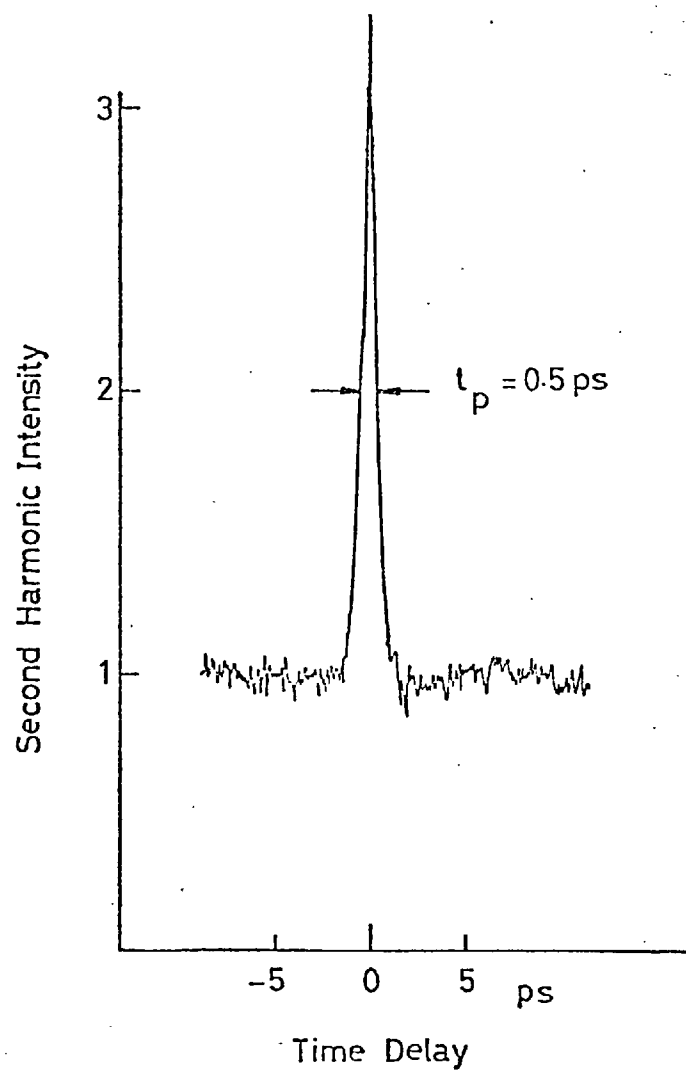
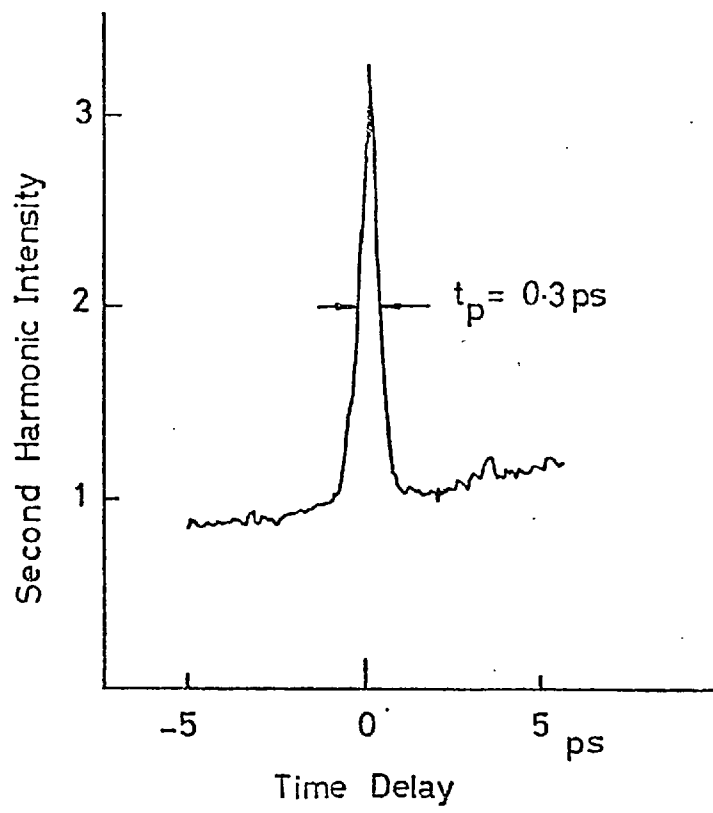


FIG:28

TABLE 4.2

<u>Pulse Profile</u>	<u>$\Delta\omega \cdot t_p / 2\pi$</u>
Gaussian	0.44
Lorentzian	0.60
Sech ²	0.32
Exponential	0.14
Exponential (single-sided)	0.11

mathematical formulation of optical pulses is briefly considered.

In Chapter 3, it was shown that for a perfectly mode-locked pulse the pulse duration and laser bandwidth contain the same information. By Parseval's theorem for the Fourier pair ωt , the total energy of the pulse is proportional to the area under either the temporal or spectral intensity profiles:

$$\int_{-\infty}^{\infty} I(t) dt = \int_{-\infty}^{\infty} i(\omega) d\omega$$

where $I(t)$ and $i(\omega)$ are the intensities in the temporal and spectral domains respectively. Hence, for a particular pulse profile, a corresponding spectral distribution exists such that the product of the full widths at half maximum intensity is a constant given by

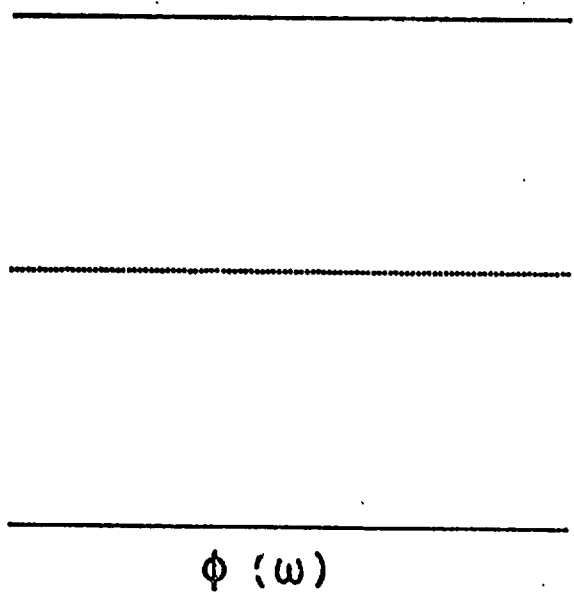
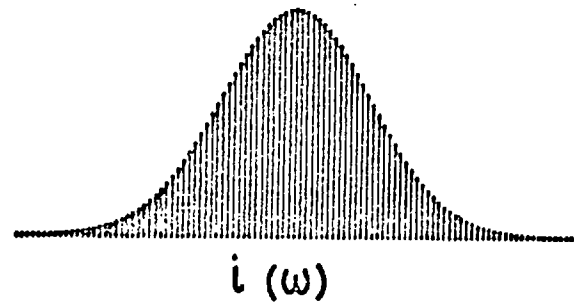
$$\Delta\omega t_p = 2\pi K$$

A laser pulse which satisfies this condition is said to be transform limited and Table 4.2 contains the theoretical values of $\Delta\omega t_p / 2\pi$ for simple analytical pulses including that for the sech^2 intensity profile fitted to the autocorrelation traces.

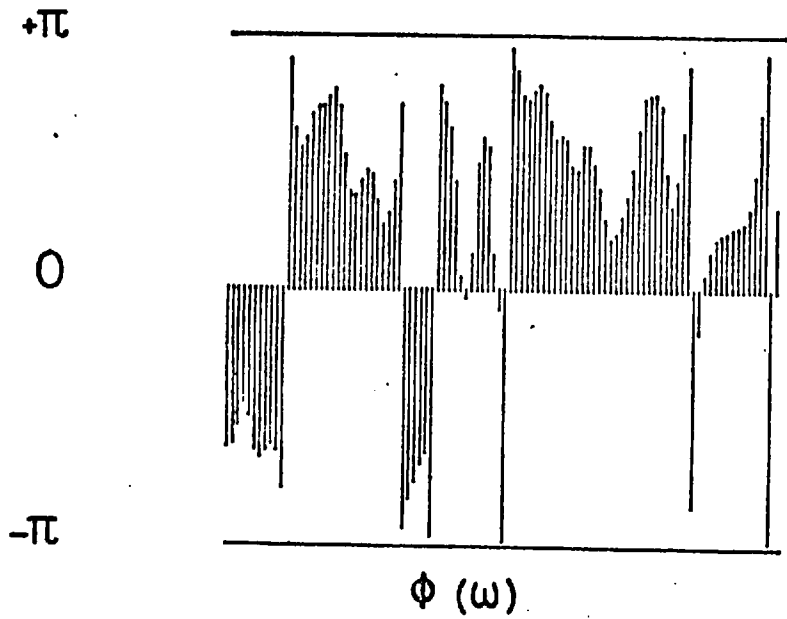
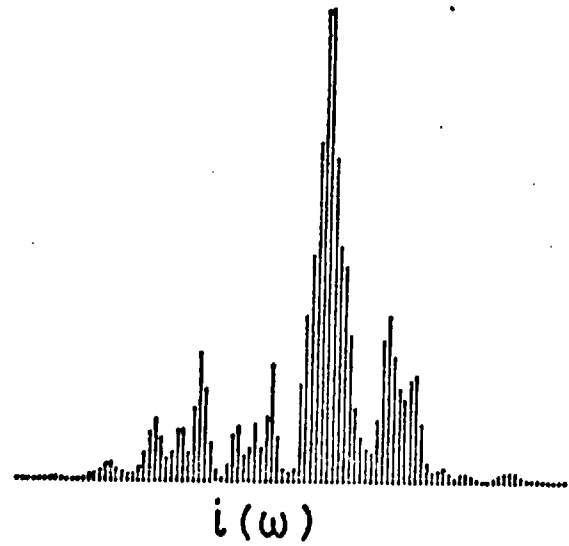
The spectrum of the ideally mode-locked laser is shown in Figure 29a in which the spectral amplitudes and phases are in a fixed relationship to each other. Figure 29b is a simulation of the situation arising in a partially mode-locked pulse in which structure is present as frequently occurs in the Nd: glass laser^{134,135}.

As anticipated with the addition of the DODCI, the creation of a stable pulse train was accompanied by spectral broadening.

FIG: 29



(a)



(b)

PLATE 12

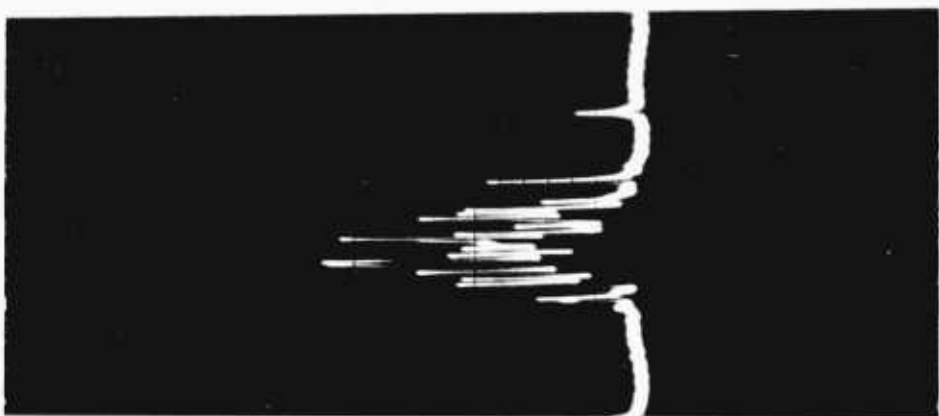
SPECTRA OF MODE-LOCKED C.W. DYE LASER

(a) Ethanol only flowing in the absorber dye cell.

(b) DODCI Concentration - $0.6 \times 10^{-5} \text{M}$

(c) DODCI Concentration - $0.8 \times 10^{-5} \text{M}$

CALIBRATION: 0.6 nm per major division



The development of the spectral broadening with concentration is illustrated in Plate 12 showing a series of spectra recorded with the scanning Fabry-Perot etalon of 1.5 nm free spectral range during the build-up of mode-locking presented previously in Plate 8. The laser linewidth increased from the C.W. value of 0.08 nm to ~ 0.6 nm for single pulses. With the 0.6 mm contacted cell, the bandwidth-pulse duration product, $\Delta\nu t_p$ was ~ 1 in the region of strongest mode-locking. Figure 30 and Plate 12c show a second harmonic trace for pulses of 3.6 ps and the corresponding spectral halfwidth of 0.4 nm. In this example the $\Delta\nu t_p$ product was ~ 1.2 and represents laser operation within a factor of 4 of the transform limit (0.32).

Along with the significant improvement in pulse duration brought about by the reduction in the cell thickness, the simultaneously recorded spectra indicated that the mode-locking was approaching the ideal case. For the subpicosecond pulses in the range 0.3 - 0.9 ps the $\Delta\nu t_p$ values were 0.4 - 0.8. The spread in these results was due to adjustments in the laser cavity and as with pulse duration was not a function of pump power. For example, at 605 nm, with pulses of 0.4 ps a bandwidth of 1.36 nm was measured at 25% above threshold. The corresponding $\Delta\nu t_p$ product was 0.45.

The greater linewidth associated with the subpicosecond pulses was recorded with the 1m spectrograph on Ilford HP4 plates which were later microdensitometered. Calibration of the exposed plates was achieved by covering part of the spectrograph entrance slit by a neutral density filter of 50% transmission to give a simultaneous indication of the spectral width at half maximum.

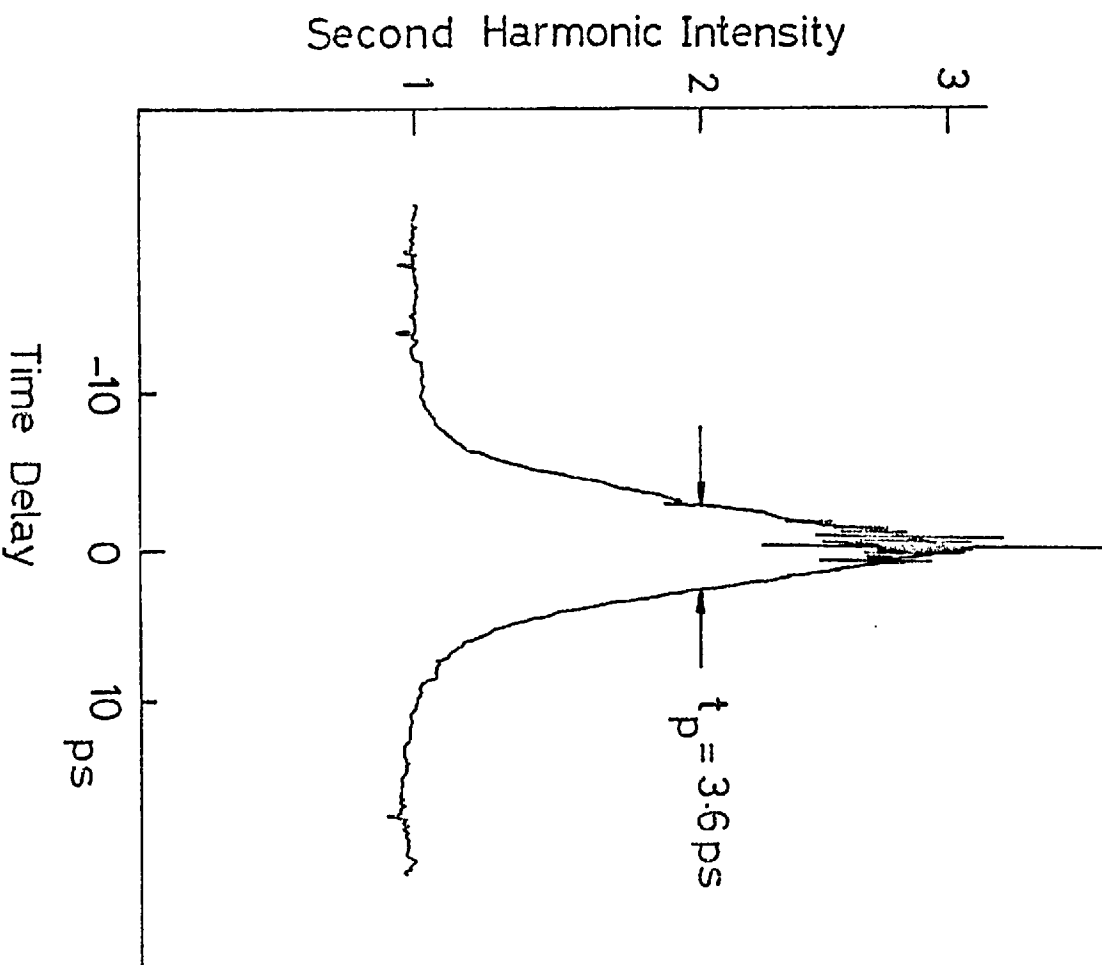


FIG:30

The second harmonic and spectral microdensitometer traces for pulses of 0.5 ps are shown in Figure 31 to which is also fitted the theoretical autocorrelation function (discrete points) for sech^2 pulses. The bandwidth-pulse duration product, $\Delta\nu t_p$, was in this example also 0.45. At higher pumping levels or at poor alignment when pulses of 1 - 1.5 ps were generated, the mode-locking remained close to the transform limited case with $\Delta\nu t_p$ in the 0.7 - 0.9 range.

The coherent subpicosecond pulses characteristic of the contacted absorber cell configuration contrasts with the chirped pulses of ~ 1 ps and spectral linewidth ~ 2.0 nm reported recently⁷⁷. The experimental arrangement used involved a non-contacted absorber in the form of a second free-flowing jet-stream and an acousto-optic cavity dumper.

With a view to quantifying the effects of the various pulse broadening and frequency chirping mechanisms present in the laser cavity the passage of a pulse through the resonator components is discussed for normal group dispersion, transverse group dispersion at a refracting surface and self-phase modulation arising from the intensity dependence of the laser media refractive index.

Mode-locking in the presence of group dispersion effects has been investigated by numerous authors^{120, 136} and they have shown that this can account in part for the magnitude of the observed frequency sweep in some solid-state lasers¹²⁵. To estimate the likely contribution of linear dispersion to the pulse duration in the C.W. dye laser, it is worthwhile considering the influence on an ideally mode-locked pulse of bandwidth e.g. 1.0 nm, oscillating in a cavity containing a 1 cm. path-length of fused silica.

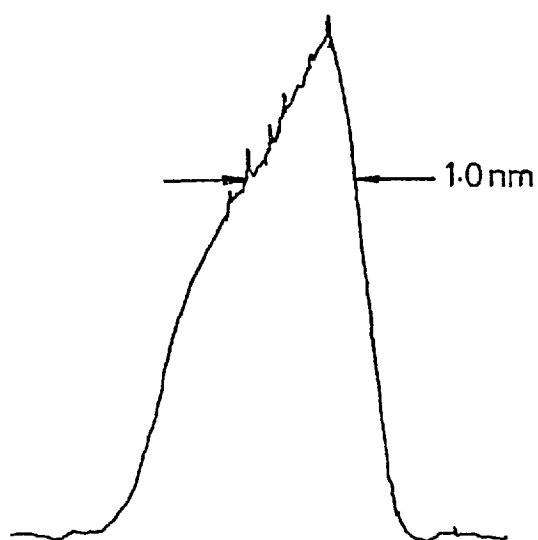
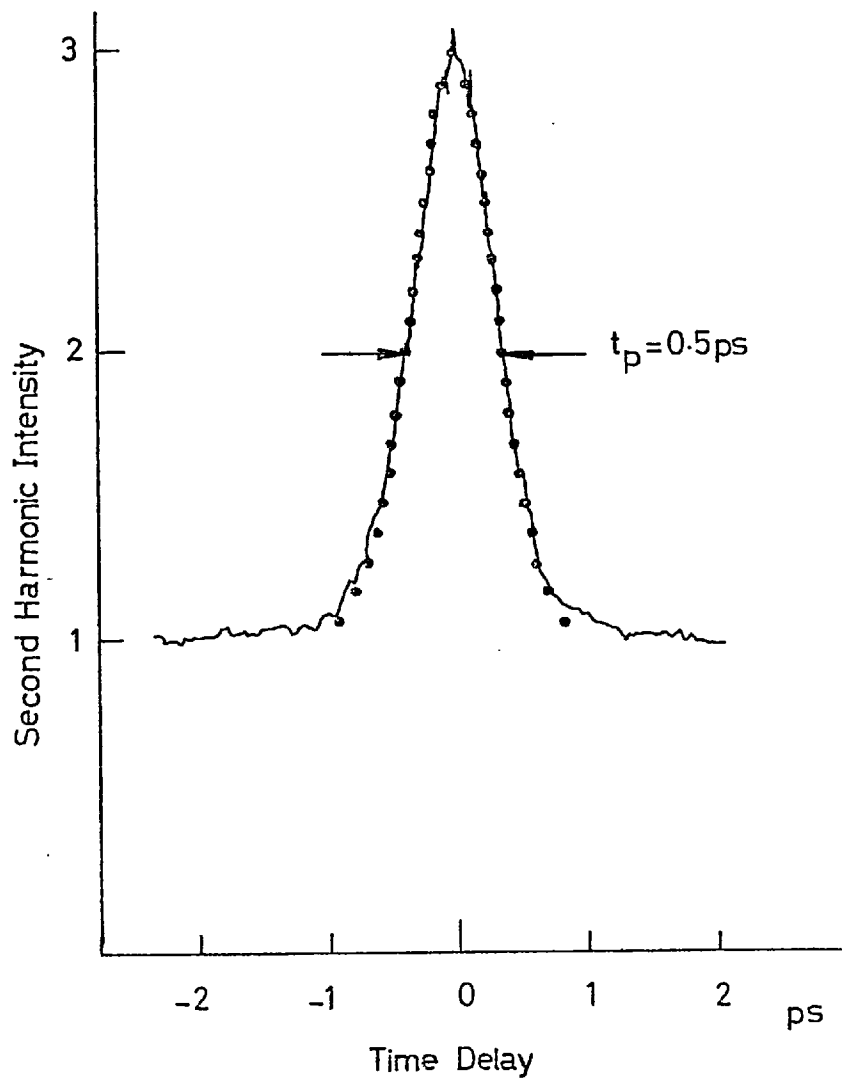


FIG:31

Following the analysis of Cubeddo and Svelto ¹³⁷, the laser mode frequencies can be represented by

$$\Omega_{\ell} = \Omega_0 \pm \ell\omega$$

where Ω_0 is the central mode frequency, ℓ is the mode number running from $-\infty$ to $+\infty$ and ω is the mode separation.

The dispersion of the refractive index n may be expanded as

$$n_{\ell} = n_0 + \frac{\partial n}{\partial \Omega} \ell\omega + \frac{1}{2} \frac{\partial^2 n}{\partial \Omega^2} (\ell\omega)^2 + \dots$$

After traversing a distance x in the medium, the electric field $E(t,x)$ of the beam is given by

$$E(t,x) = \sum_{\ell} E_{\ell} \exp i \{ (\Omega_0 + \ell\omega)\tau + \Phi_{\ell} \}$$

where E_{ℓ} is the mode amplitude, $\tau = (ct - n_{\ell}x)/c$ and

$$\Phi_{\ell} = -\ell\omega(\Omega_0) \frac{\partial n}{\partial \Omega} \frac{x}{c} - (\ell\omega)^2 \left\{ \frac{\partial n}{\partial \Omega} + \frac{\Omega_0}{2} \frac{\partial^2 n}{\partial \Omega^2} \right\} \frac{x}{c} \quad (4.1)$$

including a linear and quadratic term in ℓ . The phase term Φ_{ℓ} can be represented to first order in phase shifting due to dispersion by

$$\Phi_{\ell} = \alpha_0 + \alpha_1 \ell + \alpha_2 \ell^2 \quad (4.2)$$

where only constant and linear terms of Φ_{ℓ} would be present for perfect

mode-locking as they give the phase of the carrier wave and the time at which the pulse peak occurs respectively.

Considering only the quadratic term in λ , the electric field $E(t)$ can be written as

$$\begin{aligned}
 E &= A \exp \{i[\Omega_0 t + \phi]\} \\
 &= \exp(i\Omega_0 t) \left\{ \int_{-\infty}^{\infty} E_{\lambda} \exp i(\lambda \omega t - \alpha \lambda^2) d\lambda \right\}
 \end{aligned} \tag{4.3}$$

where $A = A(t)$ and $\phi = \phi(t)$ are the amplitude and phase respectively, and the sum over all modes is represented by the integral. For simplification, a Gaussian spectral distribution $E_{\lambda} = E_0 \exp -\beta \lambda^2$, can be assumed where E_0 is the maximum mode amplitude and β is related to the laser bandwidth $\Delta\lambda$ by

$$\Delta\lambda = \frac{\lambda^2 \omega}{2\pi c} \frac{2 \log_e 2}{\beta} \tag{4.4}$$

Integration of (4.3) gives for the amplitude and phase terms,

$$A(t) = \pi^{\frac{1}{2}} E_0 (\alpha^2 + \beta^2)^{-\frac{1}{4}} \exp \{-\beta(\omega t)^2 / 4(\alpha^2 + \beta^2)\}$$

$$\phi(t) = \{\alpha(\omega t)^2 / 4(\alpha^2 + \beta^2)\} - \frac{1}{2} \arctg (\alpha/\beta)$$

The above equations show that although the pulse width increases by a factor of $\{1 + (\alpha/\beta)^2\}^{\frac{1}{2}} \sim 1 + \frac{1}{2}(\alpha/\beta)^2$ the profile retains its Gaussian shape and a positive linear frequency sweep is introduced when $\alpha > 0$ as the phase will be a quadratic in t .

Using (4.1) and (4.4), α/β reduces to

$$\begin{aligned}\alpha/\beta &= \frac{2\pi^2 c \Delta\nu^2}{\lambda^2 \log_e 2} \cdot \left\{ \frac{\partial n}{\partial \Omega} + \frac{\Omega_0}{2} \frac{\partial^2 n}{\partial \Omega^2} \right\} \cdot x \\ &= \frac{\pi \Delta\lambda^2}{\lambda^2 \log_e 2} \cdot \left\{ \frac{\partial n}{\partial \lambda} \right\} \cdot x\end{aligned}$$

neglecting the second order terms in dispersion. Substitution of the relevant parameters for fused silica ($\partial n / \partial \lambda = 0.345 \times 10^{-4} \text{ nm}^{-1}$ at 600 nm) gives for a 1 cm path-length, $\alpha/\beta \sim 4 \times 10^{-3}$ assuming $\Delta\lambda \sim 1.0 \text{ nm}$.

This small amount of pulse broadening and frequency sweep is a negligible perturbation on the pulse compression even for durations as short as $\sim 0.1 \text{ ps}$. In the Nd: glass laser however, the presence of host dispersion evidently plays a much greater role in producing chirped pulses due to the broader oscillating bandwidth and the longer path-length in the rod. The above analysis for the C.W. dye laser should only be treated as an indication of order of magnitude for a single pass due to competition between the phase shifting of the dispersion and the locking brought about by the combined action of the amplifying and absorbing dyes which precludes extension to a large number of transits.

Likewise, the effect of self-phase-modulation (SPM) may be shown to be small in the C.W. dye laser. In flashlamp pumped mode-locked dye lasers, transform-limited pulses have been obtained by operating close to threshold thus reducing the power density in the dye solution¹⁰¹. The structure frequently encountered in Nd: glass lasers has been attributed to the effect of the laser gain profile on the SPM frequency broadening of the pulses¹³⁸.

For a Gaussian pulse, the total wavelength spread $\Delta\lambda$ is given by ¹³⁹

$$\Delta\lambda = \frac{0.7\lambda^2 z n_2 A_0^2}{c t_p} \quad (4.5)$$

where z is the distance of propagation in the medium, A_0 is the peak pulse amplitude and t_p is the pulse duration. The term n_2 is related to the intensity dependence of the refractive index by ¹²⁷

$$t_n \frac{\delta(\delta n(z,t))}{\delta t} = \delta n(z,t) - n_2 A^2(z,t)$$

where $A(z,t)$ is the instantaneous electric field amplitude at z and t , and δn is the intensity induced non-linear component of the refractive index ($n = n_0 + \delta n$) which has an exponential relaxation time t_n .

In a typical mode-locked flashlamp pumped dye laser operating at 605 nm, with peak power $\sim 4 \times 10^8$ W. cm⁻², broadening of ~ 0.1 nm per round trip has been observed for an ethanolic dye solution of 25 cms. in length. ¹⁴⁰ Extrapolating to the C.W. dye laser in which power densities of $\sim 10^8$ W.cm⁻² exist over the focal regions in the dyes of ~ 0.5 mm, SPM broadening is $\sim 10^{-4}$ nm per transit.

The mode-locked C.W. dye laser optical characteristics differ in a number of respects from those of the conventional flashlamp pumped system. The latter usually contains an etalon and a dye cuvette with Brewster windows and almost parallel surfaces such that the optical path is identical for all parts of the beam. The same is not true for the C.W. dye laser due to different optical path lengths for passage through the prism and the lens.

Group dispersion effects have been shown by Topp and Orner ¹⁴¹ to be significant in picosecond spectroscopy, especially transverse dispersion at refracting surfaces. Figure 32 shows the situation for a plane wavefront entering a prism. The extremes of the phase front (AB and CD) before and after the refracting surface are related by paths AC and BD which are identical for the wavefront to remain plane. Assuming that in air, the phase (v_ϕ) and group (v_g) velocities are equal, then

$$\frac{d}{c} = n \frac{x}{c}$$

where n is the refractive index and c is the velocity of light in air. Defining a group refractive index n_g analogous to n , such that $n_g = c/v_g$, gives for the difference in arrival times across the phase front CD

$$\begin{aligned} \Delta t &= \frac{1}{c} (n_g x - d) \\ &= \frac{x}{c} (n_g - n) = \frac{-x\lambda}{c} \cdot \frac{dn}{d\lambda} \end{aligned}$$

where the time dispersion for the surface is proportional to the difference in path length through the medium for different parts of the beam.

Tracing the path of the pulses around the mode-locked laser cavity shows that it is inverted after every transit of the prism resulting in cancellation of the lateral time delays such that at any instant only the effects of one or two traverses of the prism are present. For the fused silica prism with $dn/d\lambda = 0.345 \times 10^{-4} \text{ nm}^{-1}$ at $\sim 600 \text{ nm}$, the time delay across a 2 mm beam is $\sim 0.01 \text{ ps}$.

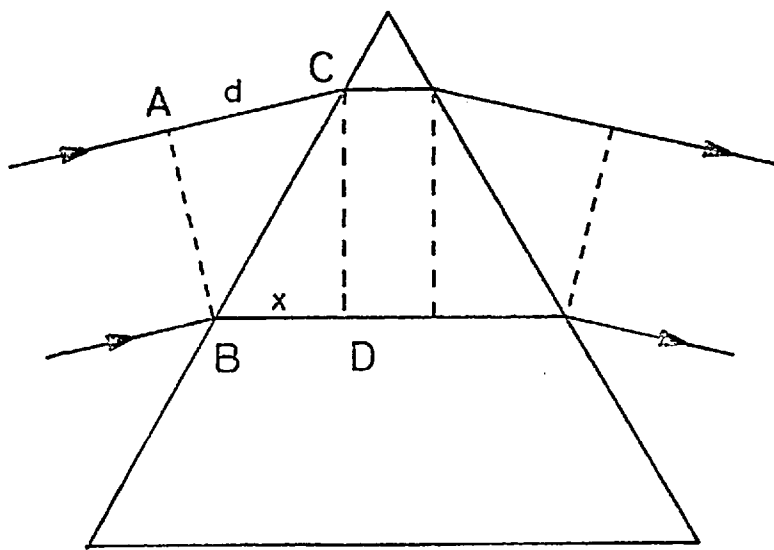


FIG:32

A similar analysis for the lens shows that although the effect does not cancel every round trip, the distortion at ~ 0.002 ps is an order of magnitude smaller.

Although the transverse group dispersion does not produce a frequency sweep as is caused by SPM and normal group dispersion in the media, the effect per transit is considerably larger. However, as it is purely a pulse broadening mechanism it is likely that its effects are compensated for by the action of the amplifying and absorbing dyes and the effect does not accumulate. The magnitude of the distortion produced by the prism suggests that shorter pulses may be more easily obtained with a low dispersion birefringent filter with parallel surfaces.

4.6f Tuning Characteristics

The subpicosecond pulses of Section 4.6d generated with the thin dye cell proved to be tunable over a broad wavelength range without significant variation in their halfwidth or power. Pulses of duration 0.3 - 0.9 ps were obtained from 598 nm to 615 nm. Outside of this region (592 - 617 nm) they increased to ~ 1.5 ps, and with the longer dye cell of 0.6 mm pulses of ~ 5.5 ps have been recorded at a long wavelength limit of 620 nm. Comparison of the performance of the two cell lengths shows as well as the reduction in pulse durations, an expected broadening of the tuning range for good mode-locking due to the stronger pulse compression with the thinner absorber. For the 0.6 mm cell, pulses of < 2 ps were not normally generated beyond ~ 610 nm whereas the long wavelength limit (for subpicosecond pulses) with the 0.2 mm cell was ~ 615 nm as already referred to. At the short wavelength extreme the difference was not so noticeable and in the region

TABLE 4.3

<u>Saturable Absorber</u>	<u>Pulse Duration and Tuning Range</u>
DQDCI	<u>0.2 mm cell</u> 0.3 - 0.9 ps (597 - 615 nm)
	<u>0.6 mm cell</u> 1.0 - 5.5 ps (592 - 620 nm)
DQOCI	<u>0.2 mm cell</u> 0.6 ps (603 nm)
	<u>0.6 mm cell</u> 1 - 2 ps (580 - 613 nm)

of 592 - 595 nm stable mode-locking was often difficult to attain. In addition, at the extremes (592 - 595 nm, 618 - 620 nm) mode-locking was only achieved close to laser threshold within $\sim 100 - 150$ mW. Above this level, multiple pulsing occurred with up to 4 - 5 equally spaced pulses oscillating in the cavity. Over the tuning range for good mode-locking it was not necessary to alter the DODCI concentration but outside of this, a reduction or increase was required to tune to the short or long wavelength limits.

Extension of the mode-locking spectrum for the flashlamp pumped Rhodamine 6G laser to shorter wavelengths (575 - 600 nm) has been facilitated by the use of DQOCI¹⁰⁸ as below 600 nm pulses of 10 - 15 ps were obtained compared to ~ 3 ps normally recorded at longer wavelengths. Similarly in the C.W. system the short wavelength limit was reduced to 580 nm using DQOCI and pulses of 1 - 2 ps were measured over 580 - 613 nm for the 0.6 mm cell thus increasing the mode-locked Rhodamine 6G tuning range by 15 nm. With the cell of 0.2 mm, subpicosecond pulses (0.6ps) at 603 nm have been observed but detailed tuning investigations have not been undertaken. An oscillogram of the DQOCI mode-locked laser is shown in Plate 13 corresponding to pulses of 1.8 ps at 602 nm. As with DODCI, the dye concentration was adjusted near the extremes of the tuning e.g. from 2×10^{-5} M at 600 nm to 3×10^{-5} M for 613 nm.

Table 4.3 summarizes the tuning behaviour of Rhodamine 6G with DODCI and DQOCI.

4.6g The Effect of Saturable Absorber Lifetime

The controversy surrounding the recovery time of DODCI was referred to in Section 4.3 and it was pointed out that bearing in

PLATE 13

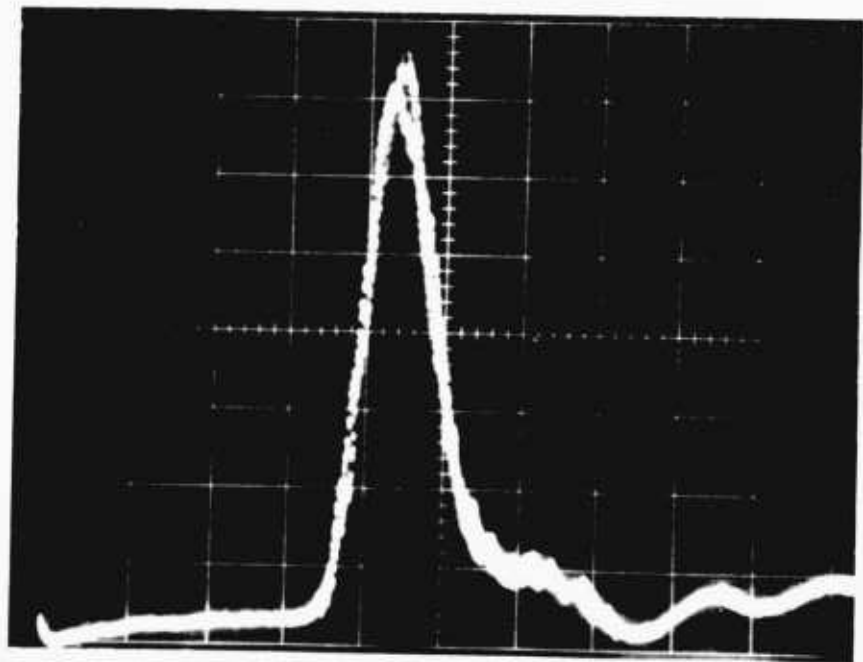
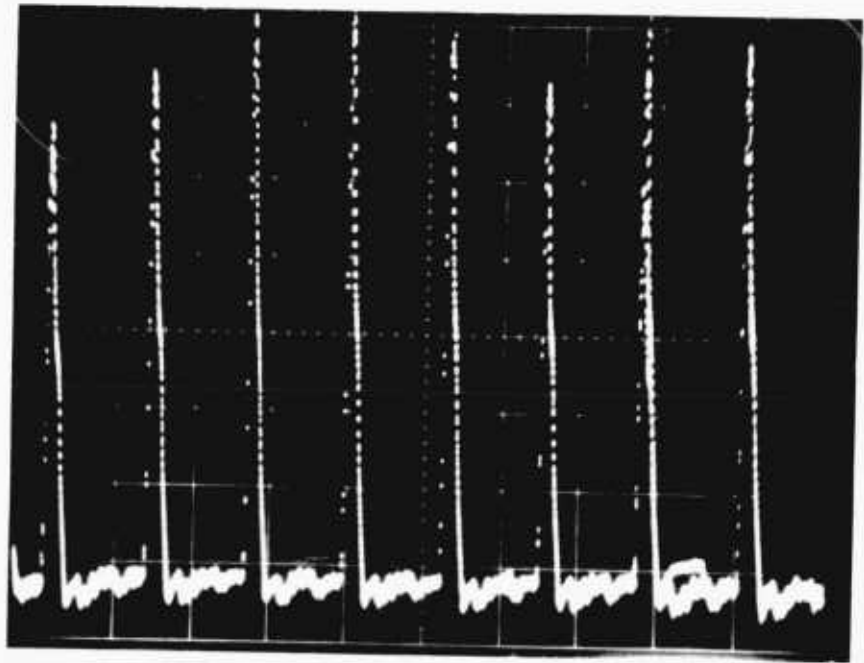
THE OUTPUT OF THE DQOCI MODE-LOCKED

C.W. DYE LASER

TIMESCALE:

(a) 10ns/DIV

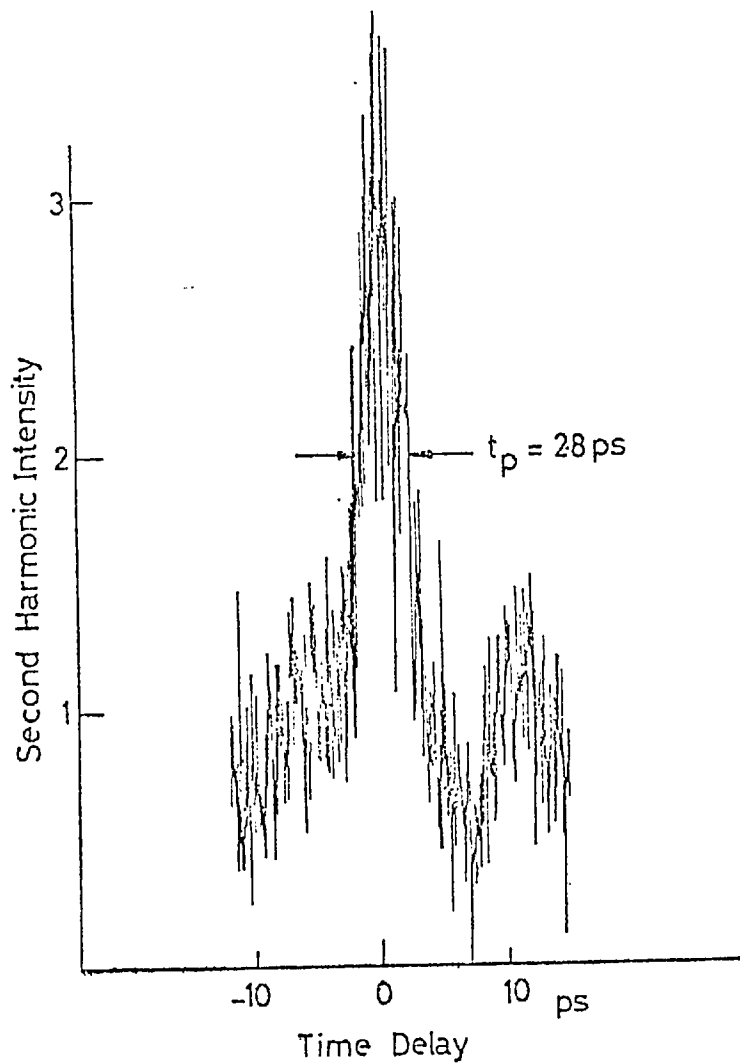
(b) 200ps/DIV



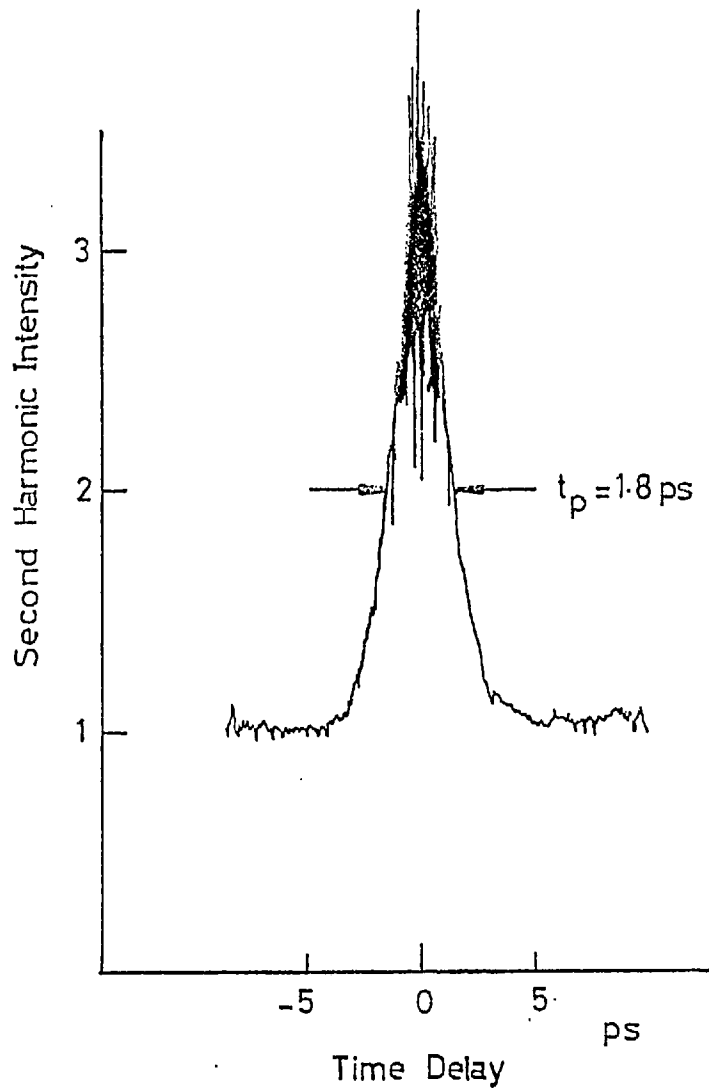
mind the different experimental methods employed, the various results are complementary. The important feature is that picosecond pulses may be produced using a saturable absorber of considerably longer lifetime ~ 300 ps. New¹¹⁴ has shown that passive mode-locking in dye lasers takes place provided certain fundamental conditions regarding the absorption cross-sections of the active and passive media are satisfied. Indeed, in a comparison of the mode-locking behaviour of solid-state and dye lasers it is apparent that in the latter, the saturable absorber lifetime plays a much smaller part in determining the steady state pulse duration. It has been demonstrated that with saturable absorbers of lifetimes $\sim 10 - 180$ ps, pulses of ~ 3 ps have been consistently recorded for a passively mode-locked Cresyl Violet Perchlorate laser whereas the same dyes generated pulses ranging from 15 ps to 105 ps when used with a ruby laser¹⁴³.

DQOCI, which has a recovery time of \sim tens of picoseconds, produced pulses of similar stability, in the C.W. laser, to those due to DODCI and from the pulse measurements of the previous section (~ 1 ps for the 0.6 mm cell, ~ 0.6 ps for the 0.2 mm cell) shows that they are independent of absorber lifetime. Both DQOCI and the DODCI photoisomer have absorption cross-sections of similar magnitude. It was interesting to note that the addition of the shorter lifetime dye to the DODCI solution when the mode-locked stability was poor resulted in an immediate improvement and a reduction in the pulse duration. The addition of DQOCI at a concentration of 1.6×10^{-6} M to 10^{-5} DODCI decreased the pulses from 2.8 ps to 1.8 ps which on further increasing the DQOCI to 1.6×10^{-5} reduced to 1.2 ps (605 nm). Second harmonic traces before and after the addition of DQOCI are shown in Figure 33. The mixed solution however did not generate

FIG: 33



(a)



(b)

pulses shorter than those obtained singly and although there was an improvement in stability there was also a reduction in the tuning range due to the presence of both dyes.

Further evidence for the independence from the absorber lifetime of the mode-locking characteristics was provided by using a Cresyl Violet Perchlorate (CVP) in ethanol solution. The measured fluorescence lifetime of CVP is ~ 3 ns¹⁴⁴ and 100% modulation of a flashlamp pumped Rhodamine 6G laser has been reported with CVP as absorber but picosecond TPF patterns were not obtained¹⁰. This was attributed to the limited number of cavity transits available for pulse compression which is expected to be slower with such a long relaxation time dye¹⁴³. In the C.W. dye laser there are an infinite number of round trips and from Figure 34 the production of short pulses is anticipated due to the magnitude and location of the CVP absorption spectrum. The presence of stimulated emission in the recovery process of CVP which can shorten the effective lifetime cannot be discounted as has been postulated for the discrepancies in the DODCI measurements.

Figure 35 shows autocorrelation traces recorded at 605 nm (cell thickness 0.2 mm) corresponding to pulses of halfwidth $t_p = 3.5$ ps and $t_p = 0.9$ ps (sech² pulses). In most respects the behaviour of this dye combination was identical to the Rhodamine 6G/DODCI system except that greater care had to be exercised in the cavity alignment. Also a long term instability in the CVP solution was apparent as the laser threshold decreased with time producing a degradation in stability and pulse characteristics. The time scale was such that at a concentration of $\sim 10^{-4}$ M, the threshold of 3W decreased to 1W

FIG:34
150

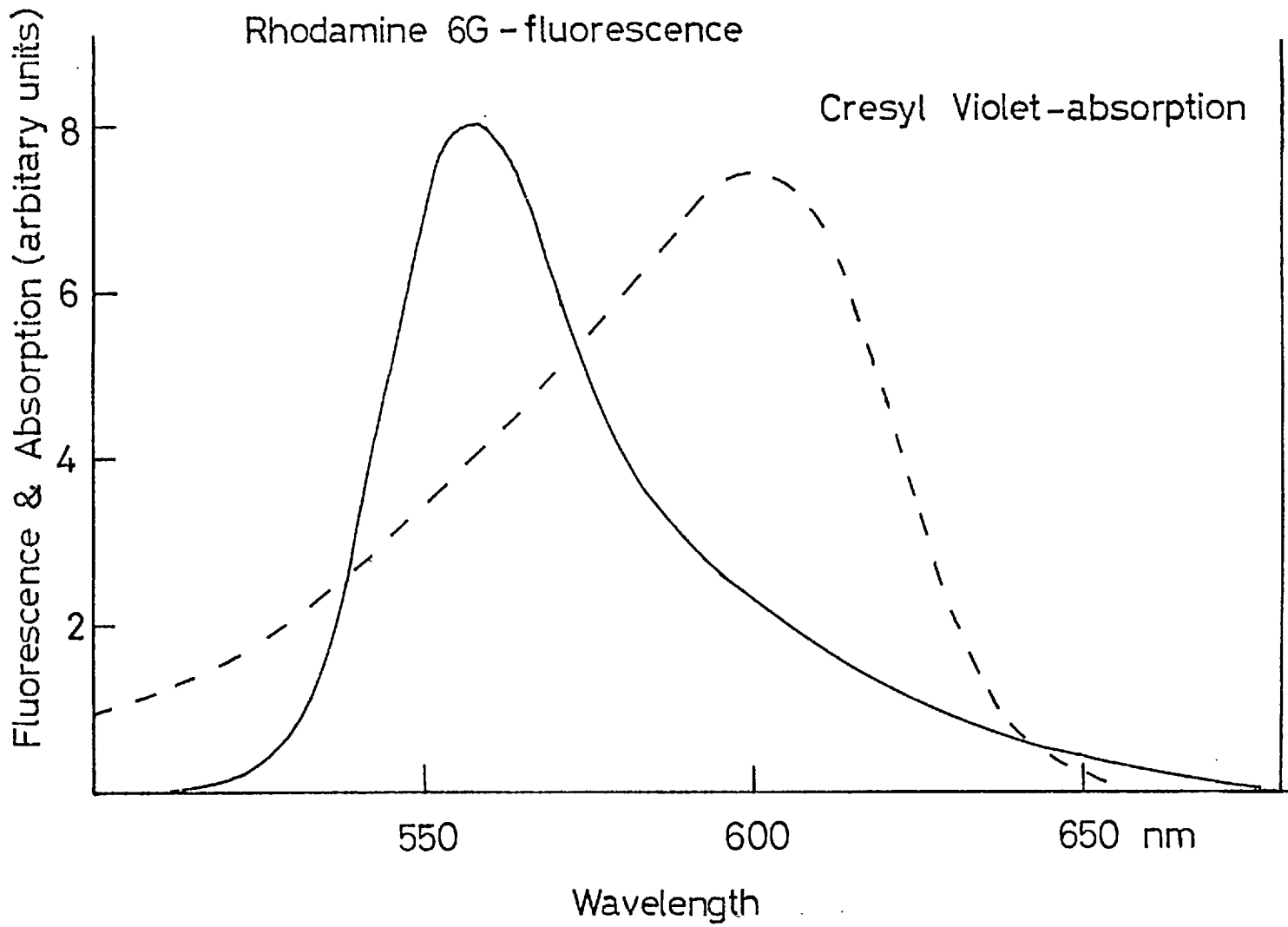
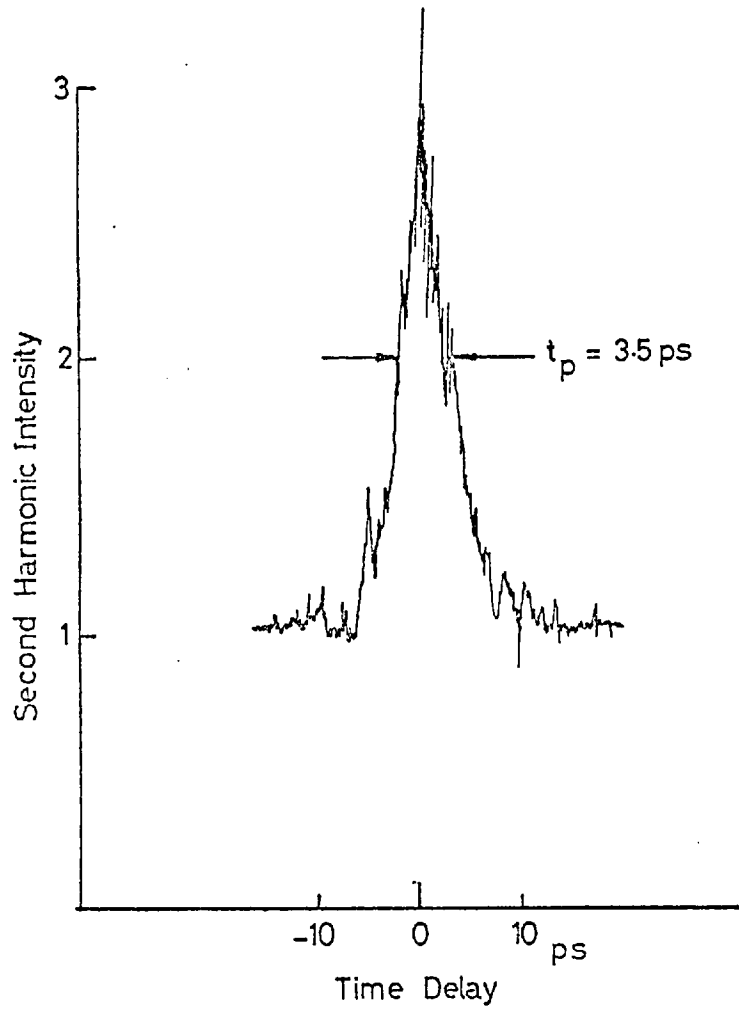
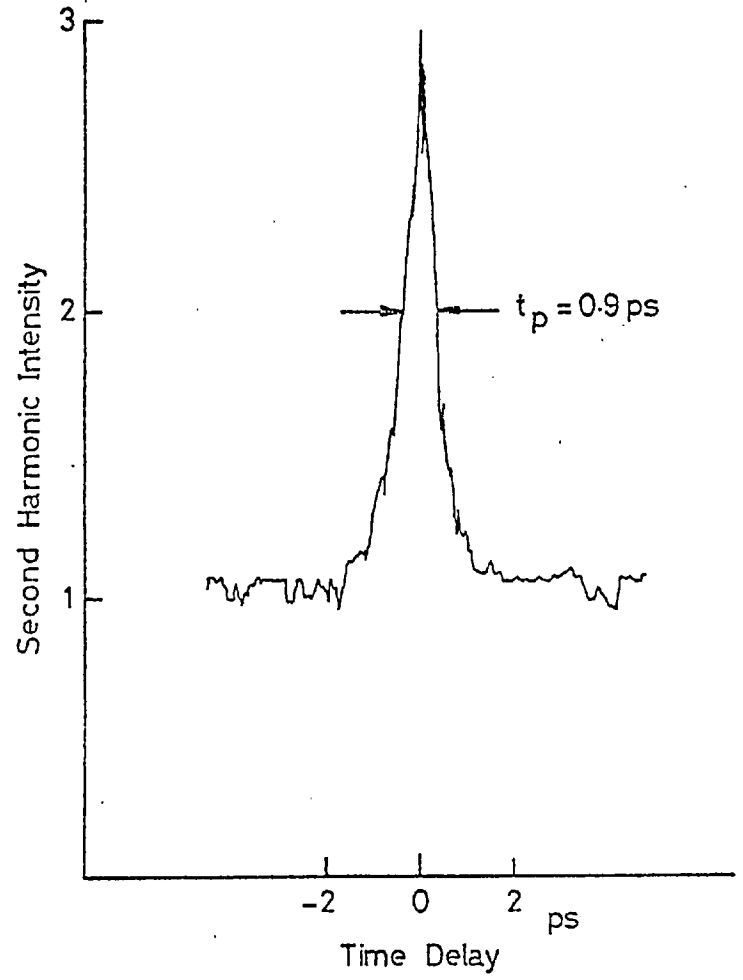


FIG : 35
151



(a)



(b)

after $\sim 1\frac{1}{2}$ hours continuous operation. This effect was also manifest in the resulting low contrast ratios of the autocorrelation measurements. Doubling the concentration raised the threshold and restored the mode-locking but eventually the same situation prevailed again. A similar instability in CVP when used as an active medium has been observed and being due to photobleaching of the molecules by the pump beam could be present under these conditions also.

4.7 Conclusion

Reliable mode-locking of the C.W. Rhodamine 6G dye laser has been demonstrated by flowing the saturable absorber in a contacted dye cell. With a low dispersion tuning element and a cell thickness of ~ 0.6 mm, pulse durations of ~ 1 ps were obtained which upon narrowing the cell to ~ 0.2 mm reduced to a minimum of ~ 0.3 ps. Spectral measurements confirmed that the subpicosecond pulses (peak power > 300 W) were close to the Fourier transform limit and that their characteristics did not depend strongly on laser power level or wavelength. The use of the saturable absorbers DQOCI and DODCI allowed continuously tunable mode-locked operation over the range 580 - 620 nm.

CHAPTER 5

TUNING OF THE MODE-LOCKED C.W. DYE LASER AND THE MODE-LOCKED CHARACTERISTICS OF THE NON-CONTACTED ABSORBER SYSTEM

5.1 Introduction

In addition to exploiting the potentially broad bandwidth of dye lasers to generate picosecond pulses, it is also essential that the subsequent mode-locking is frequency tunable as many applications require the matching of the laser wavelength to absorption bands. Flashlamp pumped dye lasers have already been mode-locked over the range 584-700nm¹⁰ by employing as active media the dyes Rhodamine 6G, Rhodamine B and Cresyl Violet Perchlorate. Mode-locking has also been reported at 465-480 nm with Esculin Monohydrate¹⁴⁵ and at 795-805 nm with DOTCI¹⁴⁶. Most published work on the passively mode-locked C.W. dye laser has concentrated on Rhodamine 6G/DODCI and the reported ranges for best mode-locking have been 590-610 nm⁹ and also at \sim 615 nm using a composite absorber of DODCI and Malachite Green⁷⁷.

In this work, using a contacted dye cell, an extension of the mode-locking spectrum to \sim 545 nm and 610 - 630 nm was achieved by mode-locking the Sodium Fluorescein and Rhodamine B lasers. Their tuning behaviour is discussed in this chapter together with an investigation of the non-contacted absorber cavity and a review of the theoretical models of the dye laser mode-locking process.

5.2 The Mode-Locked C.W. Rhodamine B Laser

To extend the spectral range over which continuous passive mode-locking is possible, the Rhodamine B laser of Chapter 2 was mode-locked with the three saturable absorbers of varying lifetimes used for

Rhodamine 6G. The longest wavelength reported for continuous pulse trains has been 670 nm¹⁴⁷ produced by pumping a Rhodamine B laser by a mode-locked argon-ion laser generating pulses of ~ 7.5 ps. In Chapter 4, passive mode-locking of Rhodamine 6G by DODCI was shown to be tunable to 620 nm.

The configuration employed for Rhodamine B was that of Figure 21a pumped by all lines of the Model 164 argon-ion laser with the active medium flowing in a dye cell. The output mirror was of 1-5% transmission over the range 610-645 nm and under these conditions typical unmode-locked thresholds were ~ 1 W for the optimum Rhodamine B concentrations (8×10^{-4} M/water + 10% Ammonyx LO) with ethanol only flowing in the absorber cell (0.6 mm). This relatively high threshold was due to the dye having a low absorption for the 488 nm pump line as well as being less efficient. When mode-locked, excitation powers of 2.5 - 3W were required.

Arthurs et al¹⁰ passively mode-locked a flashlamp pumped Rhodamine B laser over the range 605-645 nm using DODCI and DQTCI (1,3' - diethyl-4,2'-quinolythiacarbocyanine iodide) and recorded TPF patterns similar to those for Rhodamine 6G of 3-4 ps.

Likewise in the C.W. dye laser, mode-locking with DODCI closely resembled that for Rhodamine 6G. A fully mode-locked pulse train of instrument limited pulses was obtained over 608-633 nm with the normal cavity of ~ 12 ns double transit time. At the extremes, the DODCI concentration was adjusted to produce stable operation from the normal (for a 0.6 mm cell) of $\sim 10^{-5}$ M to $\sim 10^{-4}$ M. Over most of this region (610 - 630 nm) good mode-locking as evidenced by the high contrast ratio second harmonic traces of 3:1 was possible with pulse halfwidths

of 3.5 - 4.5 ps (high dispersion DEDF prism as tuning element). These results are comparable to those measured for the Rhodamine 6G dye cell cavity as initially used in this research. Shifting of the gain profile to longer wavelengths by increasing the Rhodamine B concentration to 10^{-3} M was also necessary to generate pulses of these durations at 630 nm.

Less stable mode-locking by DQOCI giving pulses of 4-5 ps was observed for 600-620 nm but at times it was difficult to obtain contrast ratios of 3:1 with most between 2.5:1 and 3:1. This may be expected from the location of the absorption maximum of DQOCI (594 nm) which although at a longer wavelength than that of DODCI does not possess a photoisomer and is restricted as an absorber to wavelengths near its peak.

As with Rhodamine 6G in Section 4.6g, picosecond pulses were recorded when Cresyl Violet Perchlorate (CVP) was introduced as absorber at a concentration of 2×10^{-5} M. Pulses of 3-4 ps were measured from 610 to 620 nm further demonstrating the independence of the mode-locking process from the dye lifetime. The problems with accurate cavity alignment and the long term instability in the CVP solution were also present as noted for Rhodamine 6G.

5.3 The Mode-Locked C.W. Sodium Fluorescein Laser

The feasibility of mode-locking at shorter wavelengths than Rhodamine 6G was investigated with the C.W. Sodium Fluorescein laser. Initially a number of dyes with absorption peaks within the tuning range of Sodium Fluorescein were unsuccessfully tried as saturable absorber without any modulation of the laser output being observed.

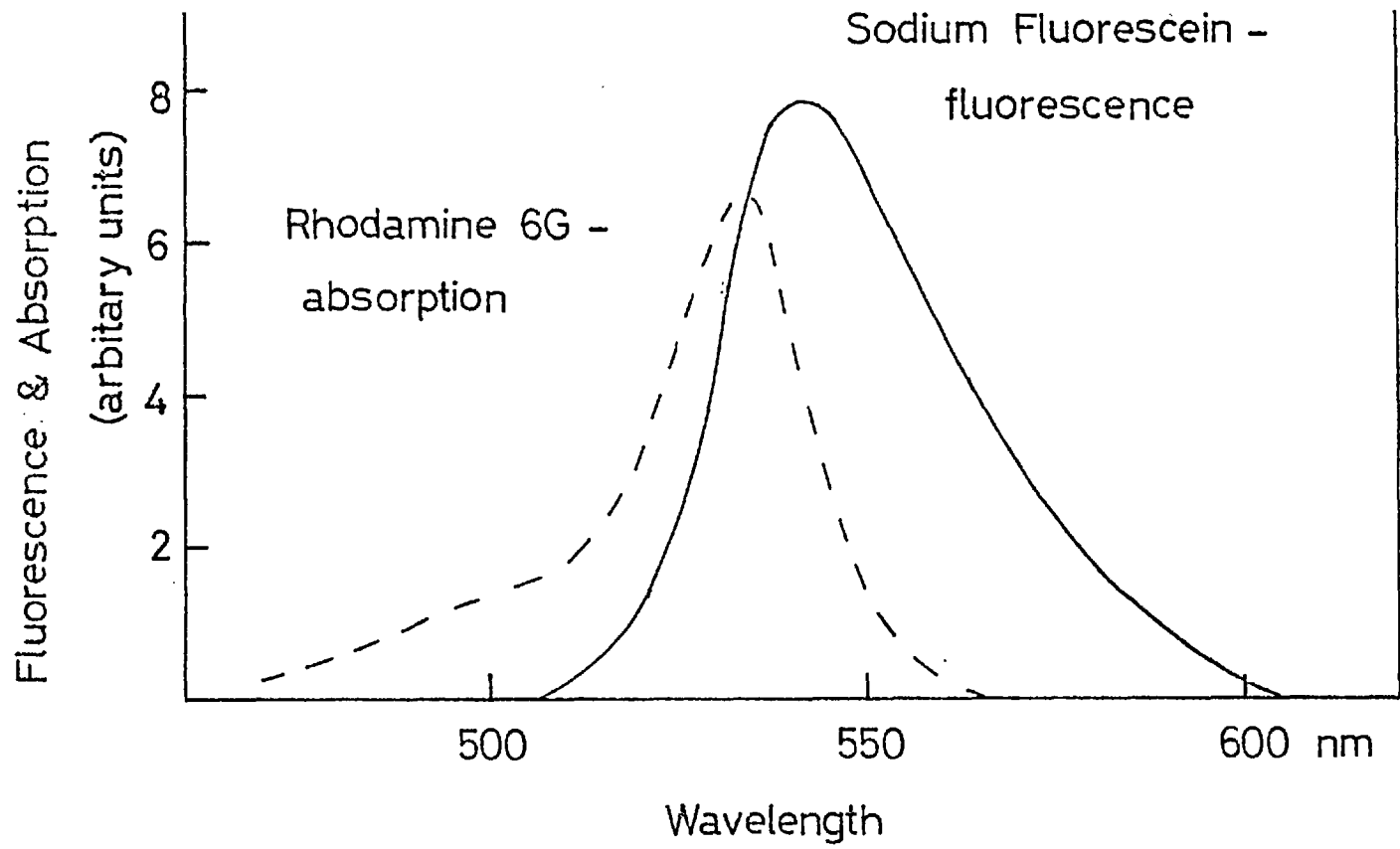
Detector limited pulses were however obtained with ethanolic solutions of Acridine Red and Rhodamine 6G, the latter producing pulses of $\sim 5-7$ ps.

The experimental arrangement was as for Rhodamine B with all lines of the pumping laser being utilized, and with the active medium (6×10^{-4} M/water + 10% Ammonyx LO + 0.05% COT) flowing in a dye cell. High contrast autocorrelation traces were only recorded for Rhodamine 6G as absorber and although Sodium Fluorescein was tunable from 532 to 580 nm, this was only possible around 545 nm. Figure 36 shows the relative positions of the Sodium Fluorescein and Rhodamine 6G fluorescence and absorption spectra respectively.

Optimum mode-locking was close to threshold (within $\sim 10\%$) and cavity adjustments were more critical than for either Rhodamine 6G or Rhodamine B mode-locked by CVP. This may have been due to the low Rhodamine 6G concentrations used as the pump power was restricted to below 2W due to COT particles burning onto the dye cell windows. The additional instability referred to in Section 2.11 was more noticeable as when the absorber was introduced the increased loss in the contacted dye cell encouraged lasing past the apex of the prism to the front mirror of the argon-ion laser.

Figure 37 shows an autocorrelation trace corresponding to pulses of 5.3 ps at 546 nm and from the simultaneously measured bandwidth of 0.26 nm, a $\Delta\nu t_p$ product of ~ 1.4 was deduced. Pulse durations measured were in the range 5-7 ps and contrast ratios were $\sim 2.5:1$ as in Figure 37. It is likely, however, that the improvements subsequently made to the laser would produce mode-locking similar to the Rhodamine 6G/Cresyl Violet combination.

FIG:36
157



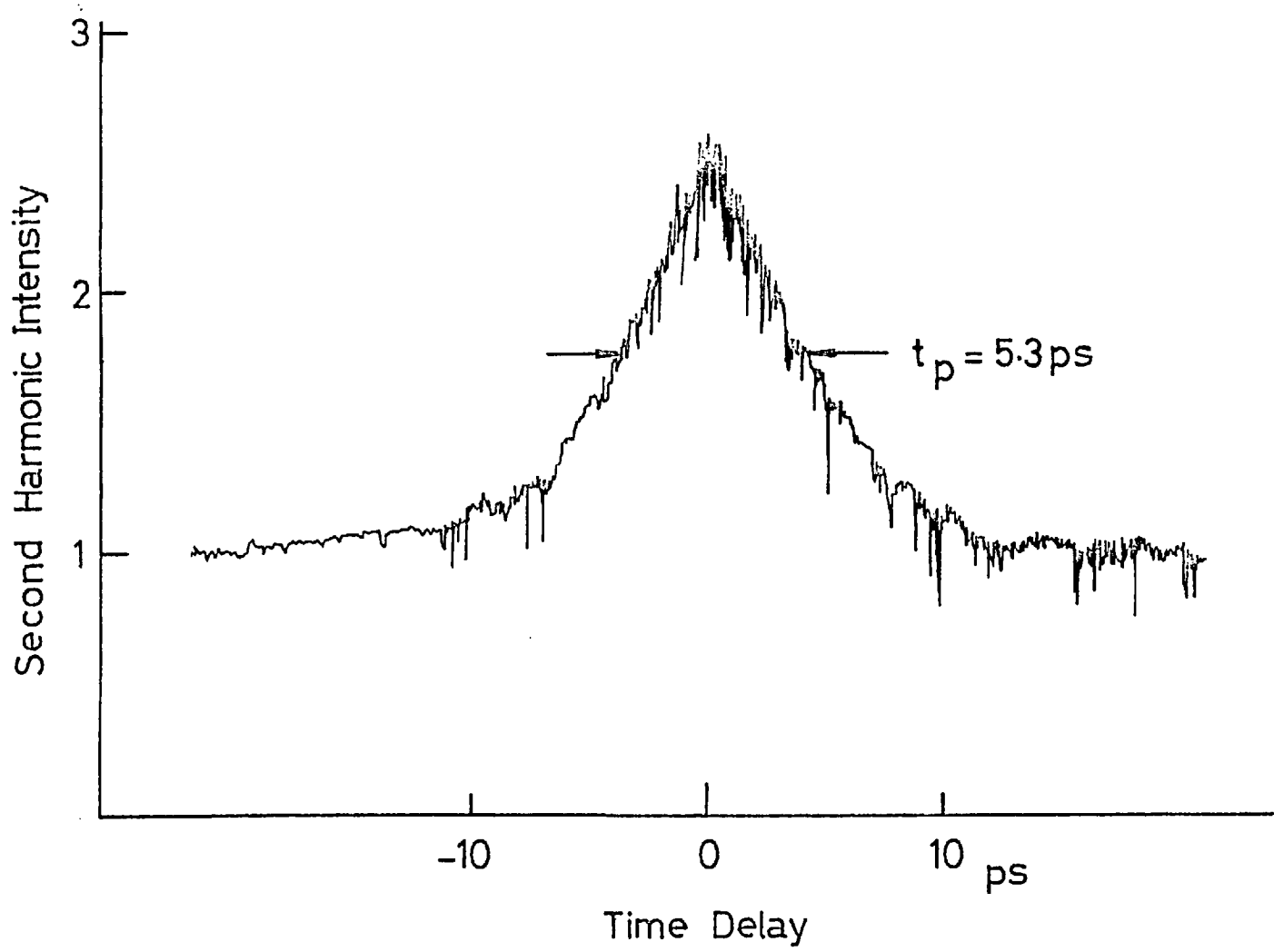


FIG: 37

5.4 The Mode-Locked C.W. Rhodamine 6G Laser- Non-Contacted Absorber

a Mode-locking Characteristics

The first passive mode-locking of the C.W. dye laser by Ippen et al⁹ involved flowing the saturable absorber in a dye cell at the focus of an astigmatically compensated cavity. Letouzey and Sari¹⁴⁸ later used a similar system but with a free-flowing jet-stream in place of the enclosed cell.

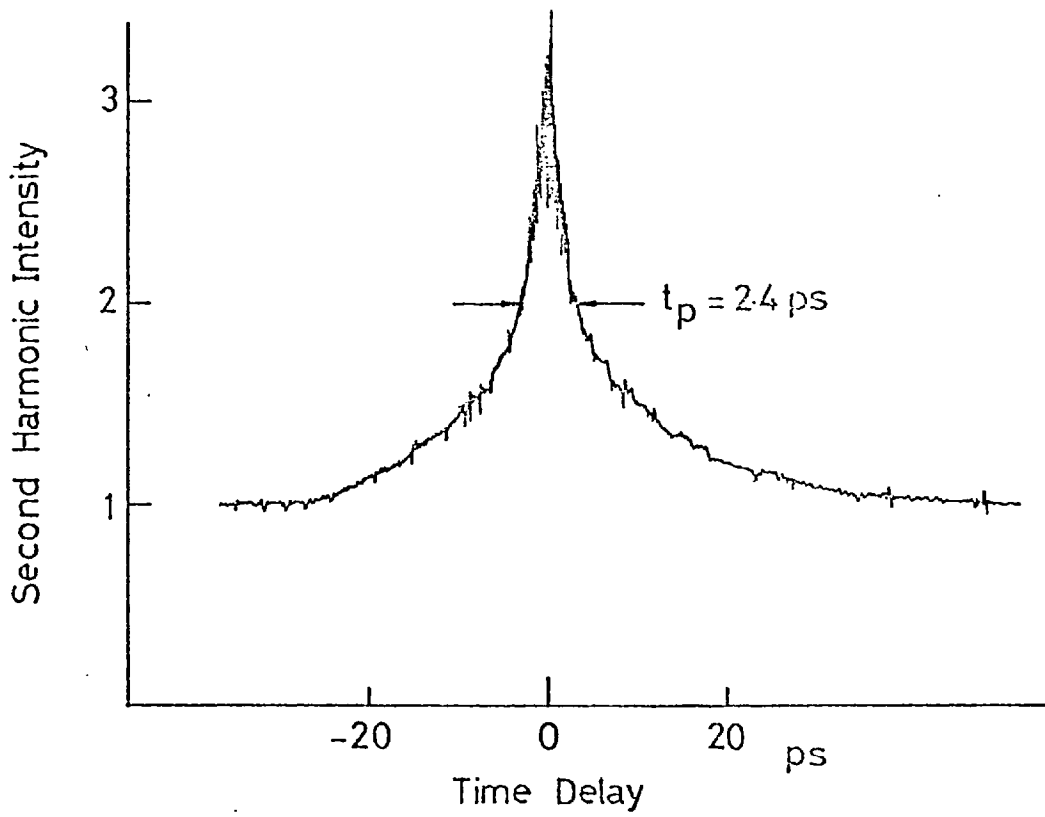
In this work, the behaviour of a non-contacted saturable absorber was investigated as a comparison with the contacted configuration. The jet-stream for the mode-locking dye in the cavity of Figure 21b was identical to that used throughout for the active medium. The same precautions were taken to ensure a stable bubble-free flow. Alignment of the second jet was accomplished by first obtaining satisfactory operation with a plane mirror in the L.H. arm of the cavity. This was then replaced by the absorber jet unit through which the solvent (ethylene glycol) was flowing. Optimum thresholds under these conditions with an output mirror of $\sim 3\%$ transmission at 600 nm were ~ 350 mW for pumping by the 514.5 nm line. The lower dispersion fused silica prism was used throughout these results. DODCI from a stock solution was added until mode-locking was observed which was normally at a concentration of $\sim 1-2 \times 10^{-5}$ M. This corresponded to a small signal transmission of $\sim 78 - 90\%$ at 600 nm for a jet of slant thickness ~ 0.4 mm.

Mode-locking with one pulse per round trip occurred with the non-contacted absorber when the laser was operated close to threshold (2 - 3 W). At ~ 200 mW above threshold double pulsing was usually

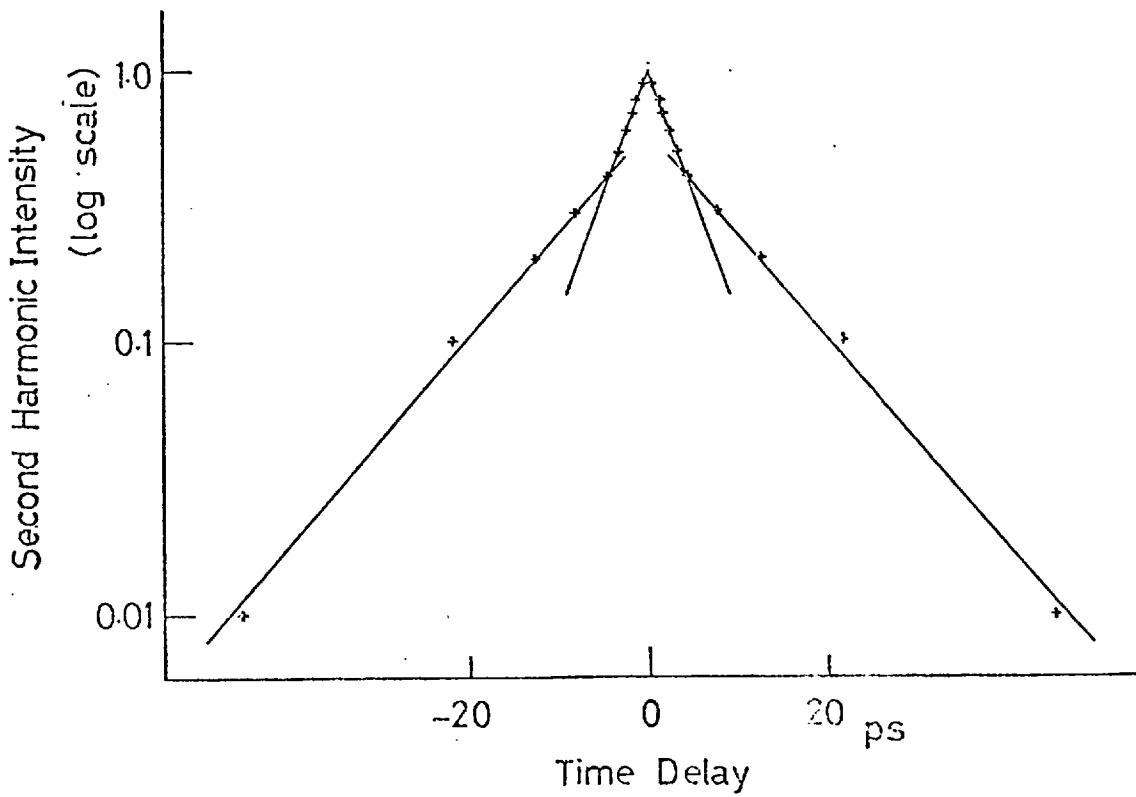
observed. An autocorrelation trace with the laser at 600 nm and close to threshold is shown in Figure 38a. In this example the DODCI concentration was $1.2 \times 10^{-5} \text{ M}$ and the pump power 2W. The pulse halfwidth of 2.4 ps was calculated assuming single-sided exponential pulses as the second harmonic curves clearly exhibit exponential "tails". In Figure 38b the previous autocorrelation is plotted logarithmically to which the best fit is by two straight lines. When close to threshold the mode-locked pulses had durations $\sim 1 - 5$ ps and were tunable in the range 595-616 nm.

The effect of pump power on the pulse characteristics is illustrated in Figure 39 which shows traces taken at threshold (1.7W) and at 2.2W in the double pulse regime at a wavelength of 605 nm. Over this interval the pulses increased from 1.6 ps to 19 ps but in Figure 39b the existence of a shoulder and spike are also apparent indicating the presence of components of ~ 1 ps under the pulse envelope. The overall contrast ratio for Figure 39b of 3:2:1 is in agreement with that expected for structured pulses⁷³. Another example of the traces recorded for double pulsing is given in Figure 40 with an overall duration of ~ 25 ps and again with structure of ~ 1 ps.

At the upper limit of single pulsing, ~ 200 mW above threshold, the autocorrelation traces changed from being smooth to having a slight shoulder at the half maximum. Figure 41a shows the shoulder and also structure signified by the peaks placed symmetrically about the central maximum. This curve was recorded immediately after that in Figure 38a. Another example of a slight shoulder for the single pulsing regime is given in Figure 41b for pulses of 2.3 ps. In the

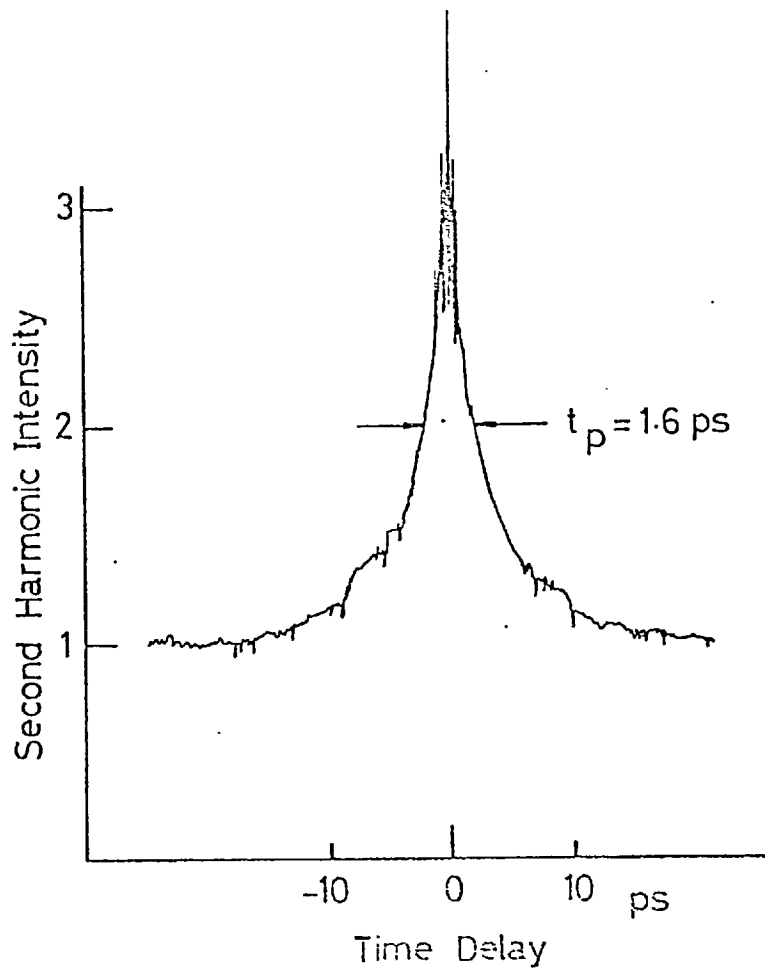


(a)

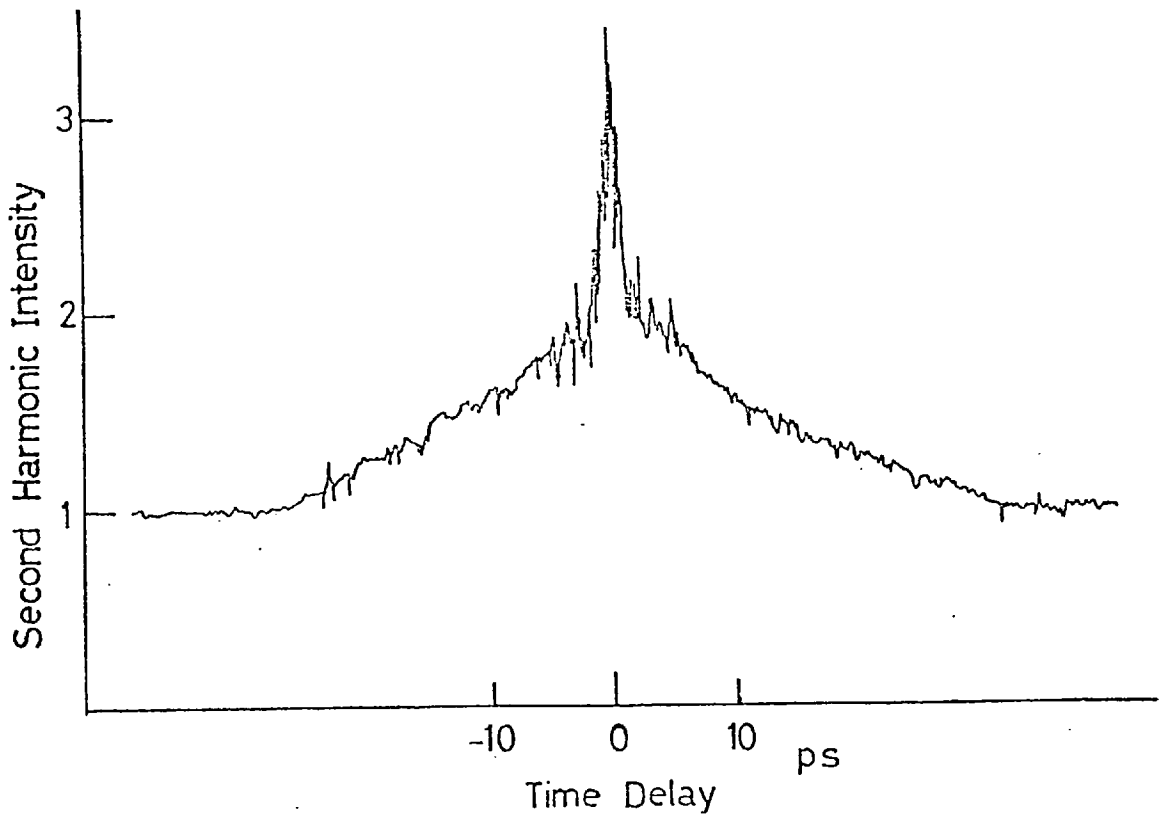


(b)

FIG: 38

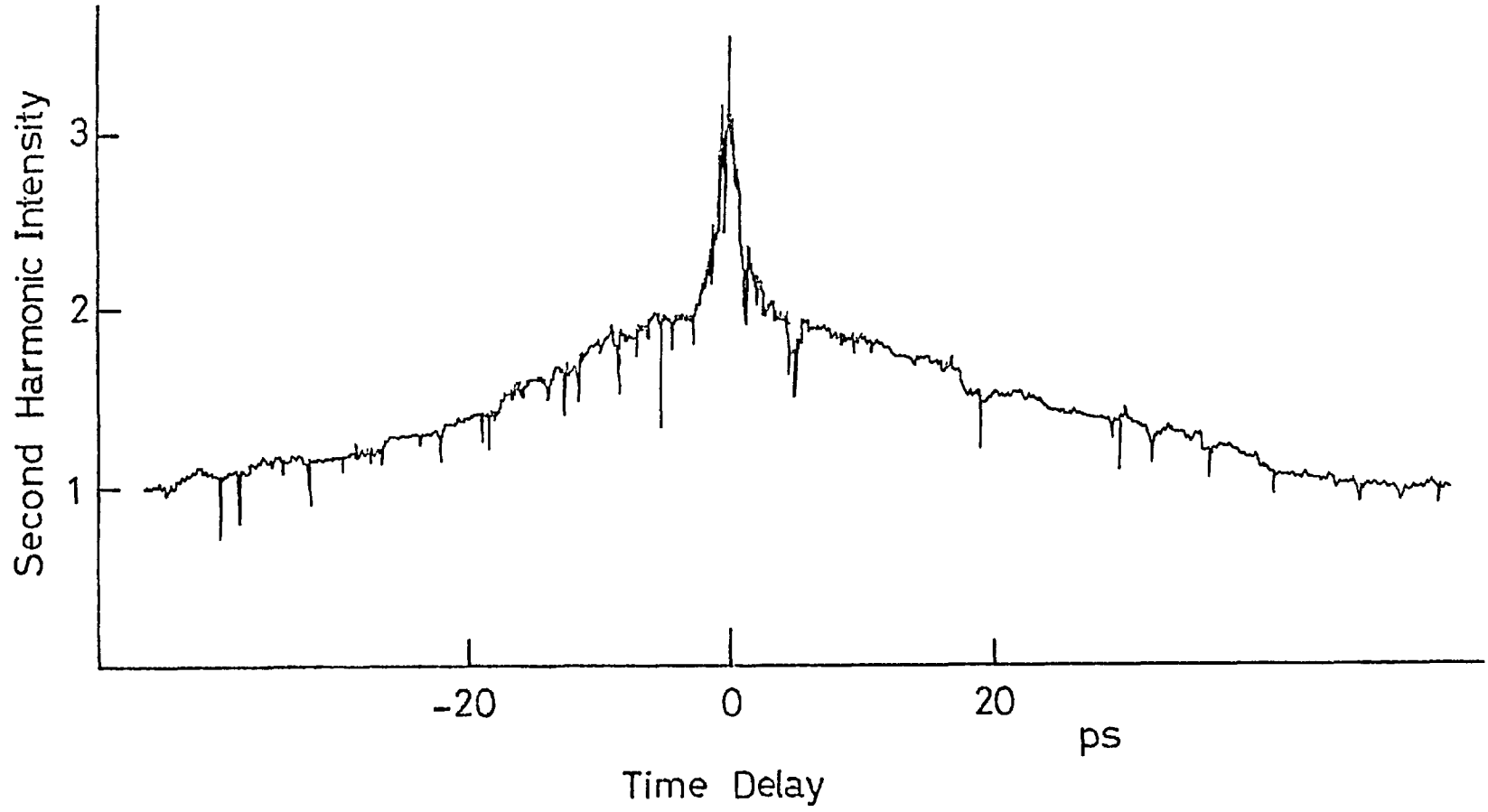


(a)



(b)

FIG: 4.0
163



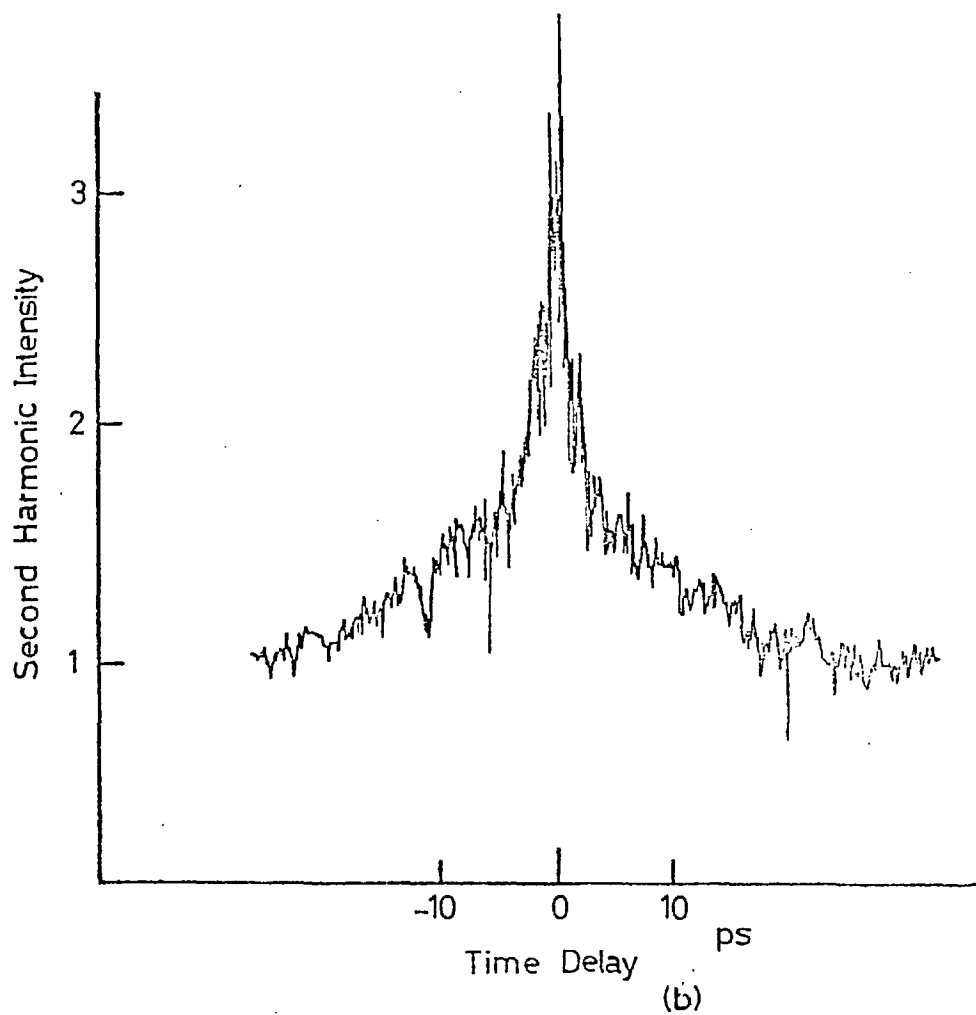
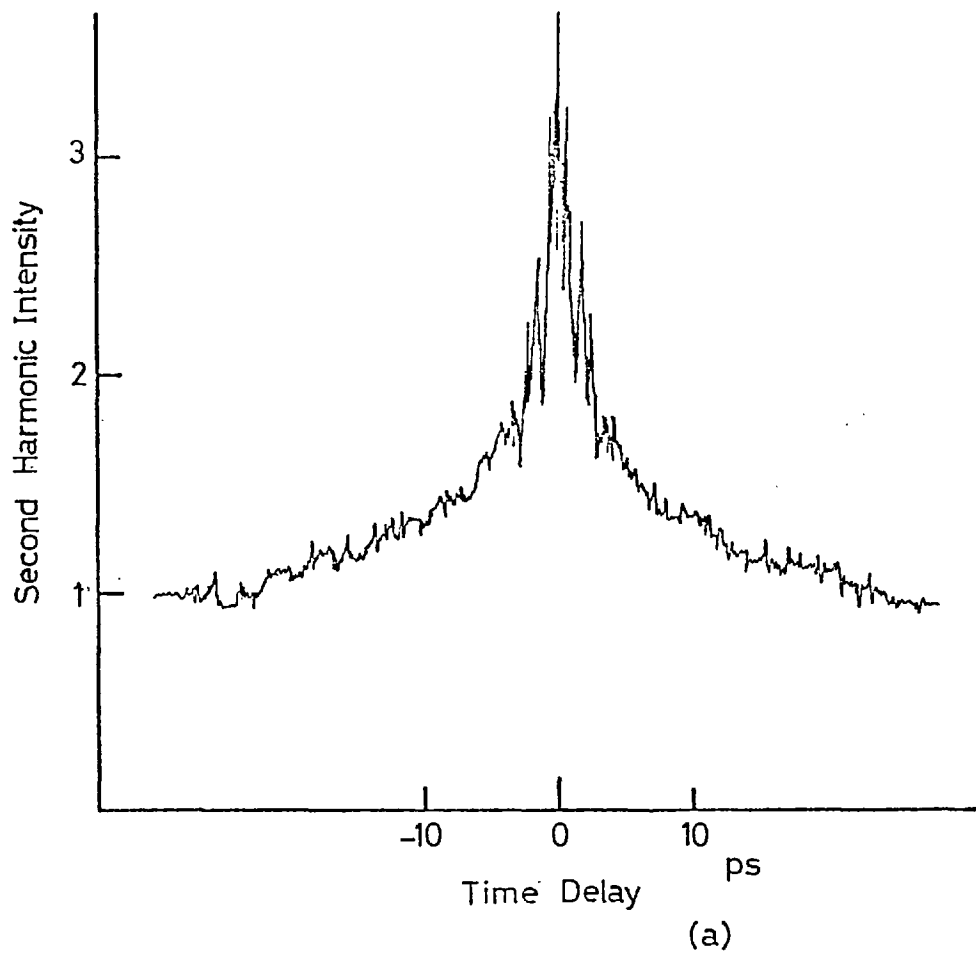


FIG: 41

course of this investigation the shortest structure measured was of 0.6 ps autocorrelation width in an envelope of 11 ps halfwidth.

At still higher pumping levels (1 W above threshold) the double pulsing degenerated into bursts of ~ 2.5 ns as shown in Plate 14 taken at an input power of 3.4W. The corresponding second harmonic trace was of low contrast with a width of ~ 4 ps. This contrast ratio is expected ⁷³ for random noise with rapid amplitude fluctuations of typical duration given by the peak width and is similar to that for a free running laser (1.5:1).

The measurements made using the second harmonic method were confirmed by examining the pulses with the electron-optical streak camera and pulse selection system described in Chapter 3. As the laser pump power was increased from threshold, the frequency of structured pulses increased and operation at power levels of ~ 200 mW above threshold gave streaks, an example of which is shown in Plate 15a along with the corresponding microdensitometer trace (Figure 42a). In this exposure, the laser was operating in the single pulse regime at 605 nm. The spacing of the two streak images was 60 ps resulting from the thickness of the optical flats in the calibration delay line. The pulse duration in Plate 15a was 11ps. This particular structured pulse exhibits a degree of asymmetry with a sharp rising edge and a decaying tail containing components of ~ 1 ps separated by 4-5ps. Plate 15b and Figure 42b display another streak made under similar conditions, again showing a decaying tail of picosecond structure. An autocorrelation trace of this type of mode-locking produces traces similar to those shown above of contrast ratio 3:2:1.

PLATE 14

OUTPUT OF NON-CONTACTED ABSORBER CONFIGURATION
AT HIGH POWER LEVELS

TIMESCALE: 2ns/DIV

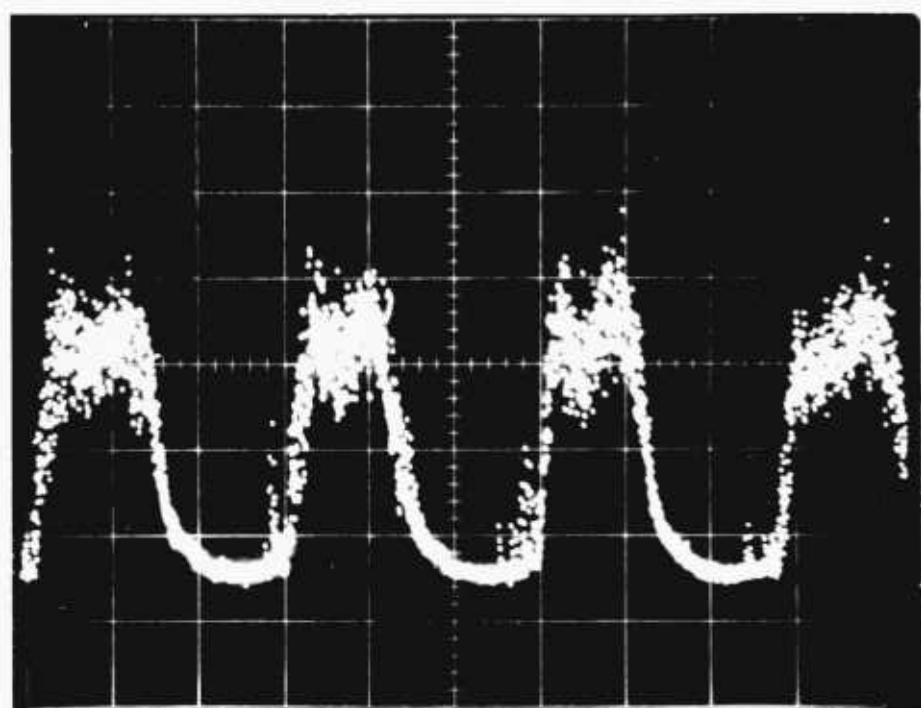


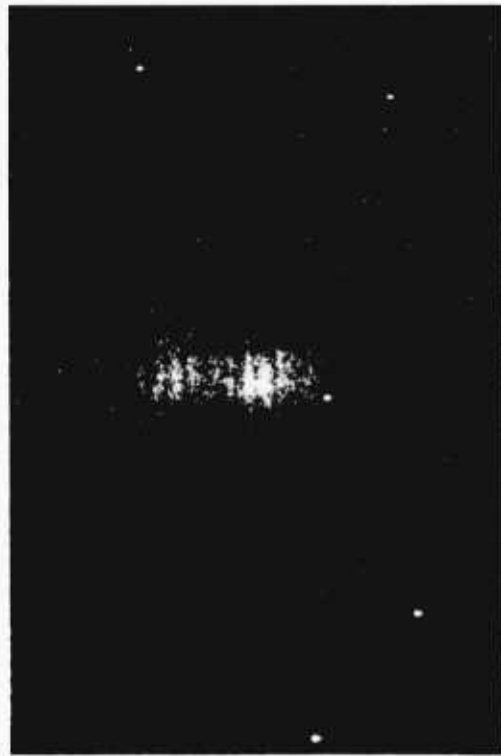
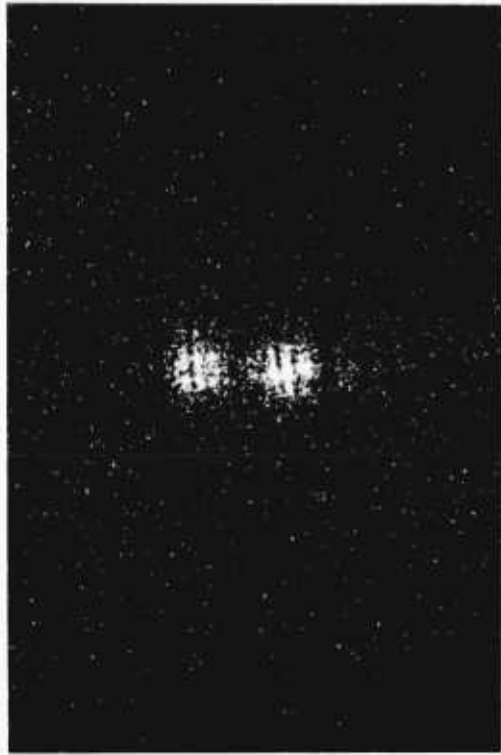
PLATE 15

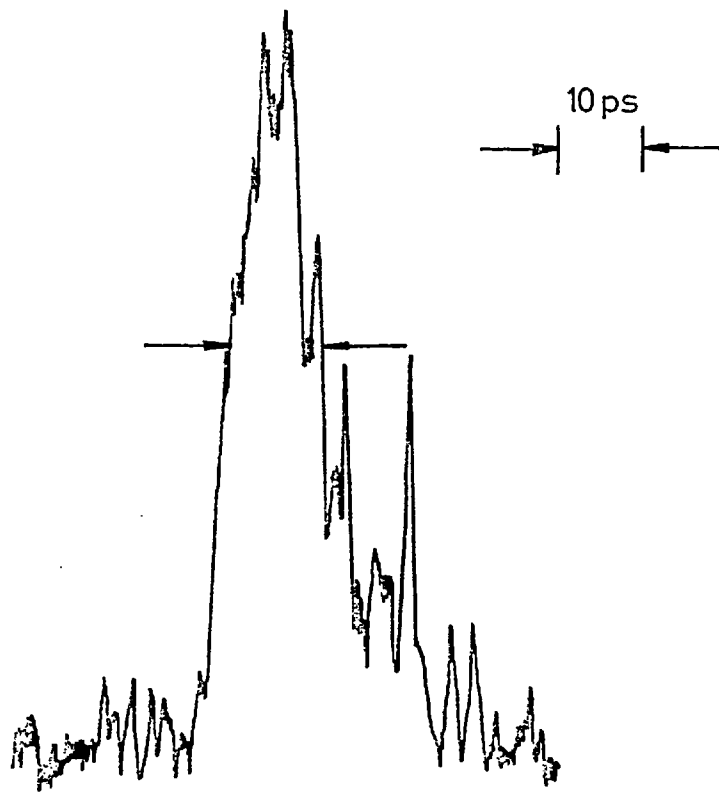
STREAKS OF NON-CONTACTED ABSORBER MODE-LOCKED

C.W. RHODAMINE 6G LASER

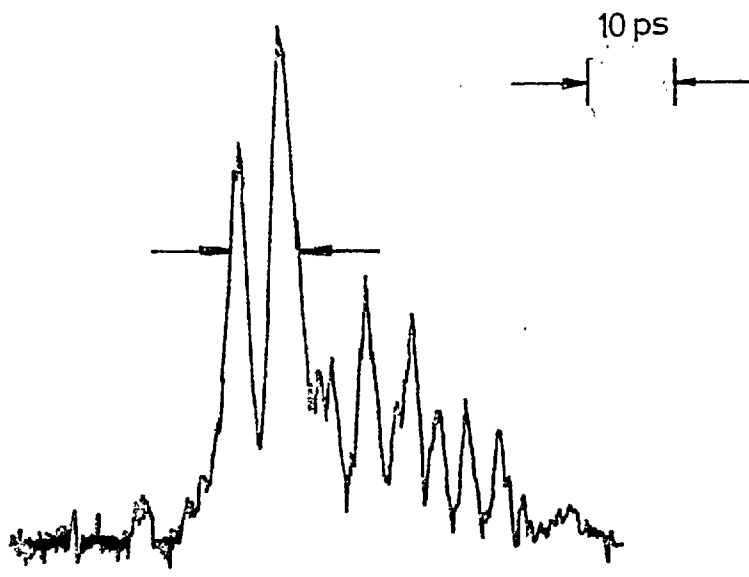
(a)

(b)





(a)



(b)

Similar results regarding the mode-locking of a double jet system have been reported^{9, 121} in which shortest pulses occur close to threshold and at higher power levels structured pulses are observed. In reference 121, the pulse profile has been shown experimentally to be a single-sided exponential. The same authors also demonstrated that the addition of the dye, Malachite Green, to the DODCI solution when already mode-locked improved laser stability and enabled operation further above threshold when tuned to ~ 615 nm, the peak of the Malachite Green absorption. The recovery time of Malachite Green has been measured in ethylene glycol to be ~ 7 ps¹² and because of this short lifetime it does not produce mode-locking by itself in the C.W. dye laser. The focussed pulses already existing due to DODCI (~ 20 MW.cm⁻²) are of sufficient intensity to create saturation when it is added to the same solution.

In this work with the non-contacted system, the addition of Malachite Green did not permit lasing at significantly greater power levels but improved stability shown by the reduced noise on the second harmonic traces and extended the region of shorter pulses (~ 1.5 ps) to ~ 616 nm where, as previously noted with DODCI only, pulses of 3 - 5 ps were normally produced over the range 610 - 616 nm.

5.4b Spectral Characteristics

With the aid of the piezoelectric scanning Fabry-Perot etalon, the linewidth of the unmode-locked jet-stream laser with ethylene glycol only flowing in the absorber jet was determined to be 0.05 nm. The addition of DODCI produced broadening of ~ 0.15 -0.5 nm. Figure 43 and Plate 16 show respectively an autocorrelation trace and the corresponding spectral photograph. The trace was recorded at a

FIG: 43
170

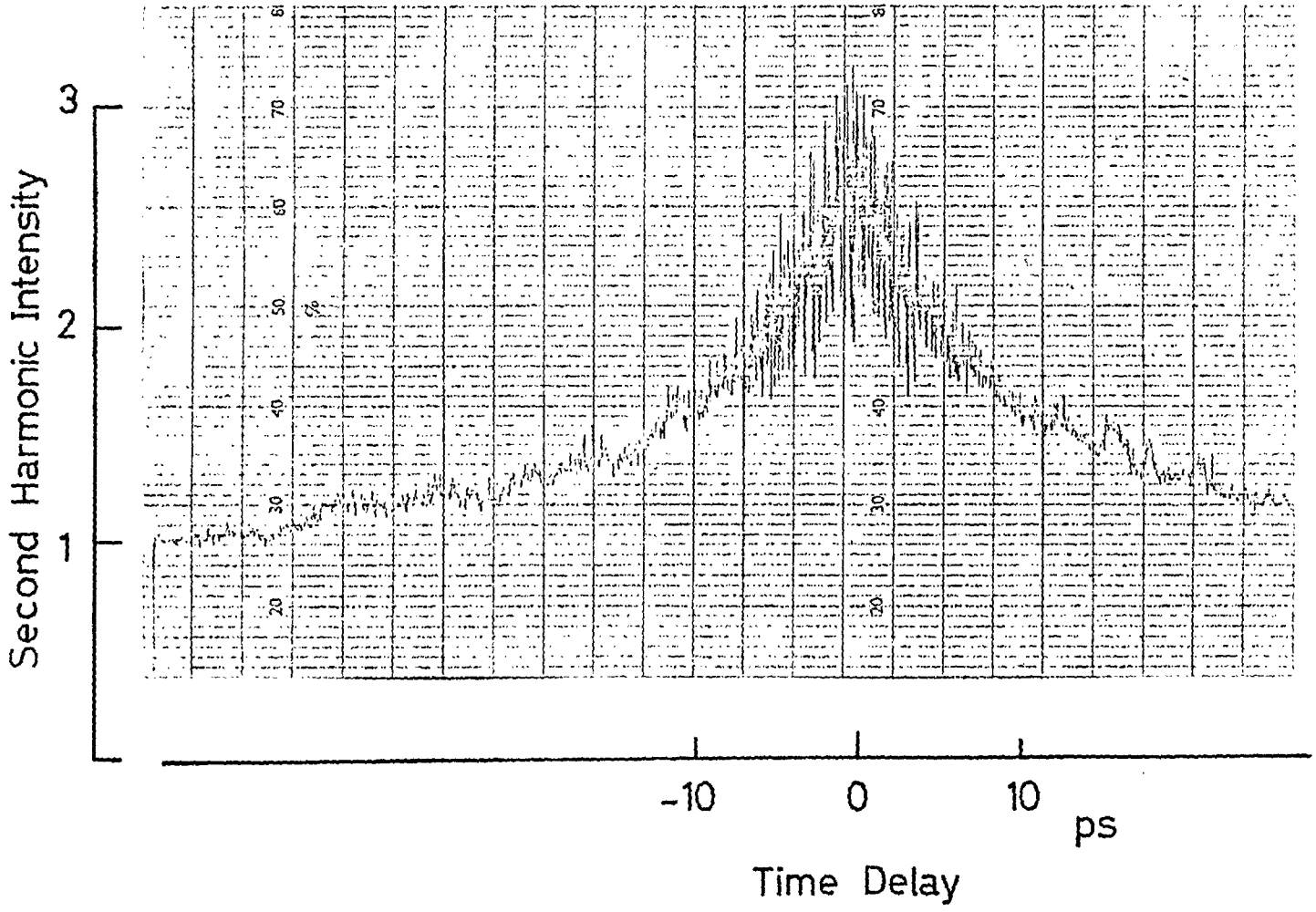
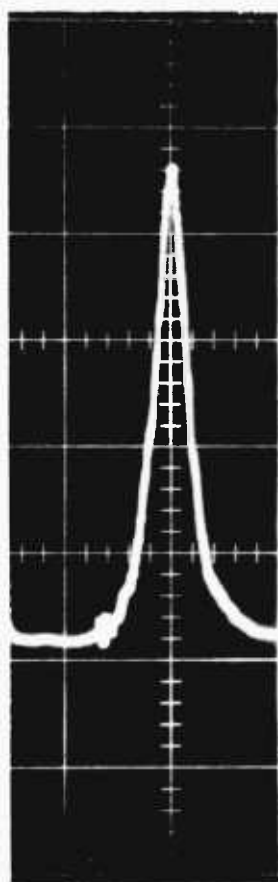


PLATE 16

SPECTRUM OF MODE-LOCKED NON-CONTACTED ABSORBER CONFIGURATION

CALIBRATION: 0.6 nm per major division



sufficiently slow scan to resolve some of the fringes across the peak. The linewidth, $\Delta\lambda=0.18$ nm, as deduced from Plate 16 gave at 608 nm a bandwidth-pulse duration product, $\Delta\nu t_p \sim 0.7$, compared with 0.11, the theoretical value for single-sided exponential pulses (as suggested by the autocorrelation traces), indicating that the mode-locking was not transform-limited.

In general, the $\Delta\nu t_p$ product for single pulses was such that the minimum values were in the range 0.57 - 0.7. It was also possible to obtain good mode-locking at similar power levels for which $\Delta\nu t_p \sim 1.0 - 1.2$ was recorded e.g. $\Delta\lambda \sim 0.45$ nm, $t_p = 3.3$ ps at 605 nm.

For the structured pulses at higher powers, $\Delta\nu t_p$ products for the spike (0.2 - 0.6) showed that the components were bandwidth limited. Similar observations have been reported for the structure in the TPF patterns of pulses from mode-locked Nd: glass lasers⁸⁹.

5.5 The Mechanism of Passive Mode-Locking

The successful operation of passively mode-locked dye lasers led to theoretical modelling of the process involved in pulse shortening where the saturable absorber lifetimes are normally considerably longer than the subsequent pulse durations e.g. DODCI, $\tau > 300$ ps^{110, 111}. Comparisons with the passively mode-locked Nd: glass or ruby lasers indicate that a different mechanism is operative in these lasers as the pulse widths are directly related to the saturable absorber dye used^{76, 142}.

Theoretical descriptions of mode-locked solid-state lasers have investigated either the beating together of the cavity modes

in the frequency domain or dealt with the statistical build-up of radiation using the fluctuation model.

Treatments of the former method have been given by Lamb¹⁴⁹, Statz et al¹⁵⁰ and Schwarz¹⁵¹, however the analysis becomes impractical when more than a few cavity modes are considered. Fleck¹⁵² has examined the influence of the saturable absorber on travelling waves in the laser cavity as distinct from the build-up of the stationary cavity modes and shown the evolution of an ultrashort pulse.

Pulse selection from the initial noise bursts and subsequent compression in solid-state lasers have been successfully modelled by the fluctuation theory^{153, 154} first proposed by Letokhov. The occurrence and evolution of the intensity fluctuation bursts in the region of linear absorption and the shaping in the non-linear absorption regime are predicted. The emission phases of the initially excited axial laser modes are random and consequently the intensity is a random function of time due to mutual interference, with spikes of average duration $\sim 1/\Delta\nu$ where $\Delta\nu$ is the total bandwidth of the fluctuations. Due to the preferred amplification of the modes near the centre of the gain curve during the period of linear development, selection occurs causing a narrowing of the spectrum of the excited modes leading to a temporal broadening of the fluctuations. Following amplification to the saturation intensity of the absorber, the selection of a noise burst occurs. The duration of this burst or pulse is determined by the relaxation time of the saturable absorber which "collapses" on the trailing edge and acts to shorten the pulse on successive transits. Hence in the mode-locked Nd: glass laser,

the shortest pulses (2 - 3 ps) are generated using the dye - Eastman Kodak No. 9860 (recovery time ~ 10 ps) ¹¹⁹. At the final stages of the pulse evolution when the intensity is sufficiently high for complete saturation of the absorber transition it would be expected that the amplification would be non-linear leading to further pulse shortening. Non-linear amplification in single pass solid-state systems has been shown by Basov et al ^{115, 155} to lead to compression by reducing the trailing edge of a pulse. This can occur if the leading edge is steeper than an exponential, satisfied experimentally by Basov using a Pockels Cell to shape the pulses. ¹⁵⁵

However, in the mode-locked solid-state laser, the non-linear pulse shaping capability is very much reduced as the pump cannot restore the inversion lost during each pass before the reflected pulse re-enters the amplifying medium. As mode-locking occurs in giant pulse solid-state lasers during the growth of the giant pulse, reliable operation requires that the time the intensity distribution takes to pass through the region of maximum absorber discrimination is sufficiently long i.e. close to the threshold. Glenn ¹⁵⁶ has shown that gain saturation does in practice play a role in slowing the growth rate of the signal in this region.

The dye laser differs considerably in that it is a continuous or quasi-continuous device as the active medium has a relaxation time of a few nanoseconds. Hence due to the resulting low storage facility of the dye together with the high stimulated emission cross-section, gain saturation becomes of prime importance. In a laser in which the combination of saturable amplification and absorption are present, pulse compression will occur as the latter acts to sharpen

the leading edge and restrain the pulse while saturable amplification depletes the trailing edge.

The theories of New^{114, 122, 157} and Haus^{121, 158, 159} to which reference has already been made in Chapter 4 will be discussed briefly here together with the conditions derived for optimum mode-locking in New's treatment.

New, in making the rate equation approximation, assumes the dephasing times of the media to be sufficiently rapid such that coherent interactions between the laser radiation and the media can be ignored. Under the conditions that the leading and trailing edge gains are less than unity, pulse selection from a perturbation on the C.W. signal and compression can be shown to take place since under "static" pulse compression only the peak of the pulse experiences gain. These restraints are realized if the relaxation time of the amplifying medium (τ) is of the same order as the cavity round trip time (T_{RT}) and if the cross-section for absorption (σ_b) is more than twice the amplification cross-section (σ_e). The experimental techniques for fulfilling these conditions were discussed in Section 4.6a.

New characterizes the second condition by the parameter s defined by

$$s = k \frac{A_e \sigma_b}{A_b \sigma_e}$$

where A_e and A_b are the respective amplifier and absorbing beam areas and $k = 2$ for a contacted dye cell (otherwise $k = 1$)¹²². For the Rhodamine 6G/DODCI or DQOCI combinations in the cavity configuration used in the experimental work, the substitution of the relevant values

gives $s \sim 9 - 10$. If this is not the case, mode-locking can still occur when the gain on either the leading or trailing edges is > 1 . The pulse is no longer fixed in local time but drifts and a slow shortening termed "dynamic" pulse compression takes place. In the C.W. dye laser focussing of the beam to a spot size in the absorber the same as that in the active medium led to the formation of long pulses $\sim 300-400$ ps due to the reduction in s to close to the minimum of ~ 2 .

The stability ranges for static pulse compression, bounded by the lines for which the leading and trailing edge gains are just unity, may be displayed in the (g_0, ξ) plane where g_0 is the unsaturated net round trip gain and $\xi = T_{RT}/\tau$. The location of these curves is in qualitative agreement with the normal operating characteristics of passively mode-locked dye lasers bearing in mind that the model best describes a ring laser or one in which the active medium is close to one end of the cavity.

As the rate equation theory of New considers only the process of pulse compression and neglects the dephasing times of the media, the pulses are expected to shorten indefinitely without a steady-state solution being reached. Garside and Lim¹⁶⁰⁻¹⁶³ employed a similar perturbation technique to that of New's in the full coherent field analysis in which the gain and loss media are characterized by phase memory times.

Using the density matrix formulation, the interaction of the media with the radiation field is governed by Maxwell's equations in the slowly varying envelope approximation such that the radiation field amplitude is coupled to the media rather than the photon flux.

In this model steady-state pulses are shown to be generated with pulse lengths tending towards the phase memory times. Experimentally, this may be taken to be a lower limit on the pulse duration as cavity parameters such as dispersion may prevent the pulse shortening from proceeding to this value. Haus^{121, 158, 159} by introducing a bandwidth limiting function into the analysis has derived approximate analytical expressions for the final pulse profiles. The journey of a pulse around the laser cavity (including passage through the tuning element) is considered and in the steady-state, the changes in the envelope add to a time delay or advance with respect to the empty cavity round trip time. Bandwidth limiting processes tend to broaden the temporal pulse profile and hence an equilibrium situation is established when these effects are balanced by pulse compression. Haus has shown that in the limit, pulses of sech^2 intensity profile are to be expected (similar to those deduced for the contacted dye cell configuration). The asymmetrical exponential pulses found by Ippen et al⁷⁷ are also valid solutions under certain conditions in which case they may or may not be transform limited.

Comparing the three models of the passively mode-locked dye laser, it is seen that they can all establish stability ranges for the cavity and being the least involved, New's is most useful in this respect. As the theories of Garside and Lim and of Haus generate closed solutions, limited in the former by the media dephasing times and in the latter by the cavity dispersion, they serve to illustrate the restraints on mode-locking but due to the experimental difficulties in determining the cavity parameters, a numerical prediction of the steady-state pulse durations has not yet been possible.

5.6 Conclusion

Passive mode-locking of Rhodamine B and Sodium Fluorescein has been demonstrated resulting in the generation of pulses over the range 610-630 nm and at 546 nm. Investigation of a non-contacted saturable absorber has shown that mode-locking only occurred within $\sim 10\%$ of threshold with autocorrelation traces similar to those produced by asymmetric exponential pulses. At higher powers, structured pulses were normally produced. A review of the current theoretical models for passively mode-locked dye lasers has also been given showing that they are in qualitative agreement with the experimental results.

GENERAL CONCLUSION

The design and operation of a C.W. dye laser has been described in detail. Flowing the active medium in a free-flowing jet-stream was shown to cause a lower insertion loss and to possess greater long term stability than a dye cell. Thermal distortion at the focus of the argon-ion laser limited the C.W. dye laser performance especially if all-lines of the pumping source were used. This may be partially compensated for by adjusting the mode size in this region. C.W. operation of the dyes, Rhodamine 6G, Rhodamine B and Sodium Fluorescein was successfully obtained in jet-stream and dye cell systems with lowest thresholds of ~ 120 mW and maximum output powers of ~ 1 W when pumped by 6 W of 514.5 nm radiation. As the out-coupling mirror was not optimized, conversion efficiencies of $\sim 30\%$ should be attainable. The use of Sodium Fluorescein in the dye cell limited the input power levels due to the effects of the necessary triplet-state quencher (COT) on the optical surfaces. Again free-flowing technology would surmount this drawback.

Passive mode-locking was achieved by the inclusion of a saturable absorber dye in either a contacted dye cell or a second jet-stream situated at a distance from the end cavity mirror. Pulse durations were determined by the second harmonic autocorrelation method and the electron-optical streak camera. The autocorrelation traces were found to be characteristic of the cavity configuration employed with those due to the contacted cell being best fitted by the autocorrelation function for pulses of sech^2 intensity profile while the non-contacted absorber generated second harmonic curves with exponential wings.

The Rhodamine 6G and Rhodamine B lasers were mode-locked by dyes possessing a range of lifetimes, tens of picoseconds (DQOCI) to

nanoseconds (Cresyl Violet), but pulses of picosecond duration were consistently recorded indicating the weak dependence in the passively mode-locked dye laser on the lifetime of the saturable absorber. Similarly, mode-locking of Sodium Fluorescein by Rhodamine 6G was also observed. These dye combinations allowed continuous tuning of the mode-locking over the range 580-630 nm and also at 546 nm increasing their potential use in picosecond spectroscopy.

Narrowing the contacted dye cell from ~ 0.6 mm to ~ 0.2 mm resulted in the production of subpicosecond pulses with the durations decreasing from ~ 1 ps to a minimum of ~ 0.3 ps for the Rhodamine 6G/DODCI combination. Mode-locked operation was also possible at power levels up to 25% above threshold and the laser was tunable over the range 595-616 nm with average output powers of ~ 15 mW corresponding to peak pulse powers in excess of 300 W. This contrasts with the non-contacted system in which single pulsing was only attainable close to threshold ($\sim 10\%$) above which structured pulses were normally observed. Spectral measurements confirmed the absence of excessive chirp and showed that the subpicosecond pulses were close to the Fourier transform limit with $\Delta\nu:tp$ (bandwidth - pulse duration) products of ~ 0.4 being recorded compared to the theoretical value of 0.32 for sech^2 pulses. Current theories of the passively mode-locked C.W. dye laser in which cavity dispersion limits pulse compression have been shown to be in qualitative agreement with the experimental system. Reductions in the pulse halfwidths were obtained by the use of a lower dispersion tuning prism. and as discussed above, the narrowing of the contacted dye cell to retain the advantages of contacting for as short a pulse as possible.

Although the other dye combinations were not studied in detail with the thin dye cell, it is anticipated that pulses of similar duration would be generated, tunable over a broader spectral range. Further engineering refinements should result in 0.1 ps pulses being achieved at which duration coherent effects in the laser media may set a lower limit to subsequent pulse shortening.

Transform limited subpicosecond pulses such as these find immediate application in photobiology, photochemistry, solid state phenomena (exciton-phonon interactions) and pulse propagation studies e.g. self-induced transparency and photon echoes. Further developments would broaden the range of applications and stimulate new ones. Synchronous pumping by a mode-locked argon-ion laser which can presently generate mode-locking of dyes for which a saturable absorber is not available, should in conjunction with passive methods lead to considerably higher peak powers and possibly shorter pulses. A variation of synchronous pumping could be an alternative approach to the production of sub-picosecond pulses. This would involve the use of a dye both as absorber and active medium such that after the passage of the original mode-locked pulse it might receive sufficient inversion to lase if a second resonator is available matched in length to the first. Such a system should be capable of subpicosecond pulses as the pumping pulses are of a few picoseconds duration. Injection mode-locking of a flashlamp pumped dye amplifier by the output of the C.W. dye laser may provide a method of generating tens of kilowatts peak power and still retain the coherent properties of the original laser. Similarly, developments in laser diagnostics such as the repetitively scanning streak camera will help to encourage and diversify the applications to which the mode-locked C.W. dye laser will be put.

REFERENCES

1. P.P. SOROKIN and J.R. LANDARD: I.B.M. J. Res. Develop., 10, 162, (1966).
2. W. SCHMIDT and F.P. SCHAFFER: Z. Naturforsch, 22a, 1563, (1967).
3. F.N. BALTAKOV, B.A. BARIKHIN, V.G. KORNILOV, S.A. MIKHNOV, A.N. RUBINOV and L.V. SUKHANOV: Sov. Phys. Tech. Phys., 17, 1161, (1973).
- 4a. G.M. GALE: Optics Comm., 7, 86, (1973).
- 4b. R.L. BARGER, J.B. WEST and T.C. ENGLISH: Appl. Phys. Lett., 27, 31, (1975).
5. O.G. PETERSON, S.A. TUCCIO and B.B. SNAVELY: Appl. Phys. Lett., 17, 245, (1970).
6. T.W. HANSCH, K.C. HARVEY, G. MEISEL and A.L. SCHAWLOW: Optics Comm., 11, 50, (1974).
7. J.M. YARBOROUGH: Appl. Phys. Lett., 24, 629, (1974).
8. W.W. SCHMIDT and F.P. SCHAFFER: Phys. Lett., 26A, 558, (1968).
9. E.P. IPPEN, C.V. SHANK and A. DIENES: Appl. Phys. Lett., 21, 348, (1972).
10. E.G. ARTHURS, D.J. BRADLEY and A.G. RODDIE: Appl. Phys. Lett., 20, 125, (1972).
11. C.V. SHANK and E.P. IPPEN: Appl. Phys. Lett., 26, 62, (1975).
12. E.P. IPPEN, C.V. SHANK and A. BERGMAN: Chem. Phys. Lett., 38, 615, (1976).
13. S.L. McCALL and E.L. HAHN: Phys. Rev. Lett., 18, 907, (1967).
14. "Dye Lasers": Topics in Applied Physics, 1, edited by F.P. SCHAFFER. Springer-Verlag, (1973).
15. B.B. SNAVELY: Proc. I.E.E.E., 57, 1374, (1969).
16. C.R. NOLLER: Chemistry of Organic Compounds (W.B. Saunders, 3rd edition, 1965).
17. D. RICARD, W.H. LOWDERMILK and J. DUCUING: Chem. Phys. Lett., 16, 617, (1972).
18. B.B. SNAVELY and O.G. PETERSON: I.E.E.E. J. Quant. Electr., QE-4, 540, (1968).
19. R.R. ALFANO, S.L. SHAPIRO and W. YUNG: Opt. Comm., 7, 191, (1973).

20. M.E. MACK: J. Appl. Phys., 39, 2483, (1968).
21. C. LIN and A. DIENES: Opt. Comm., 9, 21, (1973).
22. J.B. BIRKS: Chem. Phys. Lett., 17, 370, (1972).
23. P.M. RENTZEPIS: Chem. Phys. Lett., 3, 717, (1969).
24. O. TESCHKE, A. DIENES and G. HOLTOM: Optics Comm., 13, 318, (1975).
25. D.N. DEMPSTER, T. MORROW and M.F. QUINN: J. Photo. Chem., 2, 343, (1973/74).
26. P.P. SOROKIN and J.R. LANKARD: IBM J. Res. Develop., 11, 148, (1967).
27. S.A. TUCCIO and F.C. STROME JNR.: Appl. Optics, 11, 64, (1972).
28. T.H. FORSTER and B. SELINGER: Z. Naturforsch, 19a, 38, (1964).
29. P.P. SOROKIN, J.R. LANKARD, E.C. HAMMOND and V.L. MORUZZI: IBM J. Res. Develop., 11, 130, (1967).
30. B.B. SNAVELY and F.P. SCHAFER: Phys. Lett., 28A, 728, (1969).
31. J.B. MARLING, D.W. GREGG and L. WOOD: Appl. Phys. Lett., 17, 527, (1970).
32. O. TESCHKE and A. DIENES: Optics Comm., 9, 128, (1973).
33. J.P. WEBB, W.C. McCOLGIN and O.G. PETERSON: J. Chem. Phys., 53, 4227, (1970).
34. R. PAPPALARDO, H. SAMELSON and A. LEMPICKI: Appl. Phys. Lett., 16, 267, (1970).
35. P.K. RUNGE: Optics Comm., 4, 195, (1971).
36. R. POLLONI: Appl. Phys., 7, 131, (1975).
37. R.R. JACOBS, H. SAMELSON and A. LEMPICKI: J. Appl. Phys., 44, 263, (1973).
38. G. MAROWSKY and R. POLLONI: Appl. Phys., 8, 29, (1975).
39. M. HERCHER and H.A. PIKE: Optics. Comm., 3, 65, (1971).
40. M. HERCHER and H.A. PIKE: Optics Comm., 3, 346, (1971).
41. W. HARTIG and WALTHER: Appl. Phys., 1, 171, (1973).
42. F. O'NEILL: Optics Comm., 6, 360, (1972).

43. H. W. KOGELNIK, E.P. IPPEN, A. DIENES and C.V. SHANK: I.E.E.E. J. Quant. Electr., QE-8, 373, (1972).
44. A. DIENES, E.P. IPPEN and C.V. SHANK: I.E.E.E. J. Quant. Electr., QE-8, 388, (1972).
45. P.K. RUNGE and R. ROSENBERG: I.E.E.E. J. Quant. Electr., QE-8, 910, (1972).
46. F.Y. WU , R.E. GROVE and S. EZEKIEL: Appl. Phys. Lett., 25, 73, (1974).
47. R.A. DODGE and M.J. THOMPSON: Fluid Mechanics (McGraw-Hill, 1st edition, 1937).
48. B. WELLEGEHAUSEN, H. WELLING and R. BEIGANG: Appl. Phys., 3, 387, (1974).
49. B. WELLEGEHAUSEN, L. LAEPPLER and H. WELLING: Appl. Phys., 6, 335, (1975).
50. C.E. MOELLER, C.M. VERBER and A.H. ADELMAN: Appl. Phys. Lett., 18, 278, (1971).
51. F.A. BEISSER and D.J. EILENBERGER: I.E.E.E. J. Quant. Electr., QE-11, 372, (1975).
52. H.W. SCHRODER, H. WELLING and B. WELLEGEHAUSEN: Appl. Phys., 1, 343, (1973).
53. F.P. SCHAFER and H. MULLER: Optics Comm., 2, 407, (1971).
54. B.H. SOFFER and B.B. McFARLAND: Appl. Phys. Lett., 10, 266, (1967).
55. J.E. BJORKHOLM, F.C. DAMEN and J. SHAH: Optics Comm., 4, 283, (1971).
56. D.J. BRADLEY, W.G.I. CAUGHEY and J.I. VUKUSIC: Optics Comm., 4, 150, (1971).
57. B. SOEP: Optics Comm., 1, 433, (1970).
58. R.S. LONGHURST: Geometrical and Physical Optics (Longman, 2nd edition, 1967).
59. G.T. SCHAPPERT, K.W. BILLMAN and D.C. BURNHAM: Appl. Phys. Lett., 13, 124, (1968).
60. W.E. SPEAS: Phys. Rev., 31, 569, (1928).
61. J.B. MARLING, D.W. GREGG and S.J. THOMAS: I.E.E.E. J. Quant. Electr., QE-6, 570, (1970).
62. D.J. BRADLEY, B. LIDDY and W.E. SLEAT: Optics Comm., 2, 391, (1971).

63. J.A. GIORDMAINE, P.M. RENTZEPIS, S.L. SHAPIRO and K.W. WECHT: Appl. Phys. Lett., 11, 216, (1967).
64. H.P. WEBER: J. Appl. Phys., 38, 2231, (1967).
65. M.A. DUGUAY and J.W. HANSEN: Appl. Phys. Lett., 15, 192, (1969).
66. P.M. RENTZEPIS, C.J. MITSCHLE and A.C. SAXMAN: Appl. Phys. Lett., 17, 122, (1970).
67. R.C. ECKARDT and C.H. LEE: Appl. Phys. Lett., 15, 425, (1969).
68. A. DIENES, E.P. IPPEN and C.V. SHANK: Appl. Phys. Lett., 19, 258, (1971).
- 69a. M. BORN and E. WOLF: Principles of optics (Pergamon Press, 3rd edition, 1965).
- 69b. L. MANDEL and E. WOLF: Proc. Phys. Soc., 80, 894, (1962).
70. R.L. SMITH and C.O. ALLEY: Optics Comm., 1, 262, (1970).
71. M. DI DOMENICO, J.E. GEUSIC, H.M. MARCOS and R.G. SMITH: Appl. Phys. Lett., 8, 180, (1966).
72. C.K. CHAN and S.O. SARI: Appl. Phys. Lett., 25, 403, (1974).
73. H.P. WEBER and R. DANDLIKER: I.E.E.E. J. Quant. Electr., QE-4, 1009, (1968).
74. J.R. KLAUDER, M.A. DUGUAY, J.A. GIORDMAINE and S.L. SHAPIRO: Appl. Phys. Lett., 13, 174, (1968).
75. R.H. PICARD and P. SCHWEITZER: Phys. Rev., 1A, 1803, (1970).
76. D. von der LINDE: I.E.E.E. J. Quant. Electr., QE-8, 328, (1972).
77. E.P. IPPEN and C.V. SHANK: Appl. Phys. Lett., 27, 488, (1975).
78. R.C. MILLER: Phys. Lett., 26A, 177, (1968).
79. E.K. ZAVOISKII and S.D. FANCHENKO: Sov. Phys.- Doklady, 1, 285, (1956).
80. D.J. BRADLEY and W. SIBBETT: Appl. Phys. Lett., 27, 382, (1975).
81. W.E. SLEAT: PhD. thesis, Queen's University of Belfast, (1974).
82. A.G. RODDIE: PhD. thesis, Queen's University of Belfast, (1972).
83. F.J. McCLUNG and R.W. HELLWARTH: J. Appl. Phys., 33, 828, (1962).
84. M.H. CROWELL: I.E.E.E. J. Quant. Electr., QE-1, 12, (1965).
85. C.M. FERRAR: I.E.E.E. J. Quant. Electr., QE-5, 550, (1969).

86. A.J. DeMARIA, D.A. STETSER and H. HEYNAU: Appl. Phys. Lett., 8, 174, (1966).
87. M.E. MACK: I.E.E.E. J. Quant. Electr., QE-4, 1015, (1968).
88. D.J. BRADLEY: Opto-electronics, 6, 25, (1974).
89. D.J. BRADLEY, G.H.C. NEW and S.J. CAUGHEY: Phys. Lett., 30A, 78, (1969).
90. W.H. GLENN, M.J. BRIENZA and A.J. DeMARIA: Appl. Phys. Lett., 12, 54, (1968).
91. D.J. BRADLEY and A.J.F. DURRANT: Phys. Lett., 27A, 73, (1968).
92. M.E. MACK: Appl. Phys. Lett., 15, 166, (1969).
93. C.K. CHAN, S.O. SARI and R.E. FOSTER: J. Appl. Phys., 47, 1139, (1976).
94. H. MAHR: Private communication.
95. J.M. HARRIS, R.W. CHRISMAN and F.E. LYTLE: Appl. Phys. Lett., 26, 16, (1975).
96. P.K. RUNGE: Optics Comm., 5, 311, (1972).
97. D.J. KUIZENGA: Appl. Phys. Lett., 19, 280, (1971).
98. A.E. SIEGMAN and D.J. KUIZENGA: Opto-electronics, 6, 43, (1974).
99. P.P. SOROKIN, J.R. LANKARD, V.L. MORUZZI and E.C. HAMMOND: J. Chem. Phys., 48, 4726, (1968).
100. D.J. BRADLEY and F. O'NEILL: J. Opto-electronics, 1, 69, (1969).
101. E.G. ARTHURS, D.J. BRADLEY and A.G. RODDIE: Appl. Phys. Lett., 19, 480, (1971).
102. F. SHIMIZU: Phys. Rev. Lett., 19, 1097, (1967).
103. D.J. BRADLEY, B. LIDDY, A.G. RODDIE, W. SIBBETT and W.E. SLEAT: Optics Comm., 3, 427, (1971).
104. A. SCAVENNEC and N.S. NAHMAN: I.E.E.E. J. Quant. Electr., QE-10, 95, (1974).
105. C.V. SHANK and E.P. IPPEN: Appl. Phys. Lett., 24, 374, (1974).
106. E.B. TREACY: I.E.E.E. J. Quant. Electr., QE-5, 454, (1969).
107. E.B. TREACY: J. Appl. Phys., 42, 3848, (1971).
108. R.S. ADRAIN, E.G. ARTHURS, D.J. BRADLEY, A.G. RODDIE and J.R. TAYLOR: Optics Comm., 12, 142, (1974).

109. D.N. DEMPSTER, T. MORROW, R. RANKIN and G.F. THOMPSON: J. Chem. Soc., Faraday Tran. II, 68, 1479, (1972).
110. D. MAGDE and M.W. WINDSOR: Chem. Phys. Lett., 27, 31, (1974).
111. E.G. ARTHURS, D.J. BRADLEY and A.G. RODDIE: Chem. Phys. Lett., 22, 230, (1973).
112. E.G. ARTHURS, D.J. BRADLEY and A.G. RODDIE: Optics Comm., 8, 118, (1973).
113. H.E. LESSING, E. LIPPERT and W. RAPP: Chem. Phys. Lett., 7, 247, (1970).
114. G.H.C. NEW: Optics Comm., 6, 188, (1972).
115. N.G. BASOV, R.V. AMBARTSUMYAN, V.S. ZUEV, P.G. KRYUKOV and V.S. LETOKHOV: Sov. Phys. JETP, 23, 16, (1966).
116. T.I. KUZNETSOVA, V.I. MALYSHEV and A.S. MARKIN: Sov. Phys. JETP, 25, 286, (1967).
117. D.J. BRADLEY, G.H.C. NEW and S.J. CAUGHEY: Optics Comm., 2, 41, (1970).
118. S.J. CAUGHEY: Ph.D. Thesis, Queens University of Belfast, (1970).
119. D.J. BRADLEY and W. SIBBETT: Optics Comm., 9, 17, (1973).
120. E.M. GARMIRE and A. YARIV: I.E.E.E. J. Quant. Electr., QE-3, 222, (1967).
121. H.A. HAUS, C.V. SHANK and E.P. IPPEN: Optics Comm., 15, 29, (1975).
122. G.H.C. NEW: I.E.E.E. J. Quant. Electr., QE-10, 115, (1974).
123. J.A. ARMSTRONG: Appl. Phys. Lett., 10, 16, (1967).
124. S.L. McCALL and E.L. HAHN: Phys. Rev., 183, 457, (1969).
125. E.B. TREACY: Phys. Lett., 28A, 34, (1968).
126. E.B. TREACY: Appl. Phys. Lett., 17, 14, (1970).
127. R.A. FISHER, P.L. KELLEY and T.K. GUSTAFSON: Appl. Phys. Lett., 14, 140, (1969).
128. A. LAUBEREAU and D. von der LINDE: Z. Naturforsch., 25a, 1626, (1970).
129. E.P. IPPEN, C.V. SHANK and T.K. GUSTAFSON: Appl. Phys. Lett., 24, 190, (1974).
130. C.L. TANG and H. STATZ: J. Appl. Phys., 38, 2963, (1967).

131. E.G. ARTHURS, D.J. BRADLEY and A.G. RODDIE: Appl. Phys. Lett., 23, 88, (1973).
132. V.R. NAGIBAROV and V.V. SAMARTSEV: Chem. Phys. Lett., 5, 61, (1970).
133. I.D. ABELLA, N.A. KURNIT and S.R. HARTMAN: Phys. Rev., 141, 391, (1966).
134. D.J. BRADLEY and G.H.C. NEW: Pros. I.E.E.E., 62, 313, (1974).
135. D.J. BRADLEY, G.H.C. NEW and S.J. CAUGHEY: Phys. Lett., 32A, 313, (1970).
136. V.S. LETOKHOV and V.N. MOROZOV: Sov. Phys. JETP, 25, 862, (1967).
137. R. CUBEDDU and O. SVELTO: I.E.E.E. J. Quant. Electr., QE-5, 495, (1969).
138. R.C. ECKARDT, C.H. LEE and J.N. BRADFORD: Digest of Technical Papers, 7th International Quantum Electronics Conference, (1972).
139. S.A. AKHMANOV, A.P. SUKHORUKOV and R.V. KHOKHLOV: Sov. Phys. Uspekhi, 10, 109, (1968).
140. E.G. ARTHURS: Ph. D. Thesis, Queen's University of Belfast, (1972).
141. M.R. TOPP and G.C. ORNER: Optics Comm., 13, 276, (1975).
142. E.G. ARTHURS, D.J. BRADLEY and T.J. GLYNN: Optics Comm., 12, 136, (1974).
143. E.G. ARTHURS, D.J. BRADLEY, P.N. PUNTAMBEKAR, I.S. RUDDOCK and T.J. GLYNN: Optics Comm., 12, 360, (1974).
144. J. SHAH and R.F. LEHENY: Appl. Phys. Lett., 24, 562, (1974).
145. E.G. ARTHURS: Private Communication.
146. A. HIRTH, K. VOLLRATH, J. FAURE and D. LOUGNOT: C.R. Acad. Sci. B (France) 276, 153, (1973).
147. J. de VRIES, D. BEBELAAR and J. LANGELAAR: Digest of Technical Papers, 9th International Quantum Electronics Conference, (1976).
148. J.P. LETOUZEY and S.O. SARI: Appl. Phys. Lett., 23, 311, (1973).
149. W.E. LAMB: Phys. Rev., 134A, 1429, (1964).
150. H. STATZ, G.A. De MARS and C.L. TANG: J. Appl. Phys., 38, 2212, (1967).
151. S.E. SCHWARZ: I.E.E.E. J. Quant. Electr., QE-4, 509, (1968).
152. J.A. FLECK: J. Appl. Phys., 39, 3318, (1968).
153. V.S. LETOKHOV: Sov. Phys. JETP, 28, 562, (1969).

154. B. Ya. ZEL'DOVICH and T.I. KUZNETSOVA: Sov. Phys. Uspekhi, 15, 25, (1972).
155. N.G.BASOV, V.S. ZUEV, P.G. KRYUKOV, V.S. LETOKHOV, Yu. V. SENATSKII and S.V. CHEKALIN: Sov. Phys. JETP, 27, 410, (1968).
156. W.H. GLENN: Digest of Technical Papers, 7th International Quantum Electronics Conference, (1972).
157. G.H.C. NEW, K.E. ORKNEY and M.J.W.NOCK: Optic. Quant. Electr. 8, No. 5, (1976).
158. H.A. HAUS: I.E.E.E. J. Quant. Electr., QE-11, 736, (1975).
159. H.A. HAUS: I.E.E.E. J. Quant. Electr., QE-12, 169, (1976).
160. B.K. GARSIDE and T.K. LIM: J. Appl. Phys., 44, 2335, (1973).
161. B.K. GARSIDE and T.K. LIM: Optics. Comm., 8, 297, (1973).
162. T.K. LIM and B.K. GARSIDE: Optics Comm., 12, 8, (1974).
163. B.K. GARSIDE and T.K. LIM: Optics. Comm., 12, 240, (1974).

ACKNOWLEDGMENTS

It is with pleasure that I wish to thank Prof. D. J. Bradley FRS for his excellent supervision and untiring encouragement and for the extensive research facilities provided.

I am also indebted to Dr. W. Sibbett for his assistance with the streak camera measurements and for many stimulating discussions and also Dr. P. N. Puntambekar of the National Physical Laboratory (New Delhi) with whom part of this work was undertaken. For many helpful suggestions during the course of this research, I must express my gratitude to the other members of the Optics Section and to Dr. G. H. C. New and Mr. K. Orkney for elucidation of the theoretical aspects of passive mode-locking.

In addition, I would like to acknowledge the proficient work of the technical staff of Imperial College, London and thank Miss Joelle French for typing this thesis.

Financial support was by a Ministry of Education for Northern Ireland Postgraduate Studentship.

THE EFFECT OF SATURABLE ABSORBER LIFETIME IN PICOSECOND PULSE GENERATION. II. THE CRESYL-VIOLET LASER

E.G. ARTHURS, D.J. BRADLEY, P.N. PUNTAMBEKAR and I.S. RUDDOCK

*Optics Section, Physics Department, Imperial College,
London SW7 2BZ, England*

and

T.J. GLYNN*

*Department of Pure and Applied Physics, The Queen's University,
Belfast BT7 1NN, Northern Ireland*

Received 11 October 1974

Picosecond pulse generation in a pulsed cresyl-violet laser, mode-locked by four saturable absorbers (DTDCI, DDCI, DCI, and DCI'), of different relaxation times, has been directly studied. In contrast to the ruby laser case, the ultimate pulse duration is largely independent of the absorber lifetime. Pulses of ~ 4 psec duration are obtained from a cw Rhodamine B dye laser mode-locked with cresyl-violet.

1. Introduction

In paper I, [1], hereafter designated I, direct photoelectric measurements of the build-up phase in a ruby laser, mode-locked by DTDCI and DDCI saturable absorbers were reported. These investigations showed that the absorber relaxation time determined the pattern of pulse generation and set a lower limit to the final pulse duration. The aperture time (~ 120 psec) of the DTDCI dye cell employed was of the same duration as the shortest fluctuations at the end of the linear phase of amplification in the ruby laser, while for DDCI the corresponding time was an order of magnitude shorter. With the extension of mode-locking to the cresyl-violet laser [2] operating in the same spectral region as the ruby laser, it was possible to investigate the effect of strong amplifier saturation arising from the very short storage time (~ 3 nsec) of the dye active medium. The results obtained show that while, as in I, the aperture time of the absorber

cell strongly affects the nature of the picosecond pulse selection process, practically the same final pulse durations were produced by four mode-locking dyes of widely varying relaxation times. This independence of absorber lifetime of pulse duration in dye lasers was further emphasised by the production of single pulses as short as 3 psec, with a cw Rhodamine B laser mode-locked by a cresyl-violet dye cell.

2. The saturable absorber dyes

The absorption spectra, obtained from spectrophotometer measurements of the polymethine dyes employed for mode-locking are shown in fig. 1 together with the fluorescence spectrum of cresyl-violet. The ruby laser wavelength is also indicated. The absorption relaxation times of DDCI and DTDCI were measured by the method previously employed [1, 3] for DODCI (3,3'-diethyl-oxadiazocyanine iodide). Picosecond pulses from the mode-locked cresyl-violet laser tuned to operate at 700 nm or 654 nm, were employed for excitation and transmission measurements of DDCI

* Present address: Clarendon Laboratory, Department of Physics, University of Oxford, Parks Road, Oxford, England.

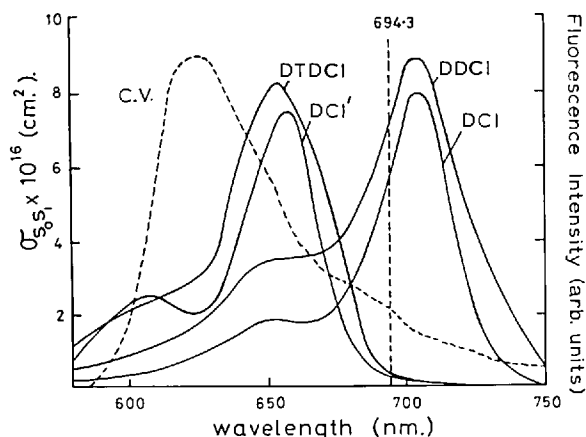


Fig. 1. Variations of absorption cross-sections of saturable absorbers as a function of wavelength. The fluorescence spectrum of cresyl-violet is also shown.

and DTDCI respectively. The value of 175 psec for DTDCI relaxation was in close agreement with the ~ 185 psec fluorescence lifetime. This was determined directly [4] from streak-camera records of the time-resolved fluorescence, emitted after excitation by a mode-locked Rhodamine 6G laser, tuned to operate at 605 nm. The fluorescence was isolated from scattered pumping beam light by spectral filtering. The decay of the side-light fluorescence from the DTDCI mode-locking dye-cell in the cresyl-violet laser was also measured with the streak-camera, giving the same result. The fluorescence lifetime of DDCI could not be measured because of its lower quantum efficiency (2.8×10^{-3}) [5] and the reduced photocathode sensitivity of the Photochron streak-tube at the longer fluorescence wavelength (750 nm). Our estimate for the fluorescence lifetime of DCI' was obtained from the product of the calculated radiative lifetime [6] and the measured quantum efficiency. The relaxation times of the saturable absorbers available for the ruby and cresyl-violet laser wavelength region thus vary from ~ 10 psec to ~ 180 psec.

The ability of DTDCI to mode-lock at 694.3 nm arises from the generation of a photoisomer with an absorption spectrum shifted to the red [7] as in the case of Rhodamine 6G mode-locked by DODCI at 625 nm [8]. The substantial difference in the fluorescence decay times reported for DCI in refs. [9] and [10] has been explained, [10], by the effect of stimulated emission, when the dye solution was excited by a high-power laser source. The resultant shortening of the fluorescent lifetime will also result in shorter ab-

Table 1

Mode-locking dye	Lifetimes		Ref.
	Absorption (psec)	Fluorescence (psec)	
1,1'-diethyl-2,2'-dicarbocyanine iodide (DDCI) in methanol	25	14	[9]
in ethanol		11	This publ. [13]
1,1'-diethyl-4,4'-carbocyanine iodide (DCI, cryptocyanine) in methanol	80	110	[10]
in ethanol		20-40	[11]
1,1'-diethyl-2,4'-carbocyanine iodide (DCI')	10	37	[9]
in ethanol		20	This publ. [12]
3,3'-diethyl-2,2'-thiadcarbocyanine iodide (DTDCI) in ethanol	175	185	This publ.
		1.2×10^3	[7]

sorption recovery times. However, the authors of [13] obtained a result in good agreement with that of [9], from the measured fluorescence quantum efficiency and the calculated radiative lifetime. Our measurements and those reported earlier [3, 4] for DODCI, were carried out in the conditions under which the saturable absorbers operate, inside the mode-locking cell in the laser cavity.

Care has also to be taken in determining the lifetime from the absorption measurement, to correct the measured dye cell absorption recovery time or aperture time. This will depend upon the particular low-light level transmission employed and the induced absorption change [3, 14]. This correction appears to have been neglected in some recent publications [15, 16]. The lifetimes thus determined are then those directly relevant to studies of laser mode-locking,* particularly for DTDCI and DODCI where photoisomer generation [3-5] adds further complications. The difference between our value and the lifetime of

* In discussion of a "DODCI controversy" the authors of [15] do not appear to have appreciated the conditions under which the lifetime measurements reported in [3] and [4] were carried out.

DTDCI from [7], could also arise from the effect of stimulated emission under the high power excitation conditions of our measurements, particularly in view of the high fluorescence quantum efficiency of DTDCI. The short fluorescence lifetimes of DDCI and DCI' are less likely to be affected by stimulated emission.

3. The cresyl-violet laser

The mode-locked dye laser arrangement was identical to that previously employed [8, 17]. The efficiency of lasing was improved by employing a mixed solution, in ethanol, of Rhodamine 6G and cresyl-violet, continuously circulated through a quartz laser dye-cell, pumped by a linear quartz ablative flaslamp. The optical length of the laser cavity was ~ 55 cm, giving a double-transit time of 4 nsec. Mirror reflectivities at the lasing wavelength were 100% (immersed in the mode-locking dye cell, of 2 mm path length) and 65%. Frequency narrowing and tuning was obtained with an optically contacted, narrow-gap ($\sim 7 \mu\text{m}$) wedged Fabry-Pérot interferometer, with dielectric coatings of $\sim 65\%$ reflectivity from 580 nm to 710 nm. The corresponding tuning range covered ~ 32 nm, near 670 nm. With ethanol only in the mode-locking dye cell the threshold pumping energy was ~ 300 J. Regular mode-locked pulse trains were produced at a pumping level of 900–1000 J. The total energy in a train depended upon the saturable absorber employed, its concentration and the operating wavelength. Generally, with optimised concentration of the absorber, total output energies of 10–30 mJ were obtained, as measured calorimetrically. Lower energy was produced at the long wavelength end of the tuning range. The longest pulse trains ($\sim 2.5 \mu\text{sec}$) were generated by DTDCI. In general the rate of picosecond pulse build-up increased with the gain of the active medium i.e. as the laser was tuned to shorter wavelengths (see figs. 1 and 2). In the untuned laser in each case, the build-up took longer than in the tuned laser operating at the same wavelength.

Details of the streak-camera system employed for directly measuring pulse durations and for studying the details of the pulse generation process have been previously, reported [1, 2, 17–19]. With all of the four mode-locking dyes, measured pulse durations of

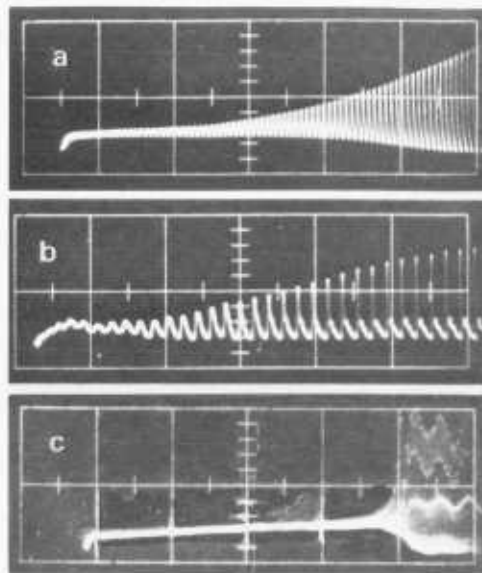


Fig. 2. Oscillograms of the initial stages of mode-locking by (a), (b) DTDCI (a) The untuned cresyl-violet laser operating at 701 nm. (Time scale 50 nsec per major division) and (b) laser output tuned to 690 nm (Time scale 20 nsec/div). (c) Mode-locking by DDCI 690 nm. (Time scale 100 nsec/div.)

5–7 psec were consistently obtained at the middle of the train, in good agreement with earlier two-photon fluorescence measurements [8]. There was negligible variation in pulse duration later in the pulse trains.

The gross differences in the initial stages of pulse evolution can be clearly seen in the oscillograms of fig. 2, recorded with a fast photodiode and Tektronix 519 oscilloscope. With DTDCI the build-up was characterized by the appearance of a single broad modulation, corresponding to the double-transit-time. This structure was transformed, at a rate depending upon the laser wavelength, into single pulses of detector limited durations. When the laser was tuned to operate at 690 nm, detector limited pulses appeared after only 20 round trips (~ 80 nsec) (fig. 2b), while a longer build-up phase (~ 250 nsec) was obtained on tuning to longer wavelengths (695–700 nm). The more abrupt generation of the pulse train produced in the tuned laser, mode-locked by DDCI, can be seen in fig. 2c. Streak camera records gave more detailed pictures. The streaking speed was reduced to $5 \times 10^8 \text{ cm sec}^{-1}$ to permit the recording of more than one double-transit time. In fig. 3 the traces (a)–(d) for DTDCI mode-locking, correspond to times 150, 300,

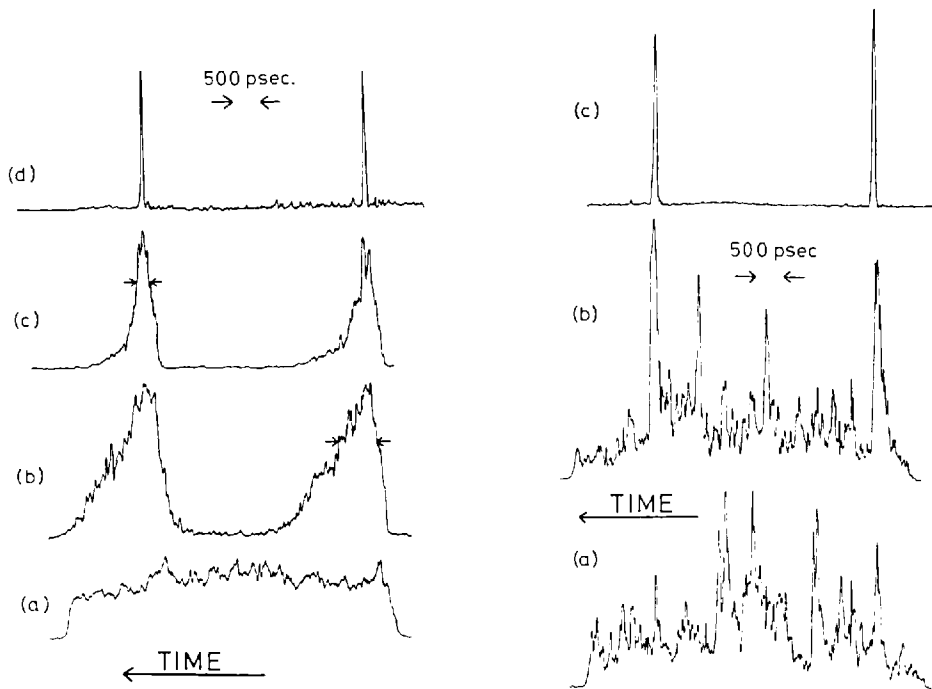


Fig. 3. Sequence of streak camera microdensitometer traces (time resolution of ~ 30 psec) showing pulse development in cressyl-violet laser mode-locked by (L.H.S.) DTDCI (untuned) and (R.H.S.) DDCI (tuned to 695 nm) (see text for details).

350 and 500 nsec after threshold was achieved. Because of the broad lasing bandwidth (~ 3 nm) of the untuned laser, the shortest initial fluctuations would have durations $\sim 2 \times 10^{-13}$ sec. The saturation of the DTDCI absorber would then be determined by the integrated energy density. A broad group of fluctuations is initially selected as for the Rhodamine 6G laser mode-locked by DODCI [2]. The shaping of the leading edge by absorber saturation is clear, even in the initial stages, while the trailing edge is attenuated by gain saturation [2, 20]. A corresponding sequence of streak records for DDCI mode-locking is also shown in fig. 3. In this case the tuned laser had an initial bandwidth of 0.5 nm. The three streaks correspond to times 85, 90 and 95 round-trips after laser threshold. Trace (c) was recorded with the laser intensity attenuated by $\times 30$ compared with that used for recording (a) and (b). These results show an evolution process similar to that obtained (1) from a ruby laser mode-locked by the same dye, but with a considerably more rapid selection rate. This arises from the greater effect of gain depletion in the cressyl-violet laser.

In the untuned dye laser mode-locked by DDCI,

the pulse generation pattern is similar except that the mode-locked train does not appear until ~ 150 round trips after threshold. Broad fluctuations in the intensity are observed after ~ 50 round trips. The effect of gain saturation is clearly seen in fig. 4. The pulse marked A,

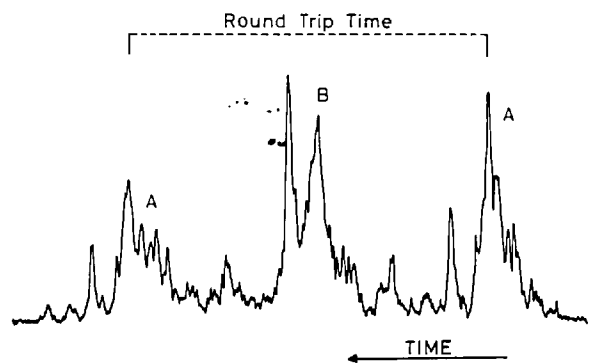


Fig. 4. Microdensitometer trace of streak recording (time resolution ~ 30 psec) showing pulse development in one round trip for the untuned cressyl-violet laser mode-locked using DDCI. This output occurred ~ 600 nsec after threshold and ~ 5 round trips before the appearance of the mode-locked output.

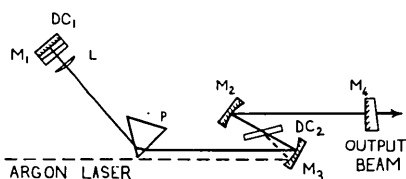


Fig. 5. Schematic diagram of cw mode-locked dye laser. Lens L focal length = 2.5 cm. Radius of curvature of mirrors M_2 , $M_3 = 10$ cm. M_1 , M_4 reflectivities = 99%.

which would otherwise have its leading edge sharpened by absorber saturation, is in fact effectively broadened and reduced in height in a single round trip because of gain depletion by the pulse marked B.

4. CW mode-locking

The above experimental results in cresyl-violet mode-locking and earlier investigations of Rhodamine lasers [2] show that picosecond pulses are produced with absorbers of lifetimes of hundreds of picoseconds. We have also investigated mode-locking of a cw Rhodamine B laser employing cresyl-violet as the saturable-absorber. The experimental system (fig. 5) combines the two different focussing arrangements used in the first mode-locked cw dye lasers [21, 22]. In this configuration all lines of the argon ion laser could be employed to produce a pumping power of 3 W. Mirrors M_1 , M_2 had 100% broad band reflectivity dielectric coatings. Tuning of the basic Rhodamine B laser over the range 599.6–650.5 nm was obtained with a 2×10^{-3} M solution in water containing 10% ammonyx L.O. When mode-locked with a 4×10^{-5} M solution in ethanol of DODCI, the laser produced pulses of durations ~ 3 psec, except at the long wavelength limit of the 610–630 nm tuning range, where the pulses lengthened to 5 psec. Pulse durations were measured by the method of second-harmonic generation in a Michelson interferometer arrangement [23]. With a solution of cresyl-violet in ethanol (2×10^{-5} M) in the saturable absorber dye cell, mode-locking from 610–620 nm, with pulse durations of 3–4 psec was obtained. The double transit time in the cavity was 10 nsec and correct optical alignment was critical for producing good mode-locking. The second harmonic trace of fig. 6 shows a pulse width of 4 psec, at 615 nm, with a 3:1 contrast ratio.

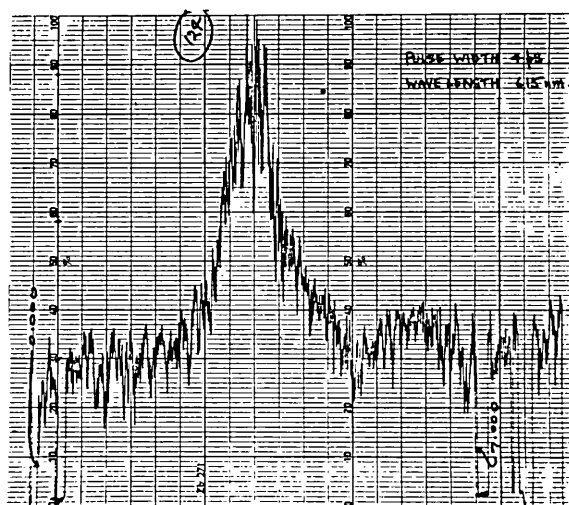


Fig. 6. Second-harmonic generation profile showing pulse duration of 4 psec at 615 nm from cw Rhodamine B laser mode-locked by cresyl-violet dye. Contrast ratio = 3:1.

5. Discussion

These results clearly show that picosecond pulses can be generated by mode-locking dye lasers with saturable absorbers of a very wide range of relaxation times. These and earlier investigations [1, 2, 17] have clarified the details of the mode-locking processes. While in dye lasers gain depletion plays a major role, the rate of ultra-short pulse generation also depends upon the relaxation time of the saturable absorber employed. The broad bandwidths available in these lasers should permit the generation of pulses as short as 10^{-13} sec. Because of reproducibility and ease of control of the various parameters further investigations of mode-locking will be more easily undertaken with cw laser systems. It will be interesting to see if molecular internal relaxation processes in the dyes will affect the generation of sub-picosecond pulses. The recent development of the Photochron II streak camera with sub-picosecond time-resolution [24] will facilitate these studies which are under way in our laboratory.

Acknowledgement

We are glad to acknowledge financial support from the Science Research Council and the Paul Instrument Fund of the Royal Society.

References

- [1] E.G. Arthurs, D.J. Bradley and T.J. Glynn, *Opt. Commun.* 12 (1974) 136.
- [2] E.G. Arthurs, D.J. Bradley and A.G. Roddie, *Appl. Phys. Lett.* 23 (1973) 88.
- [3] E.G. Arthurs, D.J. Bradley and A.G. Roddie, *Opt. Commun.* 8 (1973) 118.
- [4] E.G. Arthurs, D.J. Bradley and A.G. Roddie, *Chem. Phys. Lett.* 22 (1973) 230.
- [5] N. Dempster, T. Morrow, R. Rankin and G.F. Thompson, *Chem. Phys. Lett.* 18 (1973) 488.
- [6] T.R. Forster, *Fluoreszenz Organischer Verbindungen* (Vandenhoeck und Ruprecht, Göttingen, 1951).
- [7] D.N. Dempster, T. Morrow, R. Rankin and G.F. Thompson, *J. Chem. Soc. Faraday II* 68 (1972) 1479.
- [8] E.G. Arthurs, D.J. Bradley and A.G. Roddie, *Appl. Phys. Lett.* 20 (1972) 125.
- [9] M.A. Duguay and J.W. Hansen, *Opt. Commun.* 1 (1969) 254.
- [10] G. Mourou, G. Busca and M.M. Denariez-Roberge, *Opt. Commun.* 4 (1971) 40.
- [11] G. Mourou, B. Drouin, M. Bergeron and M.M. Denariez-Roberge, *IEEE J. Quantum Electron.* QE-9 (1973) 745.
- [12] M.W. McGeoch, *Opt. Commun.* 7 (1973) 116.
- [13] D.N. Dempster, T. Morrow, R. Rankin and G.F. Thompson, *Chem. Phys. Lett.* 22 (1973) 222.
- [14] G. Mourou, B. Drouin and M.M. Denariez-Roberge, *Appl. Phys. Lett.* 20 (1972) 453.
- [15] D. Magde and M.W. Windsor, *Chem. Phys. Lett.* 27 (1974) 31.
- [16] G.E. Busch, R.P. Jones and P.M. Rentzepis, *Chem. Phys. Lett.* 18 (1973) 178.
- [17] D.J. Bradley, *Opto-Electronics* 6 (1974) 25, and references therein.
- [18] D.J. Bradley, B. Liddy, A.G. Roddie, W. Sibbett and W.E. Sleat, *Opt. Commun.* 3 (1971) 426.
- [19] D.J. Bradley and G.H.C. New, *Proc. IEEE* 62 (1974) 313.
- [20] G.H.C. New, *IEEE J. Quantum Electron.* QE-10 (1974) 115.
- [21] E.P. Ippen, C.V. Shank and A. Dienes, *Appl. Phys. Lett.* 21 (1972) 348.
- [22] F. O'Neill, *Opt. Commun.* 6 (1972) 363; E.G. Arthurs, D.J. Bradley, B. Liddy, F. O'Neill, A.G. Roddie, W. Sibbett and W.E. Sleat, *Proc. 10th Intern. Conf. High Speed Photography.* (1972) 117.
- [23] H.P. Weber, H.G. Danielmeyer, *Phys. Rev. A2* (1970) 2074.
- [24] P.R. Bird, D.J. Bradley and W. Sibbett, *Proc. 11th Intern. Conf. High Speed Photography* (1974), in press.

Bandwidth-limited subpicosecond pulse generation in mode-locked cw dye lasers

I. S. Ruddock and D. J. Bradley

Optics Section, Physics Department, The Blackett Laboratory, Imperial College, London SW7 2BZ, England
(Received 13 April 1976)

A cw Rhodamine 6G dye laser with a thin optically contacted saturable absorber cell has been mode locked over an operating frequency range of 598–615 nm to produce pulses with durations as short as 0.3 ps. The pulses, with sech^2 intensity profiles, are practically bandwidth limited.

PACS numbers: 42.60.Eb, 42.60.Lh, 42.65.Dr

The first passively mode-locked cw dye lasers produced pulses of durations of a few picoseconds.^{1–3} Shorter pulses of durations ~ 1.0 ps were later obtained by employing a composite dye laser arrangement⁴ and by combining two saturable absorbers as the mode-locking element.⁵ However, these shorter-duration pulses were not bandwidth limited in duration. Subpicosecond pulses, as short as 0.3 ps, were obtained by compressing, with a grating pair, the frequency-chirped pulses generated in a system employing two free-flowing dye streams, for the active medium and the absorber solution, respectively.⁵ We wish to report the direct production of pulses of durations down to 0.3 ps by employing a cavity configuration incorporating an optically contacted saturable absorber dye cell. With this arrangement which is a modification of one previously published,⁶ bandwidth-limited subpicosecond pulses are readily obtained.

The laser cavity consists (Fig. 1) of an open-flowing (at Brewster's angle) "jet stream" of Rhodamine 6G/ethylene glycol situated near the center of the resonator in a conventional astigmatically compensated pumping configuration at the focus of two 10-cm-radius mirrors. The DODCI (3,3'-diethyloxadicyanine iodide) saturable absorber, dissolved in ethanol, flows in a thin variable-gap dye cell in contact with the high-reflectivity mirror. The dye laser beam is focused down into the absorber solution by a planoconvex lens of 2.5-cm focal length, to increase the power density there by 4 times. Both surfaces of the lens and the air/glass interface of the 1° wedged dye cell window are anti-reflection coated. Tuning is provided by rotation of the low-dispersion fused silica Brewster's angle prism.

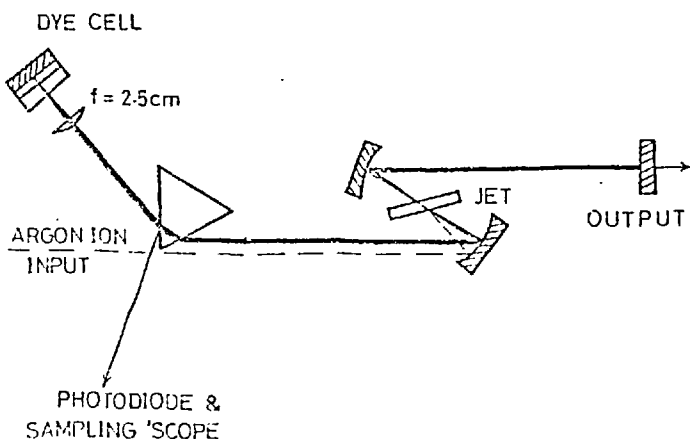


FIG. 1. Passively mode-locked cw dye laser cavity configuration.

(This arrangement also allows the use of all lines of the argon-ion pumping laser if necessary.) The output beam goes through the plane mirror, of transmission 5% at 600 nm, and the cavity length is such that the round trip is ~ 12 ns. Placing the saturable absorber dye in contact with one of the laser mirrors has previously been shown to be the optimum arrangement for the production of the shortest pulses and the most reliable mode locking in pulsed lasers.⁷

With an absorber dye cell thickness of 0.5 mm, pulse durations of 1.0–1.5 ps were readily obtained over the tuning range 595–615 nm. Pulse durations were measured both by the second-harmonic autocorrelation method and by an electron-optical streak camera, details of which have been given elsewhere.⁸ In the second-harmonic generation method an ADP crystal of 0.3-mm thickness was used to permit phase matching over the laser bandwidth. Reducing the DODCI cell length to 0.2 mm, and increasing the dye concentration to maintain the same low-light-level transmission of the cell, resulted in a reduction of the pulse durations.

A typical second-harmonic trace is shown in Fig. 2 for the laser operating at 607 nm. The best fit to the experimental curve is obtained for the autocorrelation function $G(\tau)$ of hyperbolic secant pulses of durations 0.5 ps. The pulse duration Δt (FWHM) is calculated⁹ by assuming pulses of intensity $I(t) \propto \text{sech}^2 t/T$, where $T = \Delta t/1.76$. The function $G(\tau)$, represented by the discrete points in Fig. 2, is given by

$$G(\tau) = 4T \frac{\cosh \tau/T - \tau/T \sinh \tau/T}{\sinh^3 \tau/T}$$

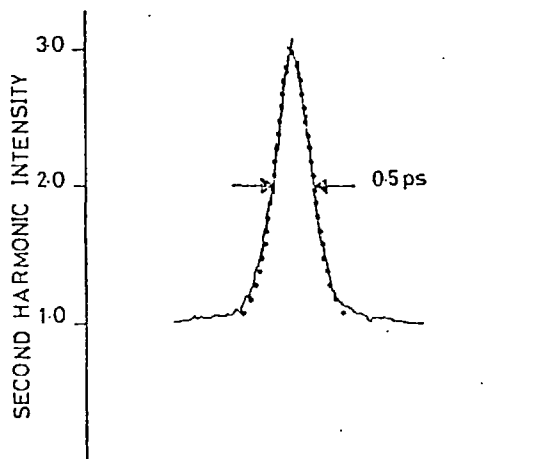


FIG. 2. Second-harmonic autocorrelation trace. Laser operating wavelength is 607 nm. The discrete points have been calculated for a sech^2 laser pulse profile.

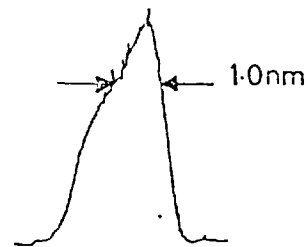


FIG. 3. Spectrum of mode-locked laser recorded simultaneously with the pulse duration measurement of Fig. 2. Arrows indicate the spectral half-width.

The full width at half-maximum, $\Delta\tau_G$, is related to the laser pulse duration Δt by $\Delta\tau_G = 1.55\Delta t$. The shortest pulses recorded had durations of 0.3 ps (at 610 nm) for a DODCI concentration of $3.6 \times 10^{-5} M$ and a pumping power level of 3 W of the argon-ion laser operating on the 514.5-nm line.

The mode-locking stability and the pulse durations do not depend on the pump level. The dye laser can operate up to 25% (0.6 W) above the threshold pumping power level of 2.4 W and still generate pulses as short as 0.3 ps. At higher pumping power levels (~30% above threshold) pulse durations increase to the 1–2-ps range and operation becomes less stable. At the optimum operating conditions, the pulse characteristics remained unchanged for periods in excess of 1 h. An average output power of 15 mW for 0.5-ps pulses has been measured, corresponding to peak pulse powers of 300 W.

Operation with the optically contacted dye cell always produces second-harmonic traces corresponding to a sech^2 pulse intensity profile, even under conditions when, for example, poor alignment causes longer structured pulses. This is in contrast to the results obtained when we, and other authors,⁵ have used a dye solution in the form of a second free-flowing jet. With this arrangement exponential wings occur on the autocorrelation traces even during optimum mode locking. In addition, with the two-jet arrangement, time-structured pulses with their characteristic autocorrelation traces, consisting of a sharp spike on a broad base, are produced at pump powers of 150–200 mW above threshold. As DODCI only is employed in the saturable absorber solution, a wide tuning range over the spectral region 598–615 nm is obtained with durations of 0.3–0.9 ps.

Confirmation that these pulses were of bandwidth-limited durations was given by simultaneous measurements of the oscillating bandwidth. A microdensitometer trace of the spectrograph plate, exposed during the recording of the autocorrelation function of Fig. 2 is shown in Fig. 3. The bandwidth of 1.0 nm at the half-intensity position (calibrated by covering part of the spectrograph entrance slit by a neutral density filter of 50% transmission) indicated that the mode-locked pulses were close to the Fourier transform limit. The corresponding "time-bandwidth product", in this example, of $\Delta\nu\Delta t = 0.45$ is to be compared with the theoretical value for sech^2 pulses of $\Delta\nu\Delta t = 0.32$. From a large number of such simultaneous spectral and temporal measurements, the $\Delta\nu\Delta t$ products for the subpicosecond pulses were found to lie in the range 0.4–0.8. Substantial frequency chirps have not been observed using the optically contacted absorber dye cell configuration, in contrast with other systems.⁵

These sech^2 pulses agree well with a recent theoretical model⁹ which predicts steady-state bandwidth-limited pulses of this shape when a bandwidth-limiting element is used. The tuning prism produces a bandwidth-limiting effect which tends to broaden the pulse intensity temporal profile. Eventually an equilibrium situation is achieved when this pulse broadening mechanism is balanced by the pulse compression produced by saturation of both the gain and the absorbing media.^{10,11} New has shown¹¹ that the optically contacted dye cell effectively increases the absorber cross section by a factor of 2, provided that the dye-cell thickness is comparable with the mode-locked laser pulse length. This advantage will thus be lost when the pulses become short compared with the cell length. The importance of a short absorber-cell path length for generating the shortest bandwidth-limited pulses has been demonstrated for the mode-locked Nd:glass laser⁸ and is seen to hold also for the mode-locked cw dye laser.

It is anticipated that with narrower dye cells and general engineering refinements the durations of these stable bandwidth-limited pulses could be decreased even further. Extension of the subpicosecond tuning range to both shorter and longer wavelengths is likely by employing other absorber-laser dye combinations. DQOCI (1,3'-diethyl-4,2'-quinolyoxacarbocyanine iodide), which has earlier mode locked the pulsed¹² and the cw¹³ Rhodamine 6G dye laser over the range 580–613 nm producing pulses of durations 1–2 ps, has generated subpicosecond pulses in the present cw system, but detailed investigations of the tuning range have not yet been carried out. The DODCI-Rhodamine B combination, with which mode locking has been achieved in the spectral region 610–630 nm⁶ should extend the tunable range to longer wavelengths.

The authors wish to thank Dr. G.H.C. New for helpful discussions and Dr. W. Sibbett for advice and for help with the measurements. Financial support from the Science Research Council is gladly acknowledged.

¹E. P. Ippen, C.V. Shank, and A. Dienes, *Appl. Phys. Lett.* **21**, 348 (1972).

²F. O'Neill, *Opt. Commun.* **6**, 360 (1972).

³E.G. Arthurs, D.J. Bradley, B. Liddy, F. O'Neill, A.G. Roddie, W. Sibbett, and W.E. Sleat, in *Proceedings of the 10th International Congress on High Speed Photography* (A.N.R.T., Paris, 1972), p. 117.

⁴C.V. Shank and E.P. Ippen, *Appl. Phys. Lett.* **24**, 373 (1975).

⁵E.P. Ippen and C.V. Shank, *Appl. Phys. Lett.* **27**, 488 (1975).

⁶E.G. Arthurs, D.J. Bradley, P.N. Puntambekar, I.S. Ruddock, and T.J. Glynn, *Opt. Commun.* **12**, 360 (1974).

⁷D.J. Bradley, G.H.C. New, and S.J. Caughey, *Phys. Lett. A* **30**, 78 (1969); D.J. Bradley and W. Sibbett, *Opt. Commun.* **9**, 17 (1973).

⁸D.J. Bradley and W. Sibbett, *Appl. Phys. Lett.* **27**, 382 (1975); D.J. Bradley and G.H.C. New, *Proc. IEEE* **62**, 313 (1974).

⁹H.A. Haus, *IEEE J. Quantum Electron.* **QE-11**, 736 (1975); H.A. Haus, *Opt. Commun.* **15**, 29 (1975).

¹⁰G.H.C. New, *Opt. Commun.* **6**, 188 (1972).

¹¹G.H.C. New, *IEEE J. Quantum Electron.* **QE-10**, 115 (1974).

¹²R.S. Adrain, E.G. Arthurs, D.J. Bradley, A.G. Roddie, and J.R. Taylor, *Opt. Commun.* **12**, 140 (1974).

¹³I.S. Ruddock, Ph.D. thesis (University of London, 1976) (unpublished).